High Pressure and Temperature Study of Cyclohexane, Methylcyclohexane, and 6-Bromo-1-hexene Pyrolysis

BY

MIROSLAW KRZYSZTOF LISZKA
B.S. University of Illinois at Chicago, 2013

THESIS

Submitted as partial fulfillment of the requirements
for the degree of Doctor of Philosophy in Mechanical Engineering
in the Graduate College of the
University of Illinois at Chicago, 2018

Chicago, Illinois

Defense Committee:

Kenneth Brezinsky, Chair and Advisor, Mechanical and Industrial Engineering
Farzad Mashayek, Mechanical and Industrial Engineering
Suresh K. Aggarwal, Mechanical and Industrial Engineering
Patrick T. Lynch, Mechanical and Industrial Engineering
Robert S. Tranter, Argonne National Laboratory

ACKNOWLEDGMENTS

I would like to thank Professor Kenneth Brezinsky for allowing me the opportunity to conduct this research and complete my doctoral studies under his guidance. I would like thank Professor Suresh K. Aggarwal for introducing me to the field of combustion research by allowing me to conduct undergraduate research under his guidance. I would like to thank the remaining committee members, Professor Farzad Mashayek, Professor Patrick T. Lynch, and Doctor Robert S. Tranter for their feedback and willingness to be part of my defense committee.

I would like to thank the current and past members of the HPST laboratory with whom I had the pleasure of working. I would particularly like to thank Doctor Aleksandr Fridlyand for taking the time to familiarize me with the laboratory equipment and procedures, and for all his feedback and suggestions in the early stages of my work. I would like to thank Juan Guzman, Xu Han, and Jai Mehta for all their help, discussions, and for making my graduate experience a memorable one.

I would like to thank my mother, Maria Liszka, and father, Kazimierz Liszka, for all their support. I would also like to thank my brother, Doctor Damian Liszka, for his advice and encouragement.

Lastly, I would like to thank David Mecha for his willingness to always provide help, advice, and tools to alleviate any mechanical problems that may have occurred in the laboratory, and for the hundreds of diaphragms without which this work would not be possible.

TABLE OF CONTENTS

LIST OF FIGURES

LIST OF ABBREVIATIONS

HPST	High Pressure Shock Tube
RMG	Reaction Mechanism Generator
GC	Gas Chromatography
CPCN	Cyclopropanecarbonitrile
TFE	1,1,1-Trifluoroethane
FID	Flame Ionization Detector
K	Kelvin
C	Celsius
cc	Cubic Centimeters
ms	Millisecond
ppm	Parts Per Million
UHP	Ultra High Purity
SSR	Solid State Relay
CFD	Computational Fluid Dynamics
SMILES	Simplified Molecular-Input Line-Entry System
InChI	International Chemical Identifier
CAS	Chemical Abstracts Service
ROP	Rate of Production
C2/C3/C4/…	Hydrocarbon Species Containing 2, 3, 4, … Carbon Atoms

SUMMARY

An extensive experimental study was completed investigating the high pressure and temperature pyrolysis of cyclohexane, methylcyclohexane, and 6-bromo-1-hexene. The experiments were completed using the High Pressure Shock Tube (HPST) at the University of Illinois at Chicago. The stable pyrolysis products were quantified with an online gas chromatography system. Experiments for all three species were completed at nominal pressures of 40, 100, and 200 bar in order to determine whether a variation in the pressure will impact the product distribution. The profiles of some of the products species were affected by the variation in the experimental pressure, but the most abundant product species did not show notable variation in their profiles. No alkylcyclopentanes were observed to form, and the only alkenylcyclopentane successfully quantified, methylencyclopentane, was observed in trace amounts. This is in contrast to the high pressure supercritical phase experiments of alkylcyclohexanes where alkylcyclopentanes were observed to be the dominant products.

An additional set of experiments was completed at a pressure of 40 bar for all three species. The fuel mole fraction for these sets was increased so that the initial fuel concentration in the reaction zone matched the fuel concentration present in the previously completed 100 bar shocks. For all three species it was found that if the initial fuel concentration in the reaction zone was kept equivalent then matching normalized product distributions can be obtained at different pressures. A set of experiments with a higher mole fraction of cyclohexane was completed at 200 bar to investigate how a further increase in the concentration may impact the product distribution. For this set of experiments, it was observed that the normalized mole fraction of the cyclic species was greater than in the previous experiments which had a lower initial mole fraction of cyclohexane in the test gas mixture. A set of experiments at 100 bar with 1,5-

hexadiene as the fuel was also completed to determine whether the 6-bromo-1-hexene decomposition does not predominately proceed through HBr loss forming 1,5-hexadiene as the primary initial 6-bromo-1-hexene decomposition product. The product distributions from the 1,5-hexadiene and the 6-bromo-1-hexene experiments varied too much for that to be the case.

Following the experimental work, the experimental data for cyclohexane and methylcyclohexane were compared against simulation results which used a recently published cyclohexane and methylcyclohexane mechanism that has been validated against atmospheric and sub-atmospheric flow reactor experimental data. It has been found that overall the model was able to well capture the present experimental results despite the large difference in the experimental conditions and different apparatuses being used for the experiments. A systematic effort to analyze the uncertainty in the mechanism and optimize the mechanism to better capture the present data was followed in a matter similar to what has been done in previous works completed in the HPST laboratory. A separate mechanism was also generated for cyclohexane and methylcyclohexane using the Reaction Mechanism Generator (RMG.) Due to RMG not being able to generate reactions for species containing bromine, a hex-5-en-1-yl and 1,5-hexadiene mechanism was generated to capture the chemistry of 6-bromo-1-hexene pyrolysis. The uncertainty in the generated mechanisms was analyzed in a similar fashion as for the literature mechanism, and an effort to optimize the mechanisms to better capture the experimental data was also undertaken.

1. INTRODUCTION

1.1 Background

In the recent years, United States has been undergoing what can be best described as an energy revolution. Consumer and personal transport vehicles have been seeing constant increases in fuel economy, reduction in the weight, and improvements to aerodynamics[1,2]. Electric personal vehicles have also managed to finally establish a firm foothold in the market and their popularity only seems to be rising. Ongoing battery research resulting in improvements in storage and charging efficiency is constantly made further adding to the popularity and ease of ownership of electric and hybrid vehicles[3–5]. Many long range commercial transport vehicles can now be seen with modifications such as trailer skirts and tails to improve aerodynamics and decrease fuel consumption[6–8]. Compressed natural gas conversions, especially on commercial short range transport and construction vehicles, are also becoming more commonplace as a result of improvements seen in emissions and thermal efficiencies[9,10]. Renewable and green energy generation and supply methods have likewise been enjoying increasing popularity and significant research funding[11].

Aerospace and aeronautical vehicles have also been affected, but due to their unique requirements and challenges the effects largely differ from those previously mentioned. Aerospace and aeronautical vehicles travel over ranges far exceeding those of other vehicles and must store enough fuel or propellant to allow them to complete the journey without refueling. The method of propulsion employed must be capable of delivering vast amounts of energy in a small timeframe, particularly during takeoff or liftoff. These requirements have limited aerospace and aeronautical vehicles to hydrocarbon fuels, and prohibited them from seeing the same alternative fuel developments as in the case of land based vehicles.

The desire to achieve longer flight ranges requires more fuel to be stored on the space or air craft; however, the minimization of the weight as well as the size of the vehicle also helps increase range by decreasing the forces that the vehicle needs to overcome while in motion. Some solutions include storing the fuel at higher pressures which increases density and decreases the volume needed for the fuel storage. Using the fuel as a coolant[12] by circulating it through the engine prior to it being consumed in the combustion process has the benefit of reducing the weight of the engine by negating the need for a separate cooling cycle. The increase in pressure, and particularly the increase in temperature in the case of the fuel being used as a coolant, causes the fuel to undergo pyrolysis and hence alter the chemical composition of the fuel prior to it even entering the combustion chamber[13]. In rocket engines, where it is advantageous to use fuel rich mixtures when the molecular weight of the fuel is lower than that of the oxidizer, pyrolysis may also have a significant impact in the engine itself as excess fuel molecules break down in the high pressure and temperature chamber. Additionally, as engine materials continue to improve it becomes increasingly desirable to increase the combustion chamber temperature and pressure which allows the engine to achieve higher thrust[14].

Aerospace and aeronautical vehicle research and development has largely focused on improvements in airframe and engine design due to the limitations in terms of fuel type. A recent example of such development can be found in SpaceX. For the past few years SpaceX has been frequently appearing in the news with their launches of Falcon 1, Falcon 9, and most recently the Falcon Heavy. Falcon 1 used the Kestrel engine, while Falcon 9 and Falcon Heavy employ the Merlin family engines[15,16]. The Kestrel engine was designed for use in missions which require smaller payloads and has a chamber pressure of approximately 10 bar while the engines in the Merlin family operate at chamber pressures of approximately 100 bar. Both these engines

use Rocket Propellant-1 (RP-1) as their fuel despite their chamber pressures varying by an order of magnitude[17]. RP-1 has been a commonly used aeronautical fuel for decades, and will likely remain so for the foreseeable future. It is a multi-component kerosene based fuel similar to jet fuels. RP-1, like other hydrocarbon rocket and jet fuels, contains a significant amount of cyclic hydrocarbons[18]. The large variation in the pressure under which the fuel reacts may cause the product distribution to change. Pyrolysis experiments of alkylcyclohexanes[19] and methylcyclohexane[20,21] conducted in the supercritical phase have found alkylcyclopentanes to be the dominant products. Alkylcyclopentanes have in turn been found to be coking[21] and sooting[22] precursors. Methylcyclohexane pyrolysis experiments conducted in the gas phase at one atmosphere have not identified alkylcyclopentanes as major products[23,24]. Currently, the literature contains no high pressure methylcyclohexane pyrolysis speciation data.

The primary use of generating speciation data for species frequently found in real fuels is to aid in the generation of chemical kinetic mechanisms that are able to correctly capture the combustion chemistry of real fuels and fuel surrogates. Significant improvements have been made from the early global chemical kinetic mechanisms that relied on a single reaction[25,26] to describe the combustion chemistry in reactors. Modern chemical kinetic mechanisms can include hundreds of species and thousands of reactions, yet they are often tailored to only correctly replicate the set of experimental data that was used to validate the mechanism. Unfortunately, the data used to validate chemical kinetic mechanisms may often span a narrow range of conditions. When such a mechanism is used for simulations at conditions varying significantly from those at which it was validated it may be found that the mechanism fails to match, or even come close, to the experimental data. The conditions in aerospace and aeronautical vehicle engines can vary widely over the course of the flight which would require

multiple chemical kinetic mechanisms to be used in order to accurately simulate the combustion process inside the engine of the vehicle. Such an approach would make the simulations time prohibitive as even computational fluid dynamic simulations for complex geometries are taxing on current computer hardware, much less combining these simulations with differential equations containing thousands of terms that must be solved for each species at each time step and grid point of the simulation.

In order to improve the accuracy of chemical kinetic mechanisms over a wider range of conditions it is necessary to conduct experiments that span a wide range of pressures and temperatures. The HPST facility at UIC is equipped to investigate the effects of pressure and temperature variation on the product composition of fuels over a wide range of experimental conditions. The shock tubes allow for experiments encompassing a pressure range from 1 to 1000 bar and 900 to 2500 Kelvin. The reaction time, or the time for which these conditions can be maintained, ranges from 0.5 to 3 milliseconds[27,28]. Dilute mixtures are used to execute the experiments in order to ensure an almost isothermal and isobaric environment for the duration of the reaction time. With such a large experimental pressure range it is possible not only to match the pressures seen in combustors presently used, but also higher pressure combustors that may be used in the future. The ability to carry out experiments at pressures higher than currently seen in use can provide fundamental understanding of the combustion characteristics that will appear if the combustor pressure is increased and help determine whether an increase in pressure, which theoretically should increase thrust, will not be negated by undesirable changes in the product composition.

1.2 Project Scope

The previous section briefly refers to the disparity between the conditions present in real combustors and the experimental conditions under which speciation data were obtained from the pyrolysis of real fuel constituents. Currently, there are only two studies which provide substantial gas phase methylcyclohexane pyrolysis speciation data[23,24]. Both the studies were completed with a flow reactor at, or below, atmospheric pressures. Methylcyclohexane has been studied in numerous other experimental works, some of which are discussed in the methylcyclohexane chapter, however, the product of those works is typically the ignition delay time. If species data is provided, it is usually only for one or two species that were used to determine when ignition occurs. Speciation data for numerous species provides more constraints for the mechanism and allows direct validation of whether the chemistry of the various species is properly captured.

Cyclohexane has also been studied extensively, but just as for methylcyclohexane, the gas phase pyrolysis speciation data is obtained at lower pressure experiments, and higher pressure experiments typically measure only the ignition delay. The high pressure pyrolysis experiments which generated speciation data for cyclohexane and alkylcyclohexanes[19] and methylcyclohexane[19–21] were conducted in the supercritical phase, and their product distributions were found to be substantially different than observed in the low pressure gas phase experiments. The current work extends the gas phase cyclohexane and methylcyclohexane pyrolysis speciation database to include high pressures (40, 100, and 200 bar) which are seen in real combustors, and to also match and exceed the pressures in the supercritical phase experiments.

The benefit of providing the combustion community with speciation data at pressures and temperatures relevant to real combustors for two species which are seen in real fuels and used in

fuel surrogates is clear since it will aid in the validation and development of chemical kinetic mechanisms. The high pressure environment in which the experiments are completed also allowed to determine whether pressure effects, such as the reactions with a reduced activation volume being preferred or the reaction rate constants reaching their high pressure limit, would result in the same product distributions as those observed in the high pressure supercritical phase experiments. Pressure also effected the initial concentration of the fuel since the test gas mixtures used for all the experiments were prepared with equivalent mole fractions of the fuel. In order to determine the effects of pressure on the product composition, an additional set of experiments was completed at 40 bar with a higher initial mole fraction of fuel that resulted in an initial fuel concentration in the reaction zone close to that observed in the 100 bar experiments.

The 6-bromo-1-hexene experiments were completed in an attempt to further study the possibility of obtaining product distributions similar to those in the high pressure supercritical phase experiments. 6-Bromo-1-hexene was used as a precursor for the hex-5-en-1-yl, or 5-hexenyl, radical which is expected to be the primary product of the cyclohexyl radical ring opening[23,29–32]. The cyclohexyl radical is highly relevant and a direct dissociation intermediate product in cyclohexane, methylcyclohexane, and alkylcyclohexane dissociation[29–35]. Using 6-bromo-1-hexene also allowed to begin the experiments further along the pathway expected to lead to the formation of methylcyclopentane or methylenecyclopentane; therefore, reducing the amount of competing reactions. The 6-bromo-1-hexene experiments were likewise completed at three pressures (40, 100, and 200 bar) with another set of experiments completed at 40 bar but with a higher initial mole fraction of the fuel in order to match the fuel concentration present in the 100 bar experiments and to determine whether any of the observed differences in

the product distributions were due to pressure effects of the difference in the initial fuel concentration.

Following the successful completion of the experiments, a comparative chemical kinetic mechanism study was undertaken. The primary purpose of this study was to compare the ability of the two mechanisms to predict the experimental data. One of the mechanisms was a recently published chemical kinetic mechanism developed to capture cyclohexane and methylcyclohexane pyrolysis chemistry[23,36]. This mechanism was created in a more classical, hierarchical fashion with the authors first utilizing an existing smaller species mechanism and then adding sub-mechanisms containing the reactions of larger species which were taken from other published works. An attempt was made at systematically determining the uncertainty in the mechanism and optimizing[37,38] the mechanism's ability to predict the high pressure data without degrading its ability to predict the lower pressure product distributions against which the mechanism was originally validated. Mechanisms for cyclohexane and methlycyclohexane were generated with the Reaction Mechanism Generator (RMG). In contrast to the literature mechanism, RMG mechanism is a computer generated mechanism which utilizes a rate based construction algorithm and 45 reaction families which result in large mechanisms (around 20,000 reactions for the mechanisms generated in this work) which are meant to fully capture the chemistry of the reactant fuel species. Uncertainty analysis for the generated mechanisms was also completed in the same fashion as for the literature model. A mechanism for hex-5-en-1-yl radical and 1,5-hexadiene was generated since RMG does not support bromine containing species. The uncertainty analysis for this mechanism was also completed.

Prior to any of the work being undertaken the online gas chromatography system was refurbished and modified to handle higher injection pressures. The system was originally

developed and optimized for sampling of 50 bar shocks[39]. Due to lack of maintenance, the time necessary for the sample pressure to stabilize would be as high as 5 to 10 minutes. The new system stabilizes the sample around 3 seconds and the areas where carbon build up may occur causing clogging and delays in the time needed for the sample pressure to stabilize have been documented. With regular maintenance the current system should be able to fulfill all the needs in the High Pressure Shock Tube (HPST) laboratory for the foreseeable future.

2. EXPERIMENTAL APPARATUS

2.1 Shock Tube Background

The scientific use and development of shock tubes began in 1899 with the work conducted by Vieille who first used pistons to measure the speed of pressure pulses by bursting glass bulbs at the end of a 6-meter-long tube[40]. Vieille then split the tube into high and low pressure sections with the use of expendable diaphragms of various materials thereby creating the first compressed gas driven shock tube. The generation of shocks can also be accomplished with detonations rather than compressed gas. The first detonation driven shock tube was used by Michel-Levy and Muraour between 1934 and 1941. It was a long tube with explosives placed on one end and was used to conduct shock wave luminosity experiments[41–43].

In 1946, the work by Payman and Shepherd was published where they noted the impact of varying the thickness of the diaphragm, the composition of the gases used in the low and high pressure sections of the shock tube, and the length of the sections of the shock tube on the speed of the shock front[44]. Their work is considered to be the first to describe the essential features and variables of a compressed gas, diaphragm shock tube[45]. The following two decades saw a rapid increase in the use of shock tubes for chemical research. Multiple studies investigating the rotational relaxation[46–48], vibrational relaxation[49–56], and dissociation[57–65] of various molecules employed the use of shock tubes in less than twenty years following the publication of Payman and Shepherd's work.

More relevant to the present work was the rapid adaptation and use of shock tubes for chemical kinetic studies in that same short time frame[66–80]. Chemical kinetic studies took advantage of both the additional increase in temperature from the reflected shock, and the rapid quenching of the product species by the rarefaction wave[77,78]. The products would then be

extracted and were typically analyzed by the means of gas chromatography or mass spectrometry[66,70,71]. Optical measurements of species, particularly intermediate species, were also conducted[67,72–74,76,80]. The continuous development of shock tubes and their widespread use in chemical kinetic research continues to the present day as evident by this work and numerous other recent shock tube studies.[81–89]

2.2 Shock Tube Theory

Figure 1a provides a simple diagram of an ideal shock tube composed of a high pressure section commonly called the driver, and the low pressure section which is filled with the experimental test gas and is referred to as the driven section. The two sections are separated by a diaphragm. Figure 1b shows the propagation of the shock wave, contact surface, and the rarefaction fan within the shock tube with respect to time after the bursting of the diaphragm occurs. Region one and region four designate the original conditions present in the driven and driver sections of the shock tube prior to the arrival of the shock wave and rarefaction fan, respectively. Region two is the region of the driven section through which the shock wave has passed but not the contact surface. Region three is the region between the contact surface and the rarefaction fan. Region five, which is of most interest in the present work, is the region through which the reflected shockwave traveled generating an additional increase in pressure and temperature near the end wall.

Figure 1c and d show the pressure and temperature distribution in the shock tube, respectively, at time t_1 at which neither incident shock wave nor the rarefaction fan have arrived and reflected off the ends of the shock tube. The subscripts indicate the pressures, P_i, and temperatures, T_i, in the regions discussed above. The relations for the conditions present in the

various region of the flow in the shock tube will be established, but prior to that the frame of reference of the flow with respect to the shock wave must be established.

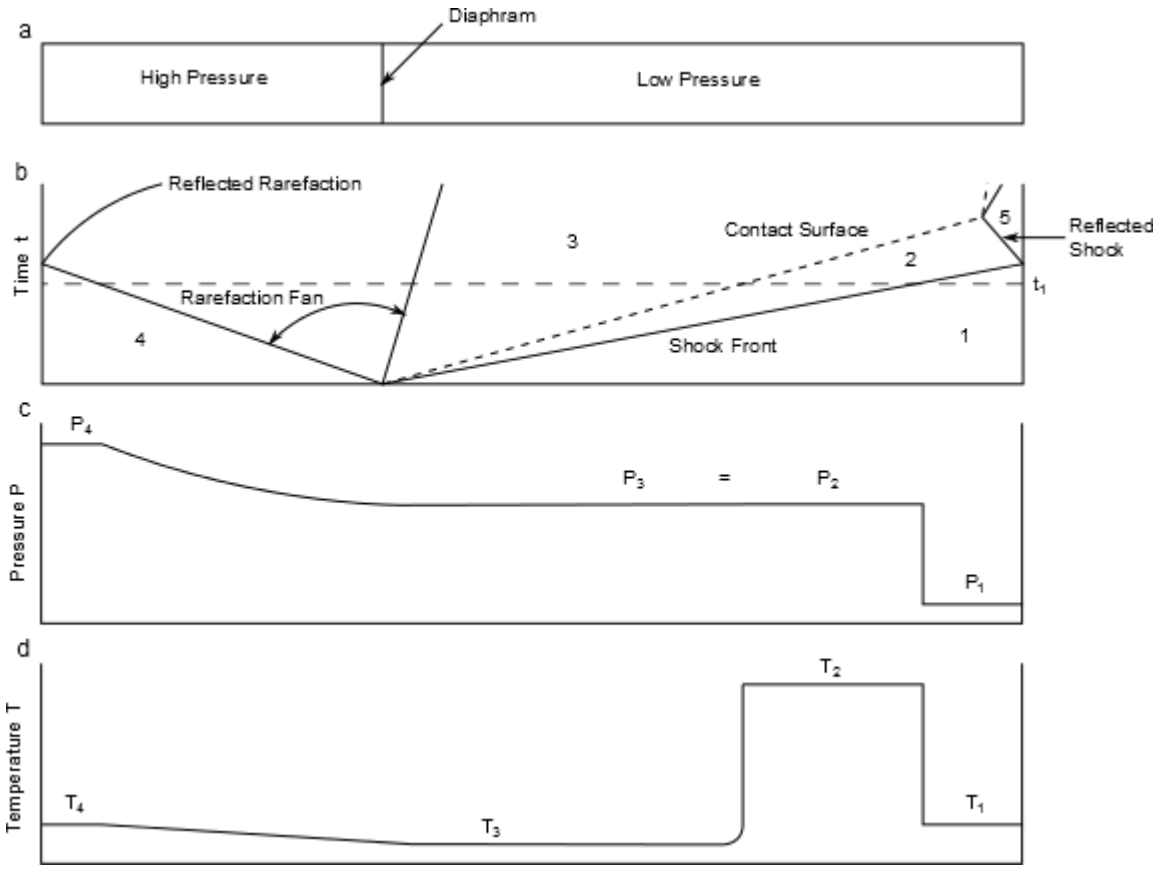

Figure 1: a) Simple diagram of an ideal shock tube, b) Position versus Time (commonly called x - T) diagram showing the propagation of the shock wave, contact surface, and rarefaction fan within the shock tube c) Pressure profile within the shock tube at time t_1, and d) Temperature profile within the shock tube at time t_1. Adapted from illustration in [45].

The definition of the frame of reference for the flow in front and behind the shock wave and all the proceeding equations are adapted from the derivations presented by Gaydon and Hurle[45]. To simplify the governing equations two relative velocities are defined: the relative velocity of the gas in front of the shock wave u_1, and the relative velocity of the gas behind the shock wave u_2 which are defined as follows:

$$u_2 = W_s - v_1 \tag{1}$$

$$u_2 = W_s - v_2 \tag{2}$$

Where W_s is the speed of the shock wave and v_1 and v_2 are the speeds of the gas in front and behind the shock wave, respectively. It is now possible to express the continuity, momentum, and energy conservation equations across the shock wave in terms of the relative velocities.

$$\rho_1 u_1 = \rho_2 u_2 \tag{3}$$

$$P_1 + \rho_1 u_1^2 = P_2 + \rho_2 u_2^2 \tag{4}$$

$$H_1 + \frac{1}{2}u_1^2 = H_2 + \frac{1}{2}u_2^2 \tag{5}$$

Where H_i are the enthalpies, P_i the pressures, and ρ_i the densities of the gas in front of the shock wave, designated with the subscript 1, and the gas behind the shock wave, denoted with subscript 2. Additional useful relations are the specific heat ratio γ, the speed of sound a, and the Mach number M which are all defined below.

$$\gamma = C_p/C_v \tag{6}$$

$$a = \sqrt{\gamma P/\rho} = \sqrt{\gamma RT/M} \tag{7}$$

$$M_i = u_i/a_i \tag{8}$$

Using the thus far developed system of equations it is now possible to obtain the relations for the ratio of pressures, densities, and temperatures across the shock wave in terms of the Mach number of the shock wave.

$$\frac{P_2}{P_1} = \frac{2\gamma M_1^2 - (\gamma - 1)}{\gamma + 1} \tag{9}$$

$$\frac{\rho_2}{\rho_1} = \frac{(\gamma + 1)M_1^2}{(\gamma - 1)M_1^2 + 2} \tag{10}$$

$$\frac{T_2}{T_1} = \frac{\left(\gamma M_1^2 - \frac{\gamma - 1}{2}\right)\left(\frac{\gamma - 1}{2} M_1^2 + 1\right)}{\left(\frac{\gamma + 1}{2}\right) M_1^2} \tag{11}$$

It is also possible to derive an implicit relation for the Mach number of the incident shock wave by noting that the rarefaction fan is isentropic and that the expression $2a/(\gamma - 1) + v$ is conserved across the rarefaction fan while also considering the adiabatic gas law and the relation for the speed of the gas behind the shock which results in the three expressions given below.

$$\frac{2a_4}{(\gamma_4 - 1)} + v_4 = \frac{2a_3}{(\gamma_3 - 1)} + v_3 \tag{12}$$

$$\frac{P_4}{P_3} = \left(\frac{a_4}{a_3}\right)^{\frac{2\gamma_4}{\gamma_4 - 1}} = \frac{P_4}{P_2} \tag{13}$$

$$v_2 = \frac{2a_1}{(\gamma_1 + 1)}\left(M_1 - \frac{1}{M_1}\right) \tag{14}$$

Using the above three equations together with equation 9 results in an implicit expression for the Mach number of the incident shock wave as a function of the initial driven and driver pressures, specific heat ratios, and speeds of sound all of which are known properties of the driven and driver sections of the shock tube.

$$\frac{P_4}{P_1} = \frac{2\gamma_1 M_1^2 - (\gamma_1 - 1)}{\gamma_1 + 1}\left\{1 - \frac{\gamma_4 - 1}{\gamma_1 + 1}\frac{a_1}{a_4}\left(M_1 - \frac{1}{M_1}\right)\right\}^{-\frac{2\gamma_4}{(\gamma_4 - 1)}} \tag{15}$$

Equation 15 together with equations 9 through 11 provide a full description of the gas conditions present behind the incident shock wave in terms of the initial loading conditions of the driven and driver sections of the shock tube. This is certainly useful, but the reaction zone for the present work is region five in Figure 1b, the region through which the reflected shock wave has passed resulting in an additional increase in the temperature and pressure of the test gas. It is

also possible to establish a set of equations for the conditions present in the zone behind the reflected shock by analogy with the equations presented so far for the conditions across the incident shock. Doing so results in a set of equations for the speed of the reflected shock and the temperature and pressure in the region behind the reflected shock in terms of the initial loading conditions of the shock tube, which are given below.

$$\frac{P_5}{P_1} = \left\{\frac{2\gamma M_1^2 - (\gamma - 1)}{\gamma + 1}\right\}\left\{\frac{(3\gamma - 1)M_1^2 - 2(\gamma - 1)}{(\gamma - 1)M_1^2 + 2}\right\} \tag{16}$$

$$\frac{T_5}{T_1} = \frac{\{2(\gamma - 1)M_1^2 + (3 - \gamma)\}\{(3\gamma - 1)M_1^2 - 2(\gamma - 1)\}}{(\gamma + 1)^2 M_1^2} \tag{17}$$

$$\frac{W_R}{W_s} = \frac{2 + \frac{2}{\gamma - 1}\frac{P_1}{P_2}}{\frac{\gamma + 1}{\gamma - 1} - \frac{P_1}{P_2}} \tag{17}$$

The only remaining useful quantity to be determined is the reaction time, or observation time, for the duration of which the conditions in region behind the reflected shock can be sustained. Gaydon and Hurl define the observation time as the time necessary for the reflected shock wave to reach the contact surface and provide the below expression for the observation time:[45]

$$\Delta\tau = \frac{\chi_1}{M_1 a_1}\left(\frac{\gamma - 1}{2\gamma}\right) \tag{18}$$

In this work the reaction time is defined as the time necessary for the pressure at the end wall to decrease to 80% of its maximum value, which will be discussed further in the following section, so the actual observed reaction times will be longer than the observation times obtained using equation 18. Nonetheless, equation 18 provides insight into what variables have an effect on the observation time. Like with most of the conditions in the reaction zone, the reaction time

is a function of the incident shock wave Mach number, with a faster speed shock decreasing the reaction time, and the speed of sound and the specific heat ratio of the driven gas. The length of the driven section, denoted by χ_1 in equation 18 is proportional to the reaction time, so longer driven sections will allow for a longer duration of the conditions in region 5 to be sustained. The reaction zone conditions in an ideal shock tube, and the time for which they can be sustained, have now fully been defined as a function of the initial conditions of the driven and driver sections by equations 15 through 18.

2.3 UIC High Pressure Shock Tube

The High Pressure Shock Tube (HPST) at the University of Illinois at Chicago was used to conduct all the experiments presented herein. The design of the HPST has been described in great detail by Dr. Robert S. Tranter and as such only a description of the most relevant and important aspects of the HPST will be provided[27]. The driven section has a modular design allowing the overall length to be varied from 37 up to 177 inches with the use of three extensions of 20, 40, and 80 inches in length. For all the experiments only the 80-inch extension was used putting the total length of the driven section at 117 inches. The driver section is 60 inches in length and its length can also be varied with the use of stainless steel plugs which range from 2 to 47 inches in length. The driven section is one inch in diameter and the driver section is two inches in diameter and contains a converging insert that reduces the diameter to one inch just before the diaphragm. A dump tank is attached to the driven section of the shock tube at a 45-degree angle shortly after the diaphragm. The dump tank allows the shock tube to function as a single pulse shock tube by dissipating the reflected shock into the dump tank rather than allowing it to reflect off the driver end wall and propagate into the driven section again.

The high driver pressures needed to fire the shocks, particularly the 200 bar shocks which require around 2000 psi of pressure in the driver section, make it prohibitive to use the helium directly from the cylinders supplied by Praxair which are pressurized to 2500 psi. Instead, the helium is boosted with a Maximator DLE-75-2-UU-M booster pump into five high pressure cylinders which are then used to fill the driver section. The high pressure cylinders were typically boosted to approximately 10,000 psi with Ultra High Purity (UHP) helium (99.999% purity) supplied by Praxair. HiPCO high pressure lines and fittings are used for all the gas connections to the shock tube due to the high pressures present in the cylinders and the driver section of the shock tube. HiPCO 22-11LF4 manual valves rated to 20,000 psi are used on all the individual high pressure cylinders to control which cylinder is in use, along the delivery lines from the cylinder to shut off the flow to the shock tube while boosting and in case of leaks, and also for exhausting the shock tube after the shock is fired. HiPCO 20-11LF4-NC pneumatic valves rated to 20,000 psi are used for controlling the filling of the driver and driven sections and are connected in series with HiPCO 60-11HF4-V metering valves rated to 60,000 psi to control and keep a more consistent rate of flow into the shock tube while the high pressure helium cylinder and test gas pressure varies. A third HiPCO-22-11LF4-NC pneumatic valve is connected at the end wall of the shock tube to extract the post shock sample.

The entire shock tube was heated to 100 degrees Celsius for all the experiments to prevent condensation of the fuel or any of the products species. Self-adhesive precision heat tape supplied by Clayborn Lab is used to heat the shock tube. The temperature control circuits are composed of three Omega CN1507-TC multi-zone temperature controllers used to monitor and control the temperature of four sections of the shock tube each, twelve Omega SSLR240DC10 Solid State Relays (SSR) used to control the power to the precision heat tape, and twelve Omega

J type thermocouples are used to measure the temperature. The entire shock tube is insulated with AMI-THERM NX08 needled cloth supplied by Auburn Manufacturing, Inc.

The experiments were conducted at three nominal pressures requiring three different types of diaphragms. All the diaphragms were punched out of 3003 grade aluminum sheets and were scored by milling to facilitate clean opening. The nominal diaphragm thicknesses used were 25 thousandths of an inch overall thickness with a 14 thousandths of an inch wall thickness, the wall thickness is the thickness of the material left in the score, 32 thousandths of an inch overall thickness with 27 thousandths of an inch wall thickness, and 50 thousandths of an inch overall thickness with 43 thousandths of an inch wall thickness which were used to generate reflected shock pressures of 40, 100, and 200 bar, respectively. The performance of the diaphragms was found to vary somewhat between batches of diaphragms most likely due to thickness variation in the supplied aluminum stock and also in the wall thickness due to milling tolerances on the score. The nominal wall thickness between batches of diaphragms would be adjusted by half or one thousand of an inch, as needed, to limit the amount of deviation in the reflected shock pressures. Figure 2 provides an example of a scored unburst diaphragm and burst diaphragm. After a new diaphragm is loaded and the shock tube is closed the driver section would be continuously evacuated with an Edwards RV8 vacuum pump until filling occurred. The driven section would first be evacuated to approximately 100 mTorr with a Leybold Trivac D2.5E vacuum pump, at which point the vacuum pump would act as a roughing pump for an Edwards EXT70 turbomolecular pump which would establish a vacuum of around 2 mTorr.

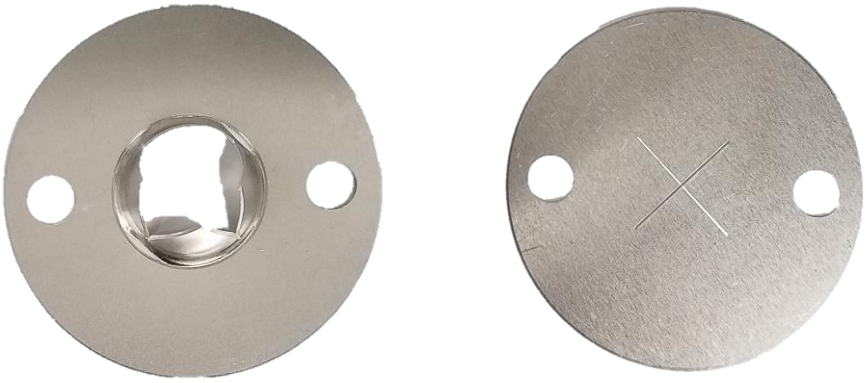

Figure 2: Example of typical 3003 grade aluminum diaphragms used for the experiments. A burst diaphragm is shown on the left, and an unused diaphragm on the right.

2.3.1 Temperature Calibration

The temperature of the shock tube is not measured directly but with an external chemical thermometer[90]. The use of an external chemical thermometer ensures that no reactions occur between the fuel mixture and the chemical thermometer, which would be possible with an internal chemical thermometer. An external chemical thermometer requires that an additional set of shocks is completed for each thermometer used. The temperature is then backed out by using the extent of reaction of the chemical thermometer, and a relation between the temperature and incident shock speed is established. The incident shock speed is measured for all the shocks with the fuel of interest in the test gas and the incident shock speed versus temperature relation established with the chemical thermometer can be used to extract the temperature.

The incident shock wave speed is captured with six PCB-113A series transducers mounted in the sidewall near the end wall of the shock tube. A seventh PCB-113A series transducer is mounted in the end wall, near the sampling port. The end wall transducer captures the reflected shock pressure profile at the end wall of the shock tube. The profile is used to obtain the pressure in the reaction zone and the reaction time. The reaction time is taken as the time it takes the maximum pressure at the end wall to decrease to 80% of its value due to the

quenching by the arriving rarefaction fan. The validity of this approach for determining the reaction time has been previously evaluated by Tang and Brezinsky[91]. Figure 3 provides an example of the end wall pressure trace as obtained and displayed by the in-house LabView program written by Dr. Robert S. Tranter. The arrows were added for clarification. The reaction time, and the arrival time of the shock wave at all seven transducers are displayed in the program. The program displays eight times in total, because the shock wave arrival time from the first transducer is sent to both the Measurement Computing PCI-DAS4020/12 data acquisition boards and due to that both the first and fifth time are equivalent.

The temperature in the reflected shock reaction zone could be obtained with the ideal shock tube relations, i.e. equation 17, since the incident shock wave speed is measured directly and all the other required properties are known; however, the ideal shock tube relations would not be adequate to capture the reflected temperature as is evident by the end wall pressure trace shown in Figure 3. The real end wall pressure profile does not retain a constant pressure after the arrival of the reflected shock, but instead exhibits an additional increase in pressure prior to the arrival of the rarefaction wave. This additional increase in the pressure would also be accompanied by an increase in temperature, whereas the ideal shock relations predict a constant temperature and pressure behind the reflected shock. The benefit of using the chemical thermometer is that it accounts for any non-ideal effects that may be present in the shock tube and provides what can be best described as a weighted average of the temperature in the reaction zone.

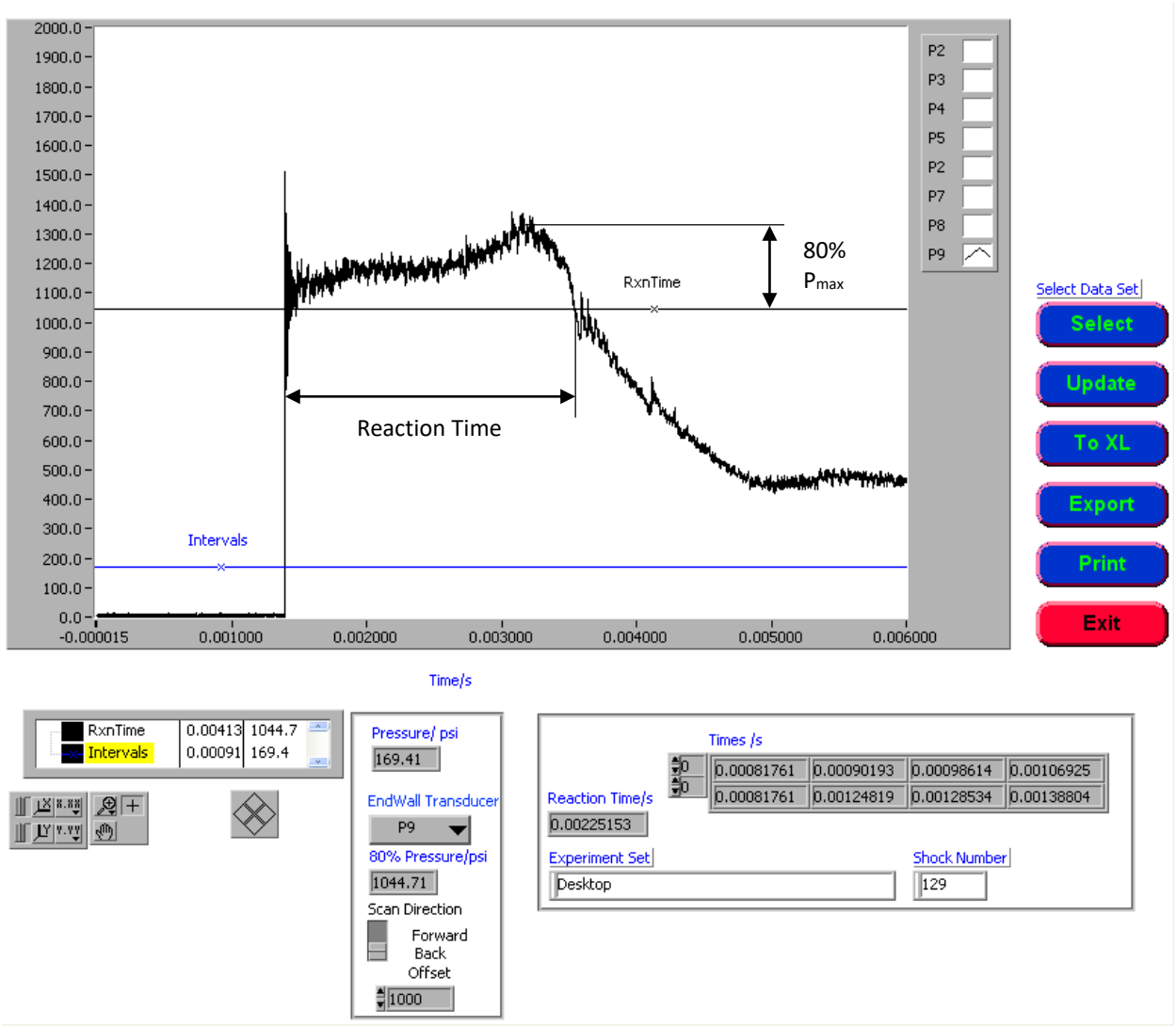

Figure 3: End wall pressure trace obtained for a 6-bromo-1-hexene shock at 100 bar as seen in the in-house LabView data acquisition program.

The two chemical thermometers used were cyclopropanecarbonitrile (CPCN) and 1,1,1-trifluouroethane (TFE.) CPCN was used to calibrate the temperature approximately over the 1000 to 1100K experimental temperature range and the rate constant coefficients used for the total CPCN isomerization rate were determined by Lifshitz et al. and are given below[92]:

$$k_{\infty} = 3.2 \times 10^{14} exp(-29106/T)[s^{-1}] \quad (19)$$

TFE was used to calibrate approximately over the 1300 to 1400K experimental temperature range and the rate constant coefficients for the decomposition to 1,1-difluoroethane were determined by Matsugi et al. to be[93]:

$$k_{\infty} = 3.33 \times 10^{14} exp(-37363/T)[s^{-1}] \tag{20}$$

With the reaction rate coefficients known, and the reaction time determined directly from the end wall pressure trace, which has been previously described, it is then possible to determine the temperature in the reflected shock reaction zone with the below equation[94].

$$T_5 = \frac{-E_a/R}{ln\left(\frac{-ln(1-x)}{At}\right)} \tag{21}$$

Where A is the pre-exponential factor in the Arrhenius equation and E_a/R is the activation energy divided by the universal gas constant. Both of these parameters for CPCN and TFE are given in equations 19 and 20, respectively. t is the reaction time which is obtained from the end wall pressure trace, and x is the extent of reaction which is defined below.

$$x = \frac{[F]_0 - [F]_f}{[F]_0} \tag{22}$$

$[F]_0$ is the initial mole fraction of the fuel or chemical thermometer, in this case either CPCN or TFE, and $[F]_f$ is the remaining amount of fuel recovered after the shock has been fired. The reactions that occur once the extent of reaction of the fuel exceeds 90% are more complex and cannot be accurately predicted by the single reaction rate constants for CPCN isomerization and TFE decomposition and are excluded from the temperature calibration. When the extent of reaction is below 10%, the fuel has not yet fully began reacting and a linear profile

cannot be established for the calibration curve and as such those points are also excluded from the temperature calibration.

Once a set of experiments has been conducted with each chemical thermometer it is possible to plot the experimentally determined temperature, obtained with equation 21, against the incident shock speed at which the temperatures were obtained and generate a temperature calibration curve such as the one shown in Figure 4. The temperature calibration curve shown in Figure 4 was obtained at 200 bar with both CPCN and TFE chemical thermometers. The temperature calibration equation is shown in the figure and was used to determine the temperature for all the 200 bar experiments. The calibration curve, and the experimental chemical thermometer temperatures, are also compared against the ideal temperature which can be obtained with equation 17. The experimentally obtained temperatures with CPCN can be seen to be closely clustered around the ideal shock relation temperature. This is because at lower temperatures the end wall pressure profile is flatter and not much additional pressure rise is observed, whereas at higher temperatures, or higher incident shock speeds, there is a larger rise observed in the end wall pressure trace and as such a larger increase in the temperature is expected.

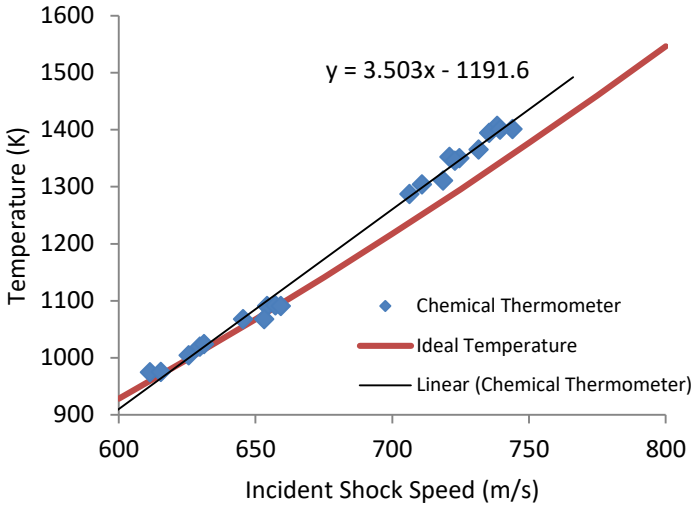

Figure 4: Temperature calibration curve for 200 bar shocks obtained using CPCN and TFE chemical thermometers. The linear trend line and the equation for the trend line are shown in the plot together with the temperature obtained using ideal shock equations.

The uncertainty in the temperature calibration has been previously evaluated and quantified as up to 30K at temperature of 1500K[37,38]. The uncertainty was determined by varying the pre-exponential factors used in equation 21 by the specified maximum uncertainty for the reaction rate constant, obtaining a new temperature calibration curve, and noting the change in the temperature at a given incident shock velocity. The uncertainty was applied to the pre-exponential factor because the uncertainty is specified for the reaction rate constant as a whole, and the pre-exponential factor is directly proportional whereas the activation energy is in the exponent. To apply an uncertainty to the activation energy this would require choosing an uncertainty to apply to the activation energy, and then applying an uncertainty to the pre-exponential factor so that the overall uncertainty would equal the uncertainty specified for the reaction rate constant. This could be done, but it shouldn't provide any further insight into the temperature uncertainty since the overall uncertainty in the temperature should end up being the same. The uncertainty determination procedure described above was repeated for the new temperature calibrations because different reaction rate coefficients were used for TFE

decomposition, and the uncertainty specified for the new TFE pre-exponential factor was 40% rather than 30% for the previously used TFE coefficients. Nonetheless, this gave a result that was very similar to the uncertainties previously obtained. Now the uncertainty at 1500K increased by only 1K, resulting with an up to 31K uncertainty in the temperature at 1500K.

2.3.2 Mixture Preparation

All the test gas mixtures used in the experiments were prepared manometrically using the mixing rig at the HPST laboratory. A recent picture of the rig is shown in Figure 5 for illustrative purposes. The test gas mixture preparation would begin by connecting, if not already connected, the 1.5 cubic foot test gas cylinder to the high pressure line and exhausting any remaining contents. The temperature of the test gas cylinder was maintained at 100 C to avoid condensation of the fuel species. The cylinder was heated with HTS/Amptek heating tape and the temperature was controlled with the same temperature controllers as described earlier in the UIC High Pressure Shock Tube section. Just as with the shock tube, the test gas cylinder is wrapped in AMI-THERM NX08 insulation. The pressure in the high pressure line of the mixing rig is measured with a Setra Systems 280E gauge pressure transducer and displayed with a Setra Systems Datum 2000 manometer. Once the test gas cylinder has been exhausted sufficiently long to achieve an atmospheric, or close to atmospheric, pressure the cylinder is closed and it is then connected to the low pressure line of the mixing rig.

The low pressure line of the mixing rig has multiple ports allowing for the connection of the test gas cylinder, up to two more gas cylinders which can be connected to the ports requiring VCR metal gasket diaphragms, the connection of the glass bulb containing the liquid fuel species, and a connection leading to an Edwards RV8 pump which is used to maintain the vacuum in the low pressure line of the mixing rig. Each line connecting to the low pressure line

contains a quarter turn valve that allows for independent shut off of each individual connection from the remainder of the low pressure line. The pressure in the low pressure line is measured with two Baratron Type 631 capacitance manometers, one with a 0 to 2 torr pressure range and the other with a 2 to 100 torr pressure range. The pressure is displayed with a MKS PDR-C-2C Power Supply Readout. The test gas cylinder is then opened and is pumped down overnight with the Edwards RV8 pump. Typically, a vacuum of approximately 20 millitorr is achieved. Once under vacuum the test gas cylinder is closed, and a bulb containing the fuel species is attached to the low pressure line with an Ultra-Torr fitting. The fuel is then degassed by submerging the bulb containing the fuel in a dewar filled with liquid nitrogen, and once frozen the bulb is exposed to the low pressure line kept under vacuum by the Edwards RV8 pump. The fuel is then allowed to thaw, and is refrozen at least two more times while continuously kept under vacuum. After the fuel is allowed to thaw for the final time, the test gas cylinder is opened and the valve on the connection to the pump closed. The fuel is then allowed to diffuse into the test gas cylinder until the desired pressure is achieved in the cylinder. A small amount (~10 torr) of neon supplied by Specialty Gases of America (99.999% purity), which is connected to one of the two other ports for gases on the low pressure line, is added as an internal standard.

The test gas cylinder is then closed and disconnected from the low pressure line of the mixing rig and connected to the high pressure line. UHP Argon supplied by Praxair (99.999% purity) is also connected to the high pressure line. The test gas cylinder remains closed while the high pressure line is filled with argon and then exhausted at least five times. This is done because a pump is not connected to the high pressure line, so the air, or any other gases, in the line are diluted with argon and exhausted repetitively. The high pressure line is then pressurized with argon, the test gas cylinder is opened, and it is filled with argon until the total desired pressure

for the test gas is achieved. It has been found that the zero reading for the high pressure line tends to drift, but the intraday change in the zero is not substantial. Additionally, the Setra Systems 280E gauge pressure transducer seems to build up charge over time which is evident once the zero reading continues to increase. Touching the transducer seems to discharge it and returns the zero reading to normal.

Figure 5: HPST laboratory mixing rig.

2.4 Analytical Technique

The samples extracted from the shock tube are analyzed with online gas chromatography (GC) sampling as described by Comandini et al[39]. Upon the arrival of the rarefaction fan and quenching of the test gas near the end wall, the pneumatic HiPCO 20-11LF4-NC valve attached to the end wall of the shock tube is opened by the LabView program and a sample is extracted and allowed to expand into the sampling system which is kept at a vacuum prior to the valve

opening. For all the experiments the time for which the valve remained opened was fixed at 200 ms. The sample pressure in the sampling lines is measured with a Baratron Type 631 capacitance manometer and displayed with a MKS PDR-C-2C Power Supply Readout. Once the sample pressure stabilizes, it is recorded and the sample is injected into the GCs. Two Hewlett-Packard (HP) 6890 GCs were used for the analysis of the products, one equipped with the Supelco Petrocol (24160-U) and the other with the Agilent GS-GasPro (113-4362) capillary column. The need for the two GCs arose from the two columns requiring substantially different temperature methods which are included in APPENDIX A. The Supelco Petrocol column provides excellent separation of C5 to C7 species, or even larger species if a sufficiently long method is used, but it requires a method with lower temperatures and a lower rate of increase in the temperature. The GS-GasPro is a more general column which can be used to quantify hydrocarbons up to C10, although it was only used to quantify products up to C4 for the present work, but it requires higher temperatures and a higher ramping rate of temperature. Both the columns were connected to Flame Ionization Detectors (FID).

Gas calibration mixtures supplied by Air Liquide and SCOTTY were used to identify the product species along with a Hewlett-Packard 5973 Mass Selective Detector. 1,3-cyclopentadiene, 1,5-hexadiene, cyclohexene, methylenecyclopentane, cyclohexane, methylcyclohexane, 1,3-cyclohexadiene, and 6-bromo-1-hexene were calibrated by vaporizing a known amount of a liquid sample containing the respective species into a treated, and heated (150 C) stainless steel vessel and injecting the sample into the GCs. A picture of the vessel used for calibrations is shown in Figure 7.

Figure 6: Recent picture of the heated 300 cc vessel used for GC calibration.

The relative uncertainty for those species is expected to be up to 10% in the extreme cases, but generally around 5 to 6% based on the observed difference in the expected mole fraction in the manometrically prepared test gas mixtures and the mole fraction obtained by GC analysis using the calibration of the same species. All the remaining species were calibrated using gas mixtures obtained from Air Liquide and SCOTTY and have uncertainties of 5% as specified by the manufacturer. The cyclohexene and 6-bromo-1-hexene calibration curves are shown in Figure 7 as an illustrative example.

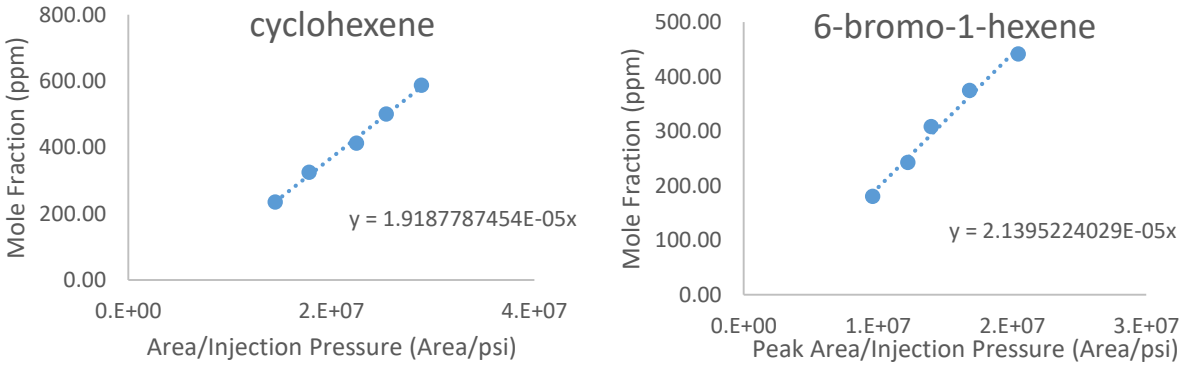

Figure 7: GC calibration curves for cyclohexene and 6-bromo-1-hexene.

Prior to any experiments being conducted the sampling lines were replaced because of diminishing performance as the time needed for the sample pressure to stabilize had become

excessively long due to clogging caused by carbon built up. Modifications were also made to allow for sampling of higher pressure shocks while limiting the risk of damaging the GC sampling valve rotors due to exposure to sample gas pressures exceeding the rating of the rotors. The three-foot-long quarter inch diameter sampling line leading from the automated sampling valve was replaced with a shorter 21-inch-long eighth inch diameter line. The reduction in the diameter of the sampling line was to restrict the flow of the extracted sample. A 150cc stainless steel vessel was attached at the end of the eighth inch sampling line to allow the sample to expand before reaching the GCs. A quarter turn valve was installed after the vessel to allow for quick shut off of the sample gas to the GCs to avoid over pressurizing the sampling valve rotors and to reduce the time needed for the sample pressure to stabilize by reducing the volume over which the sample gas has to stabilize. The quarter turn valve could be replaced with an automated value in the future that would shut off the sample flow once a desired pressure is reached in the sampling system, but the rate at which the sample flows through the sampling system can vary substantially from one shock to the next especially when high fuel concentrations are used. The automated sampling valve would not necessarily result in an increase in consistency in the sampling pressure, but it would result in a more complicated system. A helium line and a line leading to a pump were plumbed between the eighth inch sampling line and the 150cc vessel so that the sampling line and vessel can be independently flushed from the rest of the sampling system reducing the total time needed to flush and prepare the system between shocks. All the new lines, valves, fittings, and the vessel were purchased with the Sulfinert treatment offered by Restek. Other changes included the complete removal of a line leading to the exhaust as it was never used and attaching the calibration port to the rear vessel in order to minimize the number of fittings in the sampling system therefore reducing the

number of potential leak sources. The flow of sample, and calibration, gases into the GC sample loops is driven by a pressure difference achieved by pumping down the entire sampling system to a vacuum (around 0.04 psi) and allowing the higher pressure sample, or calibration gas to expand into the sampling system and to fill the GC sample loops. The typical injection pressure is around 15.5 psi, but the exhaust line was only capable of reducing the system pressure to atmospheric pressure which meant it was of little use. The GC valve bodies were also shipped to SilcoTek to be treated with their SilcoNert coating (Sulfinert equivalent) effectively resulting in all parts of the sampling system that the sample gas comes in contact with having an inert coating. Figure 8 contains the schematic of the new modified sampling system based on the sampling system originally developed by Comandini et al[39].

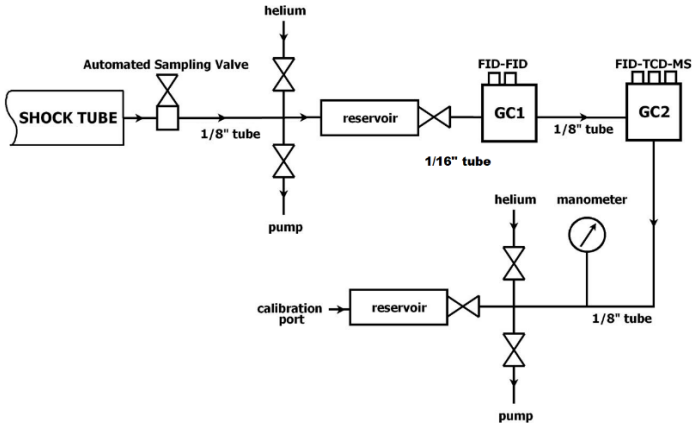

Figure 8: Modified online GC sampling system configured for acquisition of samples at higher pressures. Figure adapted and modified from [39].

3. CHEMICAL KINETIC MODELING

3.1 Chemical Kinetic Mechanisms

The experiments conducted with the HPST result in the generation of speciation data for a known quantity of a fuel of interest at known experimental conditions, i.e. pressure, temperature, and reaction time. The main purpose and use of generating this data is for the validation of chemical kinetic mechanisms. Once a chemical kinetic mechanism has been validated against a wide range of experimental data it can be reasonably expected to capture the elementary chemistry involving the fuel of interest. The chemical kinetic mechanism can then be coupled with Computational Fluid Dynamic (CFD) software and used for the simulation of various engineering combustion applications. Chemkin is a tool often used for chemical kinetic simulations and contains some basic CFD models and most of the chemical kinetic mechanisms generated utilize a Chemkin compatible format.

The information contained within a chemical kinetic mechanism for a given fuel includes all the elementary reactions which involve the fuel, and any product species that may form from the decomposition of the fuel, along with the reaction rate coefficients necessary to determine the rate at which the individual elementary reactions proceed. Only gas phase reactions will be considered and discussed since all the experimental work was completed in the gas phase.

Perhaps the most common elementary reactions are bimolecular reactions, e.g. $A + B \xrightarrow{k} C + D$, where the two reactants A and B are consumed and the two products C and D are formed. The rate of consumption of either of the reactants is equal to the rate of production of either of the products, and is proportional to the concentration of the reactants as shown below:

$$\frac{d[A]}{dt} = \frac{d[B]}{dt} = -\frac{d[C]}{dt} = -\frac{d[D]}{dt} = -k[A][B] \tag{23}$$

As shown above, the rate of consumption of the reactants A and B, and the rate of production of the products C and D, is first order with respect to both the concentrations of reactants A and B. The reaction order will always be an integer for the elementary reactions which compose a detailed chemical kinetic mechanism, but does not necessary have to be the case for lumped reactions. The reaction rate constant k is given by the Arrhenius equation, shown below, which requires the three reaction rate coefficients A, n, and E_a.

$$k(T) = AT^n exp\left(-\frac{E_a}{R_u T}\right) \tag{24}$$

Where R_u is the universal gas constant and T the temperature. Turns[95] provides a derivation for the pre-exponential factor, A, for bimolecular reactions using molecular collision theory; however, the pre-exponential factor, A, the temperature exponent, n, and the activation energy ,E_a, are usually obtained through experiments or theoretical calculations. Below is an example of an elementary bimolecular reaction as it would be found in a Chemkin compatible mechanism[23]. The reactants and products of the reaction are always specified first followed by the three reaction rate coefficients A, n, and E_a. The line may also be terminated with a short comment such as a mention of how the coefficients were obtained or a reference to where they were taken from. No more than one reaction may be specified per line in the Chemkin format.

```
CH3+CH3 = H+C2H5        4.990E+12    0.100      10600. 00        ! GRI
```

Unimolecular reactions, e.g. $A \overset{k}{\rightarrow} B$ or $A \overset{k}{\rightarrow} B + C$, are also commonly found in detailed chemical kinetic mechanisms and to a lesser extent so are termolecular or third body reactions, e.g. $A + B + M \overset{k}{\rightarrow} C + M$. The third body, M, is never consumed in the reaction but it is involved in the transfer of kinetic energy. Elementary reactions involving a third body will typically include the enhanced efficiencies for species that may act as the third body. Third body reactions

will also frequently include an additional set of reaction rate coefficients for the low pressure limit. In this case the Lindemann formulation is used to determine the reaction rate constant which depends on the low and high pressure limit reaction rate constants and on the pressure of the reactor[96]. If Troe parameters are included, then the Troe formulation is used to obtain the reaction rate constant[97]. Both the Lindemann and Troe formulations are specified in the Chemkin Theory Manual. An example of a third-body reaction which includes the low pressure limit reaction rate coefficients, the Troe parameters, and the enhanced third body efficiencies is included below[23]. The high pressure limit reaction rate coefficients are specified in the first line after the reactants and products, the low pressure limit reaction rate coefficients are in the second line, the Troe parameters in the third, and the enhanced third body efficiencies in the fourth line.

```
CH3+CH3(+M) = C2H6(+M)             2.120E+16   -0.970      620.00       ! GRI
                           LOW   /  1.770E+50   -9.670      6220.00/
                           TROE/    0.5325  151.0  1038.00  4970.0 /
                  H2/2.0/ H2O/6.0/ CH4/2.0/ CO/1.5/ CO2/2.0/ C2H6/3.0/ AR/0.7/
```

Another common approach, and one allowed in Chemkin compatible mechanisms, for handling the specification of reaction rate constants for pressure dependent reactions is the PLOG formulation. In the PLOG formulation the reaction rate coefficients are specified for at least two different pressures, and the pressures must be specified in ascending order together with their respective rate constant coefficients. If the reactor pressure is below the lowest pressure for which reaction rate constant coefficients are specified, then the reaction rate constant coefficients specified for the lowest pressure are used to determine the reaction rate constant. A similar approach is taken if the reactor pressure exceeds the highest pressure for which reaction rate constant coefficients are specified. If the reactor pressure is within 1% of any of the pressures for which reaction rate constant coefficients are specified, then the reaction rate

constant coefficients for that pressure are used directly. For reactor pressures that fall between any two pressures for which reaction rate constant coefficients are specified, and the reactor pressure is not within 1% of either of the specified pressures, then the reaction rate constant is automatically obtained by logarithmic interpolation of the reaction rate constants at the two specified pressures as shown below:

$$ln(k) = ln(k_i) + \big(ln(k_{i+1}) - ln(k_i)\big)\frac{ln(P) - ln(P_i)}{ln(P_{i+1}) - ln(P_i)} \tag{25}$$

Where k is the reaction rate constant at the desired pressure P, k_i is the reaction rate constant at pressure P_i which is the closest pressure lower than the desired pressure for which the reaction rate constant coefficients are specified, and k_{i+1} is the reaction rate constant at pressure P_{i+1} which is the closest pressure higher than the desired pressure for which the reaction rate constant coefficients are specified. An example of a reaction with reaction rate constant coefficients specified in the PLOG formulation is given below[23]. The pressure for the PLOG coefficients is specified in atm.

```
C2H2+CH3=aC3H5     8.2E+53     -13.32      33200.    ! 1999 Davis et al. RRKM
 PLOG  /0.039      4.1E+53     -13.32      33200. /  ! EST 0.1 atm /2
 PLOG  /0.1        8.2E+53     -13.32      33200. /
 PLOG  /1.0        2.7E+53     -12.82      35700. /
 PLOG  /10.0       4.4E+49     -11.40      36700. /
 PLOG  /100.0      3.8E+44     -9.63       37600. /
```

The various elementary reactions specified within a detailed chemical kinetic mechanism may also occur in the reverse order than in which the reactions are written. For the reverse reactions the reverse reaction rate constant, k_r, is related to the forward reaction rate constant, k_f, through the equilibrium constant K_{eq}.

$$\frac{k_f}{k_r} = K_{eq} = (R_u T)^{\Delta\nu} exp\left(\frac{\Delta S^0}{R_u} - \frac{\Delta H^0}{R_u T}\right) \tag{26}$$

ΔS^0 and ΔH^0 are the differences in the standard-state entropy and enthalpy, respectively, and Δv is the difference in the moles between the reactants and products. The standard-state entropy and enthalpy are obtained from thermodynamic data which must be included for all the species in the mechanism and is specified in the format used by the NASA chemical equilibrium code[98]. The standard-state specific heat, enthalpy, and entropy can be obtained using the NASA polynomial coefficients with the equations given below:

$$\frac{C_p^0}{R_u} = a_1 + a_2 T + a_3 T^2 + a_4 T^3 + a_5 T^4 \tag{27}$$

$$\frac{H^0}{R_u T} = a_1 + \frac{a_2}{2} T + \frac{a_3}{3} T^2 + \frac{a_4}{4} T^3 + \frac{a_5}{5} T^4 + \frac{a_6}{T} \tag{28}$$

$$\frac{S^0}{R_u} = a_1 ln(T) + a_2 T + \frac{a_3}{2} T^2 + \frac{a_4}{3} T^3 + \frac{a_5}{4} T^4 + a_7 \tag{29}$$

An example of the NASA polynomial coefficients for methane is shown below. Chemkin formatting allows the thermodynamic data for the species to be included either as part of the chemical kinetic mechanism file or as a separate thermodynamic file.

```
CH4               L 8/88C   1H   4   00   00G   200.000  3500.000  1000.000 1
 7.48514950E-02 1.33909467E-02-5.73285809E-06 1.22292535E-09-1.01815230E-13 2
-9.46834459E+03 1.84373180E+01 5.14987613E+00-1.36709788E-02 4.91800599E-05 3
-4.84743026E-08 1.66693956E-11-1.02466476E+04-4.64130376E+00 1.00161980E+04 4
```

3.2 Chemical Kinetic Simulations

All the simulations utilizing the chemical kinetic mechanisms described in the previous section were completed with Chemkin[99]. The “closed homogenous batch reactor”, which is a standard 0-dimensional model available within Chemkin, was used to model the HPST. The reactor is a “closed” reactor meaning there are is no inlet or outlet flow of either the product or reactant species and the reactor is “homogenous” so the species concentrations and all the physical properties are uniform spatially throughout the reactor. The Chemkin theory manual

provides a generalized form of the governing energy equation applicable to all the 0-dimensional models available within Chemkin, and even networks utilizing multiple 0-dimensional models linked together. A reduced version of the governing energy equation is given below with only the terms applicable to the "closed homogenous batch reactor" remaining.

$$\rho \sum_{k=1}^{K} Y_k c_{pk} \frac{dT}{dt} = \sum_{k=1}^{K} (h_k \dot{\omega}_k) W_k + \frac{dP}{dt} \tag{30}$$

Where c_{pk} and h_k are the specific heat and specific enthalpy of the kth species and are obtained from the NASA polynomials in the thermodynamics data which must be included with the chemical kinetic mechanism. W_k is the molecular weight of the kth species and ρ is the density in the reactor. $\dot{\omega}_k$ and Y_k are the production rate and mass fraction of the kth species, respectively, and their equations are given below.

$$\dot{\omega}_k = \sum_{i=1}^{I} (v''_{ki} - v'_{ki}) \left(k_{fi} \prod_{k=1}^{K} [X_k]^{v'_{ki}} - k_{ri} \prod_{k=1}^{K} [X_k]^{v''_{ki}} \right) \tag{31}$$

$$\rho \frac{dY_k}{dt} = \dot{\omega}_k W_k \tag{32}$$

Equation 32 is called the species conservation equation and together with equation 30 they comprise the governing system of equations for the "closed homogenous batch reactor." v'_{ki} and v''_{ki} are the stoichiometric coefficients of the reactants and products, respectively, for the kth species in the ith reaction. $[X_k]$ is the molar concentration of the kth species and k_{fi} and k_{ri} are the forward and reverse reaction rate constants for ith reaction. Reaction rate constants has been discussed in the previous section. For elementary reactions the stoichiometric coefficients will typically be one, unless a species reacts with itself in which case its stoichiometric coefficient would be two. Most reactions will typically involve no more than four species, so the production

rate term of the kth species will often include up four species per each reaction in the chemical mechanism in which the kth species participates. A chemical kinetic mechanism will frequently contain thousands of reactions; however, not every species will participate in every reaction. The molar concentration of the kth species, $[X_k]$, is related to the mass fraction of the kth species, Y_k, as shown below.

$$[X_k] = \frac{P(Y_k/W_k)}{R_u \sum_{j=1}^{K} Y_j T_j / W_j} \tag{33}$$

Where P is the pressure. This means that in order to obtain a solution for the mass fraction of each species through equation 32 a system of typically stiff ordinary differential equations must be solved. Chemkin uses a modified version of the DASPK solver to solve the equations[100]. Once a solution is obtained for the mass fractions of all the species then the governing energy equation, equation 30, can be solved. The derivation of the generalized governing energy equation is included in the Chemkin theory manual; however, Turns presents a simpler derivation for a constant pressure homogenous reactor[95]. The pressure term in the governing equation was retained because it pertains to the following discussion.

For all the simulations, the pressure was constrained and the energy equation solved as the default solution method. For an ideal shock tube this would require no further justification as the pressure behind the reflected shock is constant. An actual end wall pressure trace from the HPST, shown in Figure 3, shows that there is a pressure rise in the end wall pressure profile. Chemkin allows for a pressure profile to be specified for the simulations if the user so desires, however, this would result in additional temperature increase as shown by the pressure term in equation 30. Since the chemical thermometer, as already discussed, provides a weighted average of the temperature seen in the reaction zone then this additional increase in temperature due to

the pressure rise would be unnecessary and undesirable. Additionally, the Reaction Mechanism Generator (RMG,) which will be discussed in the following section, does now allow the use of pressure profiles for the mechanism generation[101]. The observed pressure rise also does not result in significant pressure change, such as order of magnitude or on the order of the pressure increase due to the shock wave. As such, the use of constrained pressures for the simulations is reasonable.

3.3 Reaction Mechanism Generator

The Reaction Mechanism Generator (RMG) is a free open source software in active development by the Green Group at the Massachusetts Institute of Technology used for "automatic" generation of detailed chemical kinetic mechanisms for fuel species of interest[101]. RMG was used to generate chemical kinetic mechanisms for the three fuel species used in the experimental work. The first iteration of RMG was written in Java and was developed by Song in 2004[102]. The Java version of RMG has been used in multiple published studies to develop chemical kinetic mechanisms for real fuels and constituents of real fuels[37,38,103–106]. RMG has since been rewritten in Python and is sometimes referred to as RMG-Py to distinguish it from the first iteration which was developed in Java. The cited reasons for the change in the programming language are a larger availability of useful libraries in Python, code readability, and improved exception handling[101]. The main differences for the end user are the changes in the input file formatting.

RMG utilizes chemical graph theory for the characterization of molecules and their functional groups. Adjacency lists are used to define species and to provide information about their structure which is used during the mechanism generation process. An example of an adjacency list for benzene is given below.

```
1  C u0 p0 c0 {2,D} {6,S} {7,S}
2  C u0 p0 c0 {1,D} {3,S} {8,S}
3  C u0 p0 c0 {2,S} {4,D} {9,S}
4  C u0 p0 c0 {3,D} {5,S} {10,S}
5  C u0 p0 c0 {4,S} {6,D} {11,S}
6  C u0 p0 c0 {1,S} {5,D} {12,S}
7  H u0 p0 c0 {1,S}
8  H u0 p0 c0 {2,S}
9  H u0 p0 c0 {3,S}
10 H u0 p0 c0 {4,S}
11 H u0 p0 c0 {5,S}
12 H u0 p0 c0 {6,S}
```

The index number of the atoms present in the molecule is given in the first column, followed by the element in the second column. For benzene, there will be six carbons, represented by "C," and six hydrogens, represented by "H," as shown in the adjacency list. Other currently supported elements by RMG are oxygen, "O", nitrogen, "N," silicon "Si," and sulfur, "S." The third column represents the number of unpaired electrons for each atom, followed by each atom's number of lone electron pairs in the fourth column, and the charge of each atom in the fifth column. All the remaining columns represent the bonds of each atom. Considering the first carbon atom, it has a total of three bonds with atoms two, six, and seven. The bond with atom two, a carbon atom, is a double bond represented by "D." The remaining two bonds with atom six, a carbon atom, and seven, a hydrogen atom, are single bonds represented by an "S." Triple bonds are represented by the letter "T."

The user must provide an adjacency list in the input file for every species that the user wants to be included the mechanism, regardless of whether the species is part of the fuel or simply a species that is simply desired to be included in the mechanism. The adjacency lists may be created manually, or using the "molecule search" tool on the RMG website[107]. To use the molecule search tool a species identifier must be used to generate the adjacency list. The name of the species or the Simplified Molecular-Input Line-Entry System (SMILES) identifier are the

most straightforward to use, but the International Chemical Identifier (InChI) and Chemical Abstracts Service (CAS) number can also be used.

The user must also provide a temperature and pressure that the mechanism is to be generated for. The termination criterion for the simulation must also be specified either in terms of the conversion of the fuel species or a simulation time. The reactor used for simulation is directly analogous with the zero dimensional Chemkin "closed batch reactor" discussed in the Chemical Kinetic Simulations section. Multiple reactors with different physical conditions may be specified per input file, however this increases the time necessary to generate the mechanism and each reactor is limited to a single temperature, pressure, and termination criterion. An example of one of the reactor blocks used in the input file for the methylcyclohexane mechanism is shown below.

```
simpleReactor(
    temperature = (1200,"K"),
    pressure = (199,"bar"),
    initialMoleFractions={
        "AR": 0.999819,
        "CH3cC6H11": 0.000181,
        "methylenecyclopentane": 0,
        "dimethylcyclopentane": 0,
        "benzene": 0,
        "cyclohexadiene": 0,
        "butene1": 0,
        "isobutylene": 0,
        "cyclopentadiene": 0,
    },
    terminationTime = (2.2,"ms"),
)
```

Note that all the species with a mole fraction of zero are not part of the fuel mixture, but by including them in the reactor block it ensures that they will be included in the final mechanism. The other most important block in the input file is the "database" block. An example of the database block from the input file used to generate the methylcyclohexane mechanism is given below.

```
database(
    thermoLibraries = ['Chernov', 'JetSurF2.0', 'primaryThermoLibrary'],
    reactionLibraries = [],
    seedMechanisms = ['ChernovPyrolysis', 'JetSurF2.0PyrolysisPDep'],
    kineticsDepositories = 'default',
    kineticsFamilies = 'default',
    kineticsEstimator = 'rate rules',
)
```

The thermodynamic data for the species in the generated mechanism is specified in the "thermoLibraries" line. The species thermodynamic data is typically coupled with the chemical kinetic libraries, except for the case of "primaryThermoLibrary" which does not correspond to any chemical kinetic library, but is recommended to be included to shorten the mechanism generation time. If the thermodynamic data for a species which is added to the mechanism during the mechanism generation process is not available in any of the specified thermodynamic libraries then it is estimated with Benson group additivity[108]. The order in which the thermodynamic libraries are specified matters with the former libraries taking preference over the latter in case of multiple sets of thermodynamic data being available for the same species.

The "reactionLibraries" line allows the user to specify reactions which will overwrite the estimated reaction rate constant coefficients if any of the specified reactions match the reactions added during the mechanism generation process. The "seedMechanisms" is similar in the basic premise, but has a far more powerful impact on the overall mechanism generation process. All the species, and all the reactions in the seed mechanisms are added to the initial generated mechanism. Just as with the thermodynamic libraries, if there are duplicate reactions then the reactions from the former, i.e. the seed, mechanism take preference. The RMG theory guide also stresses the importance of the quality of the seed mechanisms on the overall performance of the generated mechanism[107]. The two seed mechanisms shown in the example from the input file, "ChernovPyrolysis" and "JetSurF2.0PyrolysisPDep," were obtained by removing all the oxygen

containing species, and all the reactions which involved the oxygen containing species, from the "Chernov" and "JetSurF2.0" mechanisms which are part of the default RMG kinetics database. This was done due to RMG having no inherent option to not generate additional reactions for species containing certain elements. Since the experimental work was pyrolysis only, and the additional oxygenated species reactions increased both the time necessary to generate the mechanism as well as carry out the simulations, they were removed from the seed mechanisms. The Python script which was written to strip the unwanted reactions and species is included in APPENDIX B.

"kineticsDepositories" is an option used for testing and is left on the default value, and the only option currently available for "kineticsEstimator" is "rate rules." The "kineticsFamilies" allows the user to choose which reaction families can be used during the mechanism generation process, with the "default" option allowing all the families to be used. The settings for the remaining options in the input file are a matter of trial and error in order to achieve a convergent mechanism and user preference. The remaining options primarily involve the convergence thresholds for the reactor simulations, termination criterion for the mechanism generation, and saving additional output data which RMG is capable of generating that the user can opt to save or not. The full input files used to generate the cyclohexane, methylcyclohexane, and hex-5-en-1-yl/1,5-hexadiene mechanisms are included in APPENDIX C. Thorough descriptions for the remaining options are provided in the RMG user guide on the RMG website[107].

RMG utilizes 45 reaction families such as hydrogen abstraction, hydrogen shifts, Diels Alder addition, intramolecular Diels Alder addition, etc. to determine which elementary reactions may occur for a given species. The full list is available in [101] and in the RMG kinetics database installation directory. The reaction families have a hierarchal structure. Considering for

example the hydrogen abstraction family. At the highest, or most general level, the hydrogen abstraction may occur to molecular hydrogen, to a carbon atom bonded with hydrogen and three remaining single bonds, a carbon atom bonded with hydrogen and a double bond with another carbon atom and a remaining single bond, a carbon atom bonded with hydrogen and a triple bond with another carbon atom, etc. Then, each of those cases may have "children" which specify the functional group template in greater detail. The carbon atom bonded with hydrogen and three remaining single bonds may be methane, a methyl group, a CH2 group, or a CH group. The methyl group, as an example, may then be bonded with another carbon atom with three single bonds, or a carbon atom with a double bond with another carbon atom and a remaining single bond, etc. These functional groups templates are defined with adjacency lists which are compared against the adjacency list of the reactant species to determine whether that specific functional group is present in the reactant species. The templates also contain reaction rate parameters and a reference or a description of how those parameters were obtained.

RMG utilizes the rate-based construction algorithm developed by Susnow et al. to build the mechanism[109]. The mechanism generation process begins with all the species in the seed mechanisms and the species specified in the reactor block of the input file being added to the mechanism "core" together with all the reactions specified in the seed mechanisms. The mechanism core is composed of the species and reactions which will comprise the final generated mechanism. The 45 reaction families, or fewer if the user opts not to use all the available reaction families in the input file, are then used to determine which reactions may occur for all the species in the mechanism core. These reactions and any products which they would produce that are not already in the mechanism core are then added to the mechanism "edge". A simulation is then completed using the zero-dimensional closed batch reactor to perform reaction

flux analysis for the newly generated reactions and species in the mechanism edge. Those that exceed a user defined threshold, specified in the input file, are added to the mechanism core. The default threshold value results in mechanisms that have on the order of hundreds of species and tens of thousands of reactions. The RMG user guide suggests not lowering the threshold due to the risk of the complete chemistry not being adequately captured. Mechanism reduction may be undertaken after the final mechanism is generated. The process of determining which reactions may occur and what products may form is then repeated for the newly added core species. This process proceeds until no new species and reactions which exceed the threshold are found.

3.4 Monte Carlo Analysis

Monte Carlo (MC) analysis was utilized for the present work to obtain a graphical representation of how uncertainty in the reaction rate constants in mechanisms will manifest itself in the species profiles obtained from simulations, and as a means of systematic optimization of the mechanisms. The methodology employed was first developed and used by Fridlyand et al.[37,38] For the uncertainty analysis the mechanism is first prepared by properly formatting it and assigning an uncertainty to all the reactions present in the mechanism. The mechanism preparation is handled by a single Python script. The script originally written by Fridlyand has been modified and is included in APPENDIX B. The original script was written around only mechanism formatting found in mechanisms generated with the Java version of RMG.

The current work utilizes the Python version of RMG, and the MC analysis was also applied to a literature model. Originally, the mechanism preparation script prescribes the uncertainty to the individual reactions was unable to parse any blank lines in the mechanism, any lines containing only a comment, and it was unable to handle reactions with PLOG or Troe

parameters. Additionally, the latter scripts written by Fridlyand which read the uncertainty prescribed to each reaction and perturb the pre-exponential factor according to the prescribed uncertainty require that there is no white space present in the reaction string. This insures that when the line containing the reaction and its rate coefficients is delimited by white space then the pre-exponential factor will always have the second index in the list, making it easy to access the value and modify it as needed. The original mechanism preparation script did not complete these necessary formatting changes to the mechanism and the mechanism formatting had to be modified manually. A simple method of preparing the formatting has been applied in the rewritten script which is included in APPENDIX B. A more general approach can be taken by reading the line character by character, and has been utilized in a non-related Python script written for comparison of two mechanisms. This script is also included in APPENDIX B should anyone desire to incorporate the more general approach into the existing mechanism preparation script. Yet another Python script was written for properly handling the reaction rate constant coefficients for reactions containing PLOG coefficients, as described in the Chemical Kinetic Mechanisms section and utilizing equation 25, and is likewise included in APPENDIX B.

Once the mechanism is properly formatted and the uncertainty factors are assigned then the pre-exponential factors for all the reactions are perturbed using the Python “random.uniform()” function which generates a pseudo-random number in the desired range. The range is defined by the user as the uncertainty in the pre-exponential factor. The perturbed pre-exponential factors are then saved both in the mechanism and an additional external file and a simulation with the new mechanism with perturbed pre-exponential factors is carried out using the zero-dimensional closed batch reactor in Chemkin[99]. The results from the simulation are also saved and the process is repeated for the number of iterations defined by the user. The analysis process is

completed for a single pressure and single temperature. To span the entire desired temperature range the analysis must be repeated at multiple temperatures. After a large number of runs is completed the simulation results can be compiled and used to generate uncertainty bands in the mechanism by noting how much the species mole fractions may deviate from those obtained with the unmodified mechanism.

The perturbed pre-exponential factors and the obtained species mole fractions can be used to obtain correlation coefficients which serve as a type of global uncertainty analysis since the reaction rate constants are perturbed over what is expected to be their entire uncertainty range. One of the most common correlation coefficients is the Pearson coefficient which is defined below[110].

$$r = \frac{\sum_{i=1}^{n}(x_i - \bar{x})(y_i - \bar{y})}{\sqrt{\sum_{i=1}^{n}(x_i - \bar{x})^2}\sqrt{\sum_{i=1}^{n}(y_i - \bar{y})^2}} \tag{34}$$

Where n is the sample size and x and y are the two variables for which the correlation coefficient is being calculated. $\bar{x}$ is the mean value of x defined as $\bar{x} = \frac{1}{n}\sum_{i=1}^{n} x_i$ and similarly for $\bar{y}$ which is the mean value of y. The Pearson correlation coefficient is defined for $-1 \leq r \leq 1$ for linear relationships with -1 and 1 representing that the two variables are perfectly linearly negatively or positively, respectively, correlated. For the present case n would be the number of simulations completed, x would be the mole fractions for a given species obtained in those simulations, and y would be the pre-exponential factors for a given reaction in the mechanism. As mentioned, the Pearson correlation coefficient only determines whether the two variables are linearly correlated. The Spearman correlation coefficient can be used to determine the monotonic relationship of the two variables[111]. This is done by first ranking the two variables, x and y,

with the rank of 1 being assigned to the largest value of each variable, 2 to the second largest value of each variable, etc. Once the variables are ranked then equation 34 is applied to the ranks of the variables rather than the variables themselves. Just as the Pearson correlation coefficient, the Spearman correlation coefficient is also defined for $-1 \leq r \leq 1$ except now -1 and 1 represent a perfect positive or negative monotonic relationship between the two variables. Since a measure of the overall impact of the perturbations in the pre-exponential factors of the individual reactions on the mole fractions was desired, and whether the reactions were overall positively and negatively correlated to the mole fraction of the species rather than if they were only linearly positively or negatively correlated, the Spearman correlation coefficients were used. The Spearman correlation coefficients were obtained using the Pandas library[112].

The MC analysis was also used to optimize mechanisms. This approach is similar to the one described for the uncertainty analysis. For the mechanism optimization the experimental data must be supplied at a number of temperatures, typically nine representative temperatures were chosen in the experimental temperature range. Nine temperatures allow the experimental species profiles to be represented in sufficient detail. More temperatures could be used but that would increase the computational effort, and fewer temperatures may not represent the experimental species profiles in sufficient detail. Then as the pre-exponential factors are perturbed and simulations completed at the designated temperatures, the obtained species mole fractions from the simulation are compared against those in the experimental data and the least-squared error is calculated. The mechanism with the lowest least squared error is saved as the optimized mechanism. The Spearman correlation coefficients were used to determine which reactions to target for the mechanism optimization since it most cases only a handful of reactions were strongly correlated, negatively and positively, to the production or consumption of the

experimentally observed species. Targeting only the necessary reactions reduced the amount of simulations needed to optimize a mechanism and it also reduced the amount of overall change to the mechanism since some of the reaction rate constants may have already been validated in previous works.

4. CYCLOHEXANE PYROLYSIS

4.1 Introduction

Cyclohexane has long enjoyed interest in combustion research because it is commonly used in surrogates, and is a constituent of real jet and propulsion fuels[113–115]. One of the earliest pyrolysis experiments and modeling attempts of cyclohexane was conducted by Tsang[116]. Tsang's experiments involved a single pulse shock tube spanning a pressure range of approximately 2 to 7 bar and temperature range of 1076 to 1210 Kelvin with a reaction time of roughly 0.8 milliseconds using a test gas mixture composed of 1% of cyclohexane in a bath gas of argon. At those conditions, he found the dominant decomposition reaction of cyclohexane to be the isomerization to 1-hexene. Two other subsequent cyclohexane pyrolysis studies, a very low pressure pyrolysis study by Brown et al.[117] and atmospheric plug flow reactor work by Billaud et al.[118] also supported the isomerization of cyclohexane to 1-hexene as the initial decomposition step. More recently, a theoretical modeling study by Sirjeanet al.[119] and a lower pressure (25-200 Torr) shock tube study by Kiefer et al.[120] likewise proposed the isomerization of cyclohexane to 1-hexene through a biradical as the initial decomposition step.

It would seem that accurate reaction rate parameters for the isomerization reaction of cyclohexane to 1-hexene and a valid 1-hexene pyrolysis mechanism would be sufficient to model cyclohexane dissociation; however, El Bakali et al.[121] found that 1-hexene was not detected at a pressure of 10 atmospheres while it was at 1 atmosphere in their jet stirred reactor study of cyclohexane oxidation. In fact, El Bakali found that the production of olefins decreases as pressure increases suggesting a pressure dependence on the product distribution of cyclohexane pyrolysis. Another 1.5 to 2 bar shock tube study by Steil et al.[122] aimed at clarifying the initial cyclohexane decomposition reactions found that the two main pathways, with a branching ratio

of about 1:1, were that of isomerization to 1-hexene and then decomposition to ethylene through C-C scission, and a H-C scission first producing a cyclohexyl radical followed by H elimination resulting in cyclohexene. These two pathways were also among those suggested by Zhao et al.[123] in their plug flow reactor cyclohexane pyrolysis study. Their aim was to design the most general cyclohexane pyrolysis mechanism, and the proposed decomposition reactions were grouped into four pathways: C-C bond scission, C-H bond scission, hydrogen abstraction, and coke formation. The dominant pathways were found to be those of C-C bond scission and hydrogen abstraction. The C-C bond scission pathway was dominant at 873K with a pathway probability of 0.5420 versus that of 0.3897 for hydrogen abstraction, but the probability of hydrogen abstraction was found to increase with temperature, becoming the dominant pathway at 973K with a probability of 0.4885 versus 0.4336 for C-C bond scission. The C-H bond scission pathway was found to only have a probability of 0.0045 at 873K and increase to 0.0061 at 973K.

Two shock tube studies at around 2 bar were conducted by Peukert et al.[124,125] The first study[124] investigated the unimolecular decomposition of cyclohexane where it was found that 1-hexene is the sole initial product of cyclohexane dissociation, and the obtained rate coefficients for the reaction were in agreement with those of Tsang[116] and Kiefer et al.[120]. The second study by Peukert et al.[125] pertained to the reactions involving hydrogen abstraction of cyclohexane. First, experiments with cyclohexane and iodoethane (hydrogen donor) were completed to determine the reaction rate coefficients for the initial hydrogen abstraction from cyclohexane and formation of the cyclohexyl radical, which subsequently isomerizes to hex-5-en-1-yl. Experiments with 6-iodo-1-hexene were completed to gain insight into the decomposition of the hex-5-en-1-yl radical. Two schemes were proposed. The first involved C-C scissions of hex-5-en-1-yl, or hex-5-en-4-yl following a 1,4 hydrogen shift, that ultimately forms

ethylene and 1,3-butadiene. The second was the 5-exo-cyclization (ring contraction) which forms a cyclopentylmethyl radical that then undergoes a 1,4 shift resulting in methylcyclopentyl radical and ultimately decomposes to propene and allene. Peukert compared two literature reaction rate coefficients for the 5-exo-cyclization. The one by Sirjean et al.[126] would result in the 5-exo-cyclization reaction being the dominant reaction for the decomposition of hex-5-en-1-yl radical, while the one given by Granata et al.[127] would no longer make it the dominant reaction, but still one of importance. Peukert proposes reaction rate coefficients that fall between those of Granata and Sirjean derived from his 6-iodo-1-hexene work.

The potential energy surface for the cyclohexyl radical decomposition was calculated by Knepp et al.[128] The cyclohexyl radical is shown undergoing isomerization forming hex-5-en-1-yl radical which then can either proceed through C-C scission forming ethylene and but-3-en-1-yl, or the more energy favorable ring closure leading to cyclopentylmethyl radical that then forms methylenecyclopentane. The formation of methylcyclopentane from the cyclopentylmethyl radical is in contrast to the dissociation pathway proposed by Peukert et al.[125] This pathway is however included in the cyclohexane and methylcyclohexane models developed by Wang et al.[23,36] based on their 40 mbar cyclohexane and 30, 150, and 760 torr methylcyclohexane plug flow reactor experiments. Wang mentions that analogous ring closure reactions are possible in methylcyclohexane dissociation from C7H13 radicals, e.g. hept-6-en-1-yl radical, but that they are not included in the methylcyclohexane model due to the negligible contribution of the hex-5-en-1-yl isomerization reaction leading to the formation of methylenecyclopentane. While Wang has found the ring contraction reactions to be negligible in his work, they were observed be the dominant reactions in supercritical alkylcyclohexane[19] and methylcyclohexane pyrolysis experiments[20,21]. The products of these ring contraction

reactions, i.e. alkylcyclopentanes, have been found to be coking[21] and sooting[22] precursors, so developing a better understanding of the conditions required for these reactions to take place has practical benefits.

While the above mentioned works are by no means all-inclusive of the cyclohexane experiments conducted to date, they do show the general trend that pyrolysis studies have mostly been completed at sub or near atmospheric conditions. The higher pressure studies, such as those of El Bakali et al.[121], Lemaire et al.[129], and Sirjean et al.[130] are oxidation studies and the pressures of those experiments still fall short of the pressures achieved in the current work. Furthermore, only the work of El Bakali et al.[121] included substantial species data, the study by Lemaire et al.[129] was a low temperature oxidation study where only six carbon species were detected, and the work by Sirjean et al.[130] was an autoignition study. Cyclohexane pyrolysis is lacking high pressure and high temperature species data. Extending the current cyclohexane experimental database to high pressures and temperatures would allow for the validation of current, and creation of new, chemical kinetic mechanisms at conditions relevant to modern combustors.

4.2 Experimental Results

4.2.1 Effects of Pressure on Cyclohexane Pyrolysis

Three sets of cyclohexane shock tube experiments were completed at target pressures, the nominal pressures, with a range of experimental deviation of 40, 100, and 200 bar with a nominal (target) reaction time of 2.2 milliseconds (ms) and initial fuel mole fractions of 186, 189, and 192 parts per million (ppm,) respectively. The exact experimental conditions for each experiment are included in APPENDIX D. Care was taken during the mixture making process to achieve consistent fuel mixtures for the three sets of experiments in order to exclude any

potential concentration effects due to variation in mixture composition. The previously mentioned mole fractions of the fuel were determined through gas chromatography sampling of the fuel mixture after it has homogenized for at least 12 hours and was ready to be used in the experiments. Figure 9 contains the species product profiles of ethane, ethylene, propadiene, propyne, 1,3-butadiene, and cyclohexene obtained at the three experimental pressures. An inverse relationship was observed between the peak product mole fractions and pressure for ethane, propadiene, and propyne. The experimental pressure decrease from 200 to 100 bar resulted in approximately a 20% increase in the peak amount of ethane formed, and the pressure decrease from 100 to 40 bar resulted in roughly a 66% increase in the peak amount of ethane. For propadiene the increase was approximately 3% and 27% when the pressure was reduced from 200 to 100 bar, and 100 to 40 bar, respectively. The 3% difference is below the +/-5% analytical uncertainty due to the calibration mixture used, but since it is the same species being compared then the uncertainty in the calibration would apply at both pressures shifting the data at each pressure by the same amount. Nonetheless, the difference is small, so it is certainly possible that the reactions responsible for the production of propadiene are already at, or near, their high pressure limit at 100 bar. Propyne saw an increase of 14% and 19% in the peak mole fraction with pressure reduction from 200 to 100 bar, and 100 bar to 40 bar, respectively. For ethane, propadiene, and propyne the change in the peak amount observed was greater between the 100 and 40 bar than 200 and 100 bar experiments, but the difference was far greater in the case of ethane and propadiene than propyne. The reverse trend was observed in 1,3-butadiene, 1,3-cyclopentadiene, and cyclohexene where the peak mole fractions observed increased along with an increase in the experimental pressure. The peak mole fraction of 1,3-butadiene formed at 100 bar is only about 2.5% higher than at 40 bar, which again is below the +/-5% analytical

uncertainty in the calibration gas mixture, but the pressure increase from 100 to 200 bar results in an approximately 21% increase in the peak amount of 1,3-butadiene formed. The peak amounts of 1,3-cyclopentadiene increased by 22% with an increase of the experimental pressure from 40 to 100 bar, and 14% when the experimental pressure was increased from 100 to 200 bar. Similarly, a pressure increase from 40 to 100 bar resulted in 20% more cyclohexene produced at its peak, and 8% more when the pressure was increased from 100 to 200 bar. Both 1,3-cyclopentadiene and cyclohexene are minor product species, but other than benzene they are the two most abundant cyclic products observed in this study so their quantification and the effect of experimental pressure on their formation can provide insight into the mechanism leading to formation of benzene, and other cyclic species.

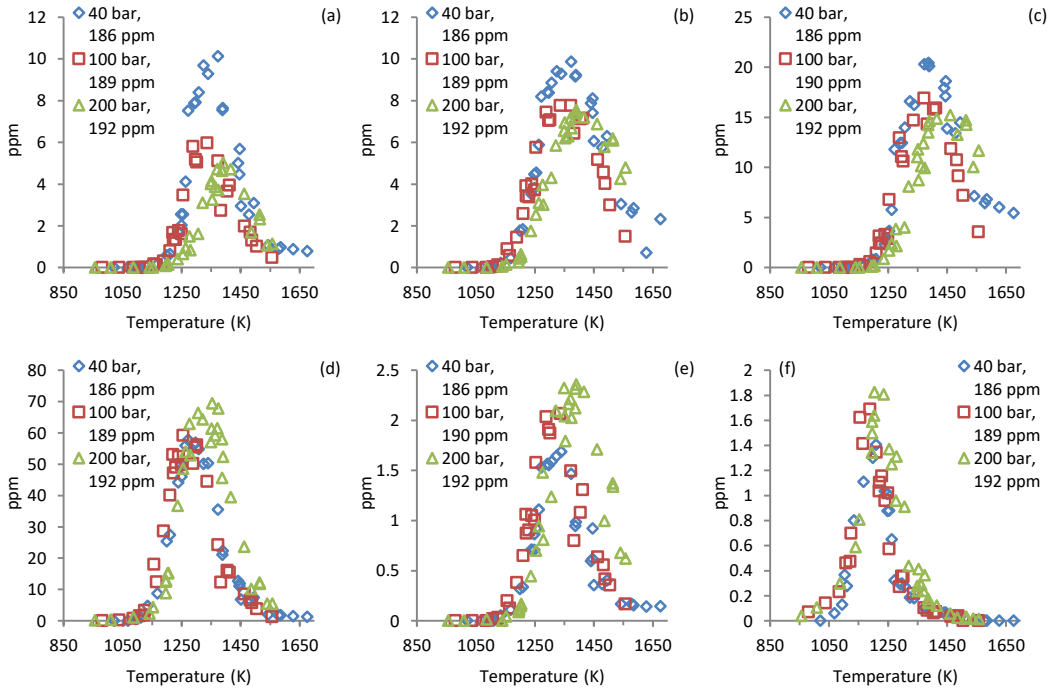

Figure 9: Species profiles of (a) ethane, (b) propadiene, (c) propyne, (d) 1,3-butadiene, (e) 1,3-cyclopentadiene, and (f) cyclohexene formed in cyclohexane pyrolysis at nominal pressures of 40, 100, and 200 bar.

Figure 10 consists of the product profiles of the most abundant species quantified in the experiments in addition to some of the other observed species namely: methane, ethylene, acetylene, propene, diacetylene, vinylacetylene, 1,2-butadiene, 1-hexene, methylenecyclopentene, benzene, touluene, and cyclohexene, or the fuel decay. Methane, ethylene, and acetylene are the most abundant products. The peak mole fraction value of acetylene was not captured in the experimental temperature range because it continues to be produced with increasing temperature, but for methane and ethylene the peak amounts observed did not seem to be effected by the variation in experimental pressure. Propene and vinylacetylene were among the products that also formed in considerable amounts, and their production did not seem to be effected by the variation in experimental pressure. The amount of propene formed at 200 bar at its peak value is about 9% higher than the 40 and 100 bar peak values, but the 200 bar mixture did have a higher mole fraction of the fuel, and there is some scatter of the 200 bar data around the peak value. For diacetylene the peak production values were not captured at any of the experimental pressures. 1,2-butadiene and 1-hexene were among the minor species observed with their peak mole fractions being below one ppm. Both of those species likewise do not show any conclusive effects on their formation due to the experimental variation in pressure. It is worth noting that 1-hexene has been successfully quantified in all three experimental pressures despite not being observed in some of the lower pressure cyclohexane experiments[121]. The remaining three cyclic species that were successfully quantified were methylenecyclopentane, benzene, and toluene. The peak mole fraction of methylenecyclopentane is approximately 34.5% higher in the 100 bar experiments over the 40 bar experiments, and 20.6% higher in the 200 bar experiments compared to the 40 bar experiments, but there is no clear increase with an increase in pressure since the peak amount observed at 100 bar is higher than at 200 bar. Additionally, the

peak amount of methylenecyclopentane does not exceed 0.2 ppm at all three experimental pressures, so it's produced in very trace amounts and near the limit of detectability of a flame ionization detector (FID,) albeit the profiles do not exhibit a significant amount of scatter. The peak amount of benzene seems to be just barely captured in the experimental temperature range at 200 bar and it does not seem to be different from the 100 and 40 bar peaks. The toluene profiles are the most scattered of all the species shown, so it is difficult to make a direct comparison between the three experimental pressures, but overall the toluene production does not seem to have been effected by the variation of the experimental pressure. The possible reason for why toluene profile is more scattered than methylenecyclopentane or 1-hexene, despite the produced amount being roughly in the same ppm range, is due to its interaction with the sampling system as it is less volatile and has a higher boiling point than methylenecyclopentane or 1-hexene. Lastly, the cyclohexane profiles compare the fuel decay at the three experimental pressures. There does not seem to be any significant differences other than the decay at 200 bar proceeding at slightly higher temperatures, which is also reflected in the product profiles.

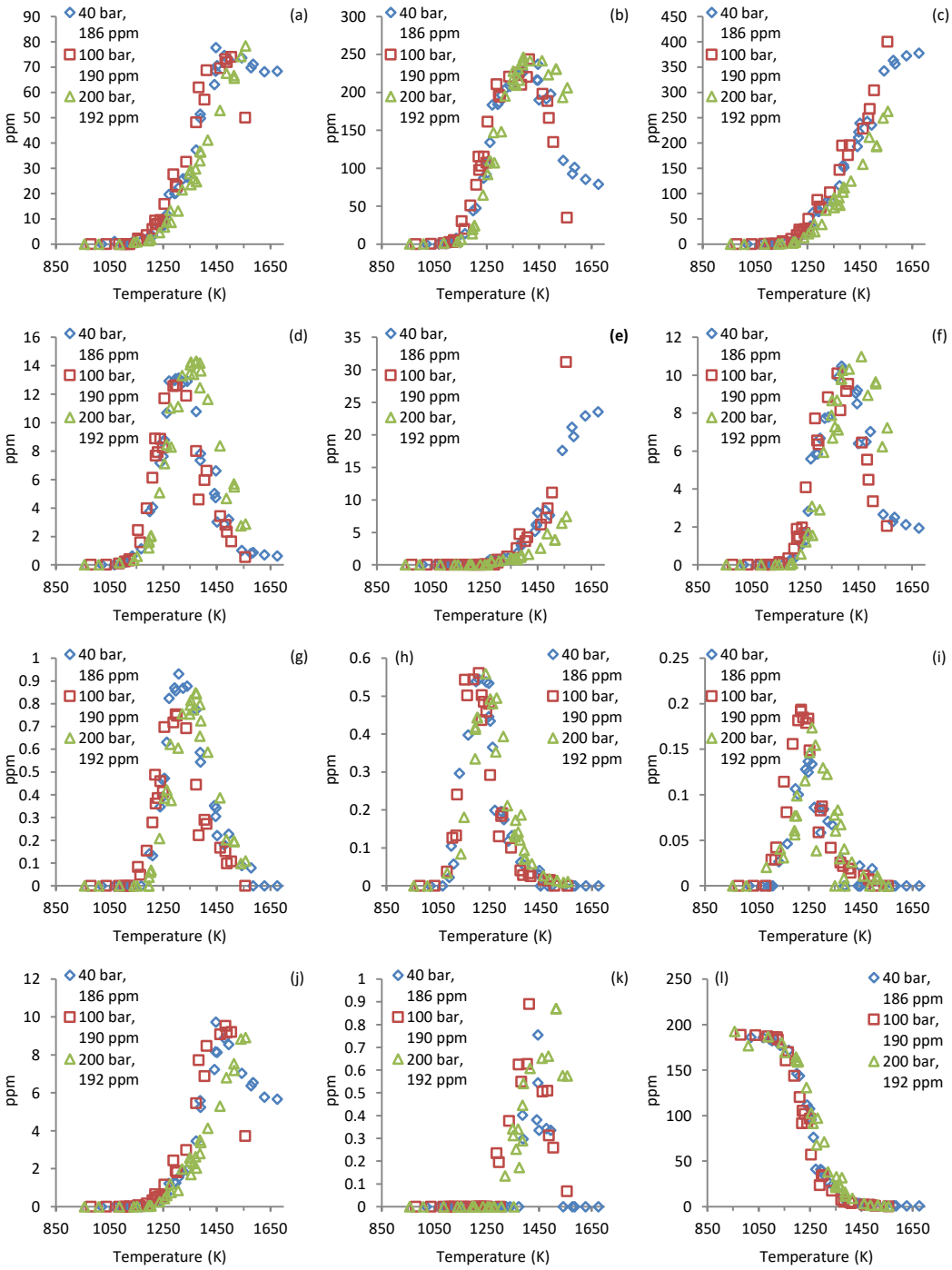

Figure 10: Species profiles of (a) methane, (b) ethylene, (c) acetylene, (d) propene, (e) diacetylene, (f) vinylacetylene, (g) 1,2-butadiene, (h) 1-hexene, (i) methylenecyclopentane, (j) benzene, (k) toluene, and (l) cyclohexane formed in cyclohexane pyrolysis at nominal pressures of 40, 100, and 200 bar.

4.2.2 Effects of Initial Fuel Concentration on Cyclohexane Pyrolysis

Thus far the products of cyclohexane pyrolysis obtained at pressures of 40, 100, and 200 bar were shown and discussed. The initial fuel mole fraction for the mixtures used for the three sets of experiments were kept approximately constant; however, the fuel concentration in the reaction zone varied considerably. Assuming ideal gas behavior, the concentration is proportional to the pressure meaning that there is an approximately 250% increase in the initial fuel concentration in the reaction zone at 100 bar compared to 40 bar, and a 500% increase in concentration in the 200 bar experiments compared to 40 bar. Higher concentrations can also be achieved at lower pressures by using a mixture with a higher fuel mole fraction. Comparing the results from a set of experiments that was conducted at a lower pressure, but with a higher mole fraction of the fuel which matches, or at least comes fairly close to, the concentration in a higher pressure set of data would allow to investigate whether the effects on the product profiles were a consequence of the change in the initial fuel concentration due to pressure, or whether they were direct pressure effects, such as various reactions approaching their high pressure rate limit, or reactions with smaller activation volumes being favored at higher pressures. To investigate the impact of the initial fuel concentration an additional set of experiments was conducted at 40 bar with a test mixture containing 484 ppm of cyclohexane. That is approximately a 260% increase in the fuel concentration compared to the previously completed 40 bar experiments where the test mixture contained 186 ppm of cyclohexane. This concentration increase is not exactly a 250% increase as predicted by the ideal gas law when the nominal experimental pressure increases from 40 to 100 bar, but it is most certainly sufficiently close to determine the impact of the initial fuel concentration on the product distribution.

Figure 11 contains the product species profiles for ethane, propadiene, propyne, 1,3-butadiene, 1,3-cyclopentadiene, and cyclohexene obtained in the 40 bar and 186 ppm of cyclohexane, 100 bar and 190 ppm of cyclohexane, and 40 bar and 484 ppm of cyclohexane experiments. All the product profiles were normalized by the initial cyclohexane mole fraction in the test mixture as otherwise the profiles obtained from the 40 bar and 484 ppm of cyclohexane experiments would be greater than those obtained from the two experiments using the lower mole fraction of cyclohexane in the test gas mixture. The species shown in Figure 11 are the same species that were shown to have their profiles effected by the experimental pressure in Figure 9. Ethane profile was impacted the most with its peak value increasing by 66% when the nominal experimental pressure was varied from 100 to 40 bar, but the 40 bar and 484 ppm set of experiments was able to reproduce the ethane data obtained at 100 bar and 190 ppm of cyclohexane very well. This demonstrates that the large difference in the amount of ethane produced observed between the 100 bar and 190 ppm of cyclohexane experiments and the 40 bar and 186 ppm of cyclohexane experiments was likely due to the initial concentration of cyclohexane present in the reaction zone rather than the difference in experimental pressure. The difference in the peak amounts of propadiene, propyene, 1,3-cyclopentadiene, and cyclohexene between the 40 bar and 100 bar experiments was originally on the order of 20% with the propadiene and propyne production increasing with a decrease in pressure, and the 1,3-cyclopentadiene and cyclohexane production increasing with an increase in pressure. The 40 bar and 484 ppm of cyclohexane set of experiments is once again able to reproduce the product profiles of propadiene, propyne, and 1,3-cyclopentadiene obtained in the 100 bar and 190 ppm of cyclohexane experiments. Again, it shows that it seems to be the initial cyclohexane concentration in the reaction zone rather than the difference in experimental pressure which

impacted the product distribution of cyclohexane pyrolysis. For the case of cyclohexene, the normalized peak amount of cyclohexene observed in the 100 bar and 190 ppm of cyclohexane experiments is 11% higher than that obtained in the 40 bar and 484 ppm of cyclohexane where originally the peak amount of cyclohexene in the 100 bar and 190 ppm of cyclohexane experiments was approximately 20% higher than in the 40 bar and 186 ppm of cyclohexane experiments. The cyclohexene peak, however, is rather narrow and it is possible that with more points around the peak the 40 bar and 484 ppm of cyclohexane profile would match the 100 bar and 190 ppm of cyclohexane profile better. Similarly, it is also possible that unlike in the case of ethane, propadiene, propyne, and 1,3-cyclopentadiene the cyclohexene production is effected by pressure and not just the initial fuel concentration. The 1,3-butadiene profile did not seem to be significantly affected by the variation in experimental pressure and its peak amount was only 3% higher in the 100 bar and 190 ppm of cyclohexane experiments compared to the 40 bar and 186 ppm of cyclohexane experiments, so unsurprisingly the 40 bar and 484 ppm of cyclohexane set of data matched the previous two sets of experiments.

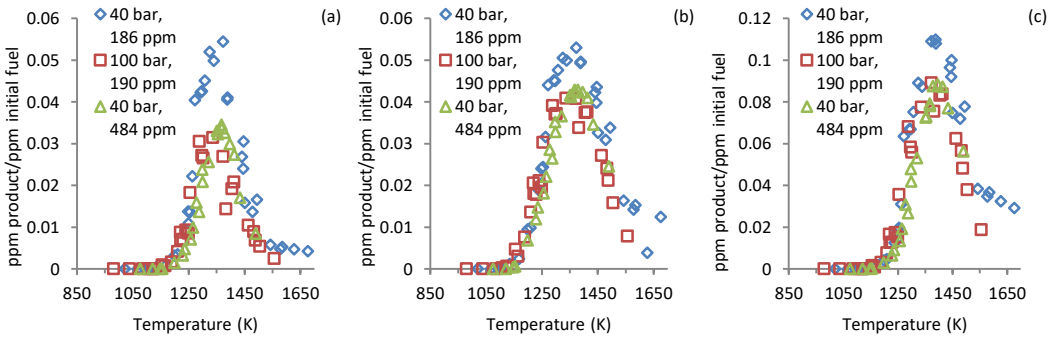

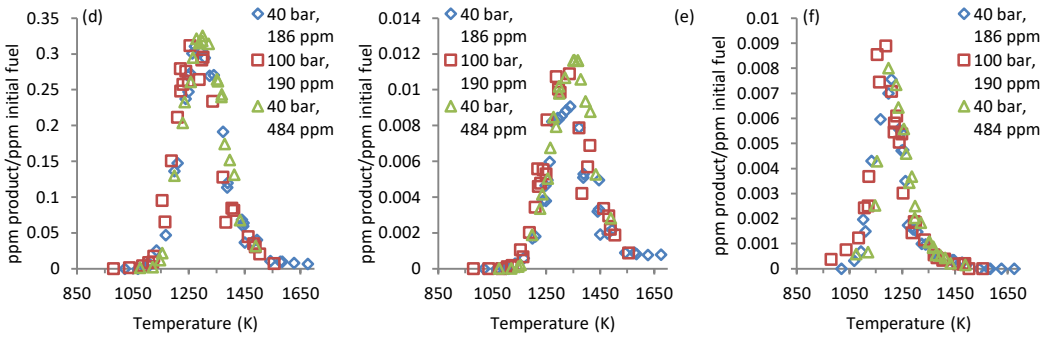

Figure 11: Comparison of species profiles of (a) ethane, (b) propadiene, (c) propyne, (d) 1,3-butadiene, (e) 1,3-cyclopentadiene, and (f) cyclohexene obtained in pyrolysis of cyclohexane at 40 bar and 186 ppm of cyclohexane, 100 bar and 190 ppm of cyclohexane, and 40 bar and 484 ppm of cyclohexane. The mole fraction of each product is normalized by the initial mole fraction of the fuel.

Figure 12 contains the species profiles of methane, ethylene, acetylene, propene, diacetylene, vinylacetylene, 1,2-butadiene, 1-hexene, methylenecyclopentane, benzene, toluene, and cyclohexane from the 40 bar and 186 ppm of cyclohexane, 100 bar and 190 ppm of cyclohexane, and 40 bar and 484 ppm of cyclohexane experiments. Just as in Figure 11, all the product profiles were normalized by the initial mole fraction of cyclohexane present in the test gas mixture for each respective set of experiments as otherwise the profiles obtained from the 40 bar and 484 ppm of cyclohexane experiments would be significantly larger than the two other sets of data with a lower initial mole fraction of cyclohexane in the test gas mixture. The data obtained from the 40 bar and 484 ppm of cyclohexane experiments matches the three major product species profiles of methane, ethylene, and acetylene from the 100 bar and 190 ppm of cyclohexane experiments, none of which seemed to exhibit any pressure dependence or have their profiles effected by the variation in experimental pressure. This illustrates that the change of the initial fuel concentration does not seem to impact the formation of methane, ethylene, and acetylene in cyclohexane pyrolysis and would imply that the rate limiting step for the formation of those species would be first order in concentration. The next three most abundant species by mole fraction, or propene, diacetylene, and vinylacetylene, also did not seem to have their

amounts of formation effected by the variation of experimental pressure, and similarly the data obtained from the 40 bar and 484 ppm of cyclohexane experiments matches the data obtained in both the 100 bar and 190 ppm of cyclohexane and 40 bar and 186 ppm of cyclohexane sets of experiments. In some of the minor species we do see some changes. The 1-hexene production did not seem to be effected by the variation in experimental pressure, so the profile from the 40 bar and 484 ppm of cyclohexane experiments matches the two lower fuel mole fraction experiments. However, the amount of 1,2-butadiene at its peak was actually about 20% higher in the 40 bar and 186 ppm of cyclohexane set of experiments compared to the 100 bar and 190 ppm of cyclohexane experiments, and this difference is reproduced in the 40 bar and 484 ppm of cyclohexane set of experiments where it matches the data obtained at 100 bar. In the case of methylenecyclopentane, the peak amount observed in the 100 bar and 190 ppm of cyclohexane experiments was approximately 30% higher than that in the 40 bar and 186 ppm of cyclohexane experiments, and the profile obtained in the 40 bar and 484 ppm of cyclohexane experiments matches that of the 100 bar set of experiments very closely.

It is worth noting that 1,2-butadiene did not exceed a peak mole fraction of 1 ppm and methylenecyclopentane did not even exceed a peak mole fraction of 0.2 ppm, as show in Figure 10, at any of the experimental pressures. With the original three sets of data that sought to investigate the effect of experimental pressure on the product distribution it certainly would be justifiable to claim that the variation present in those species profiles, even though in the case of 1,2-butadiene the difference was around 20% and for methylenecyclopetane about 30%, could be due to the experimental sets approaching the limit of detectability of an FID. Yet, this additional set of experiments illustrates that even for such minor species the product profiles can be

reproduced very well when the initial fuel concentration in the reaction zone is kept constant despite the pressures varying by a factor of 2.5.

The last three product profiles are those of benzene, toluene, and the fuel, cyclohexane. The pressure variation did not seem to effect the benzene production, so the 40 bar and 484 ppm of cyclohexane experimental data do match the previous two experimental sets well. The toluene profile was somewhat scattered making it difficult to make a meaningful comparison of the toluene data between the 40 bar and 186 ppm of cyclohexane and 100 bar and 190 ppm of cyclohexane experiments, but the toluene data obtained at 40 bar and 484 ppm of cyclohexane do match the 100 bar and 190 ppm of cyclohexane experiments other than not reproducing the single high scattered point in the 100 bar data. The cyclohexane profile, or the fuel decay, at 40 bar and 484 ppm of cyclohexane is also in line with the previous two sets of experiments which did not seem to vary significantly from one another.

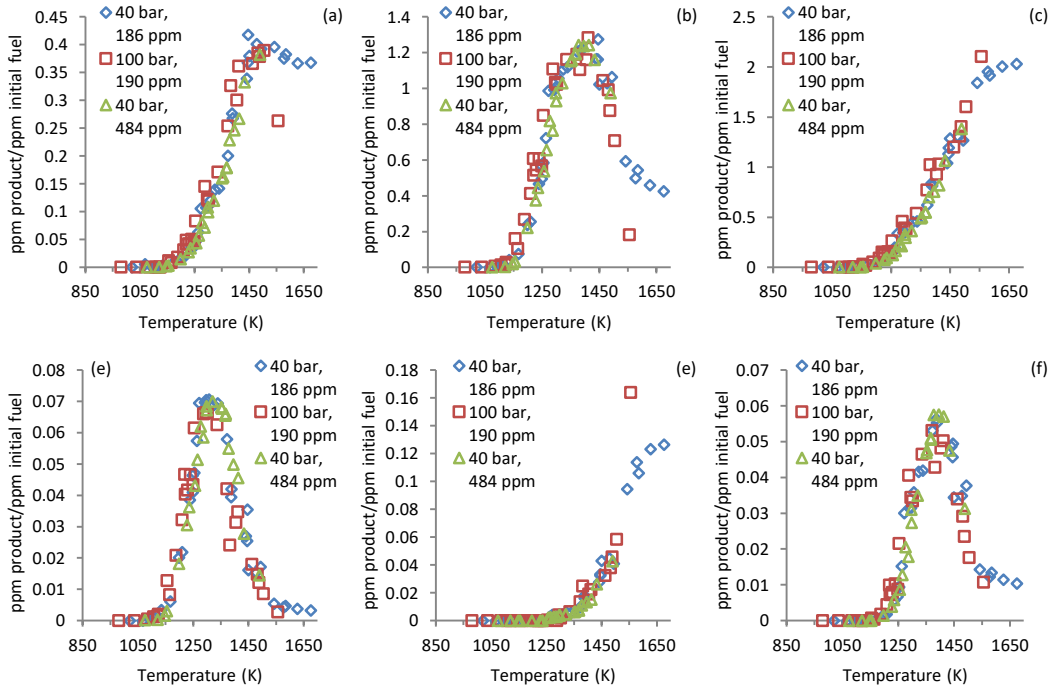

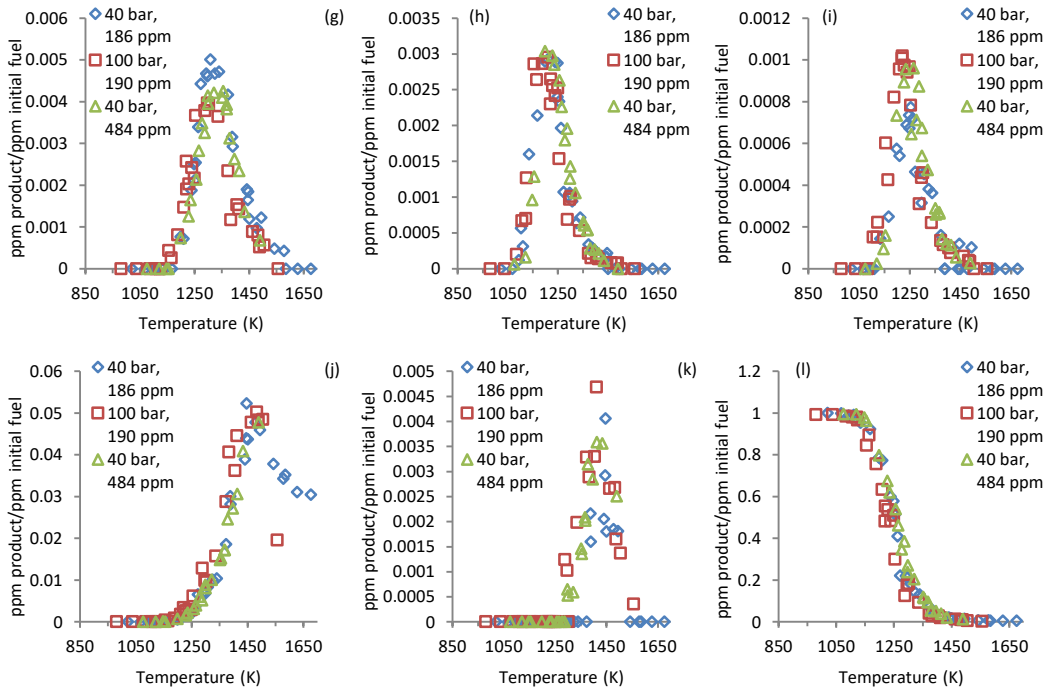

Figure 12: Comparison of species profiles of (a) methane, (b) ethylene, (c) acetylene, (d) propene, (e) diacetylene, (f) vinylacetylene, (g) 1,2-butadiene, (h) 1-hexene, (i) methylenecyclopentane, (j) benzene, (k) toluene, and (l) cyclohexane obtained in pyrolysis of cyclohexane at 40 bar and 186 ppm of cyclohexane, 100 bar and 190 ppm of cyclohexane, and 40 bar and 484 ppm of cyclohexane. The mole fraction of each product is normalized by the initial mole fraction of the fuel.

4.2.2.1 Higher Concentration Cyclohexane Pyrolysis

The cyclohexane pyrolysis product distribution was successfully reproduced at two vastly different experimental pressures which varied by a factor of 2.5, but the initial concentration of cyclohexane was kept approximately constant in the reaction zone as just discussed and illustrated in Figure 11 and Figure 12. These results would then suggest that the differences in product distributions observed at the three experimental pressures of 40, 100, and 200 bar, for which the product distributions were shown in Figure 9 and Figure 10, would be due to the variation of the initial cyclohexane concentration in the reaction zone. An additional exploratory set of experiments was completed with a high initial mole fraction of cyclohexane in the test gas

mixture to further investigate the impact of the initial concentration of cyclohexane in the reaction zone on the product distribution.

The test gas mixture utilized for the fifth set of experiments contained 3195 ppm of cyclohexane and the nominal pressure of the shocks was 200 bar. The mole fraction of cyclohexane used was not arbitrarily chosen, but rather it was the maximum amount of cyclohexane achievable in the mixture because of the limited ability to vaporize the fuel and achieve a sufficiently high gas pressure of the fuel for the high pressure test gas mixture. The shocks were completed at 200 bar in order to further increase the cyclohexane concentration in the reaction zone due to high post shock pressure.

Fewer shocks were completed for this set of experiments as its primary purpose was to serve as an exploratory set of data that could be used to observe any general trends and gain further insight into how the product distribution may be effected as the cyclohexane concentration in the fuel mixture continues to increase. Additionally, this set of experiments saw a substantial increase in the frequency of maintenance of the sampling system as clogging in the sampling system and the increase in the time needed for the sample pressure to stabilize required disassembly and cleaning of the sampling lines as often as every other shock to achieve and maintain consistent performance of the sampling system compared to the previous sets of experiments which utilized lower fuel concentrations in the test gas.

Figure 13 contains the product species profiles of ethane, propadiene, propyne, 1,3-butadiene, 1,3-cyclopentadiene, and cyclohexene from the 200 bar and 3195 ppm of cyclohexane experiments and compares them with the previously presented data from the 100 bar and 190 ppm of cyclohexane, and 200 bar and 192 ppm of cyclohexane experiments. All the product

species data are normalized by the initial mole fraction of cyclohexane present in the test gas mixture. The ethane and 1,3-butadiene profiles do not seem to be effected by the over 16-fold increase in the initial cyclohexane concentration since both the 200 bar and 3195 ppm of cyclohexane and 200 bar and 192 ppm of cyclohexane experiments produced ethane and 1,3-butadiene profiles that matched very closely. The peak normalized mole fractions of propadiene and propyne in the 200 bar and 3195 ppm of cyclohexane set of experiments are only 34% and 37%, respectively, of what was observed in the 200 bar and 192 ppm of cyclohexane experiments. However, the normalized peak amount of cyclopentadiene increased by 115%, and the normalized peak amount of cyclohexene increased by 40% in the 3195 ppm of cyclohexane set of experiments in comparison to the 200 bar and 192 ppm of cyclohexane experiments. Based on these results it would seem that a further increase in the concentration of cyclohexane in the initial fuel mixture would result in decreases to the production of C3 species, such as propadiene and propyne, while the production of cyclic species like 1,3-cyclopentadiene and cyclohexene would increase due to the cyclic species formation reactions likely being second order reactions which will begin to dominate with increasing concentrations.

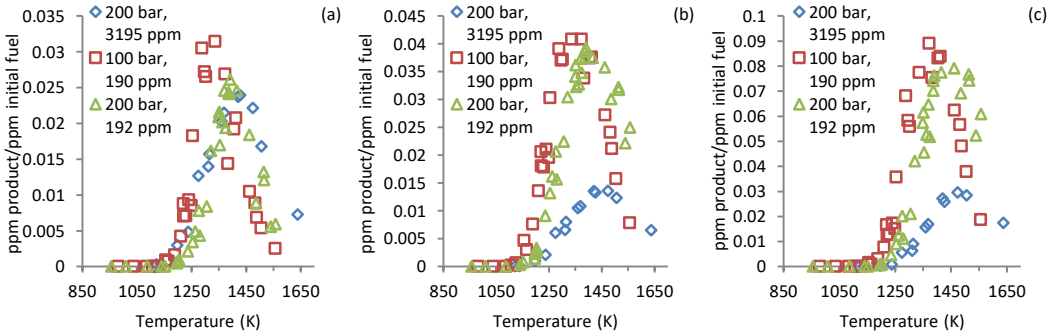

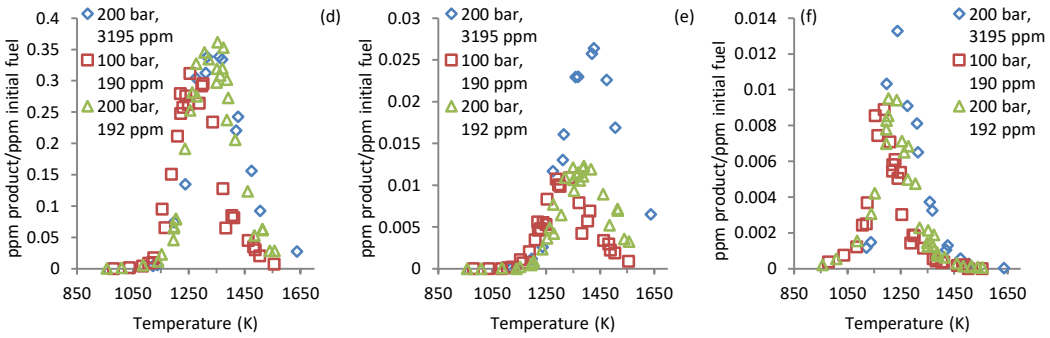

Figure 13: Comparison of species profiles of (a) ethane, (b) propadiene, (c) propyne, (d) 1,3-butadiene, (e) 1,3-cyclopentadiene, and (f) cyclohexene obtained in pyrolysis of cyclohexane at 3195 ppm of cyclohexane, 100 bar and 190 ppm of cyclohexane, and 200 bar and 192 ppm of cyclohexane. The mole fraction of each product is normalized by the initial mole fraction of the fuel.

Figure 14 contains the species profiles of methane, ethylene, acetylene, propene, diacetylene, vinylacetylene, 1,2-butadiene, 1-hexene, methylcyclopentane, benzene, toluene, and cyclohexane from the 200 bar and 3192 ppm of cyclohexane, 200 bar and 192 ppm of cyclohexane, and 100 bar and 190 ppm of cyclohexane sets of experiments. All the species data was normalized by the initial cyclohexane mole fraction for each respective set of data. Two of the most abundant products, methane and ethylene, did not seem to be effected by the large difference in concentration of cyclohexane in the test gas mixture since both the 200 bar sets of experiments have very close species profiles. For acetylene, the peak amount was not captured in the experimental temperature range, but the normalized amount formed over the temperature range encompassed, and particularly at the higher temperatures, in the 200 bar and 3195 ppm of cyclohexane experiments, was significantly lower than in either the 200 bar and 192 ppm or 100 bar and 190 ppm of cyclohexane experimental sets. Around 1500K the normalized amount of acetylene formed in the 200 bar and 3195 ppm of cyclohexane experiments was roughly half of what was observed in the 200 bar and 192 ppm of cyclohexane experiments. A similar scenario is seen in the diacetylene where around 1500 K the normalized amount of diacetylene formed in

the 200 bar and 3195 ppm of cyclohexane experiments is only around a fifth of the normalized amount formed in the 200 bar and 192 ppm of cyclohexane experiments.

There is an approximately 10% increase in the peak normalized amount of propene formed in the 200 bar and 3195 ppm of cyclohexane experiments compared to the 200 bar and 192 ppm of cyclohexane experiments. The peak normalized amounts of vinylacetylene, 1,2-butadiene, and 1-hexene observed in the 200 bar and 3195 ppm of cyclohexane experiments are approximately 76%, 68%, and 88%, respectively, of what was observed to form in the 200 bar and 192 ppm of cyclohexane experiments. The remaining three cyclic species which were quantified all showed an increase in the normalized peak amounts formed. Although the experimental temperature range was not extended to high enough temperatures to be able to determine with absolute certainty whether the peak amounts of benzene were captured in the 200 bar experiments, the maximum observed normalized amount of benzene formed in the 200 bar and 3195 ppm of cyclohexane experiments was 117% higher than in the 200 bar and 192 ppm of cyclohexane experiments. The normalized peak amount of toluene was 171% greater in the 200 bar and 3195 ppm and 200 bar and 192 ppm of cyclohexane experiments, and the normalized peak amount of methylenecyclopentane increased by approximately 47% between those two experimental sets. The fuel decay, or the cyclohexane profile, between both the 200 bar experimental sets did not seem to differ much. These results again illustrate that a continual increase of cyclohexane concentration in the initial test gas mixture results in substantial increases in the formation of cyclic species, such as benzene, toluene, and methylenecyclopetnane. Whereas C2 and C4 species such as acetylene and diacetylene, and even vinylacetylene, have far lower production amounts with an increase of cyclohexane concentration.

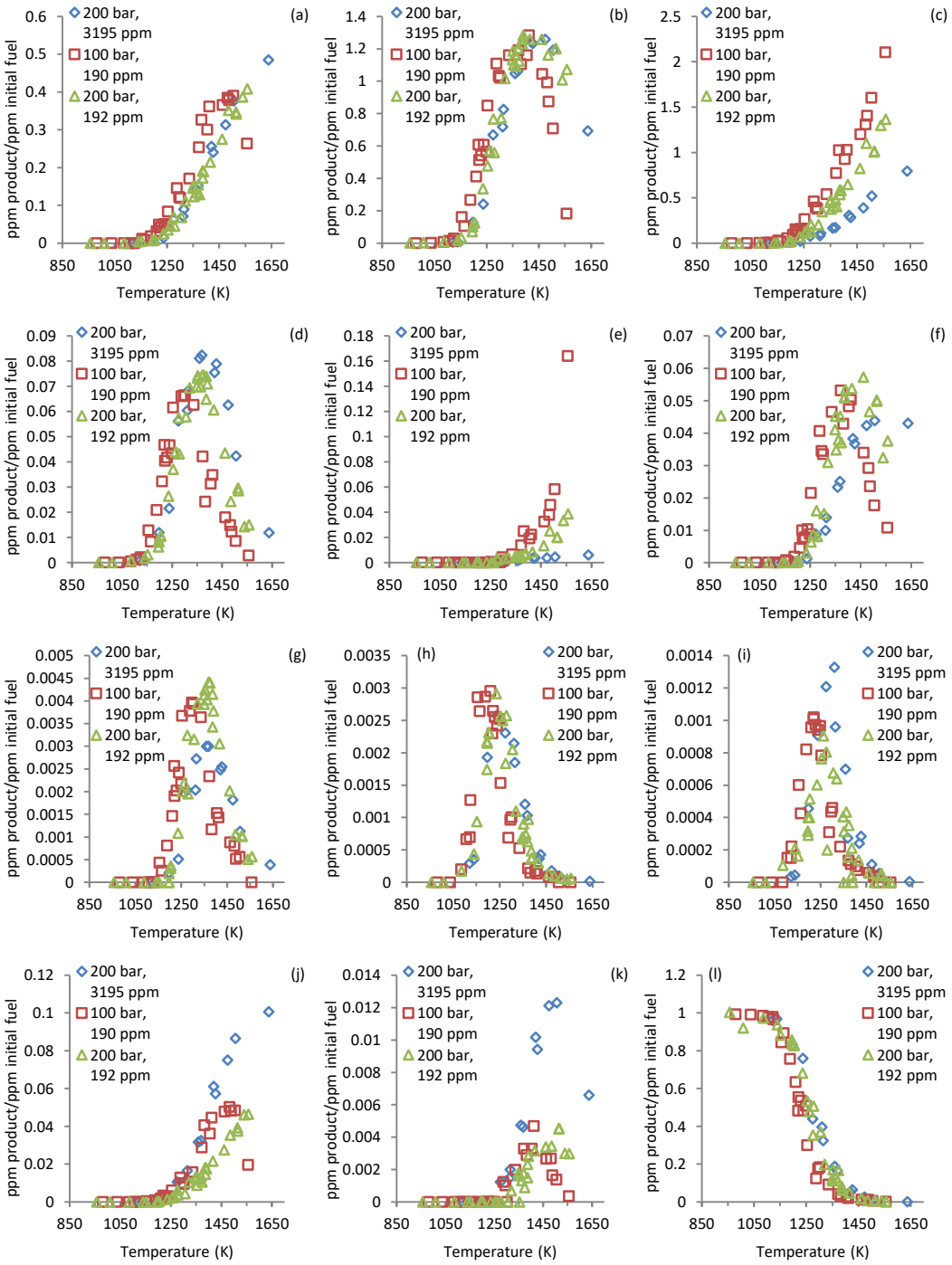

Figure 14: Comparison of species profiles of (a) methane, (b) ethylene, (c) acetylene, (d) propene, (e) diacetylene, (f) vinylacetylene, (g) 1,2-butadiene, (h) 1-hexene, (i) methylenecyclopentane, (j) benzene, (k) toluene, and (l) cyclohexane obtained in pyrolysis of cyclohexane at 3195 ppm of cyclohexane, 100 bar and 190 ppm of cyclohexane, and 200 bar and 192 ppm of cyclohexane. The mole fraction of each product is normalized by the initial mole fraction of the fuel.

4.3 Chemical Kinetic Analysis of Pressure and Concentration Dependence

Laider[94] presents common chemical kinetic rate equations some of which will be utilized for the following analysis. The analysis of a couple of these rate equations can provide possible explanations for why certain products showed a variation in their observed profiles. First, a first order reaction with respect to reactant A will be considered, e.g. $A \rightarrow Z$. The reaction may involve other reactants, e.g. $A + B + \cdots \rightarrow Z$, but if it does then it will be zeroth order with respect to any reactant other than A. The derivative form of the rate equation for this reaction is given below:

$$\frac{d[X]}{dt} = k_A([A]_0 - [X]) \tag{35}$$

$[A]_0$ is the concentration of reactant A in moles per liter at time t_0, $[X]$ is the total concentration of reactant A consumed at time t, and k_A is the reaction rate constant. The rate equation is expressed for the time derivative of the time dependent concentration of reactant A, $[X]$, but the same equation is applicable for the time derivative of the time dependent concentration of the product. In the experiments, all the species amounts were specified in mole fractions, so $[A]_0$ and $[X]$ will be redefined in terms of the mole fractions. This is done by noting that $[A]_0$ is defined as $[A]_0 = a_0[M_{tot}]$ and similarly $[X]$ as $[X] = x[M_{tot}]$ where $[M_{tot}]$ is the total number of moles per liter of the mixture and a_0 and x are the mole fractions of the reactant A at time t_0 and t, respectively. Following a separation of variables and integration of the rate equation then solving for x the below expression is obtained:

$$x[M_{tot}] = a_0[M_{tot}](1 - e^{-k_a t}) \tag{36}$$

For the three sets of experiments where the experimental pressures were varied the mole fraction of the fuel in the mixture was constant, so for those experiments $a_{0,1} = a_{0,2} = a_{0,3} = a_0$. The total moles per liter, $[M_{tot}]$, will vary between the three experimental sets due to the variation in pressure. $[M_{tot}]$ is present on both sides of the integrated rate equation, and it cannot equal zero since then no reaction would occur, so it can be cancelled, and the same rate equation is obtained for the three sets of experiments as shown below.

$$x_1 = x_2 = x_3 = a_0(1 - e^{-k_a t}) \tag{37}$$

This means that for a first order reaction the time dependent total consumed mole fraction of the reactant A, x, will be expressed by the same rate equation and the reaction will proceed at the same rate irrespective of the pressure if the initial mole fraction of the fuel is kept constant and assuming no pressure dependence in the rate coefficient. Next, the same reaction will be considered but for the two sets of experiments where the initial concentration of the fuel was kept constant, but at different pressures. For those experiments the initial mole fraction of the fuel is not equal, $a_{0,1} \neq a_{0,2}$, but the initial concentration of the fuel is equal, $[A_0] = a_{0,1}[M_{tot}]_1 = a_{0,2}[M_{tot}]_2$. By normalizing both sides of the integrated rate equation by the initial fuel concentration the below expression is obtained.

$$\frac{x_1}{a_{0,1}} = (1 - e^{-k_a t}) = \frac{x_2}{a_{0,2}} \tag{38}$$

The above expression illustrates that the same rate equation holds true for a first order reaction if the time dependent mole fraction of the fuel is normalized by the initial mole fraction of the fuel. This is also what was done for the comparison of experimental data which was obtained at different pressures, but nearly the same initial fuel concentration in the reaction zone.

The first order reaction provides an example of how the consumption of the fuel species, or production of a product species since the same equations can be used for the product, will be equivalent if the initial fuel mole fraction is kept constant. If the initial mole fraction of the fuel is not equivalent, then the time dependent mole fraction normalized by the initial mole fraction of the fuel will be equivalent. This describes the profiles of some of the species observed experimentally, but other species had matching normalized profiles if the initial concentration of the fuel was equal, but not when the initial mole fraction of the fuel was equal. An example describing this scenario can be obtained by considering a second order reaction. For the simplicity of the example, the reaction will be second order only with respect to the reactant A, even if other reactants are present, e.g. $A \rightarrow Z$ or $A + B + \cdots \rightarrow Z$. The same result would follow for a second order reaction which is first order with respect to two different reactants, but it would complicate the equations used. The rate equation for the considered reaction is given below:

$$\frac{d[X]}{dt} = k_A([A]_0 - [X])^2 \tag{39}$$

The same terms are used as in the first order reaction, so they do not need to be defined again. The concentrations will again be redefined in terms of mole fractions and the expression will be integrated and solved for x giving:

$$x[M_{tot}] = a_0[M_{tot}] - \frac{2}{k_a t a_0[M_{tot}]} \tag{40}$$

For the three experimental sets the pressure was varied but the initial mole fraction of the fuel was equivalent, $a_{0,1} = a_{0,2} = a_{0,3} = a_0$; however, the total moles per liter of the mixture in the three sets of experiments varied depending on the experimental pressure and are not

equivalent, $[M_{tot}]_1 \neq [M_{tot}]_2 \neq [M_{tot}]_3$. It is easy to see that unlike for the first order reaction, the total moles per liter cannot be eliminated from the expression and a constant initial mole fraction of the fuel is not enough to obtain equal time dependent mole fractions of the fuel, so , $x_1 \neq x_2 \neq x_3$ as shown below.

$$a_0 - \frac{2}{k_a t a_0 [M_{tot}]_1^2} \neq a_0 - \frac{2}{k_a t a_0 [M_{tot}]_2^2} \neq a_0 - \frac{2}{k_a t a_0 [M_{tot}]_3^2} \tag{41}$$

For a second order reaction the reactants will not be consumed at the same rate when the initial mole fraction of the reactant is equivalent, and the products will not be produced at the same rate. For the second case, the initial concentration of the reactant is equivalent and $[A_0] = a_{0,1}[M_{tot}]_1 = a_{0,2}[M_{tot}]_2$. Just as before, the time dependent mole fraction of the fuel is normalized by the initial mole fraction of the fuel giving the below expression.

$$\frac{x}{a_0} = 1 - \frac{2}{k_a t a_0^2 [M_{tot}]_2^2} \tag{42}$$

By using the expression for the initial concentration of the fuel the above equation can be rewritten as given below.

$$\frac{x_1}{a_{0,1}} = 1 - \frac{2}{k_a t [A]_0^2} = \frac{x_2}{a_{0,2}} \tag{43}$$

For a second order equation, the normalized mole fraction of the reactant can be expressed by the same equation if the initial concentration of the reactant is equivalent. This also means that the normalized mole fraction of the product will be equivalent since the same expression can be used to determine the production rate of the products. The second order reaction provides an example of how the observed amount of products can vary when the initial

mole fraction of the fuel is constant, but not the concentration, and how the normalized mole fraction of the product can be equivalent if the initial mole fraction of the fuel is equivalent. This entire reaction rate analysis can similarly be applied to the consumption of the intermediate products that form from the fuel following their peak because the intermediate products should follow the same unimolecular or bimolecular relationship to the fuel as the formation of the product.

4.4 Chemical Kinetic Modeling of Experimental Data

Two chemical kinetic mechanisms are compared against the experimental data obtained at 200 bar with an initial fuel mole fraction of 192 ppm of cyclohexane. The reason for using this set of experimental data is that it was shown, in Figure 9 and Figure 10, that the three major product species did not seem to be effected by the variation of the experimental pressure. For those species that were effected substantially, it was shown in Figure 11 and Figure 12 that higher pressure data, in this case obtained at 100 bar, can be replicated at a lower pressure, 40 bar, if the initial concentration of cyclohexane present in the reaction zone is equivalent at both the pressures. Both the mechanisms considered were originally validated against lower pressure data and used reaction rate constants from other mechanisms that used lower pressure data for validation. It is hypothesized that if the mechanisms are able to predict the 200 bar data successfully, perhaps through a slight adjustment of the pressure dependent reaction rate constants, then the pressure dependent rate constants can be extended to the lower pressures of 100 and 40 bar as the mechanisms have already been validated at lower pressures of around one atmosphere.

4.4.1 Wang Mechanism

The first mechanism considered is the methylcyclohexane mechanism developed by Wang et al.[23] This mechanism was chosen because it's a recently developed, fairly compact mechanism with a total of 249 species and 1570 reactions, that the authors have validated against three sets of their plug flow reactor data at pressures of 30, 150, and 760 torr in addition to also validating it against a set of their premixed flame data. The mechanism is an extension of Wang et al. cyclohexane mechanism[36] which added a methylcyclohexane sub-mechanism composed of reactions and their rate constants calculated by the authors or borrowed from JetSurf2.0 and Wang et al. ethylcyclohexane work[131], in addition to a sub-mechanism for cC7H13 radicals, and two cyclohexyl reactions. The reaction rates for the cC7H13 radicals and the two cyclohexyl reactions were calculated by the authors. The reason for using Wang's methylcyclohexane mechanism and not their cyclohexane mechanism is that of the two cyclohexyl reactions added, one is the isomerization of cyclohexyl to hex-5-en-1-yl which is expected to be a methylenecyclopentane precursor. The other cyclohexyl reaction is for the formation of cyclohexene.

Wang's cyclohexane mechanism was also validated against the authors' plug flow reactor data. The cyclohexane mechanism was an extension of Zhang et al. butene isomer mechanism[33]. This mechanism extension added reactions involving cyclohexane, 1-hexene, cyclohexyl radical, hexenyl radical, cyclohexene, benzene, and fulvene. The reaction rate constants for the cyclohexane, 1-hexene, cyclohexyl radical, and hexenyl radical reactions were taken from JetSurf2.0[132] and Kiefer's shock tube work involving 1-hexene and cyclohexane[120]. The cyclohexene reaction rate coefficients were borrowed from JetSurf2.0 and the works of Li et al.[133], Kiefer and Shah[134], and Dayma et al.[135] Lastly, the benzene

and fulvene reactions were derived from the works of Richter et al.[136], D'Anna et al.[137], Hansen et al.[138], Sivaramakrishnan et al.[139] Lindstedt and Skevis[140], and Senosiain and Miller[141].

Zhang's butene isomer mechanism has likewise been validated against the author's plug flow reactor data and mainly borrowed its reaction rate coefficients from USC Mech2[142], in addition to using reaction rate coefficients from Kiefer's 1-hexene and cyclohexane shock tube work[120], JetSurf2.0, and other works[136–138,143–150]. Wang's methylcyclohexane mechanism in total has been validated at three stages of its development and most of the reaction rate coefficients are derived from the well-known and widely validated USC Mech 2 and JetSurf2.0 mechanisms, therefore, making it a prime candidate to be compared against high pressure cyclohexane pyrolysis data.

Figure 15 contains the comparison of the simulation results obtained using the Wang mechanism with Chemkin-PRO[99] software and compares it against the experimental data from the 200 bar shocks completed with a test gas mixture containing 192 ppm of cyclohexane for all the species previously presented. Figure 15 also contains the uncertainty bounds generated using the Monte Carlo uncertainty analysis approach developed and used by Fridlyand et al.[38] where every reaction in the mechanism is randomly prescribed a perturbation to its pre-exponential "A" Arrhenius rate equation factor of up to 30%. The Monte Carlo uncertainty analysis is then completed by randomly perturbing all the reactions in the mechanism within the prescribed +/- 30% uncertainty to the pre-exponential A factor and 5000 simulations were completed at each temperature considered, starting at 900K and proceeding every 50K until 1700K, encompassing the total experimental temperature range. The perturbed A factors (input) were saved along with the species profiles generated with Chemkin-PRO (output) and Pearson correlation

coefficients[110] were calculated for each reaction in the mechanism with respect to each species detected in the experimental sets. This allowed for the generation of ranked lists of reactions that are most positively and negatively correlated to the generation or consumption, respectively, of any given species of interest. These ranked reaction correlation coefficient lists were then used to target specific reactions in the Wang mechanism for assignment of a greater uncertainty than +/-30%, while all the reactions which weren't targeted were left with a 0% uncertainty and an optimized model with the least squared error against the current experimental data was generated and plotted in Figure 15. The goal in this approach was that since the Wang mechanism has been validated against the authors' data, it would be best to target the smallest possible amount of reactions in an attempt to optimize the mechanism's ability to predict the current experimental data without compromising its performance or ability to simulate the data it has been validated against.

As shown in Figure 15, Wang's mechanism does an excellent job at predicting the current experimental data. For all the species shown, the initial formation temperatures are well captured and the peak amounts of each species formed are also well represented for most of the species. Even minor products that had their peak amounts below 1ppm, such as 1,2-butadiene, 1-hexene, and even methylenecyclopentane with its sub 0.2 ppm peak, are well represented by the model. The uncertainty bands created by the +/-30% perturbation to the pre-exponential A factors capture much of the experimental data. The data that tends to fall outside of the bands is typically at the higher temperature range above 1450K. It also has to be noted that while not shown directly in the figures so as to not obscure other plots, there is an up to 30K uncertainty in the temperature for the experimental data as previously determined[37,38]. The species uncertainty is +/-5% as previously mentioned due to the species calibration method for all

species but 1,3-cyclopentadiene, cyclohexane, methylenecyclopentane, and cyclohexane which required calibration with liquid samples rather than standard test gas mixtures and may have an uncertainty of up to +/-10%. The one species for which the model fares the poorest in predicting is benzene. Almost since its initial formation temperature, the benzene amounts observed in the experiments fall short of the model prediction, and the experimental benzene profile is outside the model uncertainty band for the majority of the experimental temperature range. At its peak, the model predicts more than double of the benzene observed in the experiments.

There are three general pathways through which benzene may be formed in Wang's mechanism: the dehydrogenation of cyclohexane which forms cyclohexene forming 1,3-cyclohexadiene and lastly benzene, the C3 + C3 species recombination, and the recombination of C2 and C4 species. The recombination reactions directly involve stable species which were observed experimentally such as propadiene, propyne, vinylacetylene, and acetylene, and radical species that were not quantified in the experiments such as propargyl, allyl, vinyl, and butynyl. Comparing both the propadiene and propyne experimental data with Wang's mechanism it can be seen that it is well represented up until about 1300K at which point Wang's mechanism predicts a peak and subsequent decay of both those species with further temperature increases, whereas the experimental data does not have those species peak and begin decaying until around 1450K. 1300K is also the temperature after which Wang's mechanism predicts the benzene formation to rapidly increase, and at that temperature the experimental data for benzene no longer falls within the mechanisms uncertainty band. A very similar case is present for vinylacetylene, with the peak and decay predicted by the mechanism to occur around 1300K whereas in the experiments it did not occur until approximately 1450K, however the difference is that vinylacetylene is actually over predicted by the mechanism. As for the benzene formation

through the cyclohexane dehydrogenation pathway, the mechanism predicts more than double the cyclohexene observed in the experiments giving an abundance of a benzene precursor.

An attempt has been made at optimizing the Wang mechanism for the current set of experimental data with the primary goal being the improvement of benzene prediction, since it was the most abundant species, particularly when accounting for carbon flux, which had the poorest approximation by the mechanism. A few approaches were taken in an attempt to optimize the mechanism while also minimizing the effect on the mechanism's ability to predict the experimental data against which the mechanism was originally validated. The mechanism optimization process has been used and described previously by Fridlyand et al.[38] However, his approach was used with mechanisms generated by the Reaction Mechanism Generator (RMG)[101] and as such the amount of reactions targeted for perturbation and change of their pre-exponential factors was much greater than what would be considered appropriate for an already validated mechanism. The mechanism in Fridlyand's optimization process with adjusted pre-exponential factors which would produce the least squared error would then be saved as the optimized mechanism. The least squares error calculation was based on the carbon flux, so species containing more carbon had a greater weight than smaller species in the error calculation.

The approaches taken for optimizing Wang's mechanism, as opposed to those used by Fridlyand, included: targeting the top two most positively and negatively correlated reactions in the experimental temperature range which were obtained every 50K for all the experimentally observed species, then using only those reactions that had pressure dependent (PLOG) data and perturbing those reactions by a maximum uncertainty factor of 2, and targeting the top ten most positively and negatively correlated reactions only for benzene and perturbing only those with PLOG data, then repeating the previous attempt but for the error calculation increasing benzene's

carbon number used in the least squared error calculations from the real value of 6 to a fictitious value of 50 to assign a greater bias toward the benzene error. Also, the previous attempt was repeated but also changing the carbon numbers of propadiene and propyne to 50. Another attempt where the carbon numbers of all the species were set to 1 so that there was no bias towards any one species. Lastly, targeting all the reactions with PLOG data regardless of their correlation coefficient and perturbing their pre-exponential factors by a maximum factor of 2. As can be seen, and as the reasoning has previously explained, only pressure dependent reactions were targeted in expectation of preserving the mechanism's ability to predict the low pressure data against which it was originally validated. Unsurprisingly, the mechanism generated in the approach which had the greatest bias assigned towards benzene in the error calculation is the one which that came closest to predicting the amount of benzene observed in the experiments, and is the one whose simulation results are plotted and shown in Figure 15.

The optimized mechanism's benzene profile falls just outside the uncertainty band of the unmodified Wang mechanisms, but at its peak the optimized mechanism still over predicts benzene by a factor of approximately 1.8. This is an improvement over the original mechanism, but there is still a substantial difference between what was observed experimentally and the prediction by the mechanism. This improvement also comes at a cost. The amount of propadiene and propyne is even further under predicted by the optimized mechanism, and 1,3-butadiene whose peak amount was previously well captured is now under predicted by about 17%. The amount of other cyclic species formed also dropped. Cyclohexene which was previously over predicted by more than a factor of 2 is now under predicted by about 27%. 1,3-cyclopentadiene, methylenecyclopentane, and toluene all see a drop in their predictions. The general trend that can be observed is that the improvement in the benzene prediction resulted in a decrease in the

amounts of benzene precursors being formed, such as propadiene, propyne, and cyclohexene, which in the case of cyclohexene was an improvement as it was significantly over predicted, but both propadiene and propyne were already under predicted in the original model. This optimization involved only the modification of reaction rates which had pressure dependent data, and since the original mechanism was validated against data obtained at atmospheric and sub-atmospheric pressure this meant that by modifying the higher pressure reaction rate constants in the PLOG formulation would allow the mechanism to retain its ability to properly predict the experimental data against which it was validated since the lower pressure PLOG reaction rate coefficients were unchanged. The inability to obtain accurate benzene prediction by only targeting PLOG reactions illustrated that many of the reactions in the benzene formation pathways are not pressure dependent.

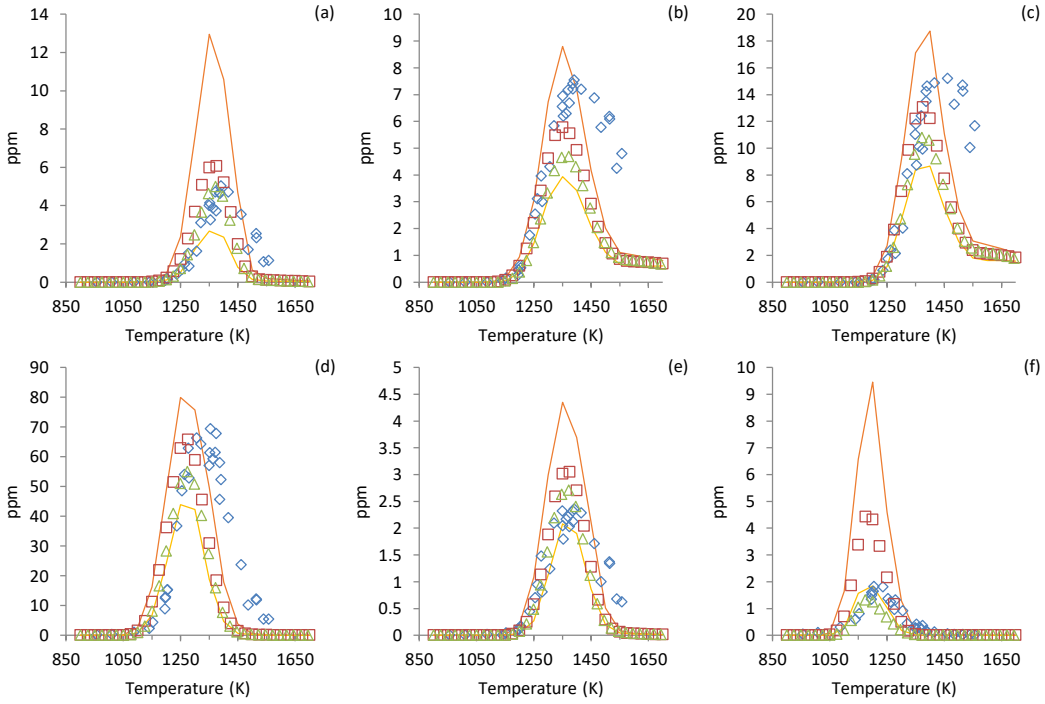

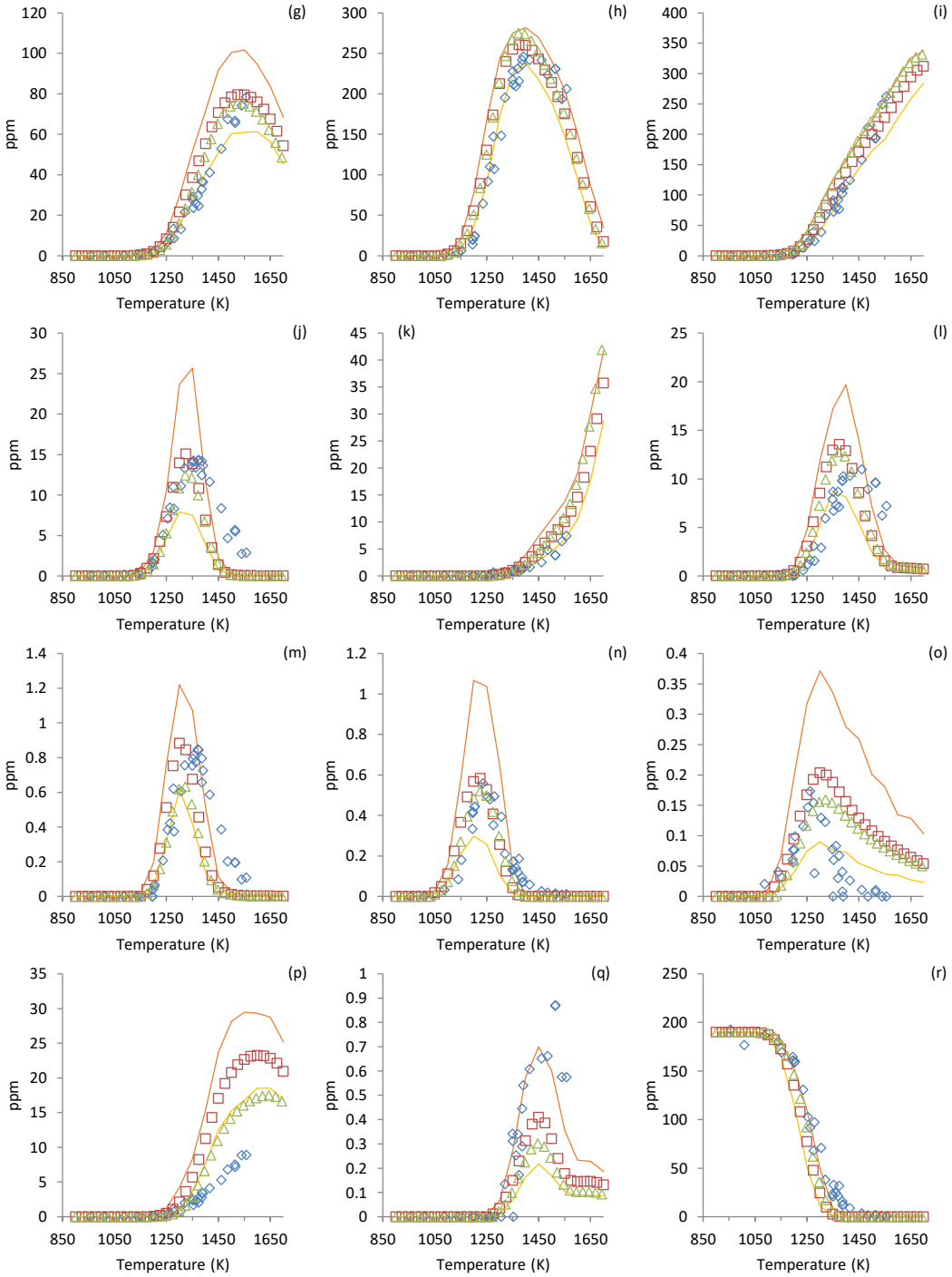

Figure 15: Comparison of species profiles of (a) ethane, (b) propadiene, (c) propyne, (d) 1,3-butadiene, (e) 1,3-cyclopentadiene, (f) cyclohexene, (g) methane, (h) ethylene, (i) acetylene, (j) propene, (k) diacetylene, (l) vinylacetylene, (m) 1,2-butadiene, (n) 1-hexene, (o) methylenecyclopentane, (p) benzene, (q) toluene, and (r) cyclohexane observed in 200 bar and 192 ppm of cyclohexane shock tube experiments versus those from a simulation using the methylcyclohexane mechanism developed by Wang[23], an optimized version of the Wang mechanism, and the bounds of uncertainty generated by prescribing a 30% uncertainty to all the A factors in the mechanism. Legend: ◇ Experimental Data, □ Wang Mechanism, △ Wang

Optimized Mechanism, —— Maximum Species Mole Fraction from Monte Carlo Analysis, —— Minimum Species Mole Fraction from Monte Carlo Analysis.

4.4.1.1 ROP Analysis

Rate of production (ROP) analysis of both the original and optimized Wang mechanism were completed for benzene at a representative temperature of 1350K and reaction time of 2.2ms to gain insight into which reactions are primarily responsible for benzene formation. Figure 16 provides a visual representation of the relative ROP analysis of the various reactions contributing to benzene formation with the percentages outside the parenthesis being the relative ROP of the original Wang mechanism and the percentages in the parenthesis are the relative ROP from the optimized Wang mechanism. The reaction of fulvene with hydrogen is the reaction with the highest contribution to the ROP of benzene with 31% of the relative ROP belonging to the reaction in the original mechanism and 42% in the optimized mechanism. Together, the C3+C3 recombination reactions account for the majority of benzene formation in the original Wang mechanism with 56% of the relative ROP of benzene stemming from C3+C3 species recombination, and 48% in the optimized Wang mechanism. The reduction in the overall contribution of the C3+C3 species recombination reactions to benzene formation is not surprising since both the amount of propadiene and propyne predicted by the optimized mechanism was reduced compared to the original Wang mechanism, as shown in Figure 15.

The propargyl radical recombination at 24% of the relative ROP in the original Wang mechanism has the largest share of the C3+C3 species recombination relative ROP, and drops to 15% of the relative ROP in the optimized Wang mechanism. The recombination of propargyl and propyne is the second most important C3+C3 species recombination reaction with 22% of the relative ROP in the original Wang mechanism and 20% in the optimized Wang mechanism. The third, and last C3+C3 species recombination reaction contributing to benzene formation is

propadiene and propargyl recombination with 10% of the relative ROP in the original Wang mechanism and 13% in the optimized Wang mechanism. The dehydrogenation of the cyclohexadienyl radical contributes 11% of the relative ROP in the original Wang mechanism and drops to 6% of the relative ROP in the optimized mechanism. This is also not surprising since the peak amount of cyclohexene predicted by the optimized Wang mechanism is just over a fourth of what the original Wang mechanism predicted.

The C4+C2 species recombination reactions in total contribute just 4% of the benzene relative ROP in the original Wang mechanism and 7% of the relative ROP in the optimized Wang mechanism. The recombination of vinylacetylene with the vinyl radical has the largest share of the C4+C2 species recombination reactions ROP at 3% for the original Wang mechanism and 5% for the optimized Wang mechanism. The recombination of acetylene and vinylacetylene has a 0% contribution to the relative ROP of benzene in the original Wang mechanism and 1% in the optimized Wang mechanism. Lastly, the acetylene and *n*C4H5 radical recombination contributes 1% of the relative ROP of benzene in both the original and optimized versions of the Wang mechanism.

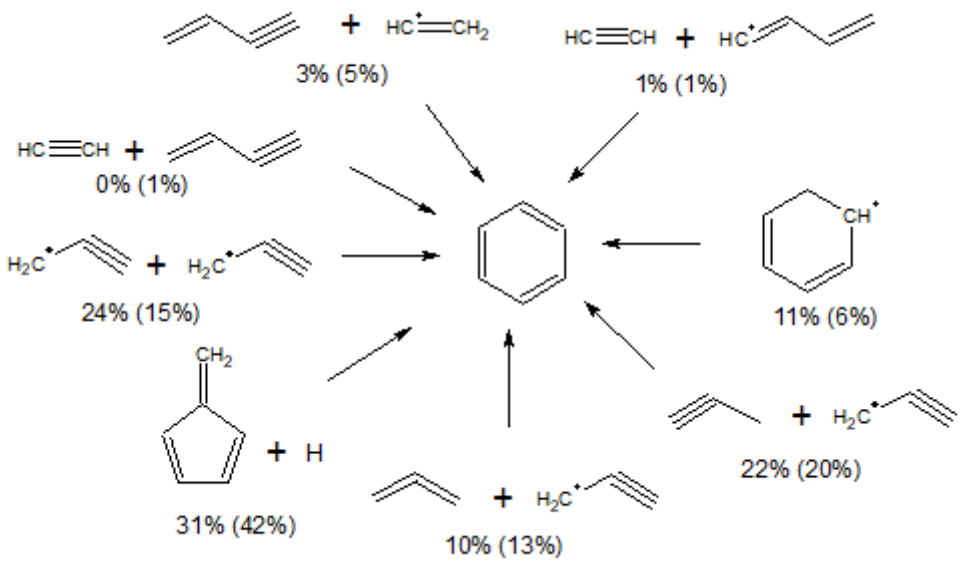

Figure 16: Visualization of the ROP analysis of benzene formation at a temperature of 1350K and reaction time of 2.2 ms. The percentages outside the parenthesis are the relative ROP from the unmodified Wang mechanism and the percentages in parenthesis are the relative ROP from the optimized Wang mechanism.

The ROP analysis was also completed for the initial cyclohexane dissociation reactions in both the original and optimized versions of the Wang mechanism. In the original Wang mechanism, the dissociation of cyclohexane into 1-hexene and the cyclohexyl radical had a branching ratio of nearly 1:1 with 52% of the relative ROP of cyclohexane belonging to the dissociation into the cyclohexyl radical and 48% to the isomerization to 1-hexene. In the optimized Wang mechanism, the dissociation into the cyclohexyl radical became more favored with 64% of the relative ROP belonging to the dissociation of cyclohexane into the cyclohexyl radical and the cyclohexane dissociation resulting in the isomerization of cyclohexane to 1-hexene having 36% of the relative ROP of cyclohexane dissociation. Figure 17 provides a visual representation of the two initial products of cyclohexane dissociation and the main pathways of the cyclohexyl radical dissociation in the Wang mechanism. The cyclohexyl radical may either form cyclohexene which will primarily dissociate into 1,3-butadiene and ethylene, or the cyclohexyl radical may undergo ring opening forming the hex-5-en-1-yl radical. The hex-5-en-1-

yl radical will then primarily either undergo beta-scission forming the but-3-en-1-yl radical and ethylene, or undergo a 1,4-hydrogen shift forming hex-5-en-4-yl radical which will in turn primarily undergo beta-scission forming 1,3-butadiene and the ethyl radical. The hex-5-en-1-yl radical may also undergo ring closure forming the cyclopentylmethyl radical which will then form methylenecyclopentane. This is a minor hex-5-en-1-yl radical dissociation pathway and is only included in the schematic due to being the only methylenecyclopentane formation pathway in the Wang mechanism, and methylenecyclopentane being the only alkenylcyclopentane observed in the current experiments.

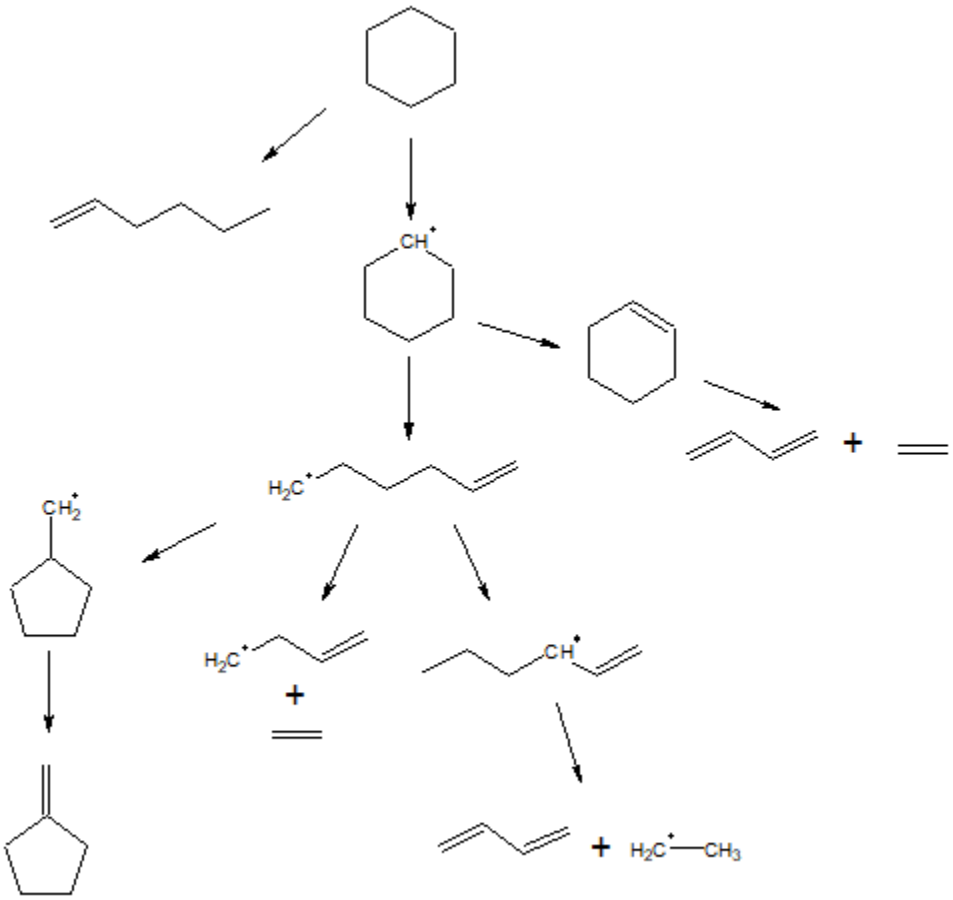

Figure 17: Main cyclohexane decomposition pathways predicted by Wang mechanism proceeding through the cyclohexyl radical at 1350K and 2.2ms

4.4.2 RMG Mechanism

The next mechanism considered is a mechanism generated using RMG[101]. RMG is an open source tool used for generation of chemical kinetic mechanisms. The mechanism was generated using the Chernov et al.[151] aromatic seed mechanism and the JetSurF2.0 seed mechanism provided in the RMG kinetics database. The Chernov mechanism is an extension of the ethane and methane flame soot precursor mechanism developed by Slavinskaya and Frank[152] with reaction rates added from other literature studies[153–157]. Attempting to generate a mechanism without the Chernov aromatic seed mechanism resulted in simulation predictions with virtually no benzene formation. Two other smaller species seed mechanisms provided in the RMG kinetics database were tested: the Curran et al. pentane mechanism[158] and the FFCM-1 mechanism[159], but both of them resulted in generated mechanisms that had noticeably worse performance and the Curran seed mechanism contains 3066 reactions both increasing the time necessary to generate the mechanism and the computation time necessary to run simulations in Chemkin-PRO. Despite what the name implies, the JetSurF2.0 seed mechanism provided in the RMG kinetics database isn't the actual JetSurF2.0 mechanism, but a smaller version of the mechanism with many of the reactions involving cyclic species removed bringing down the size of the mechanism from a total of 2163 reactions in the full JetSurF2.0 mechanism to 1439 reactions in the mechanism provided in the RMG kinetics database. Both the Chernov and JetSurF2.0 mechanisms contain oxidation reactions and oxygen containing species not needed for the present pyrolysis study. RMG does allow the user to restrict the atoms and their number allowed in the species that may be added to the mechanism generated, but the species and reactions already present in the seed mechanisms, such as the unneeded oxygen containing species, will be added to the generated mechanism regardless of whether they meet these restrictions or not. Due to RMG generated mechanisms being very large, with the number

of reactions easily exceeding ten thousand, all the oxygen containing species and all oxidation reactions were stripped from the Chernov and JetSurF2.0 seed mechanisms used to generate the mechanism for this study in order to alleviate the computation effort needed to complete the simulations.

Figure 18 contains the experimental data from the 200 bar and 192 ppm of cyclohexane shocks along with the simulation results using the RMG generated mechanisms together with the uncertainty bands which were obtained in the same procedure that was described for the Wang mechanism, and the simulation results obtained for an optimized RMG mechanism. The mechanism optimization was performed in a similar way as the first method described for the Wang mechanism. The top two most positively and negatively correlated reactions for each experimentally observed species were assigned an uncertainty of a factor of 2, but the perturbed reactions weren't limited to just PLOG reactions as this generated mechanism has not previously been validated against low pressure data as was Wang's, and the mechanism with the lowest least squared error was saved as the optimized mechanism and is plotted in Figure 18.

The generated mechanism does an excellent job of predicating the two most abundant species, ethylene and acetylene, with the optimized mechanism slightly improving the prediction. Methane and benzene profiles are also very well captured up to approximately 1450K at which point the mechanism predicts a decay with increasing temperature which isn't reflected in the experimental data. The optimized mechanism is able to capture the peak amounts and the overall profiles of 1,3-butadiene, 1,3-cyclopentadiene, cyclohexene, and vinylacetylene very well. Both propadiene and propyne are substantially under predicted by both the original and optimized generated mechanisms. Toluene is also over predicted by approximately a factor of 5. The formation of benzene in the Chernov aromatic seed mechanism is prescribed through the C3 +

C3 and C4 + C2 species recombination reactions just as in Wang's mechanism, but the Chernov mechanism does not include a benzene pathway proceeding through the dehydrogenation of cyclohexene. While benzene is very well predicted by the generated mechanism at least up to 1450K this is a consequence of both propadiene and propyne being severely under predicted. This was previously seen in Figure 15 with Wang's optimized mechanism. The over prediction of benzene was reduced, but this came at a cost of both propadiene and propyne being significantly under predicted. These results illustrate the need of further refinement of the C3 + C3 recombination reactions producing benzene since the current reaction rate parameters seem inadequate in properly capturing the benzene production at the current experimental conditions.

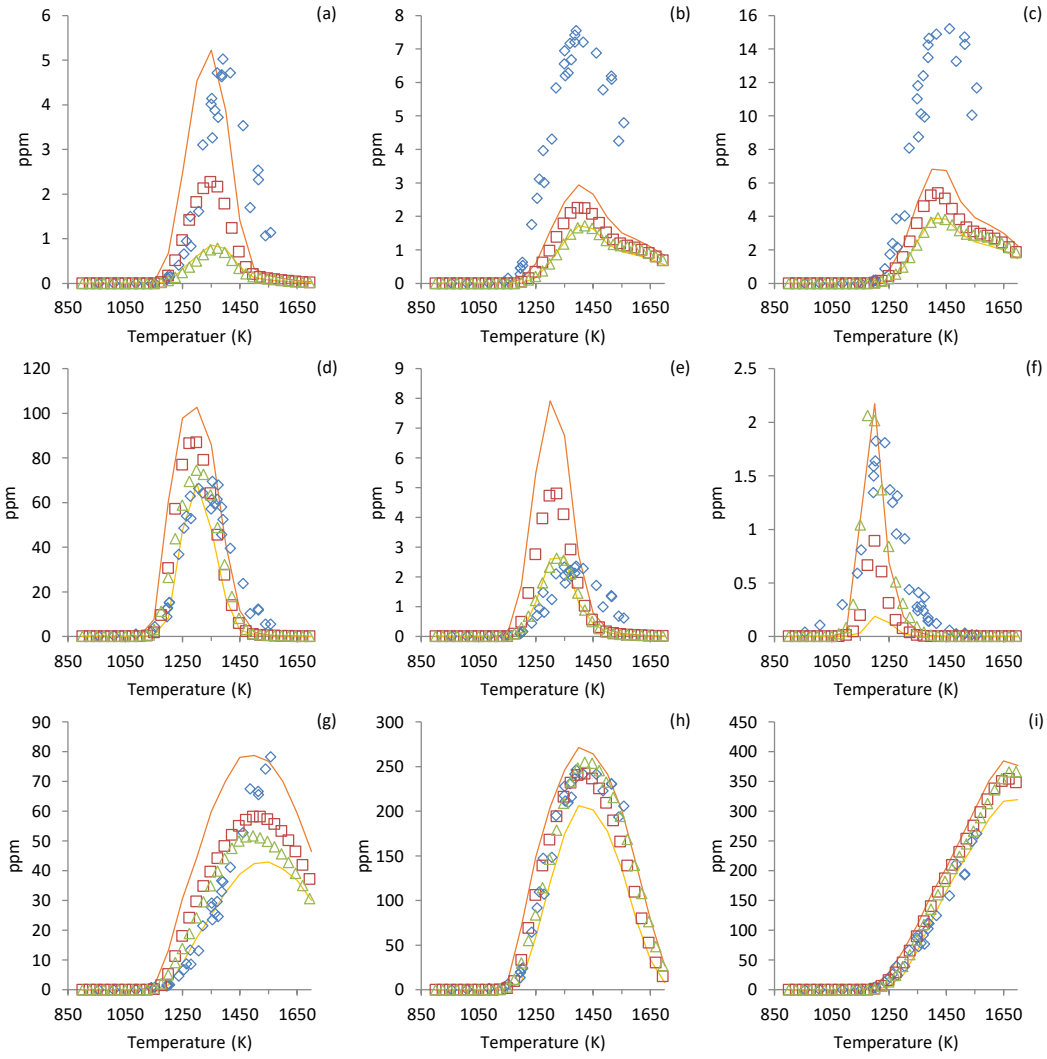

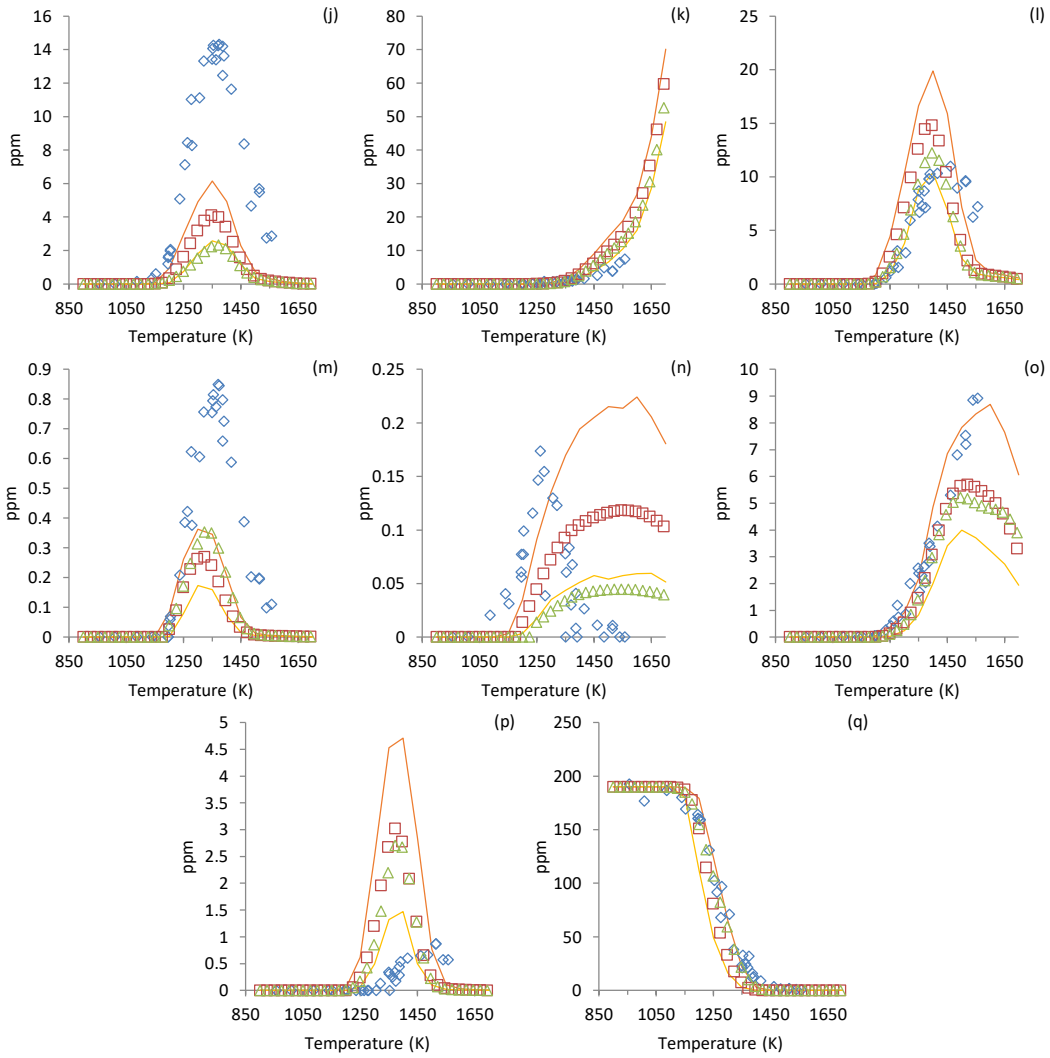

Figure 18: Comparison of species profiles of (a) ethane, (b) propadiene, (c) propyne, (d) 1,3-butadiene, (e) 1,3-cyclopentadiene, (f) cyclohexene, (g) methane, (h) ethylene, (i) acetylene, (j) propene, (k) diacetylene, (l) vinylacetylene, (m) 1,2-butadiene, (n) methylenecyclopentane, (o) benzene, (p) toluene, and (q) cyclohexane observed in 200 bar and 192 ppm of cyclohexane shock tube experiments versus those from a simulation using the RMG generated cyclohexane mechanism, an optimized version of the RMG mechanism mechanism, and the bounds of uncertainty generated by prescribing a 30% uncertainty to all the A factors in the mechanism. Legend: ◇ Experimental Data, □ RMG Mechanism, △ RMG Optimized Mechanism, — Maximum Species Mole Fraction from Monte Carlo Analysis, — Minimum Species Mole Fraction from Monte Carlo Analysis.

4.4.2.1 ROP Analysis

The benzene ROP analysis was also performed for both the unmodified and optimized versions of the RMG generated mechanism. Figure 19 contains a visual representation of the

contributions of various reactions to the formation of benzene formation at a representative temperature of 1350K and a reaction time of 2.2 ms. One immediate observation in contrast to the ROP analysis for the Wang mechanism, shown in Figure 16, is the far lower contribution from the C3+C3 recombination reactions at only 17% of the relative ROP in the unmodified RMG mechanism and 7% in the optimized RMG mechanism. It seems that both versions of the RMG mechanisms' ability to provide excellent prediction of the benzene observed experimentally up to a temperature of 1450K comes at a sacrifice of the prediction of propadiene and propyne experimental data. This is also reflected in the ROP analysis by the small contribution of the C3+C3 species recombination reactions compared to the Wang mechanism where the C3+C3 species recombination reactions accounted for 56% of the relative ROP in the unmodified mechanism, and 48% in the optimized mechanism. The recombination of propadiene with the propargyl radical contributes only 2% of the relative ROP in the unmodified RMG mechanism and 1% in the optimized mechanism. The propargyl radical recombination has the majority of the C3+C3 species recombination reactions contribution to benzene formation at 15% of the relative ROP in the unmodified RMG mechanism and 6% in the optimized mechanism.

The C4+C2 species recombination reactions have the largest contribution to the benzene formation in both versions of the RMG mechanism, as opposed to only the 4% contribution in the unmodified Wang mechanism and 6% contribution to the relative ROP in optimized Wang mechanism. The recombination of *i*C4H5 radical with acetylene has the single largest contribution with 39% of the relative ROP in the unmodified RMG mechanism and 52% in the optimized RMG mechanism. The vinylacetylene and acetylene recombination reaction has the second largest contribution with 13% of the relative ROP in the unmodified RMG mechanism

and 10% in the optimized mechanism. It is closely followed by the 2-butynyl and acetylene recombination reaction which contributes 12% of the relative ROP of benzene in the unmodified RMG mechanism and 9% in the optimized mechanism. The vinyl radical and vinylacetylene recombination contributes 5% and 3% of the relative ROP of benzene in the unmodified and modified versions of the RMG mechanism, respectively. Lastly, the vinyl radical and 1,3-butadiene recombination reaction contributes 5% and 6% of the relative ROP in the unmodified and optimized versions of the RMG mechanism, respectively. The reaction of toluene with hydrogen leading to the cleavage of the methyl group in toluene also contributes 8% of the relative ROP in the unmodified RMG mechanism and 12% in the modified mechanism.

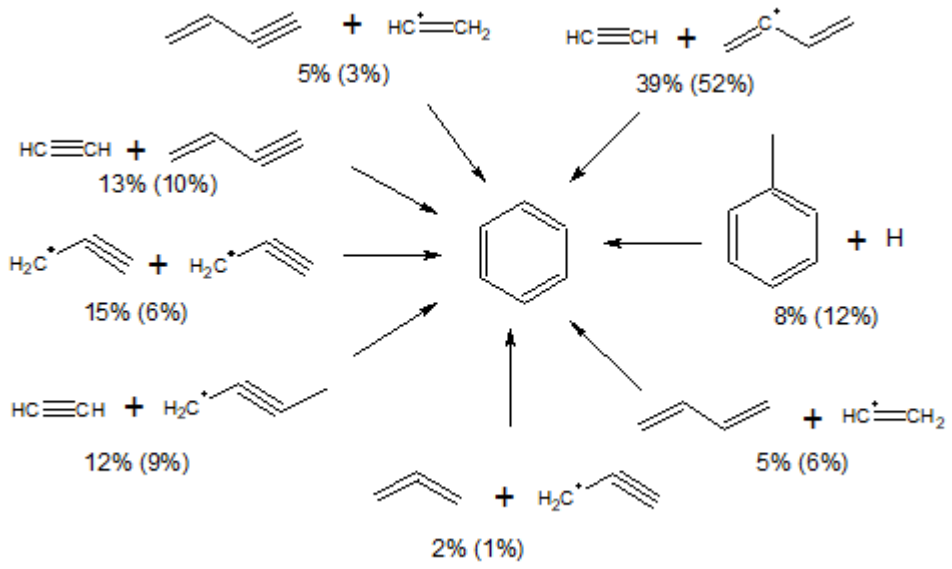

Figure 19: Visualization of the ROP analysis of benzene formation at a temperature of 1350K and reaction time of 2.2 ms. The percentages outside the parenthesis are the relative ROP from the unmodified RMG mechanism and the percentages in parenthesis are the relative ROP from the optimized RMG mechanism.

The ROP analysis was also completed for the initial dissociation pathways of cyclohexane in both the RMG mechanisms. In contrast to the ROP analysis for the Wang mechanism, in both RMG mechanisms the dissociation of cyclohexane is expected to proceed

virtually entirely through the formation of the cyclohexyl radical. This occurs primarily through hydrogen abstraction by hydrogen accounting for 79% of the relative ROP in the unmodified RMG mechanism, and 69% in the optimized mechanism followed by hydrogen abstraction by the methyl radical which accounts for 10% of the relative ROP in the unmodified RMG mechanism and 20% in the optimized mechanism. The remaining relative ROP belongs to hydrogen abstraction by other species, primarily various benzyl radicals. Figure 20 illustrated the main decomposition pathways of cyclohexane proceeding through the cyclohexyl radical at a representative temperature of 1350K and reaction time of 2.2 ms. The cyclohexyl radical may either form cyclohexene which will primarily dissociate into 1,3-butadiene and ethylene, or it may undergo ring opening forming the hex-5-en-1-yl radical. The hex-5-en-1-yl radical may then form but-3-en-1-yl and ethylene after undergoing beta-scission, or form 1,5-hexadiene. The ring closure of hex-5-en-1-yl radical to form the cyclopentylmethyl radical which then forms methylenecyclopentane is a minor pathway but is included due to methylenecyclopentane being the only alkenylcyclopentane observed experimentally. The hex-5-en-1-yl radical may also undergo either a 1,4-hydrogen shift forming the hex-5-en-4-yl radical or isomerize to the hex-4-en-3-yl radical. The hex-5-en-4-yl radical may undergo beta-scission forming 1,3-butadiene and the ethyl radical. Similarily, the hex-4-en-3-yl radical may also undergo beta-scission forming 1,3-pentadiene and the methyl radical. Both hex-5-en-4-yl and hex-4-en-3-yl may also form 1,3-hexadiene.

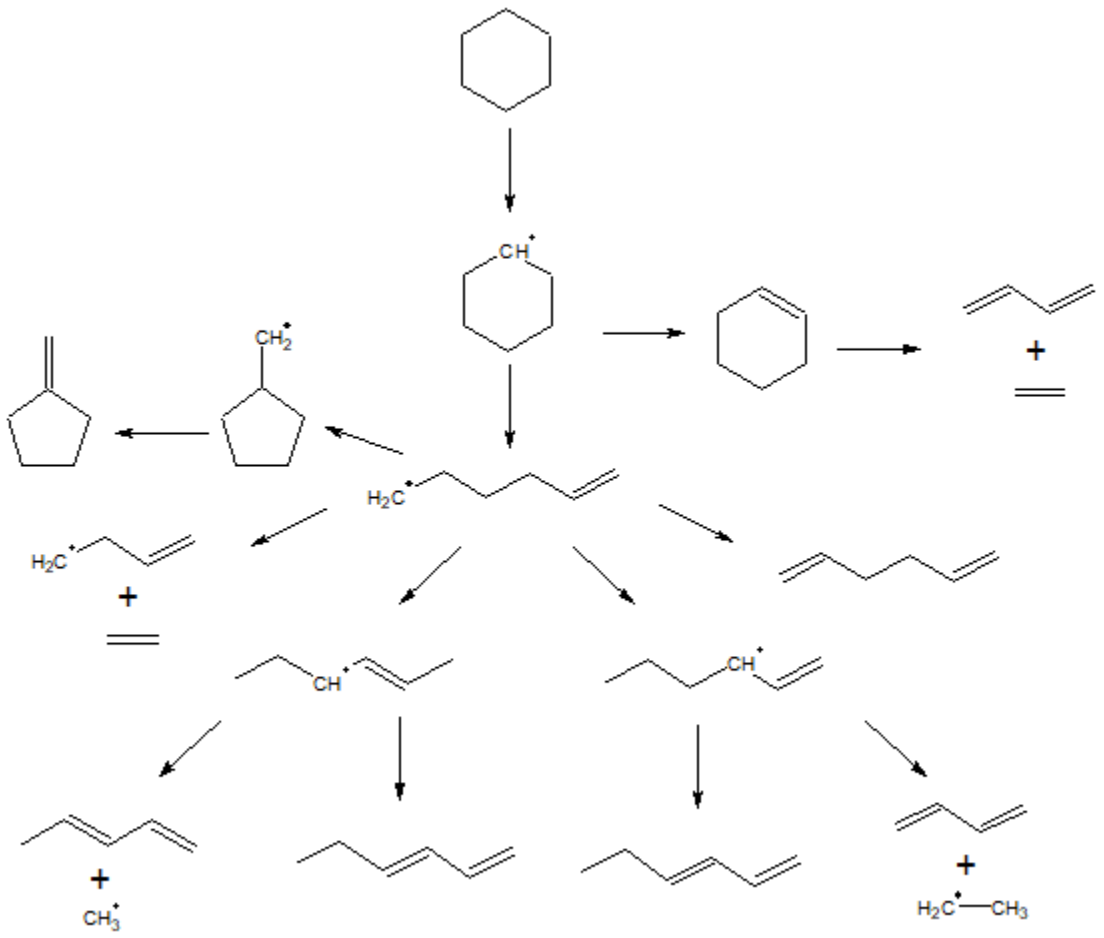

Figure 20: Main cyclohexane decomposition pathways predicted by RMG mechanism proceeding through the cyclohexyl radical at 1350K and 2.2ms.

4.4.3 Comparison of Mechanisms Against Higher Concentration Experimental Data

One consideration regarding both the mechanisms' suboptimal ability to capture the propadiene and propyne experimental profiles, and Wang's mechanism significant over prediction of benzene formation, has to do with the dilute environment of the cyclohexane fuel mixture present in the reaction zone of the current experiments. It has been shown in Figure 11 and Figure 12 that the current experimental data can be reproduced at higher pressures if the initial concentration of cyclohexane in the reaction zone is kept equivalent at both the pressures illustrating the importance of the initial fuel concentration of the product distribution.

Furthermore, in Figure 13 and Figure 14 it can be seen that the normalized profiles of propadiene and propyne for the 200 bar and 3195 ppm of cyclohexane experiments are lower than those obtained at 200 bar and 192 ppm of cyclohexane and 100 bar and 190 ppm of cyclohexane while the amount of benzene produced increases. This is in line with the results from the Wang mechanism which predicts less propadiene and propyne, but more benzene than experimentally observed as shown in Figure *15*. Also, in Figure 15 the optimized mechanism that targeted only PLOG reactions strongly correlated to benzene production showed limited improvement in being able to predict the experimental data, suggesting that the pressure dependence of the reaction rate constants does not seem sufficient in improving the mechanism's ability to capture the experimental data. Therefore, perhaps the mechanisms are able to better predict the higher concentration experimental data obtained at 200 bar.

Figure 21 contains the species profiles from the 200 bar and 3195 ppm of cyclohexane set of experiments together with the original Wang mechanism and the un-optimized RMG generated mechanism. The un-optimized mechanisms are used since the mechanism optimization was carried out against the data from the experiments using a lower initial concentration of cyclohexane, and here the aim is to test their mechanisms' performance against a set of data with a higher concentration of cyclohexane. Furthermore, it is expected that the RMG mechanism will perform poorly as it was generated for the dilute mixture conditions which were specified for the mechanism generation, so reactions which may have a higher carbon flux at higher concentrations may not be included due to them not meeting the flux threshold at dilute conditions. The main interest lies in the propadiene, propyne, and benzene profiles, but the full set of species plots is shown for completeness. The peak amount of propyne is now well predicted by the Wang mechanism, and the prediction of propadiene has also improved but is

about 25% lower than seen in the experimental data. The RMG mechanism predicts both the profiles poorly, as expected. Benzene is better captured up to about 1450K by the Wang mechanism, but then the amount of benzene produced with increasing temperature in the experiments seems to taper off while the mechanism predicts a continual increase of benzene with temperature. The RMG mechanism substantially under predicts the amount of benzene seen. Both mechanisms predict benzene to primarily dissociate into the phenyl radical and H atom.

While the Wang's mechanism is able to better capture propadiene, propyne, and benzene for the higher concentration data, some of the previous problems still remain. Cyclohexene continues to be over predicted, by a factor of two this time, and 1,3-cyclopentadiene is also over predicted by a factor of two. If the amount of cyclohexene was corrected it is possible that benzene would be captured even better by the mechanism, as was seen in the optimized Wang mechanism in Figure 15. Toluene is still under predicted, by more than a factor of two. At its maximum value, diacetylene is now over predicted by more than a factor of 20. The three major products, of methane, ethylene, and acetylene continue to be well predicted by the model. These results serve as verification that adjusting the pressure dependent parameters of the Wang mechanism would not be enough to obtain better agreement between the experimental and simulated results. The reaction rates for benzene production as well as some of the benzene precursors would have to be revisited for the mechanism to be able to better reproduced data at dilute conditions. The inability of the two considered models to capture benzene production unless propadiene and propyne concentrations are underestimated shows that the benzene formation pathways, at least at dilute conditions, are not complete. Considering the importance

of benzene in combustion the refinement of these pathways and their reaction rate coefficients should serve as motivation for further studies.

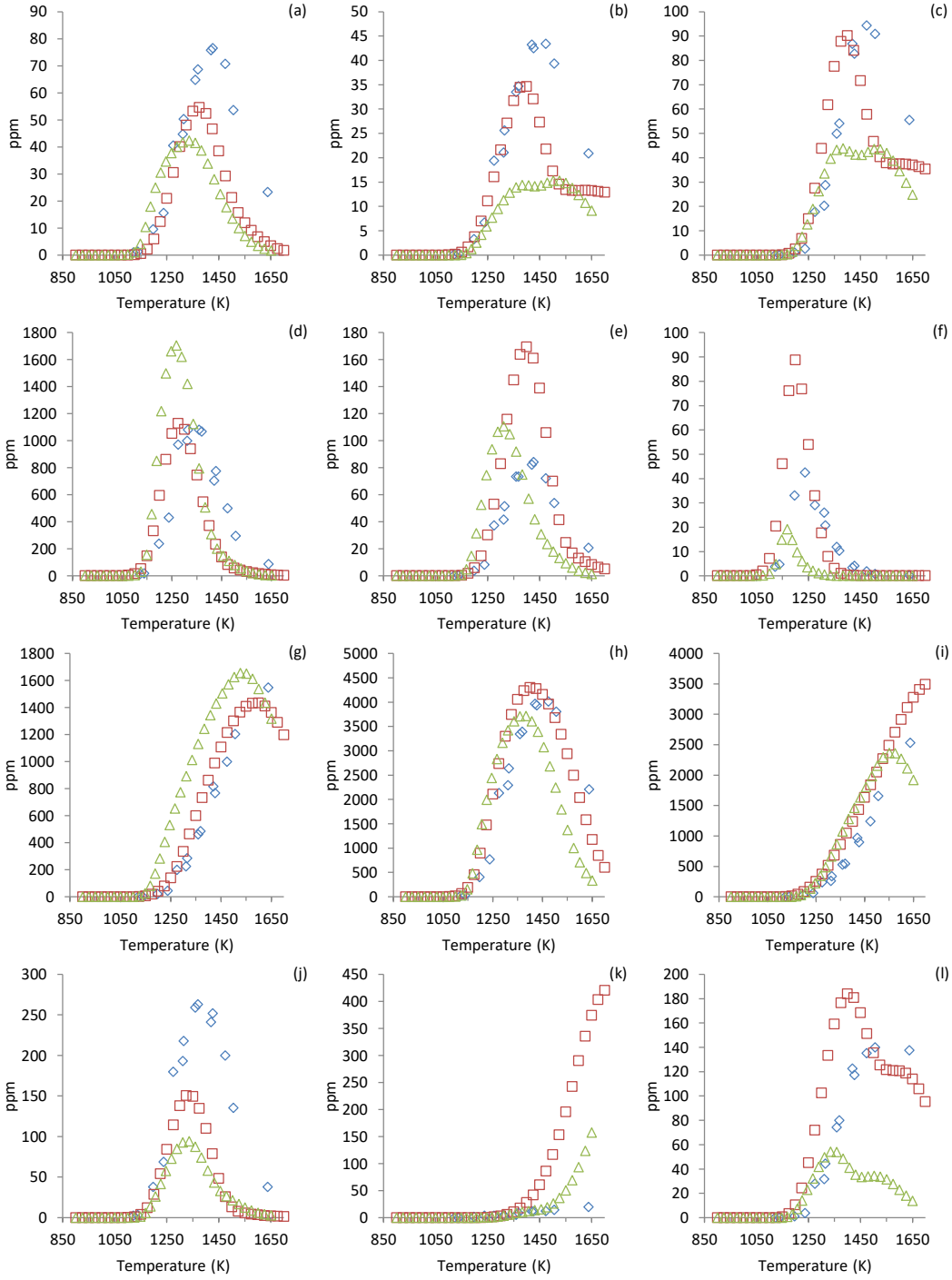

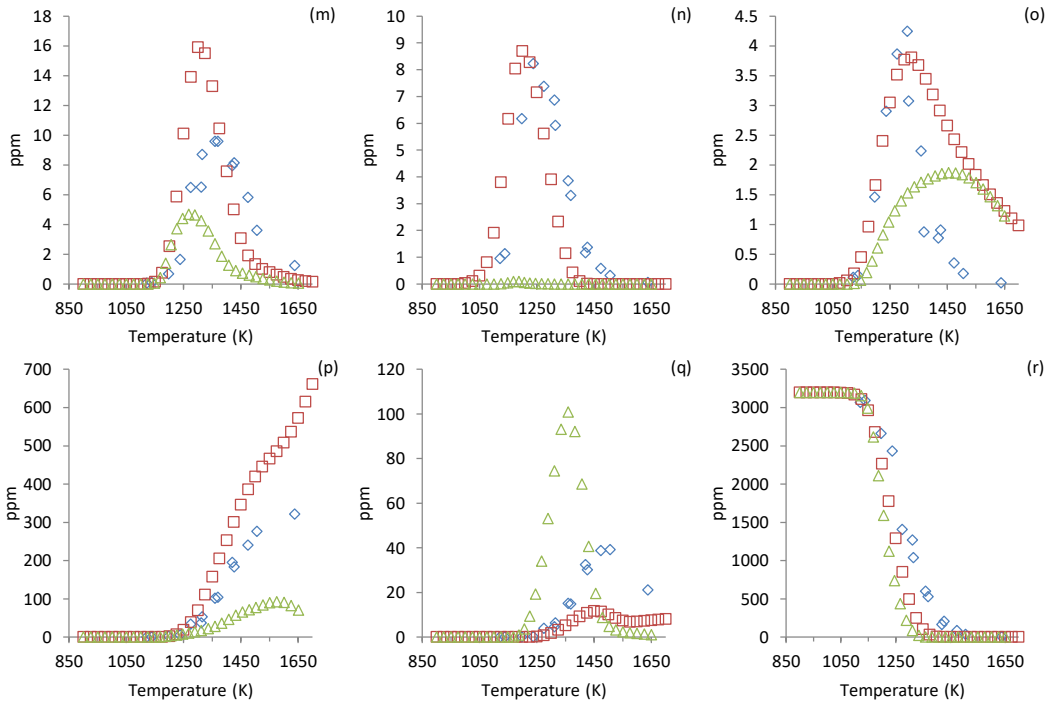

Figure 21: Comparison of species profiles of (a) ethane, (b) propadiene, (c) propyne, (d) 1,3-butadiene, (e) 1,3-cyclopentadiene, (f) cyclohexene, (g) methane, (h) ethylene, (i) acetylene, (j) propene, (k) diacetylene, (l) vinylacetylene, (m) 1,2-butadiene, (n) 1-hexene, (o) methylenecyclopentane, (p) benzene, (q) toluene, and (r) cyclohexane observed in 200 bar and 3195 ppm of cyclohexane shock tube experiments versus those from a simulation using Wang's mechanism, and the RMG generated mechanism. Legend: ◇ Experimental Data, □ Wang Mechanism, △ RMG Generated Mechanism.

4.5 Summary

An extensive experimental study was completed investigating the pyrolysis of cyclohexane under high temperature and high pressure conditions. Variation of experimental pressure resulted in some of the product species profiles being affected, particularly ethane, propadiene and propyne. However, due to the mole fraction of the fuel in the test case mixture being kept approximately equal for the three sets of experiments there was concern over the possibility of the observed product distribution changes being attributed to the fuel concentration variation in the reaction zone caused by the difference in the pressure. To investigate this an additional set of experiments was completed at a 40 bar but higher mole fraction of fuel, 484 ppm of cyclohexane, in order to match the fuel concentration expected in the 100 bar

experiments which used 190 ppm of cyclohexane as the fuel. The experimental data obtained at 40 bar and 484 ppm of cyclohexane was able to match the experimental data obtained in a higher pressure set of experiments using a lower mole fraction of fuel, 100 bar and 190 ppm of cyclohexane. This illustrated the importance of the initial fuel concentration on the product distribution, and also that at least for the conditions in the present study, matching product distributions can be obtained at significantly different pressure if the fuel concentration in the reaction zone is equivalent.

Yet another set of experiments was completed with an even higher fuel concentration of 3195 ppm of cyclohexane at a pressure of 200 bar to determine the impact on the product distribution due to a substantial increase in the initial fuel concentration. This set of experiments resulted in higher normalized mole fractions of the cyclic products: 1,3-cyclopentadiene, methylenecyclopentane, cyclohexene, benzene, and toluene compared to the 200 and 100 bar experiments which used a lower mole fraction of cyclohexane in the fuel mixture. The increase in the amount of 1,3-cyclopentadiene and methylenecyclopentane formed suggests that the high concentration environment present in the supercritical phase studies[19–21] is needed in order the see an abundance of alkylcyclopentane and alkenylcyclopentane products. Methylenecyclopentane was the only alkenylcyclopentane observed, and no alkylcyclopentane species were successfully quantified in this study.

Comparison of the experimental data at 200 bar and 192 ppm of cyclohexane with simulation results obtained with a literature[23] and generated model showed overall a good match between the simulation results and the experimental data. Both the models, however, struggled with predicting the amount of propadiene and propyne, and the literature model significantly overestimated the amount of benzene produced. Another comparison between the

experimental data obtained at 200 bar and 3195 ppm of cyclohexane and the simulation results obtained using the literature model showed improved prediction of the benzene, propadiene, and propyne production, but the prediction of diacetylene suffered. The generated model, which was generated for dilute conditions, performed worse although it still managed to capture the most abundant product species: methane, ethylene, and acetylene fairly well. These results suggest that despite the numerous previous works attempting to quantify the reactions involving C3 species, particularly their recombination to form benzene, are not complete and considering the importance of benzene in combustion systems this should motivate further studies aiming to resolve the discrepancies observed between the experimental data and model predictions in this study.

5. METHYLCYCLOHEXANE PYROLYSIS

5.1 Introduction

Methylcyclohexane has long been of interest in combustion research because it is commonly used in surrogates, and is a constituent of real jet and propulsion fuels[114,160]. One of the more recent methylcyclohexane studies was conducted by Wang et al. using a flow reactor at pressures of 30, 150, and 760 torr[23]. The experimental data were then used for the development of a chemical kinetic mechanism that is an extension of their previous cyclohexane mechanism[36]. In the mechanism, Wang et al. included a reaction pathway resulting in the formation of methylenecyclopentane that proceeds through the ring opening of the cyclohexyl radical to form hex-5-en-1-yl which subsequently undergoes 5-exo-cyclization resulting in cyclopentylmethyl which after a 1,4 hydrogen shift forms methylcyclopentyl.

A similar pathway is suggested by Peukert et al. in their work pertaining to hydrogen abstraction of cyclohexane, but Peukert proposes that rather than forming methylenecyclopentane the methylcyclopentyl radical ultimately decomposes to propene and propadiene[125]. Peukert compared two available sets of reaction rate constants for the 5-exo-cyclization reaction of the hex-5-en-1-yl radical proposed by Granata et al.[127] and Sirjean et al.[126] and found that the rates proposed by Granata would make the 5-exo-cyclization the dominant reaction involving hex-5-en-1-yl, and those by Sirjean would still result in the reaction being of importance. Peukert ultimately proposed reaction rate coefficients that fall between those of Granata and Sirjean.

The importance of the formation of methylenecyclopentane lies in that the reaction pathway is analogous to alkylcyclopentane reaction pathways, and alkylcyclopentanes have been found to be coking[21] and sooting[22] precursors. Alkylcyclopentanes have also been found to

be the dominant products in methylcyclohexane pyrolysis under supercritical conditions[19–21]. Wang mentions that the analogous ring closure reactions are possible in methylcyclohexane dissociation from C_7H_{13} radicals, e.g. hept-6-en-1-yl radical, but that they are not included in the methylcyclohexane mechanism due to the negligible formation.

The supercritical experiments in which ring contraction was observed were conducted at high pressures up to 100 bar, but at lower temperatures, around or below 800 Kelvin, and had time scales of hours[19–21]. Other examples of high pressure methylcyclohexane experiments include the studies by Vanderover and Oehlschlaeger[161] encompassing pressures up to 69.5 atm, and two works by Vasu et al.[162,163], the first with pressures near 15 atm, and the second with pressures from 1 to 50 atm. All three of these studies were autoignition studies. MacDonald et al.[164] completed a methylcyclohexane pyrolysis shock tube study with pressures up to 23 atmospheres, but only obtained species data for the fuel and ethylene.

Another notable and recent methylcyclohexane study is the modeling and experimental work by Pitz et al.[165] The experiments were completed in a rapid compression machine producing ignition delay data in the 680K to 980K temperature range at pressures of up to 20 bar. The oxidation chemical kinetic mechanism developed by Pitz was later further developed by extending it to higher temperatures and thoroughly and extensively validated against most of the notable existing methylcyclohexane experimental data by Narayanaswamy et al.[166], who validated the extended Pitz mechanism against the high pressure auto-ignition data of Pitz et al. (15 and 20 bar)[165], Vanderover and Oehlschlaeger (12 and 50 bar)[161], and both studies of Vasu et al. (20 and 45 bar)[162,163]. The limited species data of two autoignition studies was also used to validate the mechanism and included the OH and H2O profiles from the 2.1-2.2 bar shock tube work by Hong et al.[167] and the OH profiles from the 16 bar shock tube study by

Vasu et al.[162] All the detailed species validation was completed using lower pressure experimental results due to the lack of high pressure methylcyclohexane speciation data and were taken from the atmospheric pressure flow reactor study by Zeppieri et al.[24] and atmospheric pressure premixed flame data from the study by Wang et al.[23]

Another high pressure oxidation experimental and modeling study was recently completed by Weber et al.[168] Weber obtained methylcyclohexane auto-ignition data at pressures of up to 50 bar and used the experimental data to validate the modeling efforts. The model was not validated against any speciation data. Yet another experimental and autoignition study, completed in a shock tube at lower pressures of up to 4 atm, was conducted by Orme et al.[169] The authors did validate the developed methylcyclohexane mechanism against speciation data from another study using the venerable near-pyrolysis flow reactor data of Zeppieri et al.[24] The mentioned methylcyclohexane studies are not all inclusive, and a far more thorough review is presented by Pitz and Mueller[114]; however, the works discussed illustrate that the high pressure oxidation methylcyclohexane experiments only offer autoignition data or very limited species data which was used to detect the ignition of the fuel mixture, and modeling efforts which wish to include validation of detailed species data are restricted to only atmospheric pressure data presented by a couple of studies.

Currently, the only high temperature gas phase methylcyclohexane pyrolysis experiments with substantial species data are those of Wang et al.[23] and Zeppieri et al.[24] and the experiments did not exceed pressures of 1 atmosphere; however, the study by Wang did also include sub-atmospheric experiments at pressures of 30 and 150 torr. The methylcyclohexane experimental pyrolysis database is lacking gas phase high pressure and high temperature pyrolysis speciation data. Extending the current methylcyclohexane experimental database to

high pressures and temperatures would allow for the validation of current, and creation of new, chemical kinetic mechanisms at conditions relevant to modern combustors, in addition to determining whether or not the formation of alkylcyclopentanes can be observed in gas phase at high pressures.

5.2 Experimental Results

5.2.1 Effects of Pressure on Methylcyclohexane Pyrolysis

Three sets of experiments at nominal pressures of 40, 100, and 200 bar (with the exact experimental conditions for each individual experiment available in APPENDIX D) with a nominal reaction time of 2.2 milliseconds (ms) were carried out with methylcyclohexane as the fuel and the initial methylcyclohexane mole fractions at 187, 188, and 181 parts per million (ppm,) respectively. The reported fuel mole fractions were quantified by GC analysis of the test gas fuel mixture after the mixture was allowed to homogenize for a minimum of 12 hours after preparation. Figure 22 contains the product species profiles of ethane, ethylene, propadiene, propyne, 1-butene, and toluene. The peak amounts of ethane, propadiene, and propyne were observed to increase with a decrease in experimental pressure. This increase is most easily seen in ethane where the peak amount produced at 40 bar is nearly 37% greater than at 100 bar, and the increase in the peak amount from 200 to 100 bar is approximately 15%. For propadiene and propyne the increase in the peak amount is approximately 12% and 10% ppm greater, respectively, at 40 bar than produced at 100 or 200 bar. The peak amounts of both propadiene and propyne were approximately equivalent in both the 100 and 200 bar experiments, and the peak of both species was observed at a temperature approximately 50K higher in the 200 bar experiments compared to the 100 bar experiments. The reverse trend is present in the 1-butene and toluene profiles where the amounts of the products observed increase with an increase in

pressure. For 1-butene the increase in the peak amounts observed increased by approximately 20% from 40 to 100 bar and 14% from 100 bar to 200 bar, and for toluene the increase was 45% from 40 to 100 bar and 23% from 100 to 200 bar. Both of these species were minor products. The amount of ethylene produced did not seem to be effected by the variation in experimental pressure, but it is a major product species and the second most abundant product observed.

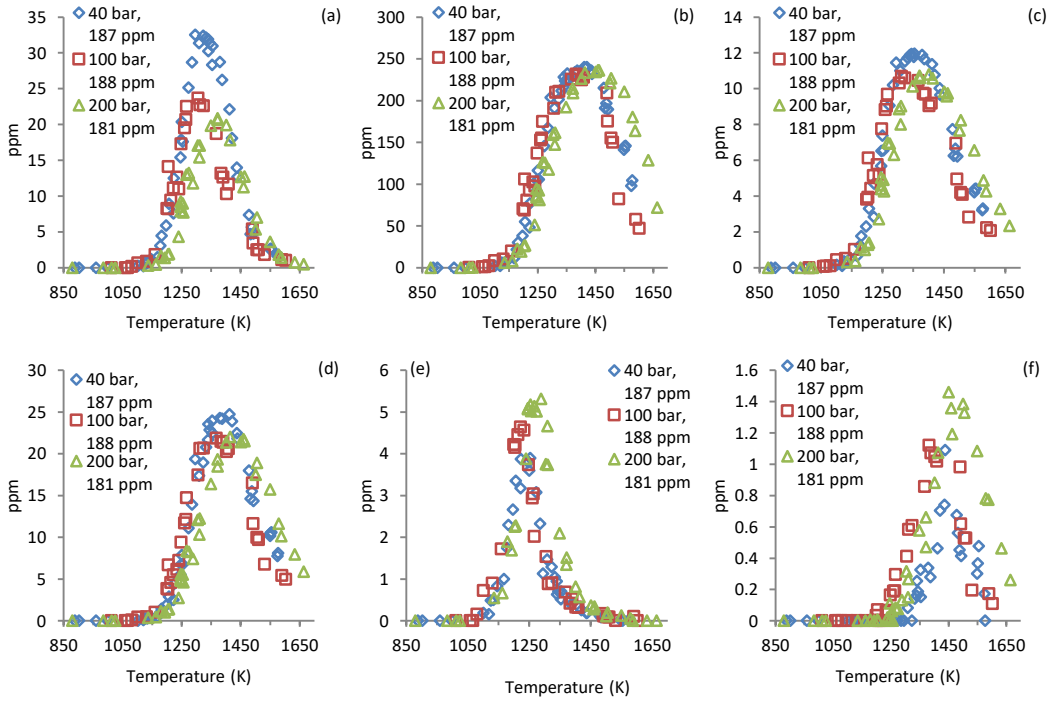

Figure 22: Species profiles of (a) ethane, (b) ethylene, (c) propadiene, (d) propyne, (e) 1-butene, and (f) toluene formed in methylcyclohexane pyrolysis at pressures of 40, 100, and 200 bar.

Figure 23 contains other quantified methylcyclohexane pyrolysis products observed at all three experimental pressures namely methane, acetylene, propene, 1,3-butadiene, diacetylene, vinylacetylene, 1,3-cyclopentadiene, methylenecyclopentane, benzene, 1,3-cyclohexadiene, cyclohexene and methylcyclohexane. Acetylene is the most abundant product quantified with a maximum composition of approximately 430 ppm being observed at 40 and 100 bar, and approximately 400 ppm at 200 bar due to the formation with respect to temperature proceeding at a lower rate at 200 bar; however, it is possible that if the experimental temperature range was

extended to higher pressures the same maximum mole fraction of acetylene would be observed at all three pressures. Methane is the second most abundant product with the 200 bar formation with respect to temperature being equivalent to that observed at 40 and 100 bar, but the peak amount of methane at 200 bar is observed at a temperature of nearly 1590K, approximately 80K higher than the temperature at which the amount of methane produced in the 40 and 100 bar experiments peaks. The peak amount of methane in the 200 bar experiments is also nearly 12% higher than in the 40 and 100 bar experiments. The diacetylene profile shows a similar formation pattern to acetylene, with the formation at 200 bar proceeding at a lower rate with respect to temperature than at either 40 and 100 bar, but once again it is possible that at higher experimental temperatures the amount observed at all three pressures may be equivalent or very close. No discernible variation in the profiles of either 1,3-butadiene and vinylacetylene with respect to the experimental pressure were observed between the three sets of data. Propene is yet another product for which the peak amount observed at 200 bar occurs is slightly, or roughly 8%, higher than observed in the 100 bar and 40 bar experiments and the peak amount is also observed at a temperature approximately 30K higher than for the remaining two sets of experiments.

All the remaining species presented are cyclic species. 1,3-Cyclopentadiene and methylenecyclopentane are the only five carbon ring species successfully quantified. Both 1,3-cyclopentadiene and methylenecyclopentane are minor species, with the peak amount of methylenecyclopentane being below 0.3 ppm which is nearing the limit of detectability of an FID, hence, the noticeable scatter in the methylenecyclopentane data. Both the species seem to exhibit slightly higher peak amounts with increasing pressure. For the case of methylenecyclopentane the pressure increase from 40 to 100 bar resulted in a 4% increase in the peak amount, and a 10% increase in the peak amount as the experimental pressure was increased

from 100 to 200 bar. For 1,3-cyclpentadiene the pressure increase from 40 bar to 100 bar resulted in a 2.6% increase in the peak amount, and a 6% increase as the pressure was increased from 100 to 200 bar. These differences are all below, or at best equal to, the uncertainty in the species calibration; however, the comparison is between same species and the same calibration curve is used and the difference in the amounts observed is quantified by the GC.

The remaining presented product species in Figure 23 are all six carbon ring species, and likewise all exhibit increased peak amounts with increasing experimental pressure. Benzene is the most abundant cyclic species quantified and showed a 14% increase in the peak amount with the pressure increase from 40 bar to 100 bar, and a much smaller 3.6% increase with the pressure increasing from 100 to 200 bar. The benzene peak also occurs at a substantially higher temperature of 1590K at 200 bar which is 90K higher than the temperature at which the peak amount of benzene is observed for both the 40 and 100 bar experimental sets. Both cyclohexene and 1,3-cyclohexadiene were very minor species. The peak amount of 1,3-cyclohexadiene increased by 18.7% from 40 to 100 bar and by 17.8% from 100 to 200 bar while the peak amount of cyclohexene increased by 6% with a pressure increase from 40 to 100 bar and 11% from 100 to 200 bar. The fuel decay, or the methylcyclohexane profile, did not seem to vary between the three experimental pressures.

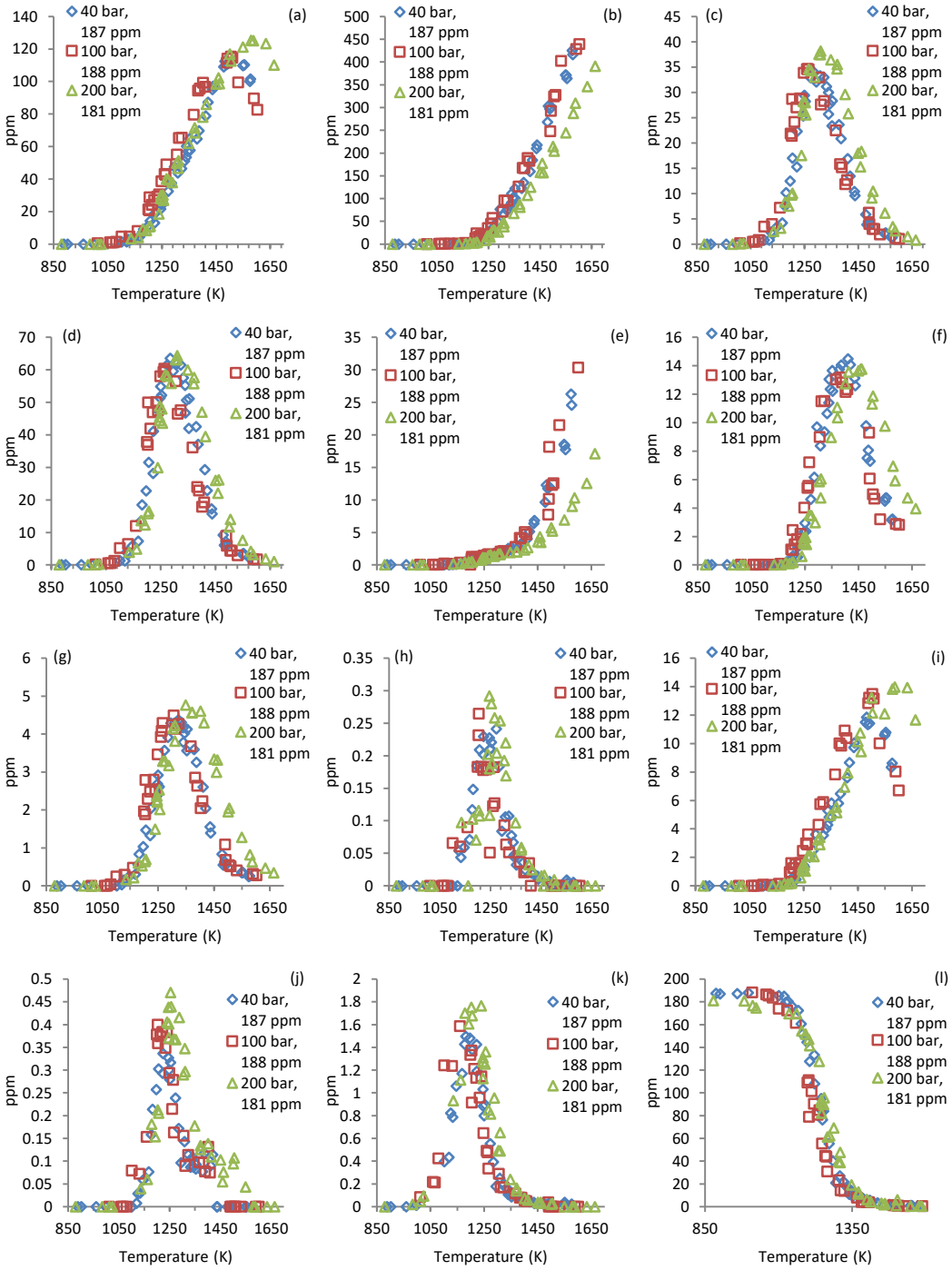

Figure 23: Species profiles of (a) methane, (b) acetylene, (c) propene, (d) 1,3-butadiene, (e) diacetylene, (f) vinylacetylene (g) 1,3-cyclopentadiene, (h) methylenecyclopentane, (i) benzene, (j) 1,3-cyclohexadiene, (k) cyclohexene and (l) methylcyclohexane formed in methylcyclohexane pyrolysis at pressures of 40, 100, and 200 bar.

5.2.2 Effects of Initial Fuel Concentration on Methylcyclohexane Pyrolysis

The results of methylcyclohexane pyrolysis at 40, 100, and 200 bar with the approximately equivalent fuel mole fractions of 187, 188, 181, respectively, were shown in Figure 22 and Figure 23 with ethane, propadiene, propyne, 1-butene, and toluene being identified as species whose profiles were most notably affected by variation of pressure. Although the mole fractions of the fuel were nearly constant at all three pressures, the fuel concentrations in the reflected shock reaction zone were not. With concentration being proportional to pressure, assuming ideal gas behavior, that meant that the fuel concentration in the reaction zone in the 100 bar shocks was 250 percent of what the fuel concentration in the reaction zone was in the 40 bar shocks, and at 200 bar the fuel concentration in the reaction zone was 500 percent of what it was in the 40 bar experiments. Rather than attributing the difference in the product profiles directly to pressure it seemed worthwhile to investigate the effects of the initial fuel concentration in the reaction zone on the product species profiles. To accomplish this goal, a set of experiments with an initial mole fraction of 507 ppm of methylcyclohexane was completed at 40 bar with a nominal reaction time of 2.2 ms. The 507 ppm fuel mixture results in a fuel concentration which is approximately 270 percent of the fuel initially present in the 40 bar and 187 ppm experiments which is not exactly equal to the expected 250 percent increase due to the pressure increase from 40 to 100 bar, but it is sufficiently close to provide insight into the effects of the initial fuel concentration.

Figure 24 contains the plots of ethane, ethylene, propadiene, propyne, 1-butene, and toluene obtained from experiments at 40 bar and 187 ppm of fuel, 100 bar and 188 ppm of fuel, and 40 bar and 507 ppm of fuel. All the species mole fractions were normalized by the initial concentration of methylcyclohexane to allow a direct comparison of the species data between all

three sets of experiments since the 40 bar and 507 ppm of fuel experiments resulted in greater mole fractions of all species. Previously, only ethylene was not affected by the variation in the experimental pressure and matching ethylene profiles were achieved for all three sets of experiments as shown in Figure 22. Similarly, the normalized ethylene profile obtained from the 40 bar and 507 ppm of fuel set of experiments matches the ethylene profiles from the 40 bar and 187 ppm of fuel and 100 bar and 188 ppm of fuel experiments.

The ethane peak previously showed the most noticeable increase with 37% more ethane being produced at its peak amount in the 40 bar and 187 ppm of fuel experiments compared to the 100 bar and 188 ppm of fuel experiments, but the 40 bar and 507 ppm of fuel set of experiments resulted in lower normalized amounts of ethane produced at its peak and the overall normalized ethane profile excellently matches the normalized profile obtained at 100 bar and 188 ppm of fuel. Both propadiene and propyne have also previously shown their peak amounts to decrease with increasing pressure, but the new set of experiments conducted at 40 bar and 507 ppm of fuel was able to produce matching normalized profiles for both propadiene and propyne to those obtained at 100 bar and 188 ppm of fuel. Inversely, the amount of 1-butene and toluene increased with increasing pressure, and once again the 100 bar and 188 ppm of fuel 1-butene and toluene profiles are excellently matched by the profiles obtained in the 40 bar and 507 ppm of fuel experiments. The ability to generate matching species data at lower pressures if the concentration of the fuel in the reaction zone is kept approximately equivalent illustrates that at least at the current experimental conditions there does not seem to be any direct pressure effects on the product species distribution, other than the effect of pressure on the initial fuel concentration.

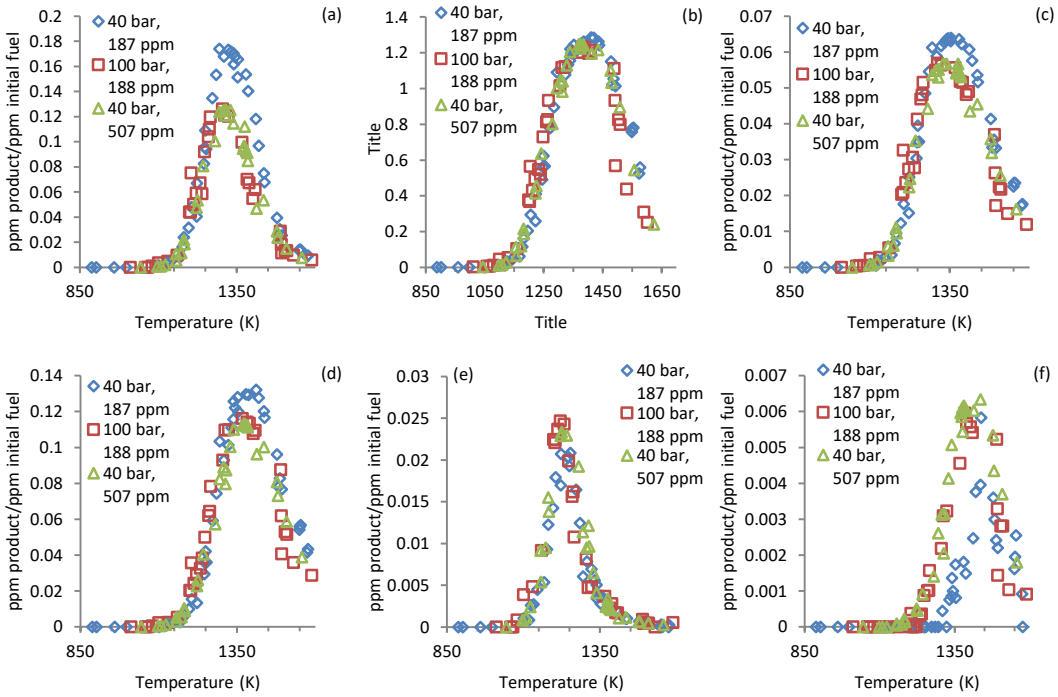

Figure 24: Comparison of product profiles of (a) ethane, (b) ethylene, (c) propadiene, (d) propyne, (e) 1-butene, and (f) toluene obtained in the pyrolysis of methylcyclohexane at 40 bar and 187 ppm, 100 bar and 188 ppm, and 40 bar and 507ppm. The mole fraction of each product is normalized by the initial mole fraction of the fuel.

Figure 25 contains all the species previously shown in Figure 23, namely methane, acetylene, propene, 1,3-butadiene, diacetylene, vinylacetylene, 1,3-cyclopentadiene, methylenecyclopentane, benzene, 1,3-cyclohexadiene, cyclohexene, and methylcyclohexane obtained in the methylcyclohexane pyrolysis experiments conducted at 40 bar and 187 ppm of fuel, 100 bar and 188 ppm of fuel, and 40 bar and 507 ppm of fuel. All the species mole fractions have once again been normalized by the initial fuel mole fraction in each respective set of experiments to allow for a direct comparison of the data obtained from all three sets of experiments. The linear product species obtained in the 40 bar and 187 ppm of fuel and 100 bar and 188 ppm of fuel experiments have previously not shown any substantial or notable variation in their initial formation temperatures, peak amounts, or the overall profiles. Similarly, the normalized species profiles obtained in the 40 bar and 507 ppm of fuel experiments match the

normalized species profiles in both the 100 bar and 188 ppm of fuel and 40 bar and 507 ppm of fuel experiments very well; however, it is worth noting that whenever there is a small difference in the normalized profile from the 100 bar and 188 ppm of fuel experiments when compared to the 40 bar and 187 ppm of fuel experiments then the profile obtained from the 40 bar and 507 ppm of fuel experiments will match more closely the profile from the 100 bar experiments.

One such example is in the methane profile where the methane production observed in the 100 bar and 187 ppm of fuel experiments proceeds at temperatures approximately 30K lower compared to the 40 bar and 187 ppm of fuel experiments. This difference is rather small and could certainly be attributed to the temperature uncertainty in the data which is also estimated to be up to 30K, but the 40 bar and 507 ppm of fuel experiments produced a profile that matched the methane profile from the 100 bar and 188 ppm of fuel experiments and likewise has an approximately 30K shift in the temperature compared to the methane profile from the 40 bar and 187 ppm of fuel experimental set. The remaining quantified linear species do not show a similar shift and the acetylene, propene, 1,3-butadiene, diacetylene, and vinylacetylene normalized profiles match very well between the three experimental sets and the normalized profiles are certainly well within the experimental temperature uncertainty of each other.

The cyclic species profiles have previously shown to have their peak amounts increase slightly with an increase in the experimental pressure. The peak amount of benzene recovered in the 100 bar and 188 ppm of fuel experiments was approximately 14% higher than the peak amount of benzene observed in the 40 bar and 187 ppm of fuel experiments. The benzene production in the 100 bar and 188 ppm of fuel experiments also proceeded at temperatures approximately 30K lower than in the 40 bar and 187 ppm of fuel experiments. The shift of the species profile has also been previously seen in the methane profile. The 40 bar and 507 ppm of

fuel experiments generated a normalized benzene profile that both captures the higher amount of benzene observed in the 100 bar and 188 ppm of fuel experiments, and also the shift in the production of benzene occurring at temperatures approximately 30K lower compared to the 40 bar and 187 ppm of fuel experiments.

The remaining cyclic species products all show the result of the 40 bar and 507 ppm of fuel experiments producing profiles which have a slightly higher peak amount compared to the 100 bar and 188 ppm of fuel experiments. The most significant increase in the peak amount is observed in methylenecyclopentane for which the peak amount increased by 29% compared to the 100 bar and 188ppm of fuel experiments that in turn had a just 4% higher peak amount of methylenecyclopentane over the 40 bar and 187 ppm of fuel experiments. The 1,3-cyclopentadiene peak amount observed in the 40 bar and 507 ppm experiments was also higher compared to the 100 bar and 188 ppm of fuel experiments by 9.4%. Similarly, the peak amount of 1,3-cyclohexadiene increased by nearly 17% and the cyclohexene peak amount by 6% in the 40 bar and 507 ppm of fuel experiments over the 100 bar and 188 ppm of fuel experiments. This result does suggest that at higher initial fuel concentrations the formation of cyclic species becomes more favorable; however, it has to be noted that other than benzene and 1,3-cyclopentadiene all the other cyclic products formed in low amounts so even a small increase in the mole fraction results in a large relative increase.

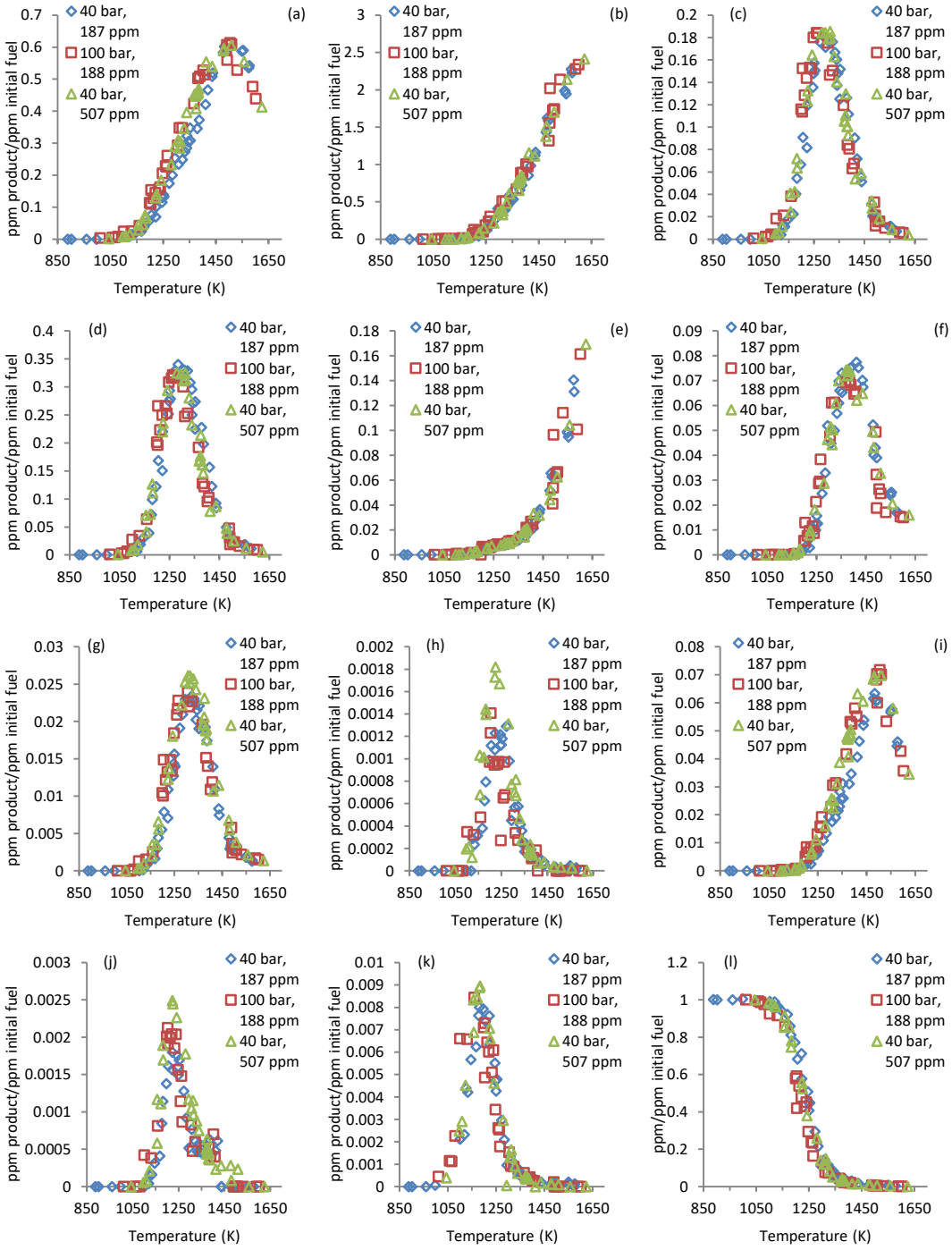

Figure 25: Comparison of product profiles of (a) methane, (b) acetylene, (c) propene, (d) 1,3-butadiene, (e) diacetylene, (f) vinylacetylene (g) 1,3-cyclopentadiene, (h) methylenecyclopentane, (i) benzene, (j) 1,3-cyclohexadiene, (k) cyclohexene and (l) methylcyclohexane obtained in the pyrolysis of methylcyclohexane at 40 bar and 187 ppm, 100 bar and 188 ppm, and 40 bar and 507 ppm. The mole fraction of each product is normalized by the initial mole fraction of the fuel.

5.3 Chemical Kinetic Modeling of Experimental Data

The 200 bar and 181 ppm of fuel methylcyclohexane experiments are compared against two chemical kinetic mechanisms. The highest pressure, or 200 bar, experimental set of data was chosen for this comparison due to the results obtained in the lower pressure and higher fuel concentration experiments conducted at 40 bar and 507 ppm of fuel being able to provide an excellent match to the higher pressure and lower fuel concentration experiments obtained at 100 bar and 188 ppm of fuel. This illustrated that at the current experimental conditions it is the initial fuel concentration in the reaction zone rather than pressure that impacts the product distribution. Additionally, one of the main interests in the present work is to generate high pressure and temperature speciation data for methylcyclohexane pyrolysis, so determining whether the mechanisms are capable of accurately predicting this new data is of particular interest.

5.3.1 Wang Mechanism

The first mechanism considered is the methylcyclohexane mechanism developed by Wang et al.[23] The mechanism was validated by Wang against low pressure methylcyclohexane pyrolysis flow reactor data obtained at pressures of 30, 150, and 760 torr and also against atmospheric pressure premixed flame data. While the mechanism has only been validated against sub-atmospheric to atmospheric pressure data, the data it has been validated against encompasses the largest amount of speciation data currently available for methylcyclohexane pyrolysis. The reaction rate constant coefficients which have been calculated by Wang were also calculated up to the high pressure limit despite the chemical kinetic mechanism being validated only against lower pressure data. Wang's methylcyclohexane mechanism is an extension of two previous iterations of the mechanism development and validation process. The previous iteration was a

cyclohexane mechanism[36], and the first iteration was a butene isomer mechanism[33]. At each point in the development process the mechanism was validated against low pressure flow reactor data. The core mechanism is comprised from reactions from USC Mech2[142], JetSurF2.0[132], the shock tube studies by Kiefer et al.[120,134] and other works[135–139,143–149].

Figure 26 contains the experimental species profiles of ethane, ethylene, propadiene, propyne, 1-butene, toluene, methane, acetylene, propene, 1,3-butadiene, diacetylene, vinylacetylene, 1,3-cyclopentadiene, methylenecyclopentane, benzene, 1,3-cyclohexadiene, cyclohexene, methylcyclohexane observed in 200 bar and 181 ppm of methylcyclohexane experiments and compares them against the simulated results obtained using Wang's mechanism, a modified version of Wang's mechanism, and the uncertainty curves obtained for the original version of Wang's mechanism which were obtained in the same fashion as described in the Cyclohexane chapter.

The main goal of the mechanism optimization was certainly to improve the mechanism's ability to capture current data; however, since the original mechanism has been validated at three stages of its development it would be prudent to allow the mechanism to retain the ability to continue to accurately capture low pressure data against which it was originally validated. To achieve this the mechanism optimization only involved modification of the reactions which had pressure dependent data in the PLOG formulation. This allowed the reaction rate constants for lower pressure data to remain as they were and only the high pressure reaction rate constants were modified.

Multiple approaches were taken in the optimization process in an attempt to achieve the best performing mechanism. These included: selecting the top two most positively (production)

and negatively (consumption) correlated reactions at each temperature from 900K to 1700K in steps of 50K for each species which was experimentally observed and predicted by the mechanism, leaving only the reactions which contain PLOG data, and assigning an uncertainty of factor of two to the remaining reactions. Selecting the top ten most positively and negatively correlated reactions to benzene from 900K to 1700K in steps of 50K and leaving only the reactions which had PLOG data which were then assigned an uncertainty of factor of two. Repeating the previous attempt, but for the carbon based least squared error calculation with respect to experimental data assigning a carbon number of 50, as opposed to the real carbon number of 6, to benzene to create an artificial bias towards capturing the benzene production accurately. Likewise repeating the previous attempt, but also assigning a carbon number of 50 to both propadiene and propyne. Lastly, assigning an uncertainty of a factor of 2 to all reactions with PLOG data regardless of their correlation coefficients with the proper carbon number for the species in the least squares error calculation.

The optimization method used has been developed and described by Fridlyand et al.[37] where the mechanism with the perturbed "A" factors and the lowest least squared error is saved as the optimized mechanism. The greatest interest in the mechanism optimization was to capture the experimental benzene profile more accurately. The importance of capturing benzene formation accurately is both practical since benzene is a soot precursor[170–173], but also the benzene observed in the experiments accounts for a substantial amount of the carbon flux. The mechanism chosen as the optimized mechanism was obtained from the optimization method which targeted the top ten most positively and negatively correlated reactions with respect to benzene in the 900K to 1700K temperature range which also contained PLOG reaction rate

coefficients since that mechanism produced results which gave the most substantial improvement in benzene prediction.

Both the original and optimized Wang mechanism predicted the initial formation temperatures of nearly all the experimentally observed species within 30K, or the estimated uncertainty in the experimental temperature. The three most abundant products observed, ethylene, methane, and acetylene, are all very well captured by both the original and optimized mechanisms. The ethylene peak is captured by both versions of the mechanism within 10% of the experimentally observed amount, and the increase and decay proceed at temperatures of approximately 30K lower than observed experimentally. The experimental methane profile is captured nearly exactly by the simulation results up to approximately 1500K at which point the simulation predicts a decay in methane whereas experimentally the peak amount and subsequent decay of methane is not observed until approximately 1600K. The acetylene prediction is also well captured but proceeding at temperatures up to 50K lower than observed experimentally until a temperature of approximately 1500K where the rate of increase of acetylene with increasing temperature begins decaying. Most of the less abundant product species such as ethane, 1-butene, propene, vinylacetylene, 1,3-cyclopentadiene, and cyclohexene are all well captured. The peak amounts are generally captured by both versions of the mechanism within 10% and the formation of the species up to the peak amount is also well captured within a temperature difference of approximately 30K. In some cases, particularly in the case of propene and vinylacetylene the decay is not as well predicted by the mechanisms, and falls outside a 30K difference in temperature; however, this is to be expected as the amount of benzene predicted by the original and optimized mechanisms is a factor of 2 and 1.7 larger than observed experimentally, so the

carbon flux to the benzene production results in a reduction of carbon flux going to the products of competing reactions.

As mentioned before, particular interest was in improving the prediction of benzene by the mechanism, and as just noted the original mechanism over predicted the peak amount of benzene observed in the experiments by a factor of two. The optimized mechanism improved the prediction, but the peak amount of benzene was still over predicted by a factor of 1.7. This improvement also came at a cost as the propadiene and propyne predictions suffered. The original mechanism was able to predict both propadiene and propyne production very well up until a temperature of approximately 1350K, which is the temperature at which the simulation predicts a peak in the amount of propadiene and propyne and a subsequent decay whereas experimentally the peak amount of propadiene and propyne is not observed until approximately 1400K and the peak amount of each species observed in the experiments is approximately 40% higher than predicted in the simulation. The modified mechanism decreased the temperature up to which the simulation predicts the experimental data down to approximately 1325K and the peak amount of propadiene observed experimentally was now approximately 60% higher than predicted by the simulation and the peak amount of propyne approximately 50% higher. Other most notable effects of the modified mechanism was an approximately 40% decrease in the peak amount of 1,3-cyclohexadiene predicted, which resulted in a better prediction of the experimental results, but the peak amount observed experimentally was still over predicted by a factor of 4. The peak amount of cyclohexene predicted by the modified mechanism also decreased by approximately 25% compared to the original mechanism, but in this case the prediction of experimental data degraded also by approximately 25%.

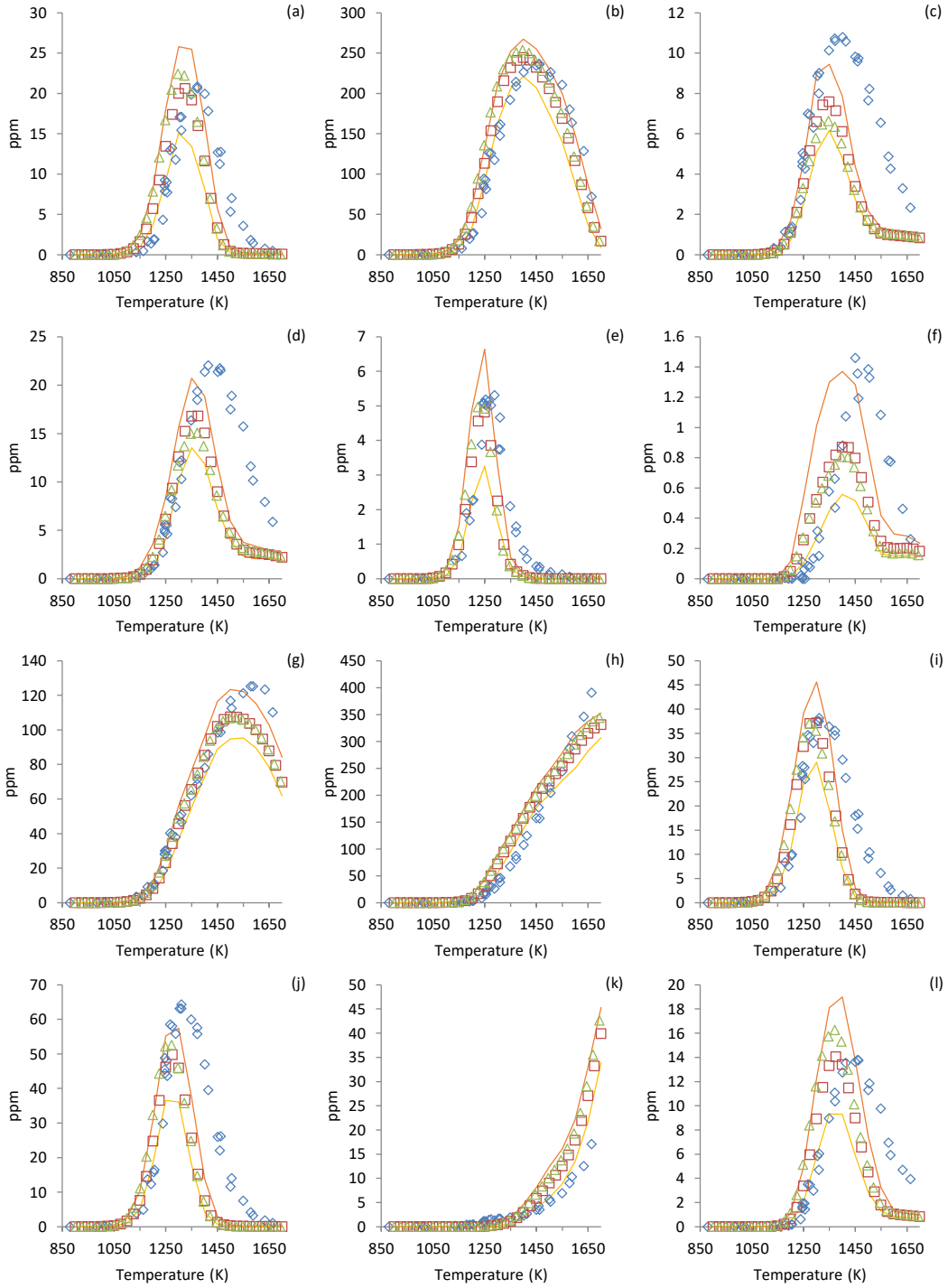
(a)
(b)
(c)
(d)
(e)
(f)
(g)
(h)
(i)
(j)
(k)
(l)
ppm
Temperature (K)
850
1050
1250
1450
1650

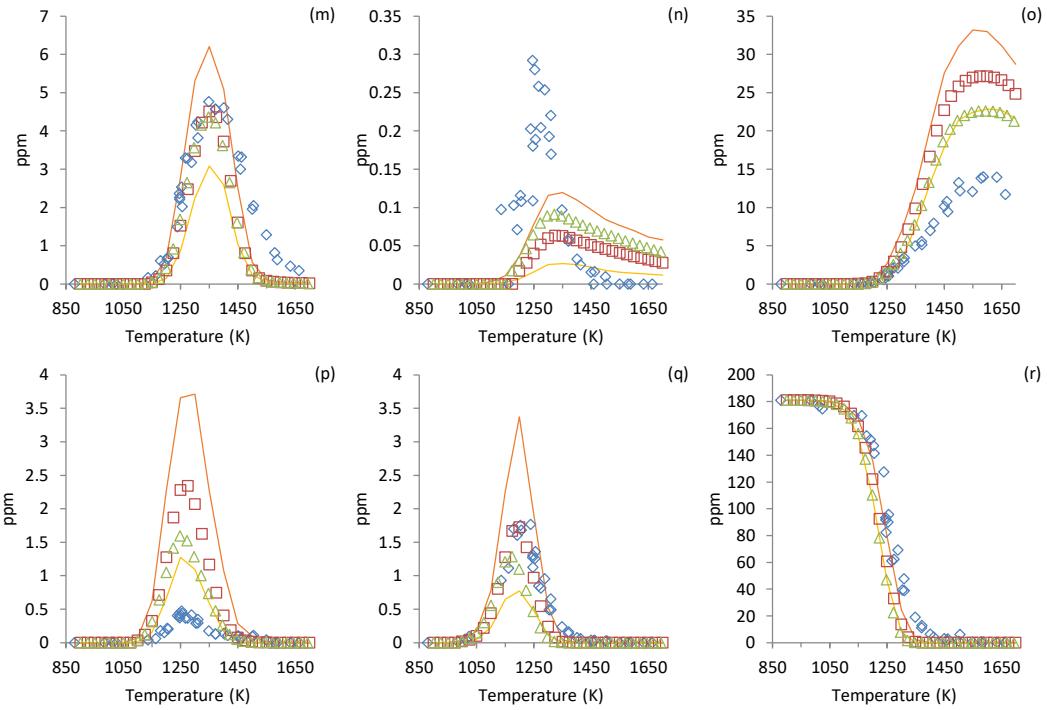

Figure 26: Comparison of species profiles of (a) ethane, (b) ethylene, (c) propadiene, (d) propyne, (e) 1-butene, (f) toluene, (g) methane, (h) acetylene, (i) propene, (j) 1,3-butadiene, (k) diacetylene, (l) vinylacetylene, (m) 1,3-cyclopentadiene, (n) methylenecyclopentane, (o) benzene, (p) 1,3-cyclohexadiene, (q) cyclohexene, (r) methylcyclohexane observed in 200 bar and 181 ppm of methylcyclohexane shock tube experiments versus those from a simulation using the methylcyclohexane mechanism developed by Wang[23], an optimized version of the Wang mechanism, and the bounds of uncertainty generated by prescribing a 30% uncertainty to all the A factors in the mechanism. Legend: ◇ Experimental Data, □ Wang Mechanism, △ Wang Optimized Mechanism, —— Maximum Species Mole Fraction from Monte Carlo Analysis, —— Minimum Species Mole Fraction from Monte Carlo Analysis.

5.3.1.1 ROP Analysis

In addition to the species data the rates of production (ROP) were obtained from the Chemkin[99] simulations for the benzene production and methylcyclohexane consumption at a representative temperature of 1350K and a reaction time of 2.2 ms. Figure 27 contains the visualization of the relative ROP analysis for benzene formation. The single most significant reaction contributing to the formation of benzene in both the original and modified versions of the Wang mechanism is the reaction of fulvene with hydrogen[138], accounting for 28% of the

relative ROP in the original mechanism and 33% in the modified mechanism. As a group, the C3 + C3 species recombination reactions account for the majority of the relative ROP for benzene with 56% of the relative ROP stemming from C3 + C3 recombination in the original mechanism and 52% in the modified mechanism. The recombination of propyne with the propargyl radical has the largest share of the relative ROP from the C3 + C3 reactions and contributes 24% of the relative ROP in the original mechanism and 26% in the modified mechanism. The propargyl recombination has the second largest share of C3 + C3 reactions with 21% of the relative ROP in the original mechanism and 15% in the modified mechanism, and propadiene and propargyl recombination contributes 11% of the relative ROP in both the mechanisms. The C4 + C2 recombination reactions have a small share in the overall relative ROP. The recombination of vinylacetylene with the vinyl radical contributes 2% of the relative ROP in the original mechanism and 3% in the modified mechanism, and the recombination of acetylene with the *n*C4H5 radical contributes 1% of the relative ROP in both mechanisms.

The ROP analysis comparison between the original and optimized mechanisms also provides another way of illustrating the impact of the modifications done to the optimized mechanism. The amount of 1,3-cyclohexadiene predicted by the mechanism has been previously been shown to decrease in Figure 26 and similarly the relative ROP from the cyclohexadienyl radical dropped from 14% to 11% in the optimized mechanism. The largest drop in the relative ROP is observed in the propargyl recombination. Propargyl has not been quantified experimentally and as such was not plotted in Figure 26, however, propadiene and propyne can both come from propargyl and have both been quantified and were observed to be predicted in lesser amounts by the modified mechanism. Fulvene has also not been quantified experimentally, and as such has not been plotted, but due to the large relative ROP stemming from the reaction of

fulvene with hydrogen it would be likely that an even better agreement between the modified model and experimental data could be achieved with a greater uncertainty than a factor of two were to be assigned to the "A" factor of that reaction.

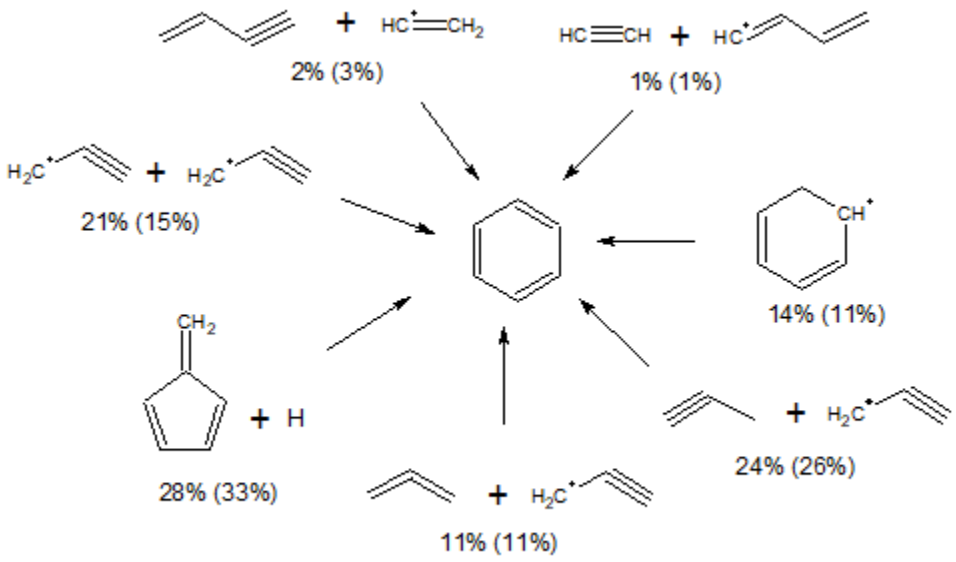

Figure 27: Visualization of the ROP analysis of benzene formation at a temperature of 1350K and reaction time of 2.2 ms. The percentages outside the parenthesis are the relative ROP from the unmodified Wang mechanism and the percentages in parenthesis are the relative ROP from the optimized Wang mechanism.

Figure 28 illustrates the visualization of the relative ROP of methylcyclohexane consumption. Half of the relative ROP of methylcyclohexane consumption results in the formation of the cyclohexyl and methyl radicals in the original mechanism and 63% in the modified mechanism. The large amount of the relative ROP resulting in the formation of the cyclohexyl radical emphasizes the importance of the cyclohexyl radical, and its decomposition pathways, not only in cyclohexane pyrolysis but also in the pyrolysis of methylcyclohexane. The formation of benzene can also proceed through the dehydrogenation of the cyclohexyl radical[23], however, the observed relative ROP from cyclohexadienyl radical decreased in the benzene ROP analysis for the optimized model illustrating that in the modified mechanism the

cyclohexyl dehydrogenation pathway has not been limited in the production of the cyclohexyl radical but further along the dehydrogenation pathway since the ROP for cyclohexyl radical increased whereas the ROP of benzene from 1,3-cyclohexadiene decreased in the optimized model. The relative ROP decreased from 9% to 6% for the 2-methyl-cyclohexyl radical, from 10% to 7% for the 3-methyl-cyclohexyl radical, and from 6% to 4% for the 4-methyl-cyclohexyl radical from the original to modified mechanism. The relative ROP of the cyclohexylmethyl radical and 1-methyl-cyclohexyl radical remained the same at 1% and 5%, respectively, between the two mechanisms. The relative ROP of the 1-heptene and 2-heptene also decreased from 3% to 2% and 10% to 8%, respectively, from the original to modified mechanism.

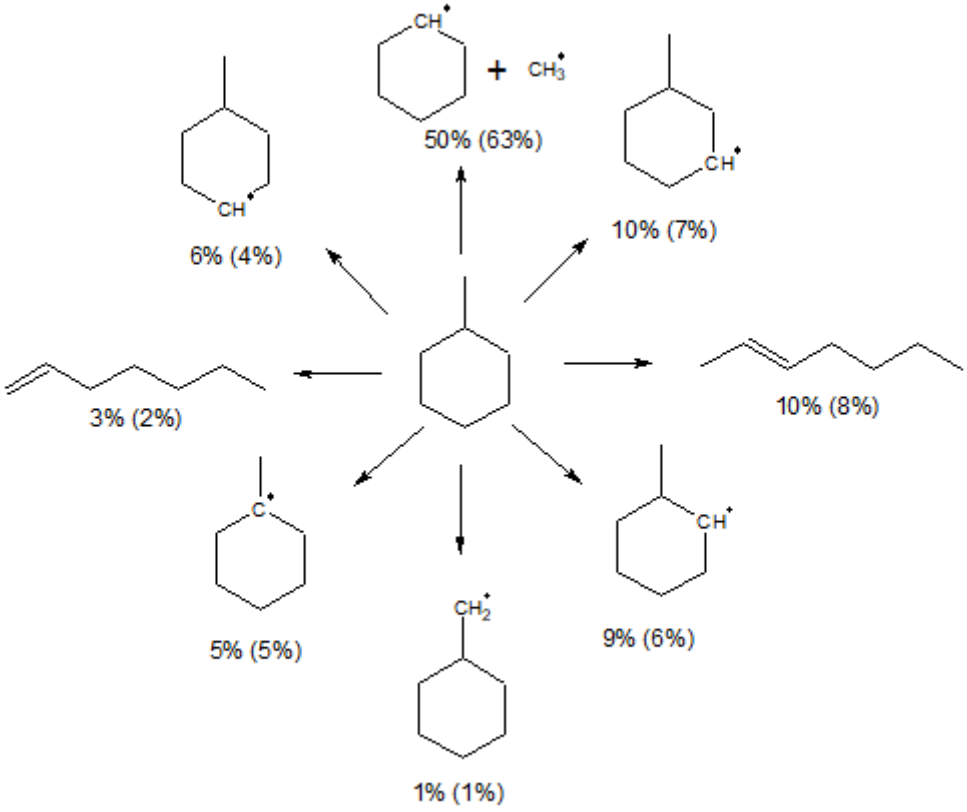

Figure 28: Visualization of the ROP analysis of methylcyclohexane consumption at a temperature of 1350K and reaction time of 2.2 ms. The percentages outside the parenthesis are the relative ROP from the unmodified Wang mechanism and the percentages in parenthesis are the relative ROP from the optimized Wang mechanism.

Figure 29 provides a visual representation of the main decomposition pathways of methylcyclohexane predicted by the Wang mechanism which proceed either through the cyclohexyl radical or the 1-methyl-cyclohexyl radical. The pathway analysis was performed using the Chemkin Reaction Path Analyzer tool[99]. The 1-methyl-cyclohexyl radical was chosen as a representative pathway for the decomposition of the remaining methyl-cyclohexyl radicals which have analogous decomposition pathways. The cyclohexyl radical will primarily either undergo ring opening to form the hex-5-en-1-yl radical, or after the loss of hydrogen will form cyclohexene which will mainly decompose into 1,3-butadiene and ethylene. The hex-5-en-1-yl radical can undergo ring closure forming the cyclopentylmethyl radical which then can form methylenecyclopentane. This is a minor pathway but is included because methylenecyclopentane was the only alkenylcyclopentane observed experimentally. The main decomposition pathways of hex-5-en-1-yl radical involve undergoing either a 1,4-hydrogen shift which results in the formation of hex-5-en-4-yl radical, or beta-scission which forms ethylene and but-3-en-1-yl radical. The hex-5-en-4-yl radical will likewise primarily undergo beta-scission forming 1,3-butadiene and ethyl radical.

The decomposition pathway proceeding through the 1-methyl-cyclohexyl radical is similar to that seen in the cyclohexyl radical in that the 1-methyl-cyclohexyl radical will either undergo hydrogen loss forming 1-methylcyclohexene or ring opening resulting in the 5-methyl-hex-5-en-1-yl radical. The 5-methyl-hex-5-en-1-yl radical will either undergo 1,4-hydrogen shift resulting in the 5-methyl-hex-5-en-4-yl radical or decompose through beta-scission forming ethylene and 3-methyl-but-3-en-1-yl radical. The 5-methyl-hex-5-en-4-yl radical will also primarily decompose through beta-scission resulting in 3-methyl-1,3-butadiene and ethyl radical.

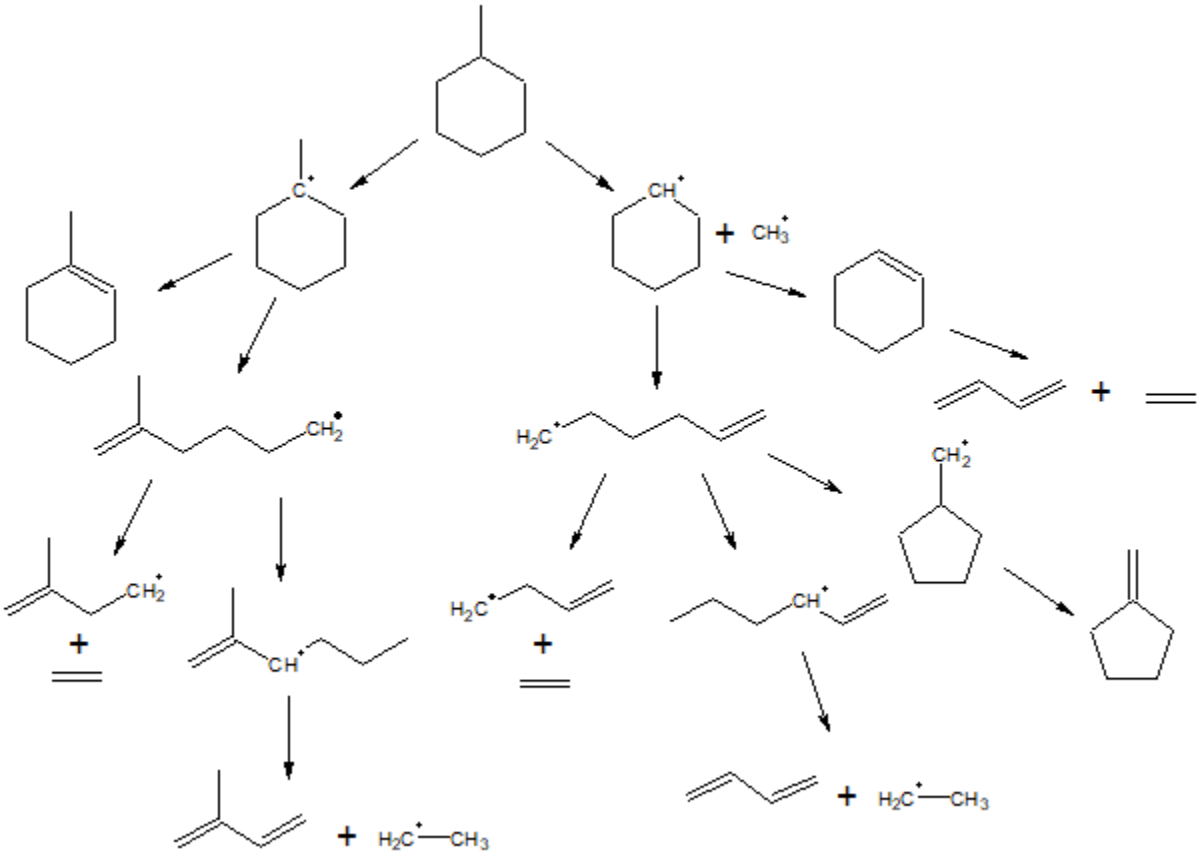

Figure 29: Main methylcyclohexane decomposition pathways proceeding through the cyclohexyl and 1-methylcyclohexyl radicals at 1350K and 2.2ms.

5.3.2 RMG Mechanism

The second mechanism to be compared with the experimental data was generated using RMG[101]. The mechanism was generated at a pressure of 200 bar and with 181 ppm of methylcyclohexane as the fuel and the option to generate PLOG coefficients, as necessary, was enabled. The 200 bar pressure environment was chosen for the generation of the mechanism due to the obtained experimental results which showed that the product distribution of higher pressure experiments can be matched at lower experimental pressures if initial fuel concentration in the reaction zone is equal in both experimental sets, at least at the present conditions. Additionally, one of the interests of this work is the investigation of whether the formation of

alkylcyclopentanes can be driven by high pressure in the gas phase, so there is interest in capturing the high pressure chemistry. Similar to the mechanism generated for Cyclohexane, the Chernov[151] and the JetSurF2.0[132] seed mechanisms were used to generate the mechanism. The mechanism uncertainty analysis and optimization were also undertaken in the exact same fashion as described previously in the Cyclohexane chapter.

Figure 30 provides a comparison of the experimental data obtained at 200 bar with 181 ppm of methylcyclohexane as the fuel and compares it against the generated RMG mechanism, the uncertainty bands due to a prescribed 30% uncertainty in the "A" factor of the reaction rate coefficients, and the optimized mechanism for the following species: ethane, ethylene, propadiene, propyne, 1-butene, toluene, methane, acetylene, propene, 1,3-butadiene, diacetylene, vinylacetylene, 1,3-cyclopentadiene, methylenecyclopentane, benzene, 1,3-cyclohexadiene, cyclohexene, and methylcyclohexane. Ethylene and acetylene, the two most abundant products, are well captured by both the original and modified versions of the RMG mechanism. For ethylene the modified mechanism better captures the peak amount formed, and there is also a slight improvement in capturing the decay compared to the original mechanism, but the decay is still predicted to occur at temperatures approximately 30K lower than observed experimentally. For acetylene, the improvement is observed at temperatures below 1600K where the original model predicted the acetylene formation to occur at temperatures approximately 10K lower than observed experimentally. The methane prediction also saw an improvement with originally the peak amount being slightly over predicted, by approximately 5%, whereas the modified model predicts the peak amount to within 1% and there is also an improvement in capturing the formation temperature, although overall the formation of methane still proceeds at temperatures up to 80K lower than observed experimentally. Propyne, propene, and 1,3-

butadiene also see as slight improvement in the modified model in terms of capturing the peak amount and the formation temperatures. There is also an improvement in capturing the formation temperatures of diacetylene, and vinylacetylene, although the optimized mechanism under predicts the peak amount of vinylacetylene formed. The remaining species such as ethane, propadiene, 1-butene, toluene, 1,3-cyclopentadiene, methylenecyclopentane, and cyclohexene were all minor products and their prediction worsened. This is not a surprising result since the optimization involves calculating the least squared error based on carbon, so species which account for a larger portion of the carbon flux will see an improvement in their profiles while the prediction of minor product species will be sacrificed to better capture the overall carbon flux.

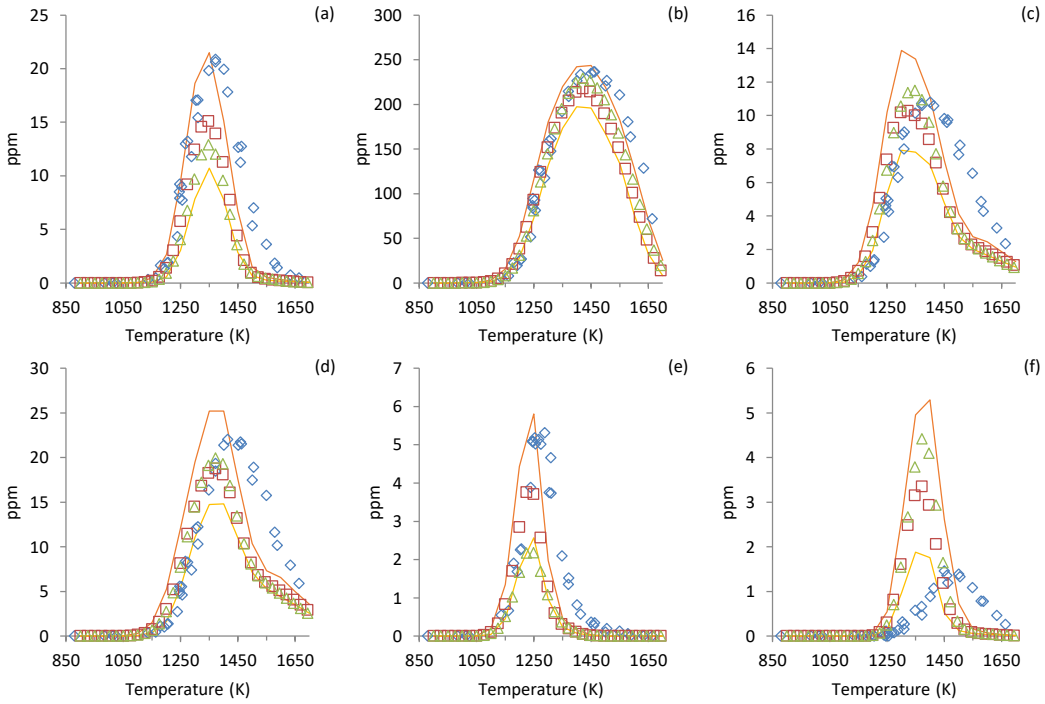

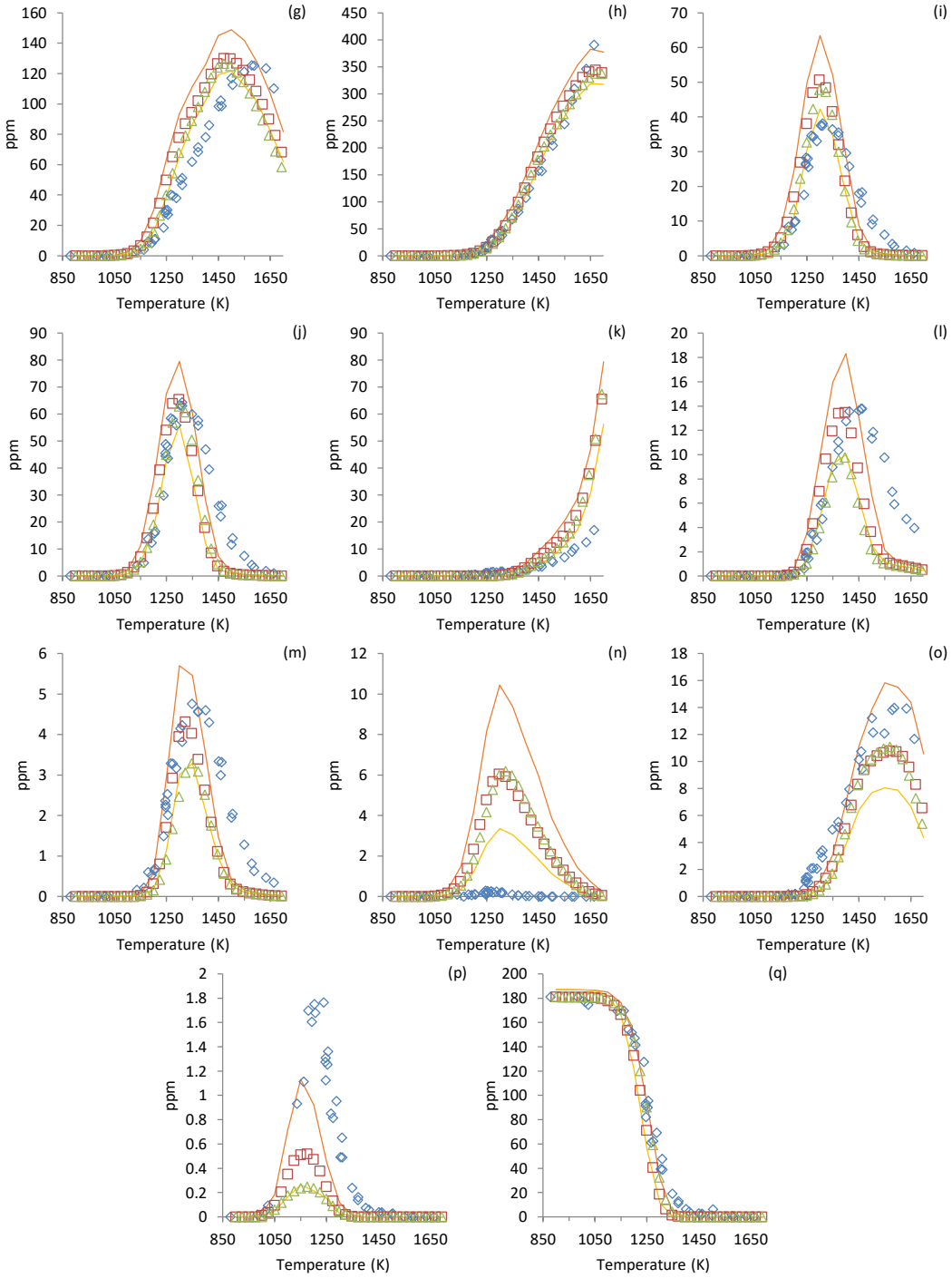

Figure 30: Comparison of species profiles of (a) ethane, (b) ethylene, (c) propadiene, (d) propyne, (e) 1-butene, (f) toluene, (g) methane, (h) acetylene, (i) propene, (j) 1,3-butadiene, (k) diacetylene, (l) vinylacetylene, (m) 1,3-cyclopentadiene, (n) methylenecyclopentane, (o) benzene, (p) 1,3-cyclohexadiene, (q) cyclohexene, (r) methylcyclohexane observed in 200 bar and 181 ppm of methylcyclohexane shock tube experiments versus those from a simulation using the methylcyclohexane mechanism generated with RMG, an optimized version of the RMG generated mechanism, and the bounds of uncertainty generated by prescribing a 30% uncertainty to all the A factors in the mechanism. Legend: ◇ Experimental Data, □ Wang Mechanism, △

Wang Optimized Mechanism, —— Maximum Species Mole Fraction from Monte Carlo Analysis, —— Minimum Species Mole Fraction from Monte Carlo Analysis.

5.3.2.1 ROP Analysis

Just as for the Wang mechanism, ROP analysis was completed for benzene formation at a representative temperature of 1350K and reaction time of 2.2 ms using the RMG generated mechanism. Figure 31 contains the visualization of the ROP analysis with the percentages outside the parenthesis being the relative ROP for the formation of benzene obtained from the original RMG mechanism and the percentages in the parenthesis are the relative ROP obtained from the optimized mechanism. One immediate difference which is observed in contrast to the benzene ROP analysis for the Wang mechanism, show in Figure 27, is that there is no benzene formation reaction involving fulvene. This is because the Chernov mechanism does not contain such a reaction. Similar to the Wang mechanism, as a group the C3+C3 recombination reactions have the greatest contribution to benzene formation accounting for 54% of the relative ROP of benzene formation in the original RMG mechanism and 61% in the optimized mechanism. The propyne and propargyl recombination reaction is not included in the Chernov mechanism, while it is in the Wang mechanism, and both the propadiene and propargyl, and propargyl recombination reactions have approximately double the contribution to the relative ROP of benzene in the RMG mechanism compared to the Wang mechanism. The increase in the contribution to the relative ROP of benzene formation by the propadiene and propargyl recombination reaction in the optimized mechanism can also be observed in the species profiles where propadiene production increased in the optimized mechanism.

The C4+C2 species recombination reactions also have a greater contribution to the production of benzene in the RMG mechanism. The *i*C4H5 radical and acetylene recombination reaction accounts for 22% of the relative ROP of benzene in the original RMG mechanism and

16% in the optimized mechanism. The remaining C4 + C2 recombination reactions include the recombination of 2-butynyl radical and acetylene, 1,3-butadiene and ethynyl radical, acetylene and vinylacetylene, and vinylacetylene and ethynyl radical. Together they account for 18% of the relative ROP in the original RMG mechanism and 15% in the optimized mechanism. The reason for this reduction can also be observed in the species profiles where the production of most of the C4 and C2 species was reduced in the optimized mechanism. The last reaction to contribute to formation of benzene is the reaction of toluene with hydrogen which results in the cleavage of the methyl group in toluene. The contribution of this reaction increases from 5% in the original mechanism to 8% in the optimized mechanism, which is not surprising since the amount of toluene predicted by the optimized mechanism increased.

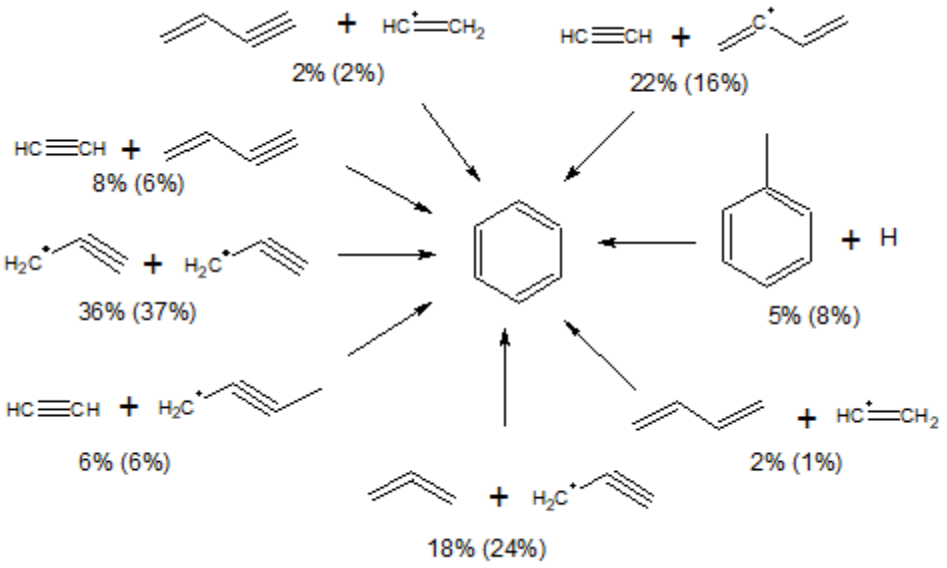

Figure 31: Visualization of the ROP analysis of benzene formation at a temperature of 1350K and reaction time of 2.2 ms. The percentages outside the parenthesis are the relative ROP from the unmodified RMG mechanism and the percentages in parenthesis are the relative ROP from the optimized RMG mechanism.

Figure 32 contains the visual representation of the ROP analysis for the initial methylcyclohexane decomposition reactions. There are fewer immediate products in the RMG mechanism since the RMG mechanism does not contain direct isomerization pathways to 1-

heptene and 2-heptene like the Wang mechanism. Also, the Wang mechanism predicted a small portion of the relative ROP, 1% for both the original and optimized Wang mechanisms, to result in the formation of the cyclohexylmethyl radical which is not predicted to form in the RMG generated mechanism. One similarity between the two mechanisms is that the main decomposition pathway results in the formation of the cyclohexyl radical for both versions of both mechanisms, although in the optimized RMG mechanism the relative ROP for the pathway drops to 32% from 40% in the unmodified RMG mechanism. The 3-methyl-cyclohexyl radical also has the largest relative ROP out of all the methyl-cyclohexyl radicals in the RMG mechanism just as in the Wang mechanism, although the relative ROP in the RMG mechanism is nearly twice as large. Likewise, the 4-methyl-cyclohexyl radical has the lowest relative ROP in both the mechanisms. The 3-methyl-cyclohexyl and the 1-methyl-cyclohexyl radicals both saw an increase in their relative ROP while the 2-methyl-cyclohexyl relative ROP dropped and the 4-methyl-cyclohexyl radical remained the same in the optimized RMG mechanism compared to the unmodified RMG mechanism.

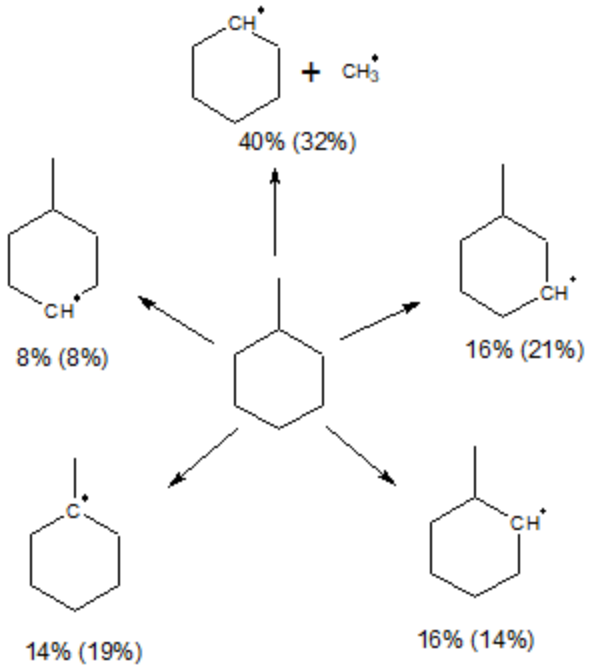

Figure 32: Visualization of the ROP analysis of methylcyclohexane consumption at a temperature of 1350K and reaction time of 2.2 ms. The percentages outside the parenthesis are the relative ROP from the unmodified RMG mechanism and the percentages in parenthesis are the relative ROP from the optimized RMG mechanism.

Figure 33 contains the main reaction paths for the methylcyclohexane decomposition proceeding through the cyclohexyl radical at a temperature of 1350K and 2.2 ms reaction time in the RMG generated mechanism which were obtained with the help of the Chemkin Reaction Path Analysis tool[99]. The cyclohexyl radical can either primarily form cyclohexene or undergo ring opening to form the hex-5-en-1-yl radical, the same as seen in the Wang mechanism reaction pathways. Cyclohexene will then primarily dissociate into 1,3-butadiene and ethylene, which is again the same as in the Wang mechanism. The hex-5-en-1-yl radical can either form 1,5-hexadiene, undergo beta-scission forming ethylene and but-3-en-1-yl, undergo a 1,4-hydrogen shift forming the hex-5-en-4-yl radical, or isomerize to the hex-4-en-3-yl. Both the hex-4-en-3-yl and hex-5-en-4-yl radicals can then either form 1,3-hexadiene or undergo beta-

scission forming 1,3-pentadiene and the methyl radical or 1,3-butadiene and the ethyl radical, respectively.

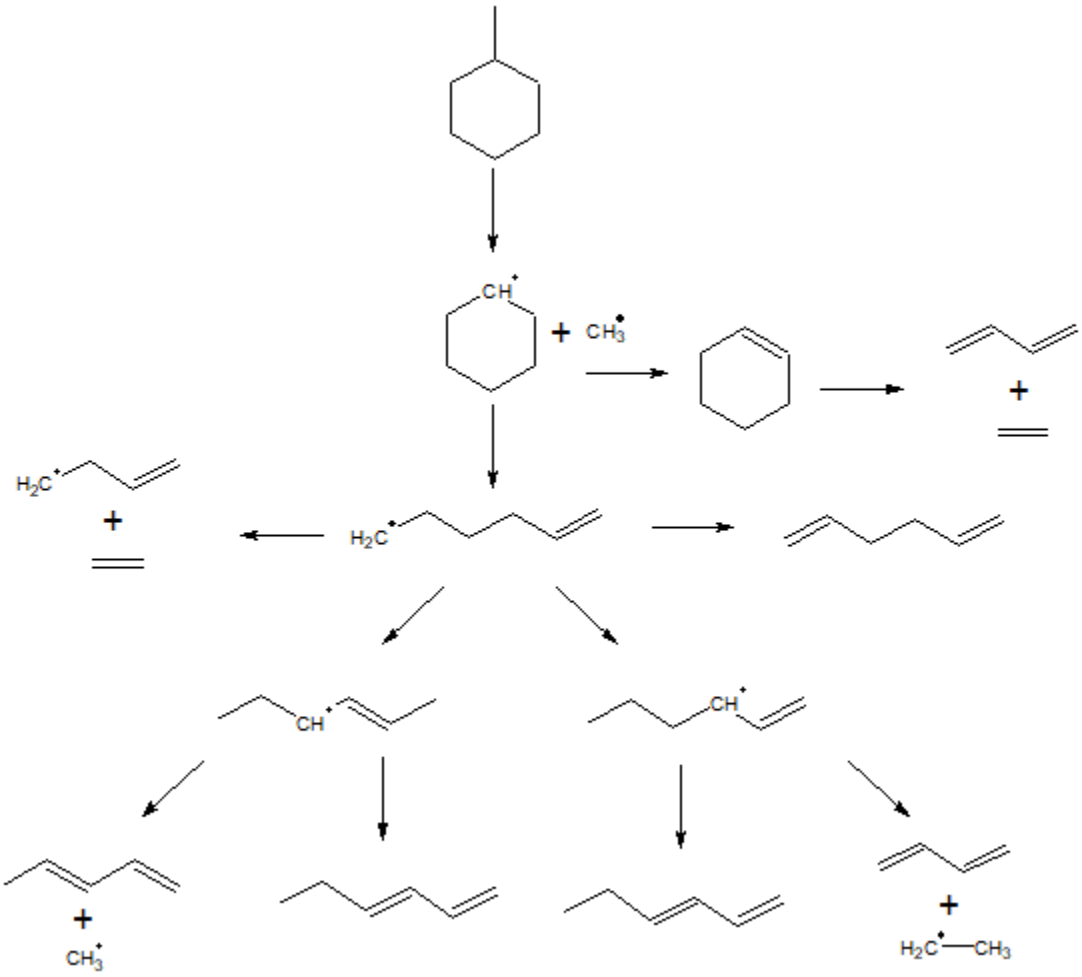

Figure 33: Main methylcyclohexane decomposition pathways proceeding through the cyclohexyl radical at 1350K and 2.2ms.

Figure 34 contains the main methylcyclohexane decomposition pathways proceeding through the 1-methyl-cyclohexyl radical at a temperature of 1350K and reaction time of 2.2ms in the RMG generated mechanism. The 1-methyl-cyclohexyl radical was chosen as a representative case for the remaining methyl-cyclohexyl radicals, and also because the main methylenecyclopentane formation pathway proceeds through the 1-methyl-cyclohexyl radical.

The 1-methyl-cyclohexyl radical undergoes ring opening forming the 5-methyl-hex-5-en-1-yl radical which can undergo beta-scission forming ethylene and 3-methyl-but-3-en-1-yl radical, just as in the Wang mechanism, ring closure forming the cyclopentyl-1,1-methyl radical, or 1,6-hydrogen shift forming the 5-methyl-hex-5-en-6-yl. The 5-methyl-hex-5-en-6-yl radical then undergoes a 6,2-hydrogen shift forming the 5-methyl-hex-5-en-2-yl radical which after beta-scission forms propene and 2-methyl-prop-2-en-1-yl radical. The formation of the cyclopentyl-1,1-methyl radical is a minor 5-methyl-hex-5-en-1-yl dissociation pathway but it is the major methylenecyclopentane production pathway which forms after the cleavage of the methyl group in the cyclopentyl-1,1-methyl radical and as such was included in the pathway diagram.

Overall, both the unmodified and optimized versions of the Wang mechanism and the RMG mechanism are able to capture the profiles of the most abundant product species, namely methane, ethylene, and acetylene. The RMG mechanism is able to better capture the peak amounts of the most abundant species, and it also does a better job of predicting the propadiene and propyne peak amounts whereas the Wang mechanism under predicts the peak amounts of both of those species. The RMG mechanism is also able to better predict the benzene profile while the Wang mechanism over predicts the amount of benzene by approximately a factor of two compared to what was observed experimentally. The improved predictions by the RMG do come at a cost as the mechanism contains 19799 reactions and 292 species compared to the 1570 reactions and 251 species in the Wang mechanism. The Wang mechanism has also been validated against the authors' own data, and it includes oxidation reactions. If computational effort and time is a concern, and/or the mechanism is to be used over a wider range of conditions then the Wang mechanism would be preferable. If the desire is to capture the chemistry at

conditions close to those in the present study and computational effort and time are not a concern, then the RMG mechanism should be used.

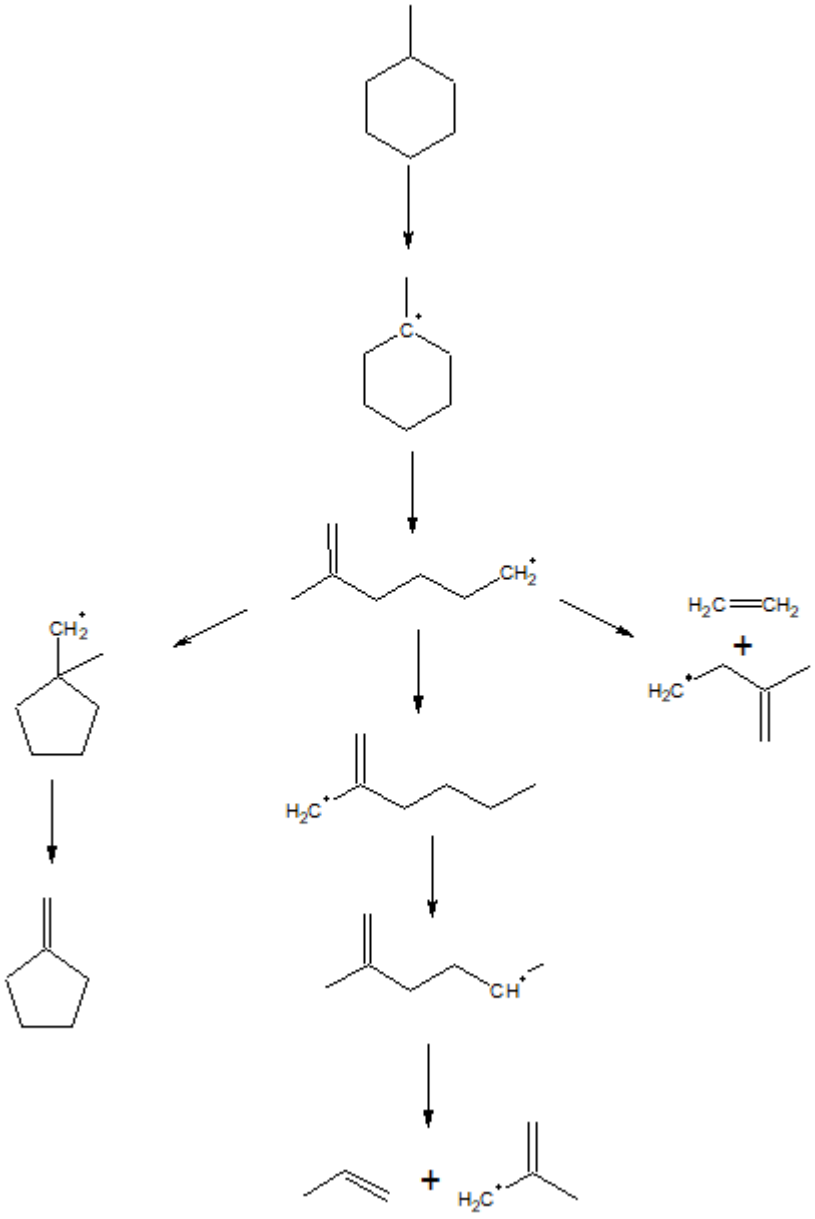

Figure 34: Main methylcyclohexane decomposition pathways proceeding through the 1-methyl-cyclohexyl radical at 1350K and 2.2ms.

5.4 Summary

Ethane, propadiene, propyne, 1-butene, and toluene were observed to have their production rates and the peak amounts effected by a variation of experimental pressure in methylcyclohexane experiments completed at nominal pressures of 40, 100, and 200 bar. It was further found that the 100 bar species data was reproducible at 40 bar when an additional set of experiments was completed at 40 bar with a higher mole fraction of the fuel in order to match the concentration in the reflected shock reaction zone present at 100 bar. This illustrated that at least at the experimental conditions present, it is the initial concentration of fuel that determines the final species composition rather than the pressure. No alkylcyclopentanes were observed to form despite the pressures in the reaction zone matching and exceeding those observed in methylcyclohexane pyrolysis experiments completed under supercritical conditions[19–21]. Unlike the supercritical methylcyclohexane experiments, the current experiments used dilute fuel mixtures and had far lower concentrations of methylcyclohexane present in the reaction zone again supporting the importance of the initial fuel concentration on the product distribution.

The experimental data was compared with two chemical kinetic mechanisms. A literature mechanism developed based on sub-atmospheric to atmospheric flow reactor data[23], and a generated mechanism with RMG[101]. Both the mechanisms were capable of predicting the major product species well. The literature mechanism was capable of capturing the current experimental results very well despite the large differences present in the experimental methods used and in experimental pressures present in the data used to validate the mechanism and those in this study; however, the mechanism struggled with the prediction of some species, mainly propadiene, propyne, and benzene and would benefit from further refinement of the mechanism. The RMG mechanism is recommended if computational effort and time are not a substantial

concern since it is able to better capture the current data. The Wang mechanism is also able to capture the current data well, contains an order of magnitude fewer reactions, and was validated against lower pressure data in addition to the current data. If the mechanism is to be used over a wide range of conditions and computational effort is a concern, then the Wang mechanism would be the appropriate choice.

6. 6-BROMO-1-HEXENE PYROLYSIS

6.1 Introduction

The hex-5-en-1-yl radical plays an important role in the dissociation of alkylcyclohexanes. An example illustrating this has been presented in a laminar flame speed study by Ji et al. which used cyclohexane and alkylcyclohexanes up to n-butylcyclohexane as fuels and included the comparison of three published mechanisms against the experimental data[29]. The mechanisms used were JetSurF1.1[174], Dagaut and Cathonnet's kerosene model[35], and Silke et al. cyclohexane oxidation model[34]. All three mechanisms predicted that over 95% of cyclohexane dissociates into the cyclohexyl radical. Dagaut's and Silke's model both predicted that approximately 95% of the cyclohexyl radical then isomerizes to the hex-5-en-1-yl radical, and JetSurF1.1 predicted that 73% of cyclohexyl radial will isomerize to hex-5-en-1-yl. JetSurF1.1 was also validated against the shock tube ignition data of Hong, with similar results obtained in the cyclohexane and cyclohexyl dissociation analysis[167]. A study similar to that of Ji[29] was completed by Liu which investigated the flame ignition temperatures of cyclohexane and alkylcyclohexanes up to n-butylcyclohexane[30], and compared the experimental results against the JetSurF2.0 mechanism[132] and Dagaut's mechanism[35] with similar findings in regards to the branching of cyclohexane and cyclohexyl dissociation. Two other modeling efforts of cyclohexane flames by McEnally and Pfefferle[31] and Zhang et al.[32] have likewise proposed the reaction pathway of cyclohexane dissociation to cyclohexyl radical which then isomerizes to hex-5-en-1-yl as the major reaction pathway.

In recent shock tube experimental and modeling work on the effect of exhaust gas recirculation on the autoignition of gasoline surrogates, it was found that the mechanism predicted all of the cyclohexane in the surrogate mixture to be converted to the cyclohexyl

radical which isomerizes to form the hex-5-en-1-yl radical[115]. Sirjean et al. proposed that the branching ratio of the dissociation of cyclohexyl radical to cyclohexene and hex-5-en-1-yl is about 1:1 in his shock tube study on the autoignition of cyclohexane[130]. Cyclopentylmethyl and cyclohexyl were suggested as the only unimolecular products of hex-5-en-1-yl radical dissociation, with the formation of cyclopentylmethyl becoming more favorable with increasing pressure, in the theoretical work by Matheu et al. about capturing the pressure dependence of the cycloalkyl reactions[175]. The possibility of hex-5-en-1-yl isomerizing to either the cyclohexyl radical or cyclopentylmethyl was also proposed by Gierczak et al. in an earlier study, and methylcyclopentane was quantified as one of the products in the cyclohexene and hydrogen sulphide photolysis experiments at pressures of 8.6 to 77 torr[176].

Peukert et al. completed two shock tube studies around a pressure of 2 bar investigating the decomposition pathways of cyclohexane[124,125]. Peukert determined in the first study that 1-hexene is the sole product of cyclohexane undergoing unimolecular dissociation[124]. Peukert's second study investigated the hydrogen abstraction reactions of cyclohexane[125]. The proposed reaction pathway in the second study was the formation of the cyclohexyl radical followed by ring opening/isomerization to the hex-5-en-1-yl radical. To study the decomposition of hex-5-en-1-yl radical, Peukert used 6-iodo-1-hexene as a precursor, and based on those experiments proposed two possible reaction pathways for the dissociation of hex-5-en-1-yl. The first involved the C-C scission of hex-5-en-1-yl, or the C-C scission of hex-5-en-4-yl radical if hex-5-en-1-yl underwent a 1,4 hydrogen shift then, or the 5-exo-cyclization which resulted in isomerization to the cyclopentylmethyl radical. Peukert determined the reaction rate coefficients for the 5-exo-cyclization reaction based on his work that were between those proposed by Granata et al.[127] and Sirjean et al.[126]

The isomerization reaction of the hex-5-en-1-yl, or more commonly 5-hexenyl, to cyclopentylmethyl is widely known and frequently utilized in organic chemistry as a radical clock for reactions with unknown rates at room or near room temperatures[177–179]. Reduction experiments of 6-bromo-1-hexene, a hex-5-en-1-yl precursor, by tributyltin hydride at temperatures of 40 to 130 degrees Celsius have found the methylcyclopentane yield to exceed 90% depending on the concentration of tributylstannane, with the yield being inversely proportional to the concentration of tributylstannane and temperature[180]. Methylcyclopentane has also been found to be a major product in cyclohexane pyrolysis experiments conducted in the supercritical phase by Lai and Song[19]. Similarly, alkylcyclopentanes have been found to be the dominant products in the pyrolysis of alkylcyclohexanes in the supercritical phase[19–21] with the proposed reaction paths analogous to the formation of methylcyclopentane in cyclohexane pyrolysis, i.e. cyclohexane -> cyclohexyl radical -> hex-5-en-1-yl radical -> cyclopentylmethyl radical -> methylcyclopentane[20]. The reaction pathway involving the hex-5-en-1-yl radical is additionally important in the pyrolysis of alkylcyclohexanes because the same reaction pathway is possible after the cleavage of the alkyl group from the alkylcyclohexane fuel resulting in the formation of cyclohexyl radical[167,169]. Alkylcyclopentanes have also been found to be both sooting[22] and coking[21] precursors; therefore, gaining a better understanding of the conditions needed for their formation is beneficial to the optimization of the performance of combustion systems.

Despite the importance of hex-5-en-1-yl in the chemical kinetic modeling of combustion and pyrolysis of cyclohexane, and alkylcyclohexanes, there has only been one experimental study conducted at combustion relevant temperatures seeking to investigate the pyrolysis of hex-5-en-1-yl, which is the work by Peukert[125] utilizing 6-iodo-1-hexene as the precursor to hex-5-

en-1-yl. Additionally, the work by Peukert only encompassed a 100 Kelvin (K) temperature range from 1060 to 1160 K, at a pressure of about 2 bar, and only the H atom profiles were measured. It is the aim of this study to investigate the pyrolysis of hex-5-en-1-yl by using 6-bromo-1-hexene as the precursor to quantify the stable species products at target, or nominal, pressures of 40, 100, and 200 bar encompassing a temperature range of approximately 900 to 1450 K. 6-Bromo-1-hexene was used rather than 6-iodo-1-hexene because the high pressure experiments required high pressure test gas mixtures, and the 6-iodo-1-hexene species is less volatile than 6-bromo-1-hexene and it was found to dissociate in the heated test gas cylinder while the test gas mixture was allowed to homogenize overnight. Figure 35 a) provides one of the proposed pathways for the formation of alkylcyclopentanes in the supercritical phase experiments[20]. Figure 35 b) illustrates an analogous pathway that begins with 6-bromo-1-hexene. The pathway in Figure 35 b) is the same pathway that is expected to occur in the pyrolysis of cyclohexane. Cyclohexane would first undergo hydrogen loss forming the cyclohexyl radical that upon ring opening would form the hex-5-en-1-yl radical. The benefit of using 6-bromo-1-hexene to investigate this pathway is that the hex-5-en-1-yl radical can be obtained immediately following the bromine loss of 6-bromo-1-hexene so the competing reaction pathways of cyclohexane dissociation (such as isomerization to 1-hexene) or the cyclohexyl radical dissociation (such as the formation of cyclohexene) will not occur. The drawback is that 6-bromo-1-hexene may also undergo HBr loss resulting in the formation of 1,5-hexadiene. For the pathway in Figure 35 b) to be truly analogous with that shown in Figure 35 a) the final product of hex-5-en-1-yl radical ring closure should be methylcyclopentane; however, the final product shown is methylenecyclopentane. The prediction of methylenecyclopentane being the final product of hex-5-en-1-yl radical ring closure is based on the cyclohexane and

methylcyclohexane pyrolysis findings, discussed in their respective chapters, in which only methylenecyclopentane was quantified, in trace amounts, and no alkylcyclopentanes were observed to form. Due to the high pressures present in the present work it will be possible to make a direct comparison of the product distribution with those observed in the supercritical phase experiments on the basis of the experimental pressure, and whether an abundance of alkylcyclopentanes will be observed to form in the gas phase.

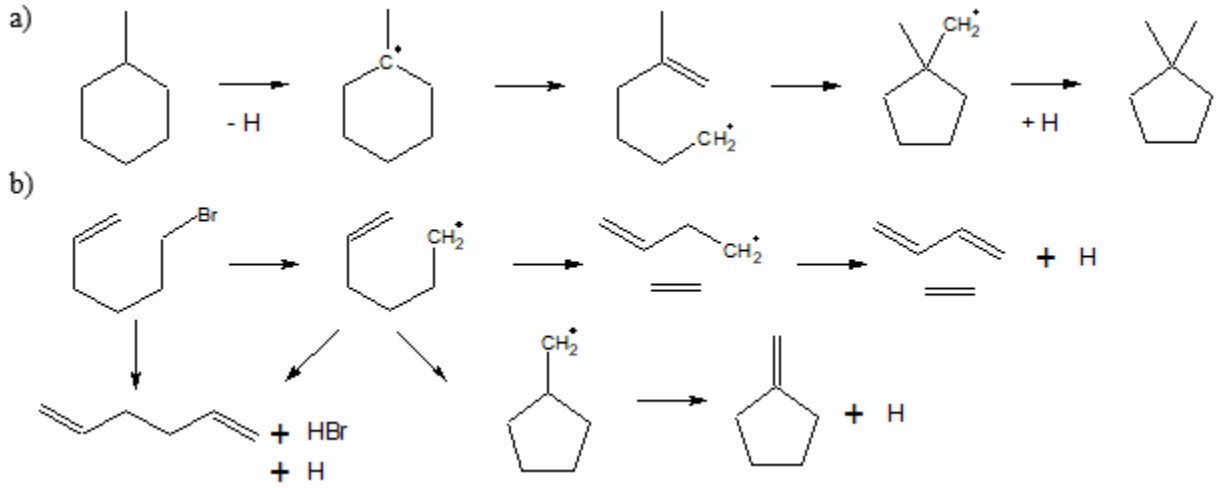

Figure 35: a) methylcyclohexane reaction pathway leading to 1,1-dimethylcyclopentane formation, b) three competing 6-bromo-1-hexene decomposition reaction pathways leading to the formation of 1,5-hexadiene, 1,3-butadiene and ethylene, and methylenecyclopentane.

6.2 Experimental Results

6.2.1 Effects of Pressure on 6-Bromo-1-hexene Pyrolysis

Three sets of shock tube pyrolysis experiments were conducted with 6-bromo-1-hexene as the fuel at three nominal pressures. The target pressures were 40, 100, and 200 bar with a nominal reaction time of 2.2 milliseconds (ms.) The actual pressure and experimental conditions for each individual experiment are included in APPENDIX D. The mole fraction of 6-bromo-1-hexene in the test gas mixture was 164, 162, and 161 ppm for the 40, 100, and 200 bar experiments, respectively. The mole fraction of the fuel in the test gas was obtained by GC

sampling of the test gas mixture after it was allowed to homogenize at least 12 hours post preparation allowing it to be ready for use in the experiments.

Figure 36 has the species mole fraction profiles as a function of temperature of ethane, ethylene, propane, propadiene, propyne, and toluene. The amount of ethane, ethylene, propane, and toluene observed in the experiments at 40 bar was lower than in the 100 and 200 bar experiments. The peak amount of ethane observed increased by approximately 144% and 36% with an increase in the experimental pressure from 40 to 100 bar, and 100 to 200 bar, respectively. A similar trend is seen in the peak amount of propane obtained with an increase of 126% when the experimental pressure increased from 40 to 100 bar, and 48% when the experiment pressure was increased from 100 to 200 bar. For both ethane and propane, the amount observed at 40 bar was lower following the initial formation temperature compared to the amount recovered at 100 and 200 bar. The difference in the species profiles was not as substantial between the 100 and 200 bar profiles, for ethane and propane, where the amounts recovered at 100 and 200 bar following the initial formation temperature were equivalent up to the 100 bar peak temperature at which point the amounts recovered at 200 bar continued increasing up until the peak temperature which is approximately 40K higher than at 100 bar.

There was no appreciable difference between the amount of ethylene and toluene formed at 100 and 200 bar, but the amounts of both species recovered at 40 bar were noticeably lower. Both ethylene and toluene formation proceeded at a greater rate with increasing temperature up to about 1100K, and following that the increase in the amount of each species observed with increasing temperature proceeded at a lower rate. This resulted in profiles that had a “hump” or an additional peak around 1100K. For ethylene, the amount recovered at the “hump” at 1100K and 100 and 200 bar was approximately 50% higher than at 40 bar, and the difference between

the amount of ethylene recovered at 100 and 200 bar compared to 40 bar decreased to being approximately 14% higher at 1360K. Similarly, for toluene the amount recovered at the "hump" at 1100K at both 100 and 200 bar was approximately 92% larger, and at 1360K the difference between the 100 and 200 bar recovered amounts was 20% higher compared to 40 bar.

For the case of propadiene and propyne, the amounts recovered at 40 and 100 bar over the entire experimental temperature range were close, but noticeably less of both species formed at 200 bar at all temperatures proceeding the initial formation temperature. The maximum amount of propadiene recovered at 100 bar was 38% higher than at 200 bar, and the maximum amount observed at 40 bar was approximately 15% higher than at 100 bar. For propyne, the maximum amount formed is approximately 32% larger at 100 bar compared to 200 bar, and about 6% higher at 40 bar than 100 bar. It should be noted that the experimental temperature range did not extend to high enough temperatures to observe the peaks of propadiene and propyne profiles at 100 and 40 bar, so it is possible that the differences at those pressures are greater than those between the maximum amounts reported.

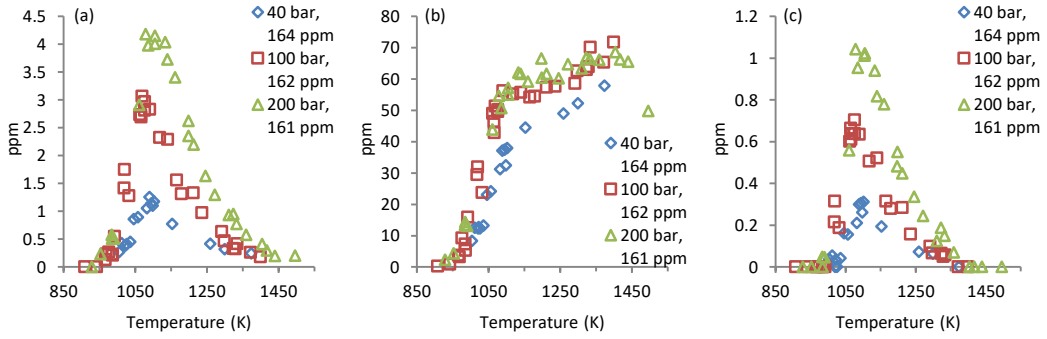

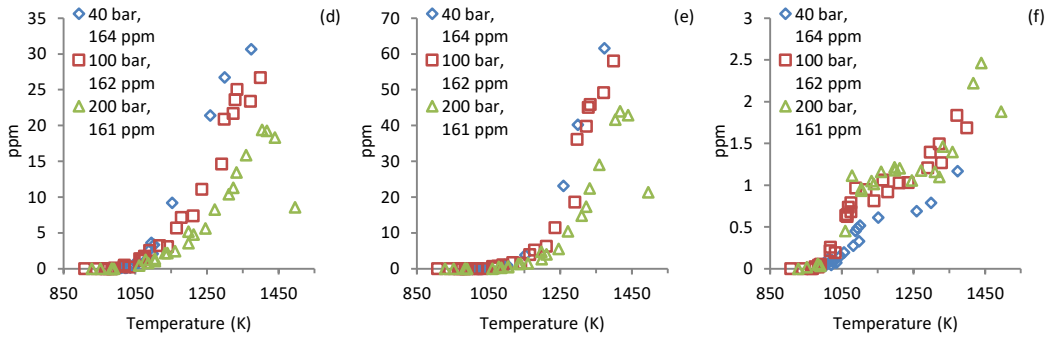

Figure 36: Species profiles of (a) ethane, (b) ethylene, (c) propane, (d) propadiene, (e) propyne, and (f) toluene formed in 6-bromo-1-hexene pyrolysis at nominal pressures of 40, 100, and 200 bar.

Figure 37 contains the species profiles of methane, acetylene, cyclopropane, propene, 1-butene, diacetylene, isobutylene, vinylacetylene, 1,3-cyclopentadiene, 1,5-hexadiene, 1-hexene, benzene, 1,3-cyclohexadiene, cyclohexene, and 6-bromo-1-hexene. The most abundant products observed were methane, acetylene, and propene. The methane profile also exhibits a "hump" at a temperature of 1100K that has been previously seen in the ethylene and toluene profiles. At the 1100K "hump" the amount of methane formed in the 100 and 200 bar experiments is approximately 48% higher than observed at 40 bar, but around 1250K the amount of methane observed at all three pressures is nearly identical. Acetylene and propene production did not seem to be effected by the experimental pressure variation and the profiles of both species were largely identical across all three experimental pressures. The only other species that did show a variation in their profiles as a result of varying experimental pressure were 1-butene and isobutylene, both were minor products. 1-butene saw an increase of 16% in the peak amount observed when the pressure decreased from 200 to 100 bar, an increase of approximately 41% when the pressure was decreased from 100 to 40 bar. For isobutylene, the peak amounts formed increased with increasing pressure with an approximately 72% increase in the peak amount formed when the pressure increased from 40 to 100 bar, and a 44% increase with the pressure increasing from 100 to 200 bar.

The remaining species did not exhibit any systematic differences in their product profiles as a result of changing experimental pressure. The only other differences between the three sets of experiments that are worthy of mention were observed in 1,3-cyclopentadiene, and cyclohexene. The decay of 1,3-cyclopentadiene with temperature at 200 bar is more rapid than at 40 or 100 bar; however, the maximum amounts observed seem in line with the amounts observed at the lower pressures. It's uncertain why this occurred, as no other profiles show such behavior even if the species were observed in lower amounts than 1,3-cyclopentadiene, so this should not be a result of poor GC quantification. The 100 bar cyclohexene experiments have two high points that are significantly higher than any other observed amounts. These high points may most likely be attributed to GC carry over from a previous run due to bromine being present in the fuel. Carry over is generally not a problem as the method used for these experiments bakes out the capillary column to purge any remnants of the sample which might still be present in the column, but nonetheless it is possible for a large, possibly bromine containing, species to remain in the column and then manifest itself as a ghost peak or coelute with the peak of another species thereby increasing the peak amount observed. These two peaks could be corrected to be in line with the amounts observed in other runs at similar temperatures, but are being presented as is. Additionally, the 200 and 40 bar experiments were not extended to as low of temperatures as the 100 bar experiments, so it is difficult to make a comparison of how much cyclohexene is expected to form at temperatures below 1000K.

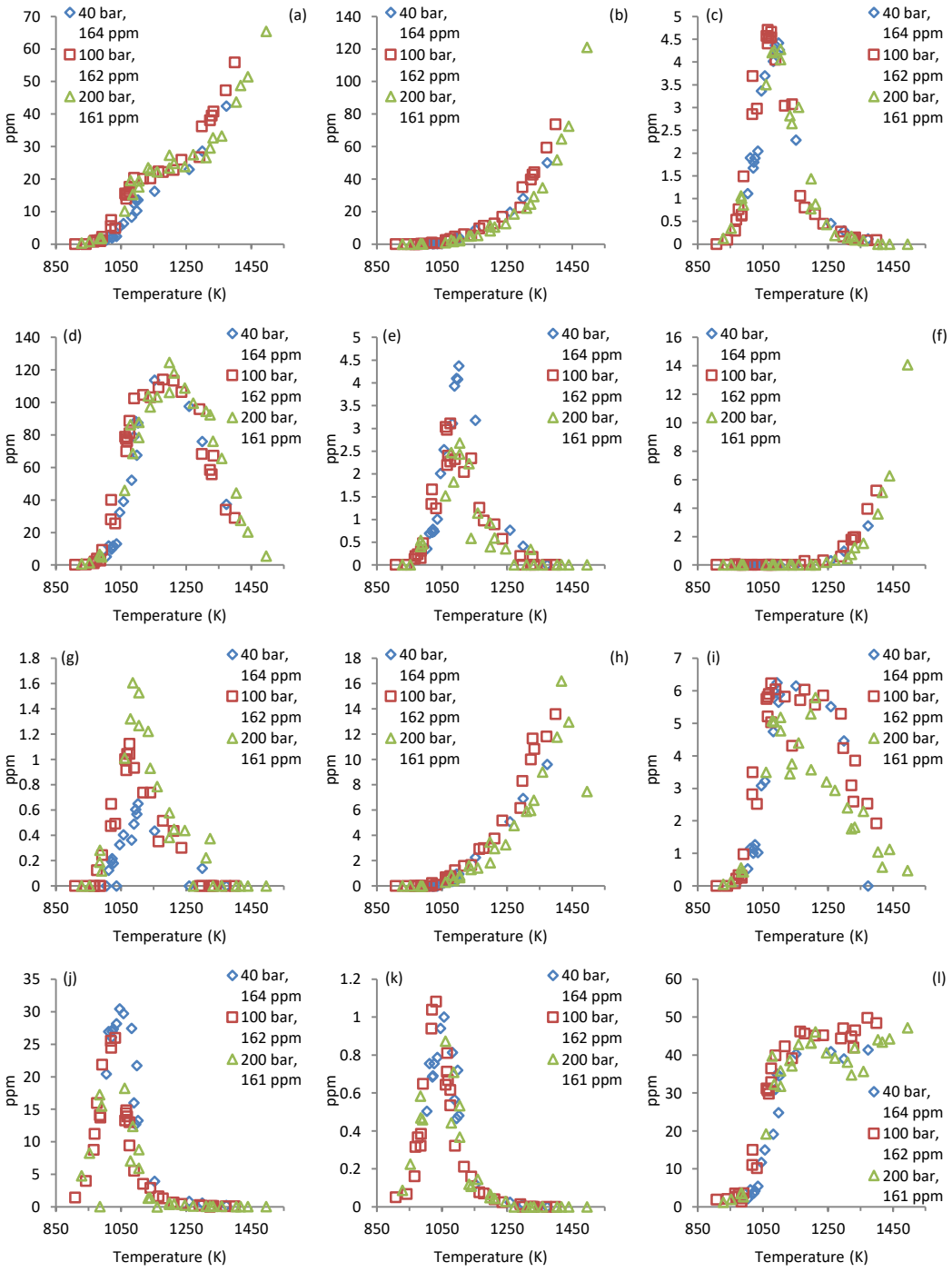
(a)
(b)
(c)
(d)
(e)
(f)
(g)
(h)
(i)
(j)
(k)
(l)
40 bar, 164 ppm
100 bar, 162 ppm
200 bar, 161 ppm
ppm
Temperature (K)

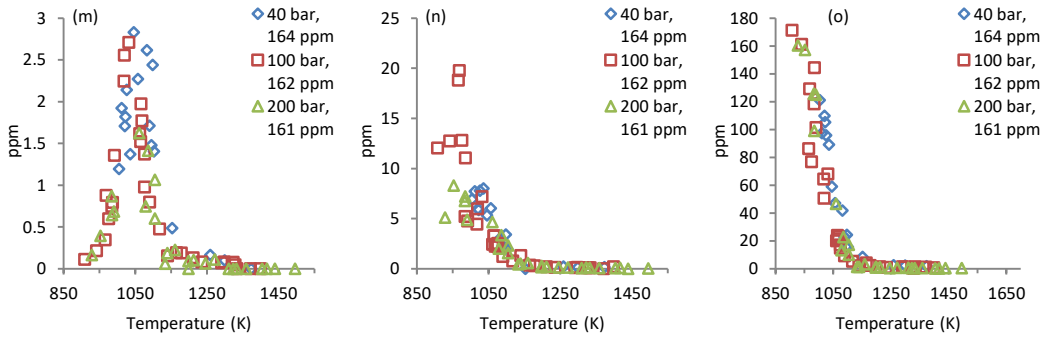

Figure 37: Species profiles of (a) methane, (b) acetylene, (c) cyclopropane, (d) propene, (e) 1-butene, (f) diacetylene, (g) isobutylene, (h) vinylacetylene, (i) 1,3-cyclopentadiene, (j) 1,5-hexadiene, (k) 1-hexene, (l) benzene, (m) 1,3-cyclohexadiene, (n) cyclohexene, and (o) 6-bromo-1-hexene formed in 6-bromo-1-hexene pyrolysis at nominal pressures of 40, 100, and 200 bar.

6.2.2 Effects of Initial Fuel Concentration on 6-Bromo-1-hexene Pyrolysis

The experimental results discussed so far were obtained at three different pressures but utilizing fuel mixtures that contained an approximately constant mole fraction of 6-bromo-1-hexene in the test gas. While the mole fraction of the fuel was nearly equivalent for the three sets of experiments the concentration varied depending on the experimental pressure, and assuming ideal gas behavior, the concentration increase would be proportional to the increase in experimental pressure. This means that while the initial mole fraction of fuel is constant, the initial concentration of the fuel in the reaction zone at 100 bar would be 250% of what is present at 40 bar, and 500% at 200 bar compared to 40 bar. Such as substantial increase in the initial fuel concentration could also lead to differences in the product distribution which prompted another set of experiments to be conducted. This set of experiments was conducted at 40 bar with 358 ppm of 6-bromo-1-hexene in the fuel mixture resulting in a fuel concentration which was approximately 218% of what was present in the previous 40 bar set which used 164 ppm of 6-bromo-1-hexene. While the increase in the fuel concentration may not be exactly equivalent to the 250% increase expected due to the increase in experimental pressure from 40 to 100 bar, it should be sufficiently close to provide insight as to whether the product distribution differences

observed were due to the difference in the initial fuel concentration present in the reaction zone or due to the variation of experimental pressure.

Figure 38 contains the same species whose product profiles were shown in Figure 37, namely ethane, ethylene, propane, propadiene, propyne, and toluene, but this time the compared species profiles were obtained from the 40 bar and 164 ppm of fuel, 100 bar and 162 ppm of fuel, and 40 bar and 358 ppm of fuel experiments. All the species mole fractions are normalized by the initial mole fraction of the fuel for each respective set of experiments as otherwise the amounts observed in the 40 bar and 358 ppm of fuel experiments would be significantly higher. Previously, an increase from 40 to 100 bar in the experimental pressure resulted in 144% more ethane observed at its peak, but the peak amount formed at 100 bar compared to the peak observed in the 40 bar and 358 ppm of fuel experiments is approximately 22% higher. Propane showed the second largest increase in the peak amount with the pressure increasing from 40 bar to 100 bar resulting in a 126% higher peak amount of propane, but the 100 bar peak compared to the 40 bar and 358 ppm of fuel peak is now approximately 20% larger. The ethylene profiles obtained in the 100 bar and 162 ppm of fuel and 40 bar and 359 ppm of fuel experiments are now virtually matched. Propadiene and propyne profiles at 40 and 100 bar previously were very similar, and the profiles obtained at 100 bar and 40 bar and 358 ppm of fuel are even closer now. For toluene, the new set of data at 40 bar and 358 ppm of fuel does not match the 100 bar set as well as in the case of ethylene, but the difference now is smaller than compared to the previous set obtained at 40 bar. It is suspected that if the fuel increase was higher, therefore coming closer to the 250% increase in the fuel concentration in the reaction zone caused by the increase in the experimental pressure, then the profiles obtained at 40 bar with increased fuel concentration would match the 100 bar profiles even better. Nonetheless, these results show that increasing the

initial fuel mole fraction in lower pressure experiments so that the fuel concentration in the reaction zone is nearly matched at two significantly different pressures results in nearly matching product species profiles at the current experimental conditions.

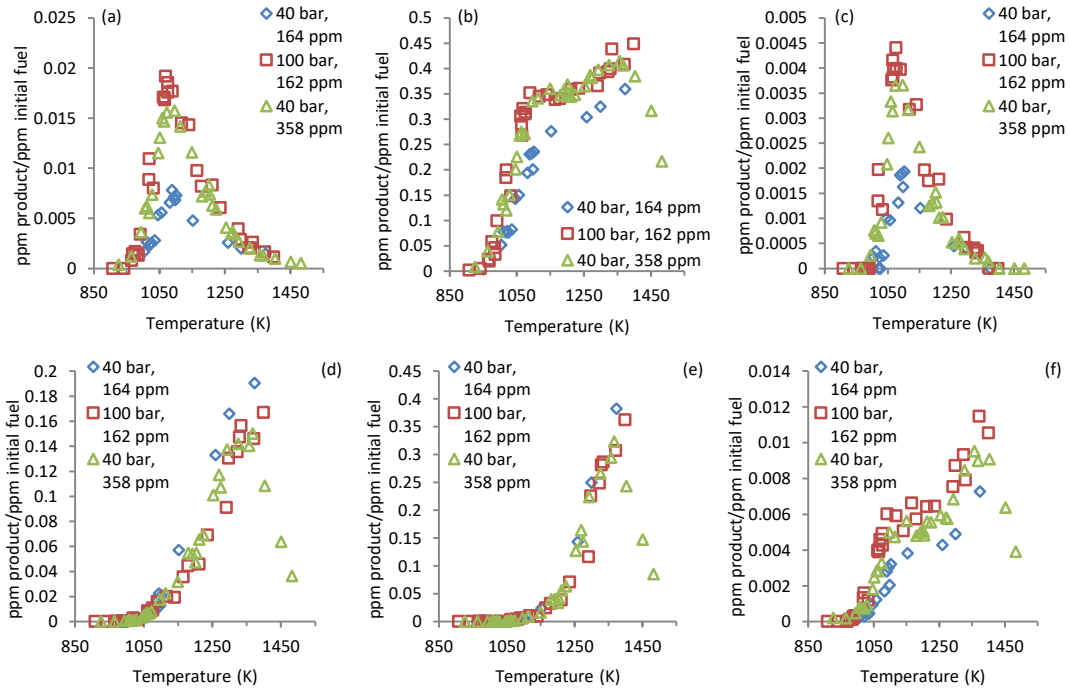

Figure 38: Comparison of species profiles of (a) ethane, (b) ethylene, (c) propane, (d) propadiene, (e) propyne, and (f) toluene formed in 6-bromo-1-hexene pyrolysis at 40 bar and 164 ppm of 6-bromo-1-hexene, 100 bar and 162 ppm of 6-bromo-1-hexene, and 40 bar and 358 ppm of 6-bromo-1-hexene. The mole fraction of each species was normalized by the initial mole fraction of 6-bromo-1-hexene for the respective data set.

Figure 39 contains the species profiles of methane, acetylene, cyclopropane, propene, 1-butene, diacetylene, isobutylene, vinylacetylene, 1,3-cyclopentadiene, 1,5-hexadiene, 1-hexene, benzene, 1,3-cyclohexadiene, cyclohexene, and 6-bromo-1-hexene from the 40 bar and 164 ppm of fuel, 100 bar and 162 ppm of fuel, and 40 bar and 358 ppm of fuel experiments. All the species profiles were normalized by the initial mole fraction of the fuel just as in Figure 38. As previously discussed, the amount of methane observed in the 40 bar and 164 ppm of fuel set of experiments was lower than in the 100 bar and 162 ppm of fuel experiments up to about 1250 K, but the amounts observed to form in the 40 bar and 358 ppm of fuel experiments match very

closely those in the 100 bar and 162 ppm of fuel experiments over the entire experimental temperature range. The remaining two most abundant product species, acetylene and propene, did not exhibit any substantial differences in their profiles when the experimental pressure was varied, and similarly the 40 bar and 358 ppm of fuel experimental data for acetylene and propene matches the data from both the 40 bar and 164 ppm of fuel and 100 bar and 162 ppm of fuel experiments. The normalized formation of the two most abundant species, acetylene and propene, not being effected by either a variation in experimental pressure or initial fuel concentration suggests that the main decomposition pathway of hex-5-en-1-yl radicals is rate limited by a unimolecular reaction, as discussed in the Chemical Kinetic Analysis of Pressure and Concentration Dependence section, at least at the experimental conditions present in this study. Likewise, cyclopropane, diacetylene, vinylacetylene, and 1,3-cyclopentadiene did not exhibit any appreciable variation in their profiles between the 40 bar and 164 ppm of fuel, 100 bar and 162 ppm or fuel, and 40 bar and 358 ppm of fuel experiments.

1-butene and isobutylene, both minor products, have previously shown to have their profiles effected by a variation in the experimental pressure. The peak amount and overall amounts observed of 1-butene have previously shown to decrease with increasing pressure. The 40 bar and 358 ppm of fuel experiments resulted in overall reduced amounts of 1-butene observed, although there were a few experimental points that were also in line with the amounts recovered in the 100 bar and 162 ppm of fuel experiments, however, these points seem to be an anomaly and scatter in the data as overall the profile exhibits reduced formation amounts of 1-butene over the majority of the experimental temperature range. The peak amount of isobutylene recovered in the 40 bar and 358 ppm of fuel experiments was approximately 34% lower than in the 100 bar and 162 ppm of fuel experiments, but the peak amount recovered was still about 15%

higher than in the 40 bar and 164 ppm of fuel experiments. The peak amount of 1,3-cyclohexadiene was also approximately 25% lower in the 40 bar and 358 ppm of fuel experiments compared to both the 100 bar and 162 ppm of fuel and 40 bar and 164 ppm of fuel experiments both of which resulted in a nearly identical peak amount of 1,3-cyclohexadiene. The reduction in the amount of 1-butene, isobutylene, and 1,3-cyclohexadiene formed in the 40 bar and 358 ppm of fuel experiments suggests that the competing reaction pathways are more sensitive to an increase of the initial fuel concentration.

1,5-hexadiene is another major product and the formation amounts observed at both 100 bar and 162 ppm of fuel and 40 bar and 358 ppm of fuel match closely, and the peak amounts observed are approximately 14% lower than in the 40 bar and 164 ppm of fuel experiments. The amounts of benzene observed to form in all three sets of experiments are fairly close up to 1100K, but with temperatures exceeding 1100K approximately 9% more benzene was recovered in the 100 bar and 162 ppm of fuel experiments compared to the 40 bar and 358 ppm of fuel and 40 bar 164 ppm of fuel experiments. The 40 bar and 358 ppm of fuel experiments did use a mixture which had a 218% increase in the fuel mole fraction compared to the 40 bar and 164 ppm of fuel experiments. It is certainly possible that if a mixture which was closer to a 250% increase in the fuel concentration, or the expected increase in the initial fuel concentration in the reaction zone due to the increase in experimental pressure, then the amount of benzene recovered in the higher fuel concentration experiments would more closely match what was observed in the 100 bar and 162 ppm of fuel experiments at temperatures in excess of 1100K. The anomaly observed in the cyclohexene profile at lower temperatures has been discussed previously. At temperatures in excess of 1000K the amount of cyclohexene recovered from all three sets of experiments is nearly equivalent. Unlike for the 100 bar and 162 ppm of fuel set of experiment,

which had a few experimental points below 1000K with high amounts of cyclohexene recovered, for the 40 bar and 358 ppm of fuel there are a few points with low amounts of cyclohexene recovered, however, those seem to be scatter points which for cyclohexene seem common at all the experimental conditions presented so far. The fuel decay between all three sets of experiments did not seem to exhibit any significant variation.

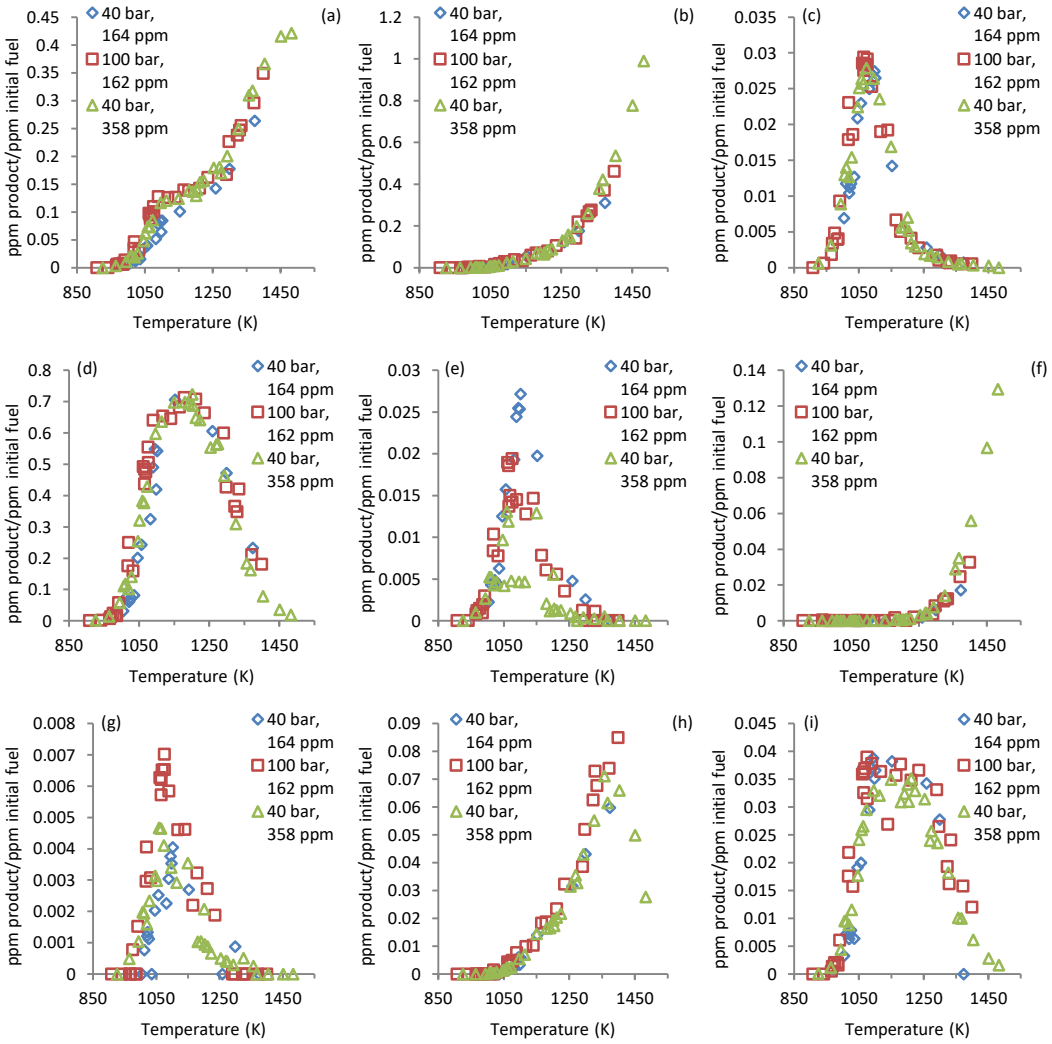

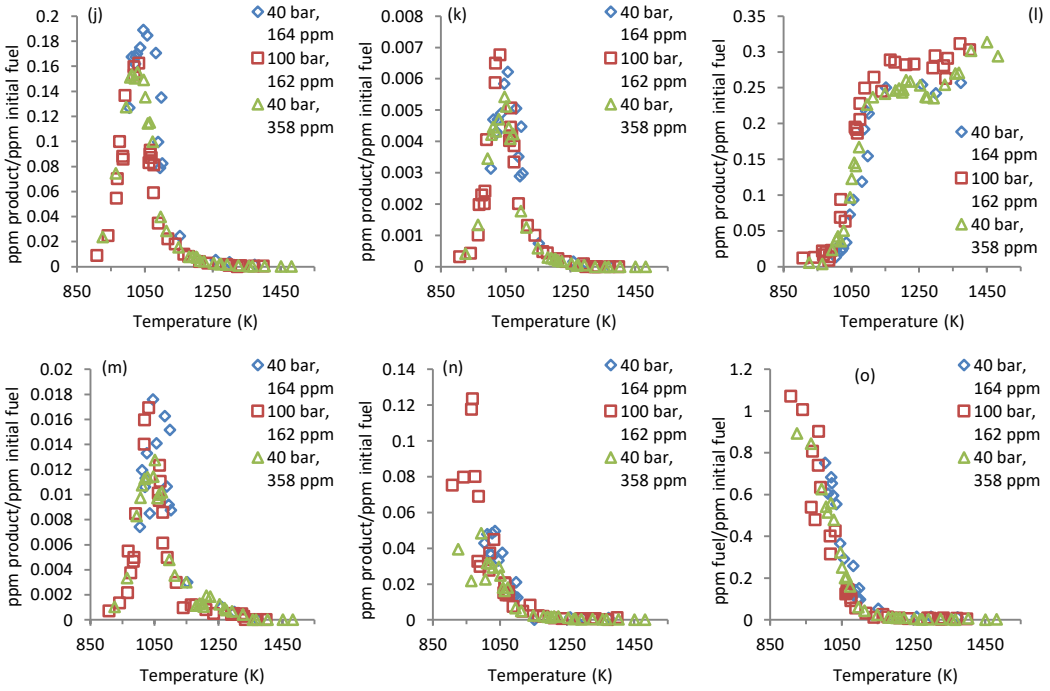

Figure 39: Comparison of species profiles of (a) methane, (b) acetylene, (c) cyclopropane, (d) propene, (e) 1-butene, (f) diacetylene, (g) isobutylene, (h) vinylacetylene, (i) 1,3-cyclopentadiene, (j) 1,5-hexadiene, (k) 1-hexene, (l) benzene, (m) 1,3-cyclohexadiene, (n) cyclohexene, and (o) 6-bromo-1-hexene formed in 6-bromo-1-hexene pyrolysis at 40 bar and 164 ppm of 6-bromo-1-hexene, 100 bar and 162 ppm of 6-bromo-1-hexene, and 40 bar and 358 ppm of 6-bromo-1-hexene. The mole fraction of each species was normalized by the initial mole fraction of 6-bromo-1-hexene for the respective data set.

6.2.3 Comparison of 1,5-Hexadiene and 6-Bromo-1-hexene Pyrolysis Product Distributions

The intent of using 6-bromo-1-hexene as the fuel was so that after undergoing a loss of the bromine atom the resulting product would be the hex-5-en-1-yl radical. It is also possible for 6-bromo-1-hexene to undergo HBr loss resulting in 1,5-hexadiene. Large amounts of 1,5-hexadiene have been observed to form in all four sets of experiments presented so far, which can be seen in product distributions shown in Figure 37 and Figure 39. To determine the significance of the HBr loss pathway in the present work, an additional set of experiments was completed at 100 bar using 170 ppm of 1,5-hexadiene as the fuel allowing the product distributions obtained in the 6-bromo-1-hexene experiments at 100 bar to be directly compared with those in the 1,5-

hexadiene experiments. Propadiene, propyne, and propene are expected to be among the primary products of 1,5-hexadiene pyrolysis[81] so particular attention to the comparison of those products' profiles will be given between the 1,5-hexadiene and 6-bromo-1-hexene experiments.

Figure 40 contains the species profiles of ethane, ethylene, propadiene, propyne, toluene, methane, acetylene, propene, 1-butene, vinylacetylene, 1,3-cyclopentadiene, 1,5-hexadiene, 1-hexene, benzene, and 1,3-cyclohexadiene obtained from the 100 bar pyrolysis experiments with 162 ppm of 6-bromo-1-hexene and 170 ppm of 1,5-hexadiene as the fuels. Propane, cyclopropane, diacetylene, isobutylene, and cyclohexene were not observed to form in the 1,5-hexadiene experiments at all, or formed in near zero amounts which did not produce any distinguishable profiles, so the plots for those species are omitted. The decay of the 1,5-hexadiene formed in the 6-bromo-1-hexene experiments occurs, and proceeds, at temperatures approximately 80K lower than observed in the 1,5-hexadiene experiments. This is due to 1,5-hexadiene being a product in 6-bromo-1-hexene pyrolysis so it decays in an environment with an already established radical pool whereas in the 1,5-hexadiene experiments, 1,5-hexadiene is the fuel and must first break down to form radical species. As mentioned and expected, propadiene, and propyne formed in abundance in the 1,5-hexadiene experiments. Despite the decay of 1,5-hexadiene in the experiments which used 1,5-hexadiene as the fuel occurring at temperatures approximately 80K higher compared to the decay of 1,5-hexadiene in the experiments which used 6-bromo-1-hexene as the fuel, the initial formation temperatures of both propadiene and propyne are approximately equivalent for both sets of experiments. The recovered amounts of propadiene begin increasing far more rapidly with temperatures in the 1,5-hexadiene experiments, and the peak amount is observed to occur at approximately 1250K. The peak amount of propadiene is not observed over the experimental range in the 6-bromo-1-hexene

experiments, and the maximum amount recovered was at 1400K, or the highest temperature for that set of experiments, and was less than half of what was observed in the peak amount of propadiene in the 1,5-hexadiene experiments. The formation of propyne in the 1,5-hexadiene experiments was also more rapid with respect to temperature, and larger amounts of propyne were recovered at lower temperatures than in the 6-bromo-1-hexene experiments. The peak amount of propyne observed in the 1,5-hexadiene experiments was recovered at approximately 1330K and was 22% larger than the maximum observed in the 6-bromo-1-hexene experiments, which just as in the case of propadiene, occurred at the highest temperature in that set of experiments at approximately 1400K.

Other major products in both sets of experiments were ethylene, methane, acetylene, and propene. The initial formation temperature for ethylene in the 1,5-hexadiene experiments is approximately 120K higher than in the 6-bromo-1-hexene experiments, and following the initial formation temperature the increase in the amount of ethylene recovered with an increase in temperature is lower than in the 6-bromo-1-hexene experiments. The ethylene profile from the 1,5-hexadiene experiments also does not exhibit the "hump" which was observed in the 6-bromo-1-hexene experiments and after which the amount of ethylene recovered in the 6-bromo-1-hexene experiments from 1090K to 1180K stays relatively constant, and only a gradual increase is observed as the temperature increases past 1180K. The difference in the methane profile between the two experimental sets is similar to that of ethylene in regards to the methane profile from the 6-bromo-1-hexene experiments exhibiting the "hump" after which the rate of production of methane with respect to temperature tapers off. The initial formation temperature of methane between the 6-bromo-1-hexene and 1,5-hexadiene experiments varies by 180K, and after approximately 1290K the amount of methane recovered from both experimental sets is very

similar. The difference in the toluene profiles between the 6-bromo-1-hexene and 1,5-hexadiene experiments are very similar to those of the methane profiles, which is understandable since both the species are heavily dependent on the availability of the methyl radical.

The acetylene profile in both the 6-bromo-1-hexene and 1,5-hexadiene experiments is very similar. The propene profile is also similar when accounting for the 80K temperature difference observed in the decay of 1,5-hexadiene in the 6-bromo-1-hexene and 1,5-hexadiene experiments, and the propene formation between the two sets of experiments is also shifted by approximately 80K, whereas the propene decay is virtually identical. At its peak amount, the amount of propene recovered in the 6-bromo-1-hexene experiments is approximately 10% higher despite the fuel mole fraction in the 6-bromo-1-hexene experiments being 3.5% lower compared to 1,5-hexadiene experiments. The 1,3-cyclopentadiene and 1,3-cyclohexadiene profiles are also similar between the two experimental sets when accounting for the temperature difference in the 1,5-hexadiene decay, and the amount of 1,3-cyclopentadiene recovered in the two sets is nearly equivalent, but approximately 16% less 1,3-cyclohexadiene was recovered and 1,3-cyclohexadiene decay proceeds at temperatures 100K lower in the 6-bromo-1-hexene experiments compared to the 1,5-hexadiene experiments.

The remaining product profiles between the two experimental sets are substantially different. The peak amount of ethane recovered in the 1,5-hexadiene experiments is over 3 times greater than in the 6-bromo-1-hexene experiments, and the peak amount 1-butene observed is more than 5 times larger in the 1,5-hexadiene experiments than in the 6-bromo-1-hexene experiments. The maximum amount of vinylacetylene is more than twice as larger in the 6-bromo-1-hexene experiments than in the 1,5-hexadiene experiments. The experimental temperature range for the 6-bromo-1-hexene experiments is not large enough to observe the

vinylacetylene peak, so it's possible that the peak amount might be even greater. The vinylacetylene peak was observed in the 1,5-hexadiene experiments, but there weren't enough experimental points around the peak to determine what the actual peak value was, however, based on the shape of the profile it shouldn't be much larger, if at all, than the maximum amount observed. The benzene profile is also substantially different, with the benzene amounts recovered in 6-bromo-1-hexene experiments increasing rapidly following the initial formation temperature of about 990K, and after a plateau amount is reached around a temperature of 1180K, the benzene amounts recovered seem to only increase slightly with increasing temperature. In the 1,5-hexadiene experiments the amount of benzene recovered increased far more gradually with increasing temperature, and the maximum amount recovered was approximately 31% lower than in the 6-bromo-1-hexene experiments.

The overall differences in the product distribution observed in the 1,5-hexadiene and 6-bromo-1-hexene experiments are too great for the 6-bromo-1-hexene decomposition to primarily proceed through HBr loss forming 1,5-hexadiene. The major products such as propadiene, propyne, ethylene, methane, and benzene as well as the lesser formed products like ethane, 1-butene, and vinylacetylene have profiles that vary too much in terms of the amount formed and/or the overall profile shape, even when accounting for the temperature difference in the 1,5-hexadiene decay between the two sets of experiments, to argue that the formation of these species proceeds through 1,5-hexadiene as an intermediate in the 6-bromo-1-hexene pyrolysis. The acetylene, and propene and 1,3-cyclopentadiene profiles, when accounting for the 1,5-hexadiene decay temperature difference, are similar between the two sets of experiments, and that is understandable as 1,5-hexadiene is observed to form in the 6-bromo-1-hexene experiments so it should also have an impact on the product distribution and there should be

shared reaction pathways between the two sets of experiments. It is also certainly possible that 1,5-hexadiene is a product of hex-5-en-1-yl radical rather than just the HBr loss from 6-bromo-1-hexene.

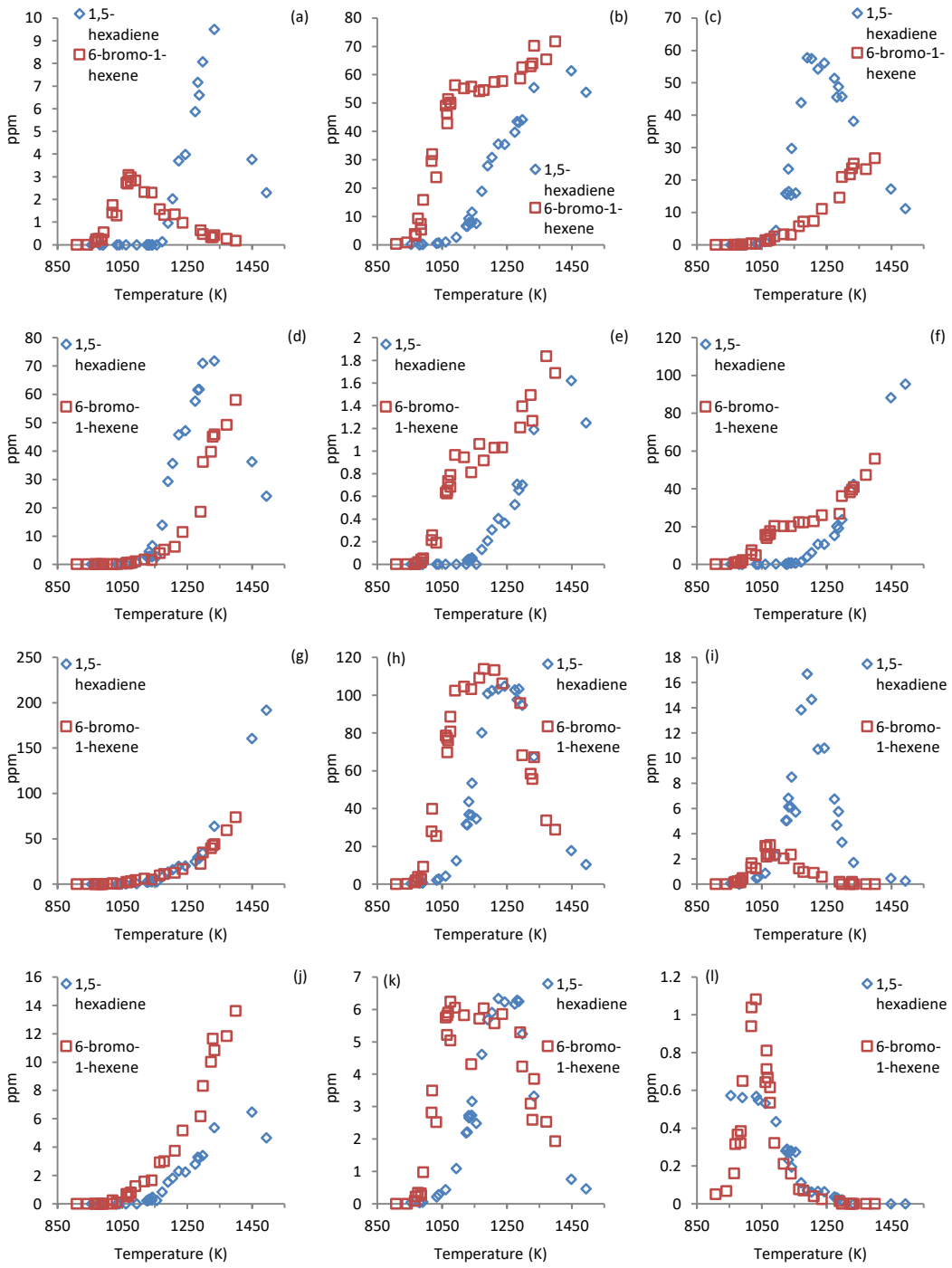

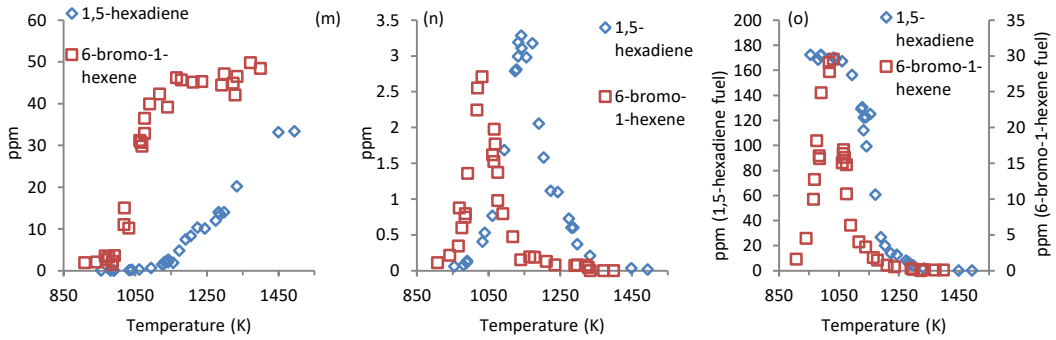

Figure 40: Comparison of species profiles of (a) ethane, (b) ethylene, (c) propadiene, (d) propyne, (e) toluene, (f) methane, (g) acetylene, (h) propene, (i) 1-butene, (j) vinylacetylene, (k) 1,3-cyclopentadiene, (l) 1-hexene, (m) benzene, (n) 1,3-cyclohexadiene, and (o) 1,5-hexadiene formed in 6-bromo-1-hexene pyrolysis at 100 bar and 162 ppm of 6-bromo-1-hexene and 1,5-hexadiene pyrolysis at 100 bar and 170 ppm of 1,5-hexadiene as the fuel.

6.3 Chemical Kinetic Modeling of Experimental Data

The Reaction Mechanism Generator (RMG)[101] was used to generate a Chemkin[99] compatible mechanism to model the hex-5-en-1-yl pyrolysis. RMG does not allow the generation of mechanisms involving bromine containing species making it impossible to directly generate a mechanism for 6-bromo-1-hexene. Instead, a mechanism was generated for a fuel mixture composed of 81 ppm of hex-5-en-1-yl and 80 ppm of 1,5-hexadiene with a balance of argon. 1,5-hexadiene was included in the fuel due to the substantial amounts of 1,5-hexadiene forming at the lower range of experimental temperatures covered. This suggests that 6-bromo-1-hexene may also undergo HBr loss resulting in production of 1,5-hexadiene, and not just Br loss resulting in hex-5-en-1-yl which was desired. It is possible to manually add reactions involving 6-bromo-1-hexene to the generated mechanism, but there are no reaction rate coefficients available for 6-bromo-1-hexene pyrolysis currently in literature. Peukert estimated the reaction rate coefficients for the loss of iodine in 6-iodo-1-hexene pyrolysis, but he did not consider HI loss resulting 1,5-hexadiene[125]. There is also a lack of available thermochemistry data for 6-bromo-1-hexene which is required by Chemkin. The mechanism was generated for a pressure of 200 bar with the option to generate pressure dependent reaction rate coefficients in the PLOG format as needed.

The reason for generating the mechanism at the highest experimental pressure was due to the demonstrated ability to produce matching, or very closely matching, experimental data at lower pressures if the initial fuel concentration in the reaction zone is equivalent, or very close, to that in higher pressure experiments. Additionally, one of the aims of this study was to investigate whether high pressure may drive the formation of alkylcyclopentanes, so there is particular interest in modeling the high pressure chemistry.

Just as for the generated Cyclohexane and Methylcyclohexane mechanisms, the RMG mechanism was generated using the Chernov[151] and JetSurF2.0[132] seed mechanisms as provided in the RMG database. Monte Carlo uncertainty analysis was completed for the generated mechanisms as described previously in the Cyclohexane chapter. Two sets of simulations were completed using the generated mechanism, one with purely hex-5-en-1-yl as the fuel and one with a fuel mixture composed of 81 ppm of hex-5-en-1-yl and 80 ppm of 1,5-hexadiene. The Monte Carlo uncertainty analysis was completed for both fuel mixtures, but is only presented for the one using purely hex-5-en-1-yl as the fuel in order to retain clarity in the plots.

6.3.1 Simulation of the Expected Immediate 6-Bromo-1-hexene Product Pyrolysis

Figure 41 contains the 200 bar and 161 ppm of 6-bromo-1-hexene experimental data, the simulation results for both the 161 ppm of hex-5-en-1-yl fuel and the 81 ppm of hex-5-en-1-yl with 80 ppm of 1,5-hexadiene fuel, and the uncertainty curves for the 161 ppm of hex-5-en-1-yl fuel simulation for ethane, ethylene, propane, propadiene, propyne, toluene, methane, acetylene, propene, 1-butene, diacetylene, isobutylene, vinylacetylene, 1,3-cyclopentadiene, 1,5-hexadiene, 1-hexene, benzene, and cyclohexene. Cyclopropane, 1,3-cyclohexadiene, and 6-bromo-1-hexene were not predicted by the mechanism so their plots are omitted. One result immediately worth

noting are the simulation predictions for 1,5-hexadiene. Even for the case with only hex-5-en-1-yl as the fuel the amount of 1,5-hexadiene predicted exceeds the amount observed in the experiments. Although the peak amount of 1,5-hexadiene has not been captured in the 200 bar experiments due to lack of points near the peak, it can be estimated based on the 40 and 100 bar experiments to be around 25 ppm whereas 28 ppm is predicted if the fuel is purely hex-5-en-1-yl, and a maximum of 88 ppm is predicted for the hex-5-en-1-yl/1,5-hexadiene fuel mixture.

Despite the hex-5-en-1-yl/1,5-hexadiene fuel mixture resulting in a substantial over prediction of 1,5-hexadiene, using it as the fuel results in noticeably better prediction of the remaining product species compared to using purely hex-5-en-1-yl as the fuel. Using purely hex-5-en-1-yl as the fuel results in over prediction of the peak amount of ethane in excess of 8 fold, ethylene by nearly 3 fold, and propane by more than 3 fold. The hex-5-en-1-yl/1,5-hexadiene fuel mixture also results in over prediction of those species, but not by such substantial amounts. For ethane and propane, the hex-5-en-1-yl/1,5-hexadiene fuel mixture provides reasonable match with the experimental data up to a temperature of approximately 1050K, after which the simulation results predict further increase in the amount of both ethane and propane whereas decay was observed in the experimental results. For ethylene, the hex-5-en-1-yl/1,5-hexadiene mixture continues to provide reasonable prediction of the experimental data up to approximately 1300K, after which the simulation results show an increase with increasing temperature whereas the amount of ethylene observed experimentally remains constant.

The pure hex-5-en-1-yl fuel simulation results under predict the experimentally observed peak amount of propene in excess of a factor of 6, and the experimental peak amounts of both propadiene and propyne by approximately a factor of 5. The simulation which used the hex-5-en-1-yl/1,5-hexadiene mixture predicts the overall propene profile reasonably well with an

approximately 18% under prediction of the peak amount. The peak amount of propadiene is over predicted by approximately 27%, and the peak amount of propyne is under predicted by approximately 36% by the hex-5-en-1-yl/1,5-hexadiene mixture. The propadiene formation is predicted to proceed at lower temperatures than experimentally observed, but the experimentally used fuel is 6-bromo-1-hexene which has to undergo Br loss to form hex-5-en-1-yl and 1,5-hexadiene whereas those two are the initial fuel for the simulation. The propyne prediction is reasonable up to approximately 1350K after which point the simulation predicts a decay which is not experimentally observed until approximately 1440K.

The pure hex-5-en-1-yl fuel simulation predicts the overall methane profile rather well over the entire experimental temperature range and even captures the "hump" around 1100K which is not captured with the hex-5-en-1-yl/1,5-hexadiene fuel mixture simulation. The simulation with either fuel results in reasonable prediction of both the experimentally observed acetylene and diacetylene profiles, although the pure hex-5-en-1-yl as fuel simulation predicts diacetylene slightly better over the other simulation, whereas the reverse is true for acetylene. Both fuels substantially over predict the formation of 1-butene and under predict isobutylene, both of which were minor experimental products. The vinylacetylene and cyclopentadiene peak amounts are reasonable captured by either fuel, but more so by the hex-5-en-1-yl/1,5-hexadiene mixture. 1-hexene is another minor product which is significantly over predicted in simulations with either fuel. Experimentally, a peak value of about 1 ppm of 1-hexene was observed while the simulation using the hex-5-en-1-yl/1,5-hexadiene fuel mixture predicted 19 ppm of 1-hexene to form, and the simulation with pure hex-5-en-1-yl as the fuel predicted 45.6 ppm of 1-hexene. The simulations with either fuel also predict substantial amounts of 1,3-butadiene, with a peak amount of 58 ppm predicted by the hex-5-en-1-yl/1,5-hexadiene fuel mixture and 94 ppm

predicted by the pure hex-5-en-1-yl fuel which are not plotted. 1,3-butadiene was not quantified successfully in any of the experiments involving 6-bromo-1-hexene as the fuel due to significant scatter in the data. The most probable reason for this is carryover of bromine containing species from a previous run, however, a distinct pattern or reason for the scatter was not found and attempts at experimenting with the post run bake out of the capillary column to remove the carryover species while still retaining a manageable overall method run time were not successful. No other species was impacted by such significant scatter other than 1,3-butadiene. Despite the scatter, the estimated peak amount of 1,3-butadiene based on the experimental data is not expected to exceed 20 ppm, so the use of either fuel results in substantial over prediction in the formation of 1,3-butadiene.

The large amounts of benzene observed experimentally are not captured by the simulations with either fuel. 1,3-cyclohexadiene is not predicted in the simulations at all, and cyclohexene is under predicted. The inability of the simulation results to capture the large amounts of benzene observed to form experimentally suggests incorrect reaction rates or missing fundamental reaction pathways in hex-5-en-1-yl pyrolysis. The Chernov seed mechanism, which is the source of the aromatic formation reactions for the RMG generated mechanism, does not contain the cyclohexene dehydrogenation pathway leading to the formation of benzene or the isomerization of fulvene to benzene. However, the inclusion of the dehydrogenation of cyclohexene pathway would not improve the results significantly, because cyclohexene is substantially under predicted by the simulation. Recent experimental and modeling combustion studies have suggested that the hex-5-en-1-yl radical forms from the cyclohexyl radical, and then can either isomerize to the cyclopentylmethly radical or dissociate into smaller species[29–32,115,125,130,167]. The isomerization of the hex-5-en-1-yl radical to the cyclohexyl radical

has also been proposed[175,176]. Based on the current experimental results it seems that the isomerization of hex-5-en-1-yl to the cyclohexyl radical which then forms cyclohexene and undergoes the dehydrogenation pathway to form 1,3-cyclohexadiene and then benzene is the most probable. This hypothesis is based on the experimental observation that both cyclohexene and 1,3-cyclohexadiene decay to zero, or near zero, ppm at approximately 1150K which is the same temperature at which benzene reaches its plateau value, until more benzene is produced at higher temperatures which is expected to be due to C3+C3 species recombination. This also seems to be supported by the generated model in which benzene formation sub-mechanism predominately relies on the recombination of C3 + C3 species which is observed to occur at higher temperatures.

The cyclopentylmethyl radical could also act as an intermediate in the formation of benzene by forming either methylenecyclopentane or one of the methylcyclopentene isomers which would then dehydrogenate to fulvene and isomerize to benzene. Neither methylenecyclopentane nor and methylcyclopentene isomers were detected in this work; however, cyclopentadiene was quantified in the experiments and it could form following the cleavage of the methyl group on the methylcyclopentene isomers which would be a competing reaction pathway with the dehydrogenation to fulvene. However, cyclopentadiene formation peaks at a temperature of approximately 1100K whereas the benzene peak is not observed until about 1150K, which would either mean that the isomerization of hex-5-en-1-yl radical to cyclohexyl radical which then forms cyclohexene that proceeds to dehydrogenate to benzene is the more favorable pathway, or that the cleavage of the methyl group in the methylcyclopentene isomers because less favorable with increasing temperature. Nonetheless, the large amount of benzene observed to form in the experimental, and the inability of the model to predict the

benzene formation illustrate the need for refinement and further development of pathways in which the hex-5-en-1-yl radical acts as a benzene precursor, especially due to the current literature supporting the formation of hex-5-en-1-yl as a significant pathway in the pyrolysis of the cyclohexyl radical.

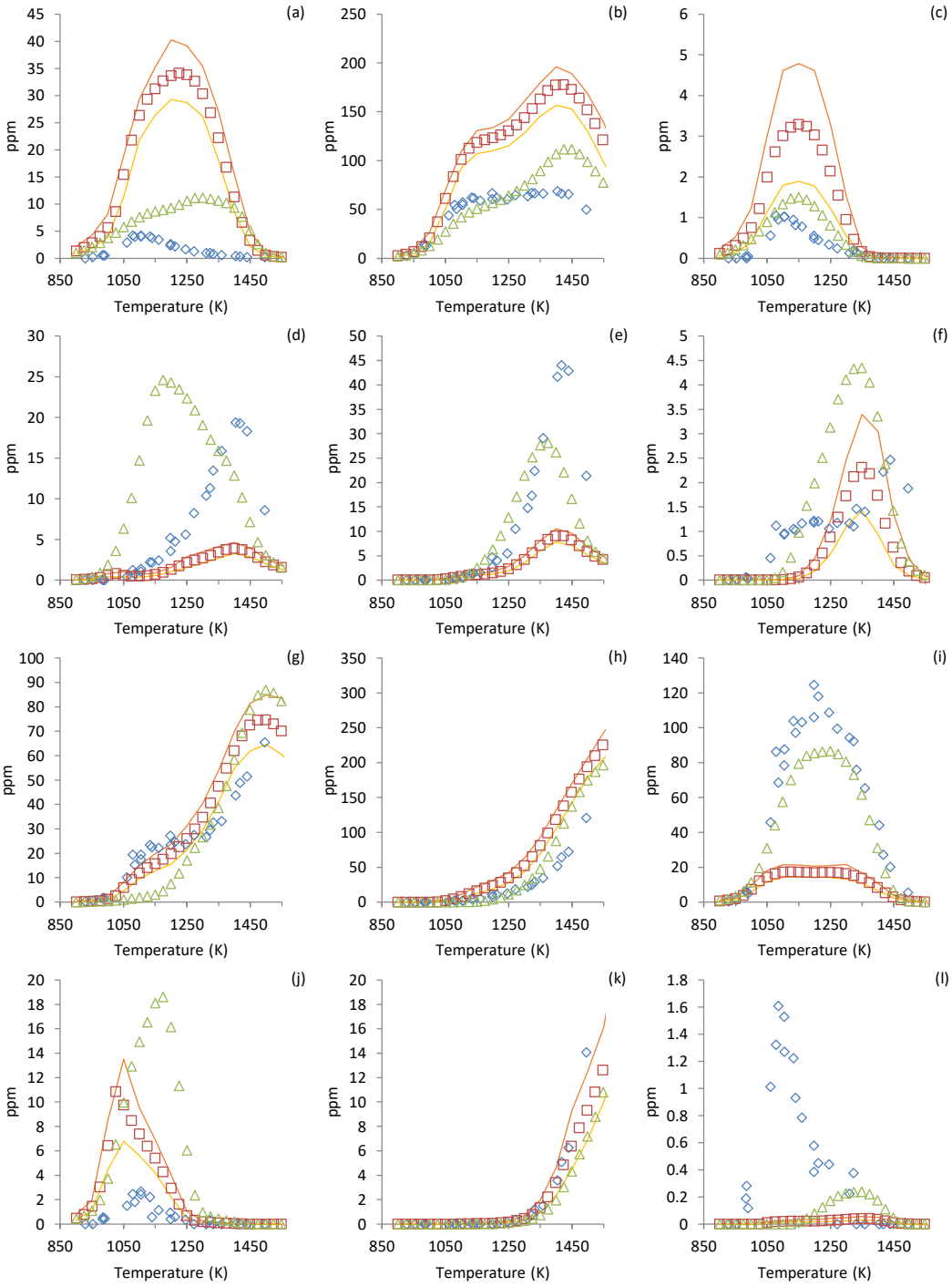

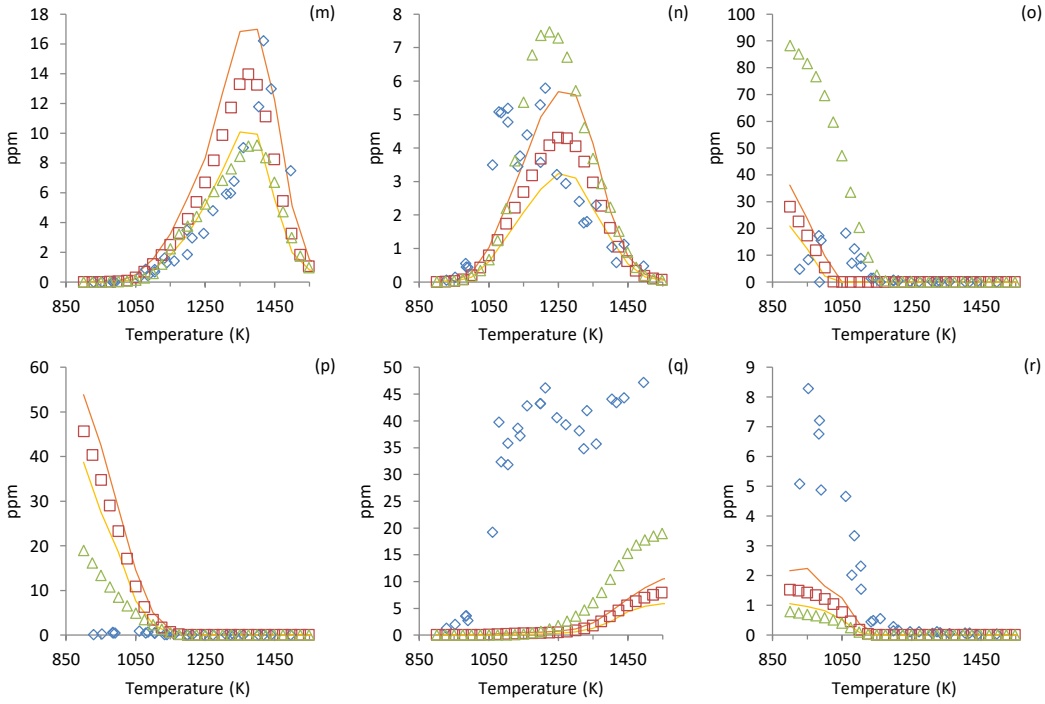

Figure 41: Comparison of species profiles of (a) ethane, (b) ethylene, (c) propane, (d) propadiene, (e) propyne, (f) toluene, (g) methane, (h) acetylene, (i) propene, (j) 1-butene, (k) diacetylene, (l) isobutylene, (m) vinylacetylene, (n) 1,3-cyclopentadiene, (o) 1,5-hexadiene, (p) 1-hexene, (q) benzene, and (r) cyclohexene formed in 6-bromo-1-hexene pyrolysis at 200 bar and 161 ppm of 6-bromo-1-hexene as the fuel against the simulation results obtained from the RMG generated mechanism using 161 ppm of hex-5-en-1-yl as the fuel, and another simulation result obtained using the same mechanism but 81 ppm of hex-5-en-1-yl and 80 ppm of 1,5-hexadiene as the fuel. The uncertainty bands obtained by prescribing an uncertainty of 30% to all the A factors in the mechanism are plotted for the simulation set which was obtained with 161 ppm of hex-5-en-1-yl as the fuel. Legend: ◇ Experimental Data, □ Simulation Results using 161 ppm of hex-5-en-1-yl as Fuel, △ Simulation Results using 81 ppm of hex-5-en-1-yl and 80 ppm of 1,5-hexadiene as Fuel, ——— Maximum Species Mole Fraction from Monte Carlo Analysis for the 161 ppm of hex-5-en-1-yl fuel Simulation, ——— Minimum Species Mole Fraction from Monte Carlo Analysis for the 161 ppm of hex-5-en-1-yl fuel Simulation

6.3.1.1 ROP Analysis

The rate of production (ROP) analysis for benzene was completed at a representative temperature of 1350K and reaction time of 2.2 ms for the simulation using 161 ppm of hex-5-en-1-yl as the fuel, and the simulation using 80 ppm of 1,5-hexadiene and 81 ppm of hex-5-en-1-yl as the fuel. The ROP analysis was completed for benzene because it is one of the most abundant products observed experimentally. It is also an important species in combustion chemistry, and it

is significantly under predicted by the generated model indicating missing pathways or incorrect reaction rates. The ROP analysis will provide insight into which benzene producing reactions are included in the mechanism, and which reactions may be missing resulting in the under prediction of benzene by the model. Figure 42 illustrates the contribution of various reactions to the benzene formation for the 161 ppm of hex-5-en-1-yl fuel simulation. The C4 + C2 species recombination reactions in total contribute 63% of the relative ROP. The acetylene and the *i*C4H5 recombination reaction has the largest share of the relative ROP at 32%. The acetylene and vinylacetylene recombination and the acetylene and 2-butynyl and and acetylene recombination reactions also have a substantial portion of the relative ROP at 14% and 11%, respectively. The two remaining C4+C2 species recombination reactions are the recombination of the vinyl radical and vinylacetylene, and the recombination of 1,3-butadiene and the vinyl radical which have 4% and 2% of the relative ROP. The propargyl recombination reaction has the second largest impact on benzene formation with 21% of the relative ROP. The only other C3+C3 recombination reaction is the recombination of propadiene and propargyl which contributes 9% of the relative ROP. The reaction of toluene with hydrogen which results in the cleavage of the methyl group contributes 6% of the relative ROP. All the reactions, and their overall contribution to the formation of benzene are very similar to those obtained in the ROP analysis for benzene production in the RMG mechanism generated for cyclohexane. The methylcyclohexane RMG mechanism also had the same reactions contributing to the benzene formation, but the contribution from the C3+C3 recombination reactions, i.e. propargyl recombination and the propadiene and propargyl recombination reactions had a slightly higher contribution.

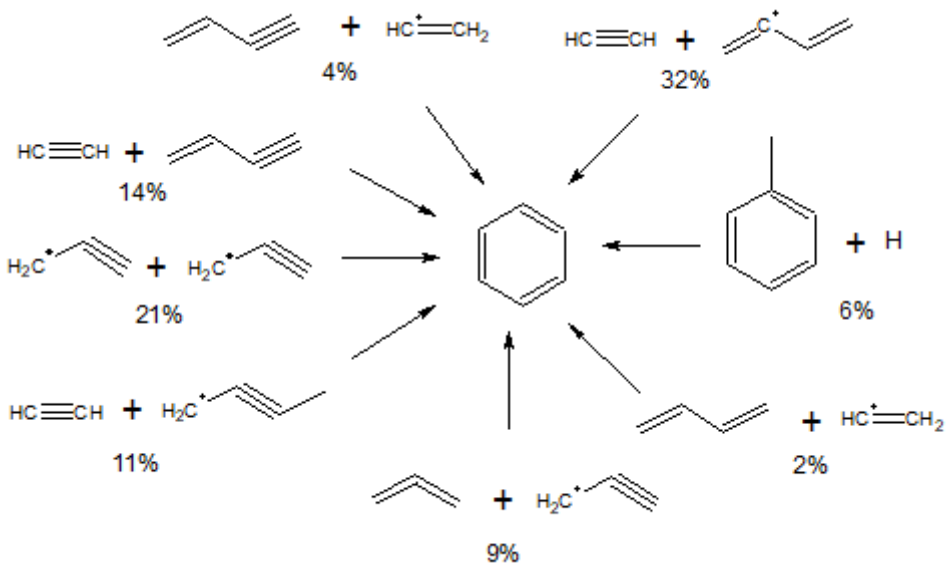

Figure 42: Visualization of the ROP analysis of benzene formation at a temperature of 1350K and reaction time of 2.2 ms for a simulation using 161 ppm of hex-5-en-1-yl as the fuel.

Figure 43 visualizes the contribution of the primary benzene formation reactions for the simulation which used 80 ppm of 1,5-hexadiene and 81 ppm of hex-5-en-1-yl as the fuel at a temperature of 1350K and reaction time of 2.2 ms. The simulation results obtained with the fuel mixture of 80 ppm of 1,5-hexadiene and 81 ppm of hex-5-en-1-yl have resulted in a larger amount of benzene being predicted, although still substantially less than observed experimentally especially at lower temperatures, and also a larger amount of both propadiene and propyne being predicted. This is likewise reflected in the ROP analysis where the C3+C3 recombination reactions now have a substantially larger share, at 86% of the relative ROP, compared to the simulation which used only hex-5-en-1-yl as the fuel. The propargyl recombination reaction alone contributes 56% of the relative ROP, and the propadiene and propargyl recombination reaction contributes 30%. The C4 + C2 species recombination reactions now only contribute 10% of the relative ROP. 5% is a result of the *i*C4H5 and acetylene recombination, 3% comes from acetylene and vinylacetylene recombination, and 2% from acetylene and 2-butynyl recombination. The reaction of toluene with hydrogen also contributes 4% of the relative ROP.

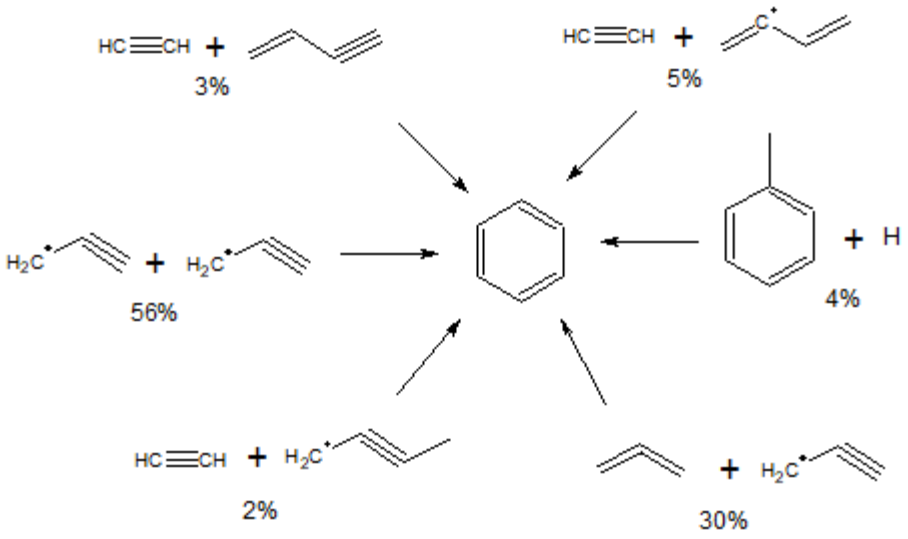

Figure 43: Visualization of the ROP analysis of benzene formation at a temperature of 1350K and reaction time of 2.2 ms for a simulation using 80 ppm of 1,5-hexadiene and 81 ppm of hex-5-en-1-yl as the fuel

Figure 44 illustrates the main decomposition pathways of the hex-5-en-1-yl radical as predicted by the RMG generated mechanism. The reaction pathways were obtained with the help of Chemkin Reaction Path Analyzer. The dominant decomposition pathway for both the fuel mixture simulations is the 1,4-hydrogen shift resulting in the formation of hex-5-en-4-yl. For the simulation using 161 ppm of hex-5-en-1-yl as the fuel the pathway results in nearly 91% of the relative ROP of hex-5-en-1-yl consumption and 94% for the simulation using 80 ppm of 1,5-hexadiene and 81 ppm of hex-5-en-1-yl as fuel. The second most important hex-5-en-1-yl decomposition pathway is the beta-scission of hex-5-en-1-yl which forms ethylene and the but-3-en-1-yl radical. For both fuel mixtures this pathway has approximately 4.5% of the relative ROP of hex-5-en-1-yl consumption. For the simulation using 80 ppm of 1,5-hexadiene and 81 ppm of hex-5-en-1-yl as fuel the third most important hex-5-en-1-yl radical dissociation pathway is the ring closure to form the cyclohexyl radical at approximately 1% of the relative ROP. All the remaining pathways for that fuel mixture combined have a relative ROP of less than 1%. For the

mixture utilizing 161 ppm of hex-5-en-1-yl as the fuel the third most important pathway is the formation of 1,5-hexadiene at approximately 2.5% of the relative ROP of hex-5-en-1-yl dissociation, followed by isomerization to the hex-5-en-2-yl radical or ring closure to form the cyclohexyl radical, both at approximately 1% of the relative ROP of hex-5-en-1-yl dissociation. All the remaining reactions have a contribution of less than 1% to the relative ROP of hex-5-en-1-yl dissociation. The formation of the cyclopentylmethyl radical which can then form methylenecyclopentane is also possible, but has a negligible contribution to the relative ROP of hex-5-en-1-yl radical dissociation. In both the simulation, the cyclohexyl radical will primarily form cyclohexene which will then mostly dissociate into 1,3-butadiene and ethylene. The hex-5-en-2-yl radical can either undergo beta-scission forming propene and the allyl radical, or form 1,5-hexadiene. The hex-5-en-4-yl radical can similarly undergo beta-scission forming 1,3-butadiene and the ethyl radical or form 1,3-hexadiene.

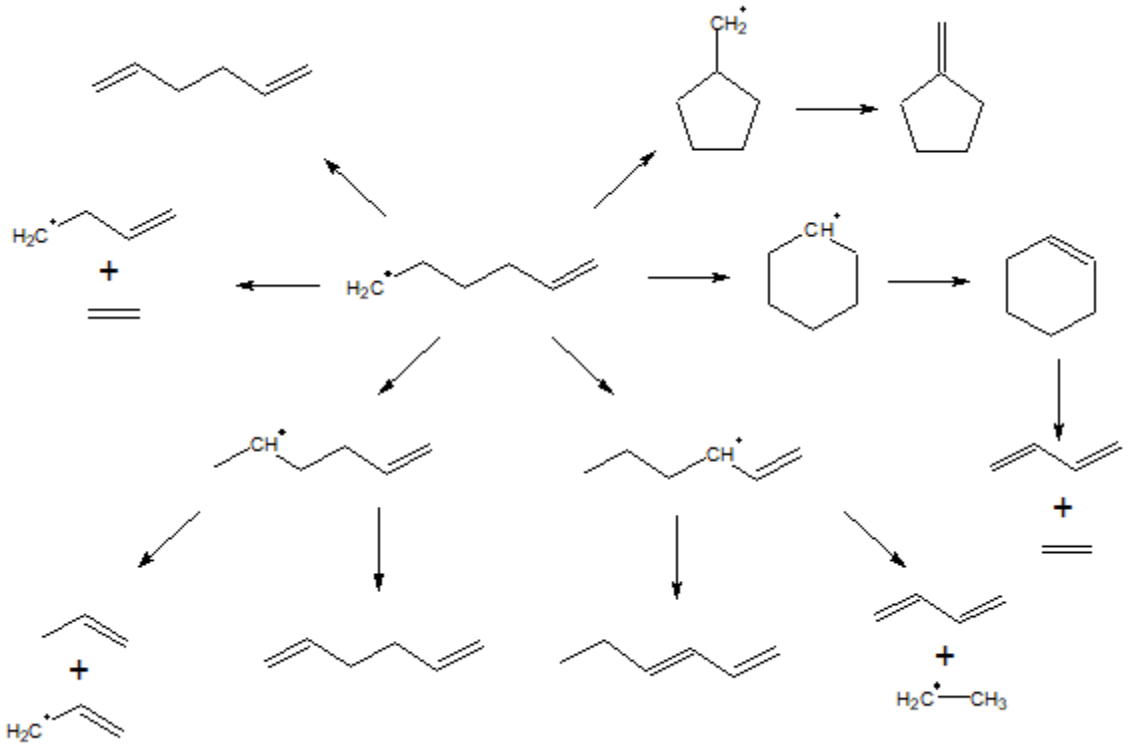

Figure 44: Main hex-5-en-1-yl radical decomposition pathways predicted by RMG mechanism at 1350K and 2.2ms.

6.3.2 Simulation of 1,5-Hexadiene Pyrolysis

Due to the availability of 1,5-hexadiene experimental data which was obtained as part of this study, and the substantial amount of 1,5-hexadiene observed in the pyrolysis of 6-bromo-1-hexene, the generated mechanism is also compared against the 1,5-hexadiene experimental results. Particular interest lies in the ability of the mechanism to predict the benzene formation in the 1,5-hexadiene experiments since the C3 species, such as propadiene, propyne, and propene, were observed to form in abundance and the benzene formation sub mechanism in the generated mechanism heavily relies on C3 + C3 species recombination. Nonetheless, all the typical products have also been plotted except for propane and cyclopropane which were not observed experimentally or predicted by the model, and 1,3-cyclohexadiene and cyclohexene which were not predicted by the model.

Figure 45 contains the species profiles of ethane, ethylene, propadiene, propyne, toluene, methane, acetylene, propene, 1-butene, diacetylene, isobutyelene, 1,3-cyclopentadiene, 1,5-

hexadiene, and benzene from the 100 bar 1,5-hexadiene pyrolysis experiments and the simulation profiles obtained using the RMG generated mechanism for hex-5-en-1-yl and 1,5-hexadiene pyrolysis. The mechanism is able to excellently predict the propyne, methane and acetylene profiles over the entire experimental temperature range, and all three species were major products. For the other two most abundant species, propadiene and propene, the decay is well captured, but the formation is predicted to proceed at temperatures approximately 70K lower than observed experimentally, and the peak amount are over predicted by over 40%, but the peak temperature is well captured. Ethylene is also a major product species, and the peak amount is captured within 16%, but the formation is predicted to initially proceed slower with increasing temperature than observed experimentally. The toluene formation is well predicted, and the 1-butene formation and decay are well captured, but the peak amount of each species is under predicted.

All the other product species are generally reasonably well captured by the model; however, the 1,5-hexadiene decay is predicted to proceed at temperatures approximately 50K lower than observed experimentally. Lastly, and most importantly, the model excellently captured the benzene experimental data. This result illustrates the model's ability to capture benzene formation when it is expected to primarily proceed through the recombination of C3 + C3 species, which are plentiful in the pyrolysis of 1,5-hexadiene. This also reiterates that the large amount of benzene forming at lower temperatures in 6-bromo-1-hexene which proceeds through the hex-5-en-1-yl is not a result of C3 + C3 species recombination, and requires further modeling efforts to capture accurately.

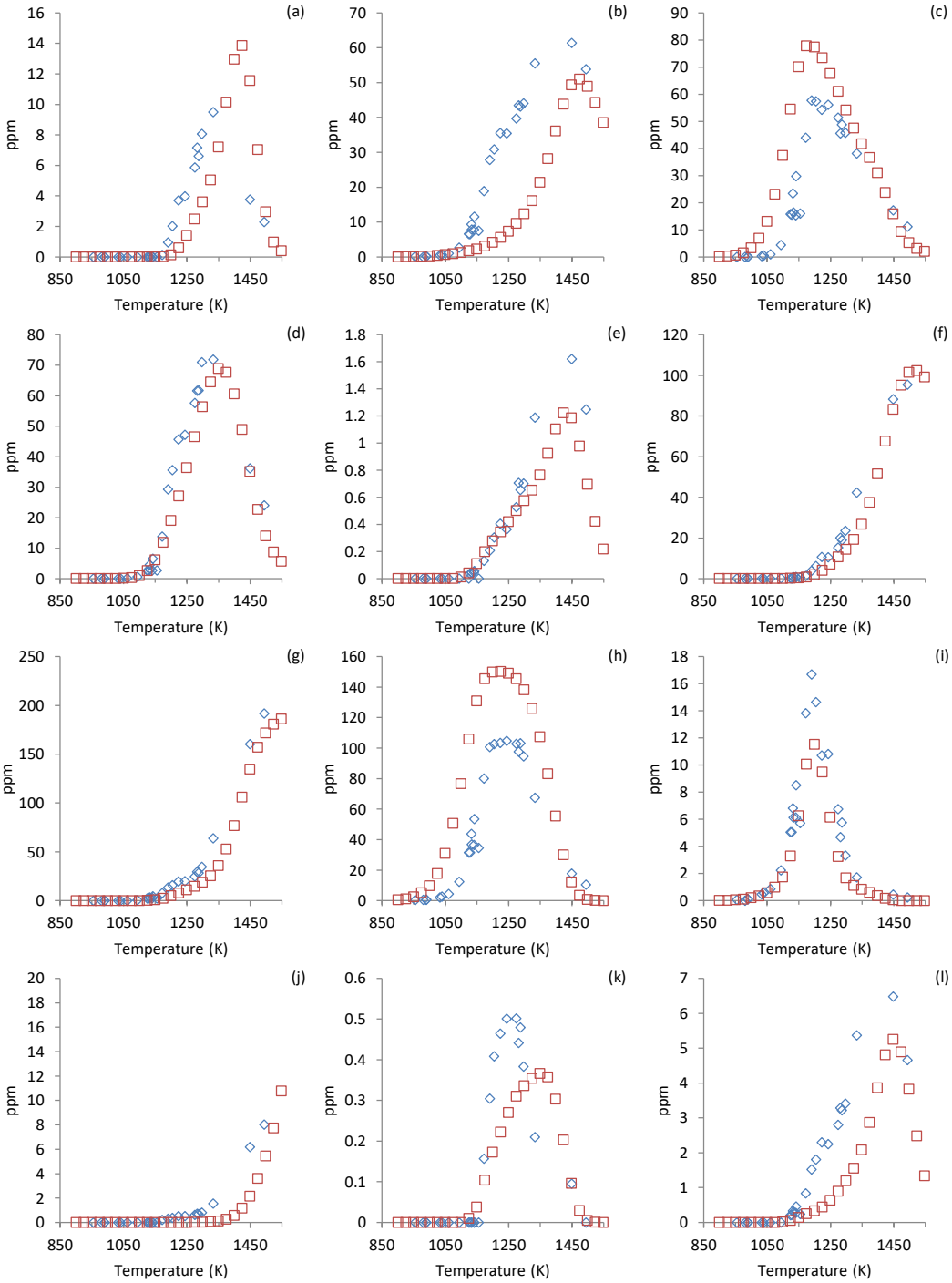
(a)
(b)
(c)
(d)
(e)
(f)
(g)
(h)
(i)
(j)
(k)
(l)
ppm
Temperature (K)
850
1050
1250
1450

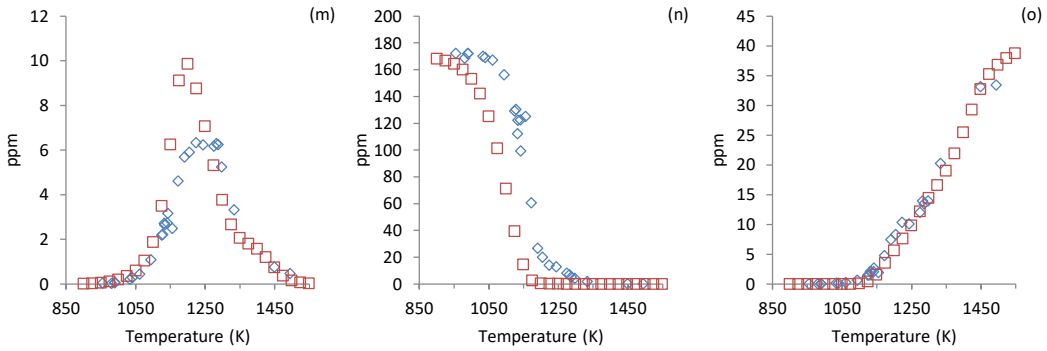

Figure 45: Comparison of species profiles of (a) ethane, (b) ethylene, (c) propadiene, (d) propyne, (e) toluene, (f) methane, (g) acetylene, (h) propene, (i) 1-butene, (j) diacetylene, (k) isobutylene, (l) vinylacetylene, (m) 1,3-cyclopentadiene, (n) 1,5-hexadiene, and (o) benzene formed in 1,5-hexadiene pyrolysis at 100 bar and 170 ppm of 1,5-hexadiene as the fuel against the simulation results obtained from the RMG generated mechanism. Legend: ◇Experimental Data, □ Simulation Results using 170 ppm of 1,5-hexadiene as fuel.

6.4 Summary

A 6-bromo-1-hexene pyrolysis study was completed at high pressures and temperatures seeking to investigate the effects of pressure on the pyrolysis of the hex-5-en-1-yl radical and also whether a high pressure environment is sufficient to drive the formation of alkylcyclopentanes which have been detected in supercritical phase pyrolysis of alkylcyclohexanes. The use of a hex-5-en-1-yl precursor allowed the study to be completed further along the reaction pathway expected to result in the formation of methylenecyclopentane, and perhaps alkylcyclopentanes, based on the proposed analogous pathway in the study of methylcyclohexane pyrolysis in the supercritical phase[20], see Figure 35. Neither methylenecyclopentane nor any alkylcyclopentanes were observed in the current work, indicating the pressure alone is not sufficient to drive the formation of alkylcyclopentanes. Varying the experimental pressure between the three target pressures of 40, 100, and 200 bar did impact the product distribution. Most noticeably the product profiles of ethane, ethylene, propane, propadiene, propyne, and toluene were affected by the variation of the experimental pressure. The experiments at all three pressures were conducted with fuel mixtures that contained

approximately an equivalent mole fraction of 6-bromo-1-hexene in the test gas, but assuming ideal gas behavior, the fuel concentration in the reaction zone is expected to vary proportionally with the experimental pressure. An additional set of experiments was conducted at a pressure of 40 bar, but with a higher fuel mole fraction so that the fuel concentration in the reaction zone comes close to that in the 100 bar experiments, and the product distribution obtained matched closely that at 100 bar. This result emphasized that at the current experimental conditions the product distribution is sensitive to the initial fuel concentration.

An additional set of experiments was conducted using 1,5-hexadiene as the fuel in order to generate 1,5-hexadiene pyrolysis data at experimental conditions relevant to this study. This was done due to large amounts of 1,5-hexadiene being observed to form at low temperatures in the 6-bromo-1-hexene pyrolysis. The main intent of the 6-bromo-1-hexene pyrolysis work was to study the decomposition of the hex-5-en-1-yl radical, but if the primarily reaction pathway proceeded through the HBr loss resulting in the formation of 1,5-hexadiene then the production distributions from 6-bromo-1-hexene and 1,5-hexadiene pyrolysis would be expected to be similar if not the same, but this was found not to be the case.

A hex-5-en-1-yl and 1,5-hexadiene chemical kinetic mechanism was generated with the help of RMG in an attempt to model the experimental data. RMG is unable to generate mechanisms for species containing bromine, hence why the mechanism was instead generated for the two main expected initial products, or hex-5-en-1-yl and 1,5-hexadiene. The mechanism was unable to accurately predict the large amounts of benzene which formed at relatively low temperatures, and it substantially under predicted cyclohexene and did not predict any 1,3-cyclohexadiene formation. When the same mechanism was used to simulated the 1,5-hexadiene set of experiments it was able to capture the benzene profile exceptionally well. In 1,5-hexadiene

the benzene pyrolysis proceeds through the C3 + C3 species recombination, which are formed in abundance; however, these are not expected to be the main pathways which result in the benzene formation from the hex-5-en-1-yl radical. Instead, the proposed pathways proceed through the isomerization of hex-5-en-1-yl radical to the cyclohexyl radical which then forms cyclohexene that undergoes dehydrogenation ultimately forming benzene. The other pathway involves the cyclopentylmethyl radical, which is the more traditionally proposed isomerization product of hex-5-en-1-yl radical. The cyclopentylmethyl radical would then either form methylenecyclopentane, or the methylcyclopentene isomers which would undergo dehydrogenation forming fulvene that would then isomerize to benzene; however, no alkylcyclopentanes, alkylcyclopentanes or alkenylcyclopentanes, which were observed in the supercritical phase pyrolysis of alkylcyclohexanes, were observed experimentally in the present work to suggest that this is pathway occurs. The large amounts of benzene observed experimentally, and the importance of hex-5-en-1-yl in the cyclohexyl radical isomerization, should act as motivation for further refinement of pathways of the hex-5-en-1-yl radical acting as a benzene precursor.

7. CONCLUDING REMARKS AND FUTURE WORK

The presented work resulted in substantial amounts of speciation data for three species: cyclohexane, methylcyclohexane, and 6-bromo-1-hexene, all three of which are relevant to real fuels. The experiments were conducted at high pressures of up to 200 bar rarely seen in gas phase experiments. The high pressure conditions used for the present work matched, and surpassed, the experimental pressures of previous works investigating the pyrolysis of cyclohexane and alkylcyclohexanes at supercritical conditions[19–21]. No alkylcyclopentanes were observed to form in the present work, in contrast to the supercritical pyrolysis studies where alkylcyclopentanes were the main products, and only methylenecyclopentane was observed in trace amounts in the present cyclohexane and methylcyclohexane studies. This led to the conclusion that high pressures alone are not sufficient to drive the formation of alkylcyclopentanes, and that the high concentration environment present in the supercritical phase studies must be needed. This conclusion is further supported by the high mole fraction (3195 ppm) cyclohexane experimental data set where an increase in the production of cyclic products was observed compared to the experiments which used lower mole fractions of cyclohexane (~200 ppm).

The HPST could be used to conduct further experiments with higher initial concentrations of the fuel. This could be achieved by using higher initial fuel mole fractions, e.g. on the order of 10,000 ppm, and higher experimental pressures since the shock tube was designed to operate at pressures of up to 1000 bar. It is expected that such experimental work would be time consuming due to the need for frequent cleaning and maintained of the sampling system due to the carbon build up. Further experiments with higher initial concentrations of the fuel would provide insight as to whether the formation of cyclic species continuous to increase with increasing initial fuel

concentration, and whether a quantifiable amount of alkylcyclopentanes could form in the gas phase.

The speciation data obtained in the present work was also used for the purpose of chemical kinetic modeling using an open source tool. The speciation data is freely available and is included in APPENDIX D. It can be used for further chemical kinetic mechanism development and validation. The present data was also compared against a recently published methylcyclohexane mechanism[23]. It was found that the mechanism was unable to capture the amount of benzene observed to form in the cyclohexane and methylcyclohexane experiments. The amount of benzene predicted by the mechanism would typically be double of what was observed experimentally. The amount of propadiene and propyne by the mechanism was under predicted compared to the cyclohexane and methylcyclohexane experimental data. An attempt was made at systematically improving the mechanism's ability to predict the current data, without degrading its ability to predict the lower pressure data against which it was validated. The ability to predict the benzene formation was improved, but it was still substantially over predicted over the majority of the experimental temperature range. Further refinement of the reaction rate constants for the dominant benzene formation reactions, such as C3 + C3 species recombination, is suggested to better capture experimental data at conditions relevant to those in the present study.

Chemical kinetic mechanisms were generated for cyclohexane and methylcylohexane using RMG. RMG does not currently allow the inclusion of bromine containing species in the generated mechanisms, so a mechanism for the hex-5-en-1-yl radical and 1,5-hexadiene, the expected two initial products of 6-bromo-1-hexene dissociation, was generated instead. The methylcyclohexane mechanism was able to predict the experimental data well, and did not have

difficulty predicting benzene unlike the literature mechanism. The cyclohexane mechanism was able to predict the experimental benzene profile well up to a temperature of approximately 1450K, but it significantly under predicted both the amount of propadiene and propyne observed experimentally. Furthermore, the hex-5-en-1-yl and 1,5-hexadiene mechanism was unable to capture the significant amounts of benzene observed experimentally. The hex-5-en-1-yl radical is expected to be the primary product of the cyclohexyl radical ring opening, and the cyclohexyl radical is in turn the expected primary product of cyclohexane dissociation. These findings suggest that the current cyclohexane and cyclohexyl radical dissociation pathways are incomplete and that the reaction rate constants for those pathways need further refinement. The current experimental data should aid in the refinement of future mechanisms, particularly the 6-bromo-1-hexene study which was used to investigate the hex-5-en-1-yl radical dissociation. Only one similar study[125] has been previously conducted, at lower pressures of around 2 bar, much smaller temperature range (1060-1160K) and with species data only for the hydrogen atom. The current work spans a much larger temperature range (900-1500K), multiple pressures (40, 100, and 200 bar) and provides speciation data for over 20 species.

The large amounts of benzene observed in the hex-5-en-1-yl radical dissociation experiments illustrated that the hex-5-en-1-yl radical dissociation pathways are more complex than currently modeled. It may also be worthwhile to experimentally determine whether the hex-5-en-1-yl radical truly is the dominant product of cyclohexyl radical dissociation. This could be done by completing experiments using bromocyclohexane and comparing the product distribution to that of 6-bromo-1-hexene, which should be very close according to current literature mechanisms which primarily predict the cyclohexyl radical to dissociate to hex-5-en-1-yl radical.

CITED LITERATURE

[1] M. Sivak, B. Schoettle, Eco-driving: Strategic, tactical, and operational decisions of the driver that influence vehicle fuel economy, Transp. Policy. 22 (2012) 96–99. doi:10.1016/j.tranpol.2012.05.010.

[2] T. Klier, J. Linn, The price of gasoline and new vehicle fuel economy: Evidence from monthly sales data, Am. Econ. J. Econ. Policy. 2 (2010) 134–153. doi:10.1257/pol.2.3.134.

[3] A. Khaligh, Z. Li, Battery, ultracapacitor, fuel cell, and hybrid energy storage systems for electric, hybrid electric, fuel cell, and plug-in hybrid electric vehicles: State of the art, IEEE Trans. Veh. Technol. 59 (2010) 2806–2814. doi:10.1109/TVT.2010.2047877.

[4] K. Clement-Nyns, E. Haesen, J. Driesen, The impact of Charging plug-in hybrid electric vehicles on a residential distribution grid, IEEE Trans. Power Syst. 25 (2010) 371–380. doi:10.1109/TPWRS.2009.2036481.

[5] G. Fontaras, P. Pistikopoulos, Z. Samaras, Experimental evaluation of hybrid vehicle fuel economy and pollutant emissions over real-world simulation driving cycles, Atmos. Environ. 42 (2008) 4023–4035. doi:10.1016/j.atmosenv.2008.01.053.

[6] Z. Mohamed-Kassim, A. Filippone, Fuel savings on a heavy vehicle via aerodynamic drag reduction, Transp. Res. Part D Transp. Environ. 15 (2010) 275–284. doi:10.1016/j.trd.2010.02.010.

[7] J. Ortega, K. Salari, A. Brown, R. Schoon, Aerodynamic drag reduction of class 8 heavy vehicles: a full-scale wind tunnel study, 2013. https://e-reports-ext.llnl.gov/pdf/741852.pdf (accessed April 23, 2018).

[8] L.L.N. Laboratory, DOE's, DOE ' s Effort to Reduce Truck Aerodynamic Drag through Joint Experiments and Computations, (2012). doi:10.2514/6.2004-2249.

[9] R.G. Papagiannakis, C.D. Rakopoulos, D.T. Hountalas, D.C. Rakopoulos, Emission characteristics of high speed, dual fuel, compression ignition engine operating in a wide range of natural gas/diesel fuel proportions, Fuel. 89 (2010) 1397–1406. doi:10.1016/j.fuel.2009.11.001.

[10] T. Korakianitis, A.M. Namasivayam, R.J. Crookes, Natural-gas fueled spark-ignition (SI) and compression-ignition (CI) engine performance and emissions, Prog. Energy Combust. Sci. 37 (2011) 89–112. doi:10.1016/j.pecs.2010.04.002.

[11] P. Hartmann, V. Apaolaza-Ibáñez, Consumer attitude and purchase intention toward green energy brands: The roles of psychological benefits and environmental concern, J. Bus. Res. 65 (2012) 1254–1263. doi:10.1016/j.jbusres.2011.11.001.

[12] Q. Zhang, G. Liu, L. Wang, X. Zhang, G. Li, Controllable decomposition of methanol for active fuel cooling technology, in: Energy and Fuels, American Chemical Society, 2014: pp. 4431–4439. doi:10.1021/ef500668q.

[13] T. Edwards, Cracking and deposition behavior of supercritical hydrocarbon aviation fuels, Combust. Sci. Technol. 178 (2006) 307–334. doi:10.1080/00102200500294346.

[14] P.G. Hill, C.R. Peterson, Mechanics and Thermodynamics of Propulsion, 2nd ed., Addison-Wesley Publishing Co., Reading, MA, 1992.

[15] A. Young, Game Changer: SpaceX, in: Springer, Cham, 2015: pp. 15–28. doi:10.1007/978-3-319-18929-1_2.

[16] J. Foust, United States Space Launch Programs, in: Handb. Sp. Secur., Springer New York, New York, NY, 2015: pp. 725–742. doi:10.1007/978-1-4614-2029-3_32.

[17] A. Mazzetti, L. Merotto, G. Pinarello, Paraffin-based hybrid rocket engines applications: A review and a market perspective, Acta Astronaut. 126 (2016) 286–297. doi:10.1016/j.actaastro.2016.04.036.

[18] B. Kehimkar, B.A. Parsons, J.C. Hoggard, M.C. Billingsley, T.J. Bruno, R.E. Synovec, Modeling RP-1 fuel advanced distillation data using comprehensive two-dimensional gas chromatography coupled with time-of-flight mass spectrometry and partial least squares analysis, Anal. Bioanal. Chem. 407 (2015) 321–330. doi:10.1007/s00216-014-8233-6.

[19] W.C. Lai, C. Song, Pyrolysis of alkylcyclohexanes in or near the supercritical phase. Product distribution and reaction pathways, Fuel Process. Technol. 48 (1996) 1–27. doi:10.1016/0378-3820(96)01030-2.

[20] J.F. Stewart, Supercritical Pyrolysis of the Endothermic Fuels Methylcyclohexane, Decalin and Tetralin, Princeton University, 1999. http://adsabs.harvard.edu/abs/1999PhDT.....388S.

[21] J. Kim, S.H. Park, C.H. Lee, B.-H. Chun, J.S. Han, B.H. Jeong, S.H. Kim, Coke Formation during Thermal Decomposition of Methylcyclohexane by Alkyl Substituted C_5 Ring Hydrocarbons under Supercritical Conditions, Energy & Fuels. 26 (2012) 5121–5134. doi:10.1021/ef3007678.

[22] C.S. McEnally, L.D. Pfefferle, An Experimental Study in Non-Premixed Flames of Hydrocarbon Growth Processes that Involve Five-Membered Carbon Rings, Combust. Sci. Technol. 131 (1998) 323–344. doi:10.1080/00102209808935766.

[23] Z. Wang, L. Ye, W. Yuan, L. Zhang, Y. Wang, Z. Cheng, F. Zhang, F. Qi, Experimental and kinetic modeling study on methylcyclohexane pyrolysis and combustion, Combust. Flame. 161 (2014) 84–100. doi:10.1016/j.combustflame.2013.08.011.

[24] S. Zeppieri, K. Brezinsky, I. Glassman, Pyrolysis studies of methylcyclohexane and oxidation studies of methylcyclohexane and methylcyclohexane/toluene blends, Combust. Flame. 108 (1997) 266–286. doi:10.1016/S0010-2180(96)00125-3.

[25] F.L. Dryer, C.K. Westbrook, Simplified Reaction Mechanisms for the Oxidation of Hydrocarbon Fuels in Flames, Combust. Sci. Technol. 27 (1981) 31–43. doi:10.1080/00102208108946970.

[26] W.P. Jones, R.P. Lindstedt, Global reaction schemes for hydrocarbon combustion, Combust. Flame. 73 (1988) 233–249. doi:10.1016/0010-2180(88)90021-1.

[27] R.S. Tranter, K. Brezinsky, D. Fulle, Design of a high-pressure single pulse shock tube for chemical kinetic investigations, Rev. Sci. Instrum. 72 (2001) 3046–3054. doi:10.1063/1.1379963.

[28] A. Fridlyand, K. Brezinsky, A. Mandelbaum, N-Heptane Pyrolysis and Oxidation in Ethylene – Methane and Iso-Octane Mixtures, J. Propuls. Power. 29 (2013) 732–743. doi:10.2514/1.B34875.

[29] C. Ji, E. Dames, B. Sirjean, H. Wang, F.N. Egolfopoulos, An experimental and modeling study of the propagation of cyclohexane and mono-alkylated cyclohexane flames, Proc. Combust. Inst. 33 (2011) 971–978. doi:10.1016/j.proci.2010.06.099.

[30] N. Liu, C. Ji, F.N. Egolfopoulos, Ignition of non-premixed cyclohexane and mono-alkylated cyclohexane flames, Proc. Combust. Inst. 34 (2013) 873–880. doi:10.1016/j.proci.2012.05.104.

[31] C.S. McEnally, L.D. Pfefferle, Experimental study of fuel decomposition and hydrocarbon growth processes for cyclohexane and related compounds in nonpremixed flames, Combust. Flame. 136 (2004) 155–167. doi:10.1016/j.combustflame.2003.09.012.

[32] H.R. Zhang, L.K. Huynh, N. Kungwan, Z. Yang, S. Zhang, Combustion modeling and kinetic rate calculations for a stoichiometric cyclohexane flame. 1. Major reaction

pathways, J. Phys. Chem. A. 111 (2007) 4102–4115. doi:10.1021/jp068237q.

[33] Y. Zhang, J. Cai, L. Zhao, J. Yang, H. Jin, Z. Cheng, Y. Li, L. Zhang, F. Qi, An experimental and kinetic modeling study of three butene isomers pyrolysis at low pressure, Combust. Flame. 159 (2012) 905–917. doi:10.1016/j.combustflame.2011.09.005.

[34] E.J. Silke, W.J. Pitz, C.K. Westbrook, M. Ribaucour, Detailed chemical kinetic modeling of cyclohexane oxidation, J. Phys. Chem. A. 111 (2007) 3761–3775. doi:10.1021/jp067592d.

[35] P. Dagaut, M. Cathonnet, The ignition, oxidation, and combustion of kerosene: A review of experimental and kinetic modeling, Prog. Energy Combust. Sci. 32 (2006) 48–92. doi:10.1016/j.pecs.2005.10.003.

[36] Z. Wang, Z. Cheng, W. Yuan, J. Cai, L. Zhang, F. Zhang, F. Qi, J. Wang, An experimental and kinetic modeling study of cyclohexane pyrolysis at low pressure, Combust. Flame. 159 (2012) 2243–2253. doi:10.1016/j.combustflame.2012.02.019.

[37] A. Fridlyand, S.S. Goldsborough, K. Brezinsky, S.S. Merchant, W.H. Green, Influence of the double bond position on the oxidation of decene isomers at high pressures and temperatures, Proc. Combust. Inst. 35 (2015) 333–340. doi:10.1016/J.PROCI.2014.06.020.

[38] A. Fridlyand, S.S. Goldsborough, K. Brezinsky, Chemical Kinetic Influences of Alkyl Chain Structure on the High Pressure and Temperature Oxidation of a Representative Unsaturated Biodiesel: Methyl Nonenoate, J. Phys. Chem. A. 119 (2015) 7559–7577. doi:10.1021/acs.jpca.5b00914.

[39] A. Comandini, T. Malewicki, K. Brezinsky, Online and offline experimental techniques for polycyclic aromatic hydrocarbons recovery and measurement, Rev. Sci. Instrum. 83 (2012) 34101. doi:10.1063/1.3692748.

[40] P. Vieille, Sur les discontinuités produites par la détente brusque de gaz comprimés., Comptes Rendus. 129 (1899) 1228.

[41] H. Muraour, Étude spectrale de la détonation dans le vide des explosifs d'amorçage, J. Phys. Le Radium. 7 (1936) 411–416. doi:10.1051/jphysrad:01936007010041100.

[42] H. Muraour, A. Michel-Lévy, E. Burlot, Étude des phénomènes lumineux qui accompagnent la propagation des ondes de choc dans différents gaz, J. Phys. Le Radium.

8 (1937) 330–331. doi:10.1051/jphysrad:0193700808033000.

[43] H. Muraour, A. Michel-Lévy, Obtention de spectres de métaux par rencontre d'ondes de choc, J. Phys. Le Radium. 1 (1940) 260–264. doi:10.1051/jphysrad:0194000107026000.

[44] W. Payman, W.C.F. Shepherd, Explosion Waves and Shock Waves. VI. The Disturbance Produced by Bursting Diaphragms with Compressed Air, Proc. R. Soc. A Math. Phys. Eng. Sci. 186 (1946) 293–321. doi:10.1098/rspa.1946.0045.

[45] A.G. Gaydon, I.R. Hurle, The shock tube in high-temperature chemical physics, Chapman and Hall, 1963.

[46] E.F. Greene, G.R. Cowan, D.F. Hornig, The thickness of shock fronts in argon and nitrogen and rotational heat capacity lags, J. Chem. Phys. 19 (1951) 427–434. doi:10.1063/1.1748241.

[47] E.F. Greene, D.F. Hornig, The shape and thickness of shock fronts in argon, hydrogen, nitrogen, and oxygen, J. Chem. Phys. 21 (1953) 617–624. doi:10.1063/1.1698978.

[48] W.H. Andersen, D.F. Hornig, The structure of shock fronts in various gases, Mol. Phys. 2 (1959) 49–63. doi:10.1080/00268975900100051.

[49] E.F. Smiley, E.H. Winkler, Shock-tube measurements of vibrational relaxation, J. Chem. Phys. 22 (1954) 2018–2022. doi:10.1063/1.1739984.

[50] W. Griffith, D. Brickl, V. Blackman, Structure of Shock Waves in Polyatomic Gases, Phys. Rev. 102 (1956) 1209–1216. doi:10.1103/PhysRev.102.1209.

[51] V. Blackman, Vibrational relaxation in oxygen and nitrogen, J. Fluid Mech. 1 (1956) 61–85. doi:10.1017/S0022112056000056.

[52] I.R. HURLE, A.G. GAYDON, Vibrational Relaxation and Dissociation of Carbon Dioxide behind Shock Waves, Nature. 184 (1959) 1858–1859. doi:10.1038/1841858a0.

[53] W. Roth, Vibrational Relaxation of CN in the Shock Tube, J. Chem. Phys. 31 (1959) 720–721. doi:10.1063/1.1730451.

[54] M. Camac, A. Vaughan, O2 Dissociation Rates O2-Ar Mixtures, J. Chem. Phys. 34 (1961) 460–470. doi:10.1063/1.4757209.

[55] M. Camac, O2vibration relaxation in oxygen-argon mixtures, J. Chem. Phys. 34 (1961) 448–459. doi:10.1063/1.4757208.

[56] P.R. Monson, J.J. Allport, F. Robben, Comparative studies of vibrational relaxation in nitric oxide, Planet. Space Sci. 3 (1961) 86–93. doi:10.1016/0032-0633(61)90231-8.

[57] D. Britton, N. Davidson, G. Schott, SHOCK WAVES IN CHEMICAL KINETICS THE RATE OF DISSOCIATION OF MOLECULAR IODINE, Discuss. Faraday Soc. 17 (1954) 58–68. http://pubs.rsc.org/-/content/articlepdf/1954/df/df9541700058 (accessed April 10, 2018).

[58] D. Britton, N. Davidson, W. Gehman, C. Schott, Shock waves in chemical kinetics: Further studies on the rate of dissociation of molecular iodine, J. Chem. Phys. 25 (1956) 804–809. doi:10.1063/1.1743127.

[59] H.B. Palmer, D.F. Hornig, Rate of dissociation of bromine in shock waves, J. Chem. Phys. 26 (1956) 98–105. doi:10.1063/1.1743272.

[60] H.S. Glick, W.H. Wurster, Shock Tube Study of Dissociation Relaxation in Oxygen, J. Chem. Phys. 27 (1957). doi:10.1063/1.1743976.

[61] J.P. Chesick, G.B. Kistiakowsky, Gaseous detonations. X. Study of reaction zones, J. Chem. Phys. 28 (1958) 956–961. doi:10.1063/1.1744304.

[62] S.R. Byron, Measurement of the rate of dissociation of oxygen, J. Chem. Phys. 30 (1959) 1380–1392. doi:10.1063/1.1730209.

[63] D.L. Matthews, Interferometric Measurement in the Shock Tube of the Dissociation Rate of Oxygen, Phys. Fluids. 2 (1959) 170. doi:10.1063/1.1705908.

[64] J.P. Rink, H.T. Knight, R.E. Duff, Shock tube determination of dissociation rates of oxygen, J. Chem. Phys. 34 (1961) 1942–1947. doi:10.1063/1.1731797.

[65] H.T. Knight, J.P. Rink, Dissociation Energy of Cyanogen and Related Quantities by X-Ray Densitometry of Shock Waves, J. Chem. Phys. 35 (1961) 199–208. doi:10.1063/1.1731891.

[66] J.N. Bradley, SHOCK-WAVE DECOMPOSITION OF NITROPARAFFINS PART 1.-MASS-SPECTROMETRIC STUDY OF NITROMETHANE DECOMPOSITION, Trans. Faraday Soc. 57 (1961) 1750–1756. http://pubs.rsc.org/-/content/articlepdf/1961/tf/tf9615701750 (accessed April 11, 2018).

[67] M.N. Plooster, D. Garvin, The Hydrogen-Bromine Reaction at Elevated Temperatures, J. Am. Chem. Soc. 78 (1956) 6003–6008. https://pubs.acs.org/doi/pdf/10.1021/ja01604a013 (accessed April 11, 2018).

[68] H.S. Glick, J.J. Klein, W. Squire, Single-Pulse Shock Tube Studies of the Kinetics of the Reaction N 2 +O 2 ⇄2NO between 2000–3000°K, J. Chem. Phys. 27 (1957) 850–857.

doi:10.1063/1.1743864.

[69] S.-C. Lin, W.I. Fyfe, Low-Density Shock Tube for Chemical Kinetics Studies, Phys. Fluids. 4 (1961) 238. doi:10.1063/1.1724434.

[70] J.N. Bradley, G.B. Kistiakowsky, Shock Wave Studies by Mass Spectrometry. I. Thermal Decomposition of Nitrous Oxide, J. Chem. Phys. 35 (1961) 256–263. doi:10.1063/1.1731897.

[71] J.N. Bradley, G.B. Kistiakowsky, Shock wave studies by mass spectrometry. II. Polymerization and oxidation of acetylene, J. Chem. Phys. 35 (1961) 264–270. doi:10.1063/1.1731898.

[72] C.F. Aten, E.F. Greene, THE PYROLYSIS OF ACETYLENE IN SHOCK WAVES, Discuss. Faraday Soc. 22 (1956) 162–166. http://pubs.rsc.org/-/content/articlepdf/1956/df/df9562200162 (accessed April 11, 2018).

[73] C.F. Aten, E.F. Greene, The high temperature pyrolysis of acetylene 1400° to 2500° K, Combust. Flame. 5 (1961) 55–64. doi:10.1016/0010-2180(61)90073-6.

[74] R.K. Lyon, P.H. Kydd, Gaseous Detonations. XIV. The CH Radical in Acetylene Oxygen Detonations, J. Chem. Phys. 34 (1961) 1069–1070. doi:10.1063/1.1731648.

[75] T. Carrington, N. Davidson, Shock waves in chemical kinetics: The rate of dissociation of N204., J. Phys. Chem. 57 (1953) 418–427.

[76] G. Schott, N. Davidson, Shock Waves in Chemical Kinetics: The Decomposition of N2O5 at High Temperatures., J. Am. Chem. Soc. 80 (1958) 1841–1853.

[77] H.S. Glick, W. Squire, A. Hertzberg, A new shock tube technique for the study of high temperature gas phase reactions., Symp. Combust. 5 (1955) 393–402.

[78] E.F. Greene, R.L. Taylor, W.L. Patterson Jr, Pyrolysis of simple hydrocarbons in shock waves., J. Phys. Chem. 62 (1958) 238–243.

[79] G.B. Skinner, R.A. Ruehrwein, Shock tube studies on the pyrolysis and oxidation of methane., J. Phys. Chem. 63 (1959) 1736–1742.

[80] M. Steinberg, W.E. Kaskan, The ignition of combustible mixtures by shock waves., Symp. Combust. 5 (1955) 664–672.

[81] A. Fridlyand, P.T. Lynch, R.S. Tranter, K. Brezinsky, Single pulse shock tube study of allyl radical recombination, J. Phys. Chem. A. 117 (2013) 4762–4776. doi:10.1021/jp402391n.

[82] R.S. Tranter, P.T. Lynch, J.B. Randazzo, J.P.A. Lockhart, X. Chen, C.F. Goldsmith, High temperature pyrolysis of 2-methyl furan, Phys. Chem. Chem. Phys. (2018). doi:10.1039/C7CP07775K.

[83] P.T. Lynch, Note: An improved solenoid driver valve for miniature shock tubes, Rev. Sci. Instrum. 87 (2016) 56110. doi:10.1063/1.4953115.

[84] K.P. Lynch, J.L. Wagner, Time-resolved pulse-burst tomographic PIV of impulsively-started cylinder wakes in a shock tube, in: 2018 AIAA Aerosp. Sci. Meet., American Institute of Aeronautics and Astronautics, Reston, Virginia, 2018. doi:10.2514/6.2018-2038.

[85] P.T. Lynch, T.P. Troy, M. Ahmed, R.S. Tranter, Probing combustion chemistry in a miniature shock tube with synchrotron VUV photo ionization mass spectrometry, Anal. Chem. 87 (2015) 2345–2352. doi:10.1021/ac5041633.

[86] P.T. Lynch, G. Wang, Chemical thermometry in miniature HRRST using 1,1,1-trifluoroethane dissociation, Proc. Combust. Inst. 36 (2017) 307–314. doi:10.1016/j.proci.2016.05.057.

[87] J.B. Randazzo, C.J. Annesley, K. Bell, R.S. Tranter, A shock tube laser schlieren study of cyclopentane pyrolysis, Proc. Combust. Inst. 36 (2017) 273–280. doi:10.1016/j.proci.2016.05.038.

[88] J.B. Randazzo, R.S. Tranter, Note: An improved driver section for a diaphragmless shock tube, Rev. Sci. Instrum. 86 (2015) 16117. doi:10.1063/1.4906758.

[89] R.K. Hanson, D.F. Davidson, Recent advances in laser absorption and shock tube methods for studies of combustion chemistry, Prog. Energy Combust. Sci. 44 (2014) 103–114. doi:10.1016/j.pecs.2014.05.001.

[90] R.S. Tranter, R. Sivaramakrishnan, N. Srinivasan, K. Brezinsky, Calibration of reaction temperatures in a very high pressure shock tube using chemical thermometers, Int. J. Chem. Kinet. 33 (2001) 722–731. doi:10.1002/kin.1069.

[91] W. Tang, K. Brezinsky, Chemical kinetic simulations behind reflected shock waves, Int. J. Chem. Kinet. 38 (2006) 75–97. doi:10.1002/kin.20134.

[92] A. Lifshitz, C. Tamburu, F. Dubnikova, Reactions of 1-naphthyl radicals with ethylene. Single pulse shock tube experiments, quantum chemical, transition state theory, and multiwell calculations, J. Phys. Chem. A. 112 (2008) 925–933. doi:10.1021/jp077289s.

[93] A. Matsugi, K. Yasunaga, H. Shiina, Thermal decomposition of 1,1,1-trifluoroethane revisited, J. Phys. Chem. A. 118 (2014) 11688–11695. doi:10.1021/jp510227k.

[94] K.J. Laidler, Chemical kinetics, 3rd ed., Harper & Row, New York, 1987.

[95] S.R. Turns, An Introduction to Combustion: Concepts and Applications, 2nd ed., McGraw-Hill, 2000.

[96] F.A. Lindemann, S. Arrhenius, I. Langmuir, N.R. Dhar, J. Perrin, W.M. Lewis, Discussion on "the radiation theory of chemical action," Trans. Faraday Soc. 17 (1922) 598–606.

[97] R.G. Gilbert, K. Luther, J. Troe, Theory of Thermal Unimolecular Reactions in the Fall-off Range. II. Weak Collision Rate Constants, Berichte Der Bunsengesellschaft Für Phys. Chemie. 87 (1983) 169–177. doi:10.1002/bbpc.19830870218.

[98] S. Gordon, B.J. McBride, Computer program for calculation of complex chemical equilibrium compositions rocket performance incident and reflected shocks, and Chapman-Jouguet detonations, Comput. Progr. Calc. Complex Chem. Equilib. Compos. Rocket Perform. Incid. Reflected Shock. ChapmanJouguet Detonations. (1971) 250. https://ntrs.nasa.gov/search.jsp?R=19780009781 (accessed April 19, 2018).

[99] Reaction Design, ANSYS CHEMKIN-Pro 18.0, (2016).

[100] S. Li, L. Petzold, Software and algorithms for sensitivity analysis of large-scale differential algebraic systems, J. Comput. Appl. Math. 125 (2000) 131–145. doi:10.1016/S0377-0427(00)00464-7.

[101] C.W. Gao, J.W. Allen, W.H. Green, R.H. West, Reaction Mechanism Generator: Automatic construction of chemical kinetic mechanisms, Comput. Phys. Commun. 203 (2016) 212–225. doi:10.1016/j.cpc.2016.02.013.

[102] J. Song, Building robust chemical reaction mechanisms : next generation of automatic model construction software, Thesis (Ph. D.)--Massachusetts Inst. Technol. Dept. Chem. Eng. 2004. (2004). https://dspace.mit.edu/handle/1721.1/30058 (accessed April 21, 2018).

[103] M.R. Harper, K.M. Van Geem, S.P. Pyl, G.B. Marin, W.H. Green, Comprehensive reaction mechanism for n-butanol pyrolysis and combustion, Combust. Flame. 158 (2011) 16–41. doi:10.1016/j.combustflame.2010.06.002.

[104] J.W. Allen, A.M. Scheer, C.W. Gao, S.S. Merchant, S.S. Vasu, O. Welz, J.D. Savee, D.L. Osborn, C. Lee, S. Vranckx, Z. Wang, F. Qi, R.X. Fernandes, W.H. Green, M.Z. Hadi, C.A. Taatjes, A coordinated investigation of the combustion chemistry of diisopropyl

ketone, a prototype for biofuels produced by endophytic fungi, Combust. Flame. 161 (2014) 711–724. doi:10.1016/j.combustflame.2013.10.019.

[105] G.R. Magoon, J. Aguilera-Iparraguirre, W.H. Green, J.J. Lutz, P. Piecuch, H.W. Wong, O.O. Oluwole, Detailed chemical kinetic modeling of JP-10 (exo-tetrahydrodicyclopentadiene) high-temperature oxidation: Exploring the role of biradical species in initial decomposition steps, Int. J. Chem. Kinet. 44 (2012) 179–193. doi:10.1002/kin.20702.

[106] S. V. Petway, H. Ismail, W.H. Green, E.G. Estupiñán, L.E. Jusinski, C.A. Taatjes, Measurements and automated mechanism generation modeling of OH production in photolytically initiated oxidation of the neopentyl radical, J. Phys. Chem. A. 111 (2007) 3891–3900. doi:10.1021/jp0668549.

[107] RMG - Reaction Mechanism Generator, (n.d.). http://rmg.mit.edu/ (accessed April 22, 2018).

[108] S.W. Benson, J.H. Buss, Additivity rules for the estimation of molecular properties. Thermodynamic properties, J. Chem. Phys. 29 (1958) 546–572. doi:10.1063/1.1744539.

[109] R.G. Susnow, A.M. Dean, W.H. Green, P. Peczak, L.J. Broadbelt, Rate-based construction of kinetic models for complex systems, J. Phys. Chem. A. 101 (1997) 3731–3740. doi:10.1021/jp9637690.

[110] K. Pearson, Note on Regression and Inheritance in the Case of Two Parents, Proc. R. Soc. London. 58 (n.d.) 240–242. doi:10.2307/115794.

[111] C. Spearman, “General Intelligence,” Objectively Determined and Measured, Am. J. Psychol. 15 (1904) 201. doi:10.2307/1412107.

[112] W. McKinney, Data Structures for Statistical Computing in Python, Proc. 9th Python Sci. Conf. 1697900 (2010) 51–56. https://pdfs.semanticscholar.org/f6da/c1c52d3b07c993fe52513b8964f86e8fe381.pdf (accessed April 4, 2018).

[113] E. Ranzi, A wide-range kinetic modeling study of oxidation and combustion of transportation fuels and surrogate mixtures, Energy and Fuels. 20 (2006) 1024–1032. doi:10.1021/ef060028h.

[114] W.J. Pitz, C.J. Mueller, Recent progress in the development of diesel surrogate fuels, Prog. Energy Combust. Sci. 37 (2011) 330–350. doi:10.1016/j.pecs.2010.06.004.

[115] H. Li, L. Yu, S. Sun, S. Wang, X. Lu, Z. Huang, A Shock Tube Experimental and Modeling Study of Multicomponent Gasoline Surrogates Diluted with Exhaust Gas Recirculation, Energy & Fuels. 32 (2018) 3800–3813. doi:10.1021/acs.energyfuels.7b01028.

[116] W. Tsang, Thermal stability of cyclohexane and 1-hexene, Int. J. Chem. Kinet. 10 (1978) 1119–1138. doi:10.1002/kin.550101103.

[117] T.C. Brown, K.D. King, T.T. Nguyen, Kinetics of primary processes in the pyrolysis of cyclopentanes and cyclohexanes, in: J. Phys. Chem., 1986: pp. 419–424. doi:10.1021/j100275a013.

[118] F. Billaud, P. Chaverot, M. Berthelin, E. Freund, Thermal decomposition of cyclohexane at approximately 810 °c, Ind. Eng. Chem. Res. 27 (1988) 759–764. doi:10.1021/ie00077a007.

[119] B. Sirjean, P.A. Glaude, M.F. Ruiz-Lopez, R. Fournet, Detailed kinetic study of the ring opening of cycloalkanes by CBS-QB3 calculations, J. Phys. Chem. A. 110 (2006) 12693–12704. doi:10.1021/jp0651081.

[120] J.H. Kiefer, K.S. Gupte, L.B. Harding, S.J. Klippenstein, Shock tube and theory investigation of cyclohexane and 1-hexene decomposition, J. Phys. Chem. A. 113 (2009) 13570–13583. doi:10.1021/jp905891q.

[121] A. El Bakali, M. Braun-Unkhoff, P. Dagaut, P. Frank, M. Cathonnet, Detailed kinetic reaction mechanism for cyclohexane oxidation at pressure up to ten atmospheres, Proc. Combust. Inst. 28 (2000) 1631–1638. doi:10.1016/S0082-0784(00)80561-5.

[122] U. Steil, C. Naumann, P. Frank, Experimental Study of the Pyrolysis of Cyclohexane at Shock Tube Relevant Conditions Institute of Combustion Technology German Aerospace Centre, Proc. Eur. Combust. Meet. (2005) 1–6. http://www.dlr.de (accessed March 18, 2018).

[123] Y. Zhao, B. Shen, F. Wei, Quantitative interpretation to the chain mechanism of free radical reactions in cyclohexane pyrolysis, J. Nat. Gas Chem. 20 (2011) 507–514. doi:10.1016/S1003-9953(10)60233-2.

[124] S. Peukert, C. Naumann, M. Braun-Unkhoff, U. Riedel, Formation of H-atoms in the pyrolysis of cyclohexane and 1-hexene: A shock tube and modeling study, Int. J. Chem. Kinet. 43 (2011) 107–119. doi:10.1002/kin.20539.

[125] S. Peukert, C. Naumann, M. Braun-Unkhoff, U. Riedel, The reaction of cyclohexane with H-atoms: A shock tube and modeling study, Int. J. Chem. Kinet. 44 (2012) 130–146. doi:10.1002/kin.20595.

[126] B. Sirjean, P.A. Glaude, M.F. Ruiz-Lopèz, R. Fournet, Theoretical kinetic study of thermal unimolecular decomposition of cyclic alkyl radicals, J. Phys. Chem. A. 112 (2008) 11598–11610. doi:10.1021/jp805640s.

[127] S. Granata, T. Faravelli, E. Ranzi, A wide range kinetic modeling study of the pyrolysis and combustion of naphthenes, Combust. Flame. 132 (2003) 533–544. doi:10.1016/S0010-2180(02)00465-0.

[128] A.M. Knepp, G. Meloni, L.E. Jusinski, C.A. Taatjes, C. Cavallotti, S.J. Klippenstein, Theory, measurements, and modeling of OH and HO2 formation in the reaction of cyclohexyl radicals with O2, Phys. Chem. Chem. Phys. 9 (2007) 4315. doi:10.1039/b705934e.

[129] O. Lemaire, M. Ribaucour, M. Carlier, R. Minetti, The production of benzene in the low-temperature oxidation of cyclohexane, cyclohexene, and cyclohexa-1,3-diene, Combust. Flame. 127 (2001) 1971–1980. doi:10.1016/S0010-2180(01)00301-7.

[130] B. Sirjean, F. Buda, H. Hakka, P.A. Glaude, R. Fournet, V. Warth, F. Battin-Leclerc, M. Ruiz-Lopez, The autoignition of cyclopentane and cyclohexane in a shock tube, Proc. Combust. Inst. 31 I (2007) 277–284. doi:10.1016/j.proci.2006.07.247.

[131] Z. Wang, H. Bian, Y. Wang, L. Zhang, Y. Li, F. Zhang, F. Qi, Investigation on primary decomposition of ethylcyclohexane at atmospheric pressure, Proc. Combust. Inst. 35 (2015) 367–375. doi:10.1016/j.proci.2014.05.119.

[132] H. Wang, E. Dames, B. Sirjean, D.A. Sheen, R. Tangko, A. Violi, J.Y.W. Lai, F.N. Egolfopoulos, D.F. Davidson, R.K. Hanson, A high-temperature chemical kinetic model of n-alkane (up to n-dodecane), cyclohexane, and methyl-, ethyl-, n-propyl and n-butyl-cyclohexane oxidation at high temperatures, JetSurF version 2.0, (2010). http://web.stanford.edu/group/haiwanglab/JetSurF/JetSurF2.0/index.html.

[133] W. Li, M.E. Law, P.R. Westmoreland, T. Kasper, N. Hansen, K. Kohse-Höinghaus, Multiple benzene-formation paths in a fuel-rich cyclohexane flame, Combust. Flame. 158 (2011) 2077–2089. doi:10.1016/j.combustflame.2011.03.014.

[134] J.H. Kiefer, J.N. Shah, Unimolecular dissociation of cyclohexene at extremely high

temperatures: Behavior of the energy-transfer collision efficiency, J. Phys. Chem. 91 (1987) 3024–3030. doi:10.1021/j100295a076.

[135] G. Dayma, P.A. Glaude, R. Fournet, F. Battin-Leclerc, Experimental and modeling study of the oxidation of cyclohexene, Int. J. Chem. Kinet. 35 (2003) 273–285. doi:10.1002/kin.10127.

[136] H. Richter, S. Granata, W.H. Green, J.B. Howard, Detailed modeling of PAH and soot formation in a laminar premixed benzene/oxygen/argon low-pressure flame, Proc. Combust. Inst. 30 (2005) 1397–1404. doi:10.1016/j.proci.2004.08.088.

[137] A. D'Anna, A. D'Alessio, J. Kent, A computational study of hydrocarbon growth and the formation of aromatics in coflowing laminar diffusion flames of ethylene, Combust. Flame. 125 (2001) 1196–1206. doi:10.1016/S0010-2180(01)00238-3.

[138] N. Hansen, J.A. Miller, P.R. Westmoreland, T. Kasper, K. Kohse-Höinghaus, J. Wang, T.A. Cool, Isomer-specific combustion chemistry in allene and propyne flames, Combust. Flame. 156 (2009) 2153–2164. https://www.sciencedirect.com/science/article/pii/S0010218009002041?via%3Dihub (accessed March 18, 2018).

[139] R. Sivaramakrishnan, R.S. Tranter, K. Brezinsky, High pressure pyrolysis of toluene. 1. Experiments and modeling of toluene decomposition, J. Phys. Chem. A. 110 (2006) 9388–9399. doi:10.1021/jp060820j.

[140] R.P. Lindstedt, G. Skevis, Chemistry of Acetylene Flames, Combust. Sci. Technol. 125 (1997) 73–137. doi:10.1080/00102209708935656.

[141] J.P. Senosiain, J.A. Miller, The Reaction of n- and i-C4H5 Radicals with Acetylene, J. Phys. Chem. A. 111 (2007) 3740–3747. doi:10.1021/jp0675126.

[142] H. Wang, X. You, A. V Joshi, S.G. Davis, A. Laskin, F. Egolfopoulos, C.K. Law, USC Mech Version II. High-Temperature Combustion Reaction Model of H2/CO/C1-C4 Compounds., (n.d.). http://ignis.usc.edu/USC_Mech_II.htm.

[143] A. Miyoshi, Computational studies on the reactions of 3-butenyl and 3-butenylperoxy radicals, Int. J. Chem. Kinet. 42 (2010) 273–288. doi:10.1002/kin.20478.

[144] K. Yasunaga, Y. Kuraguchi, R. Ikeuchi, H. Masaoka, O. Takahashi, T. Koike, Y. Hidaka, Shock tube and modeling study of isobutene pyrolysis and oxidation, Proc. Combust. Inst. 32 I (2009) 453–460. doi:10.1016/j.proci.2008.06.144.

[145] G. Blanquart, P. Pepiot-Desjardins, H. Pitsch, Chemical mechanism for high temperature combustion of engine relevant fuels with emphasis on soot precursors, Combust. Flame. 156 (2009) 588–607. doi:10.1016/j.combustflame.2008.12.007.

[146] J.A. Miller, J.P. Senosiain, S.J. Klippenstein, Y. Georgievskii, Reactions over multiple, interconnected potential wells: Unimolecular and bimolecular reactions on a C3H5potential, J. Phys. Chem. A. 112 (2008) 9429–9438. doi:10.1021/jp804510k.

[147] S.G. Davis, C.K. Law, H. Wang, Propyne Pyrolysis in a Flow Reactor: An Experimental, RRKM, and Detailed Kinetic Modeling Study, J. Phys. Chem. A. 103 (1999) 5889–5899. doi:10.1021/jp982762a.

[148] V. Detilleux, J. Vandooren, Experimental and kinetic modeling evidences of a C7H6 pathway in a rich toluene flame, J. Phys. Chem. A. 113 (2009) 10913–10922. doi:10.1021/jp905954g.

[149] G.B. Bacskay, J.C. Mackie, The pyrolysis of cyclopentadiene: quantum chemical and kinetic modelling studies of the acetylene plus propyne/allene decomposition channels, Phys. Chem. Chem. Phys. 3 (2001) 2467–2473. doi:10.1039/b101317n.

[150] R. Sivaramakrishnan, K. Brezinsky, H. Vasudevan, R.S. Tranter, A shock-tube study of the high-pressure thermal decomposition of benzene, Combust. Sci. Technol. 178 (2006) 285–305. doi:10.1080/00102200500292340.

[151] V. Chernov, M.J. Thomson, S.B. Dworkin, N.A. Slavinskaya, U. Riedel, Soot formation with C1 and C2 fuels using an improved chemical mechanism for PAH growth, Combust. Flame. (2014). doi:10.1016/j.combustflame.2013.09.017.

[152] N.A. Slavinskaya, P. Frank, A modelling study of aromatic soot precursors formation in laminar methane and ethene flames, Combust. Flame. 156 (2009) 1705–1722. doi:10.1016/j.combustflame.2009.04.013.

[153] A. Raj, M. Celnik, R. Shirley, M. Sander, R. Patterson, R. West, M. Kraft, A statistical approach to develop a detailed soot growth model using PAH characteristics, Combust. Flame. 156 (2009) 896–913. doi:10.1016/j.combustflame.2009.01.005.

[154] K. Narayanaswamy, G. Blanquart, H. Pitsch, A consistent chemical mechanism for oxidation of substituted aromatic species, Combust. Flame. 157 (2010) 1879–1898. doi:10.1016/j.combustflame.2010.07.009.

[155] R.K. Robinson, R.P. Lindstedt, On the chemical kinetics of cyclopentadiene oxidation,

Combust. Flame. 158 (2011) 666–686. doi:10.1016/j.combustflame.2010.12.001.

[156] R. Fournet, J.C. Bauge, F. Battin-Leclerc, Experimental and modeling of oxidation of acetylene, propyne, allene and 1,3-butadiene, Int. J. Chem. Kinet. 31 (1999) 361–379. doi:10.1002/(SICI)1097-4601(1999)31:5<361::AID-KIN6>3.0.CO;2-K.

[157] A. Laskin, A. Lifshitz, Thermal decomposition of indene. Experimental results and kinetic modeling, in: Symp. Combust., Elsevier, 1998: pp. 313–320. doi:10.1016/S0082-0784(98)80418-9.

[158] J. Bugler, B. Marks, O. Mathieu, R. Archuleta, A. Camou, C. Grégoire, K.A. Heufer, E.L. Petersen, H.J. Curran, An ignition delay time and chemical kinetic modeling study of the pentane isomers, Combust. Flame. 163 (2016) 138–156. doi:10.1016/j.combustflame.2015.09.014.

[159] G.P. Smith, Y. Tao, H. Wang, Foundational Fuel Chemistry Model Version1.0 (FFCM-1), (2016). http://nanoenergy.stanford.edu/ffcm1.

[160] S. Humer, A. Frassoldati, S. Granata, T. Faravelli, E. Ranzi, R. Seiser, K. Seshadri, Experimental and kinetic modeling study of combustion of JP-8, its surrogates and reference components in laminar nonpremixed flows, Proc. Combust. Inst. 31 I (2007) 393–400. doi:10.1016/j.proci.2006.08.008.

[161] J. Vanderover, M.A. Oehlschlaeger, Ignition time measurements for methylcylcohexane- and ethylcyclohexane-air mixtures at elevated pressures, Int. J. Chem. Kinet. 41 (2009) 82–91. doi:10.1002/kin.20370.

[162] S.S. Vasu, D.F. Davidson, R.K. Hanson, OH time-histories during oxidation of n-heptane and methylcyclohexane at high pressures and temperatures, Combust. Flame. 156 (2009) 736–749. doi:10.1016/j.combustflame.2008.09.006.

[163] S.S. Vasu, D.F. Davidson, Z. Hong, R.K. Hanson, Shock tube study of methylcyclohexane ignition over a wide range of pressure and temperature, Energy and Fuels. 23 (2009) 175–185. doi:10.1021/ef800694g.

[164] M.E. MacDonald, W. Ren, Y. Zhu, D.F. Davidson, R.K. Hanson, Fuel and Ethylene Measurements during n-dodecane, methylcyclohexane, and iso-cetane pyrolysis in shock tubes, in: Fuel, Elsevier, 2013: pp. 1060–1068. doi:10.1016/j.fuel.2012.09.068.

[165] W.J. Pitz, C. V. Naik, T. Ní Mhaoldúin, C.K. Westbrook, H.J. Curran, J.P. Orme, J.M. Simmie, Modeling and experimental investigation of methylcyclohexane ignition in a

rapid compression machine, Proc. Combust. Inst. 31 I (2007) 267–275. doi:10.1016/j.proci.2006.08.041.

[166] K. Narayanaswamy, H. Pitsch, P. Pepiot, A chemical mechanism for low to high temperature oxidation of methylcyclohexane as a component of transportation fuel surrogates, Combust. Flame. 162 (2015) 1193–1213. doi:10.1016/j.combustflame.2014.10.013.

[167] Z. Hong, K.Y. Lam, D.F. Davidson, R.K. Hanson, A comparative study of the oxidation characteristics of cyclohexane, methylcyclohexane, and n-butylcyclohexane at high temperatures, Combust. Flame. 158 (2011) 1456–1468. doi:10.1016/j.combustflame.2010.12.019.

[168] B.W. Weber, W.J. Pitz, M. Mehl, E.J. Silke, A.C. Davis, C.J. Sung, Experiments and modeling of the autoignition of methylcyclohexane at high pressure, Combust. Flame. 161 (2014) 1972–1983. doi:10.1016/j.combustflame.2014.01.018.

[169] J.P. Orme, H.J. Curran, J.M. Simmie, Experimental and modeling study of methyl cyclohexane pyrolysis and oxidation, J. Phys. Chem. A. 110 (2006) 114–131. doi:10.1021/jp0543678.

[170] H. Böhm, H. Jander, D. Tanke, PAH growth and soot formation in the pyrolysis of acetylene and benzene at high temperatures and pressures: Modeling and experiment, in: Symp. Combust., Elsevier, 1998: pp. 1605–1612. doi:10.1016/S0082-0784(98)80570-5.

[171] H. Böhm, H. Janderb, PAH formation in acetylene–benzene pyrolysis, Phys. Chem. Chem. Phys. 1 (1999) 3775–3781. doi:10.1039/a903306h.

[172] Y. Kobayashi, T. Furuhata, K. Amagai, M. Arai, Soot precursor measurements in benzene and hexane diffusion flames, Combust. Flame. 154 (2008) 346–355. doi:10.1016/j.combustflame.2008.03.022.

[173] B. Öktem, M.P. Tolocka, B. Zhao, H. Wang, M. V. Johnston, Chemical species associated with the early stage of soot growth in a laminar premixed ethylene-oxygen-argon flame, Combust. Flame. 142 (2005) 364–373. doi:10.1016/j.combustflame.2005.03.016.

[174] B. Sirjean, E. Dames, D.A. Sheen, F.N. Egolfopoulos, H. Wang, D.F. Davidson, R.K. Hanson, H. Pitsch, C.T. Bowman, C.K. Law, W. Tsang, N.P. Cernansky, D.L. Miller, A. Violi, R.P. Lindstedt, A high-temperature chemical kinetic model of n-alkane, cyclohexane, and methyl-, ethyl-, n-propyl and n-butyl-cyclohexane oxidation at high

temperatures, JetSurF version 1.1, (2009). http://melchior.usc.edu/JetSurF/JetSurF1.1.

[175] D.M. Matheu, W.H. Green, J.M. Grenda, Capturing pressure-dependence in automated mechanism generation: Reactions through cycloalkyl intermediates, Int. J. Chem. Kinet. 35 (2003) 95–119. doi:10.1002/kin.10106.

[176] T. Gierczak, J. Gawlowski, J. Niedzielski, Isomerization of excited cyclohexyl, 1-hexen-6-yl and cyclopentylmethyl radicals, J. Photochem. Photobiol. A Chem. 55 (1990) 25–35. doi:10.1016/1010-6030(90)80015-P.

[177] C. Chatgilialoglu, V.I. Timokhin, M. Ballestri, One-Carbon Ring Expansion in Cyclopentanones as a Free-Radical Clock., Sect. Title Phys. Org. Chem. 63 (1998) 1327–1329. doi:10.1021/jo9716338.

[178] Y. Fu, R.Q. Li, L. Liu, Q.X. Guo, Solvent effect is not significant for the speed of a radical clock, Res. Chem. Intermed. 30 (2004) 279–286. doi:10.1163/156856704323034012.

[179] M.K. Abdel Latif, J.N. Spencer, M. Paradzinsky, J.M. Tanko, Does Metal Ion Complexation Make Radical Clocks Run Fast? An Experimental Perspective, J. Phys. Chem. A. 121 (2017) 9682–9686. doi:10.1021/acs.jpca.7b07575.

[180] C. Walling, A. Cioffari, C. Walling, Cyclization of 5-Hexenyl Radicals1, J. Am. Chem. Soc. 94 (1972) 6059–6064. doi:10.1021/ja00772a020.

APPENDIX A

GC Method for the GC containing the GS-GasPro column.

```
                          INSTRUMENT CONTROL PARAMETERS:    Instrument #2
                          ---------------------------------------------

   C:\msdchem\2\METHODS\Liq10(3).M

Control Information
------- -----------

Sample Inlet      :  GC
Injection Source  :  Manual
Injection Location:  Rear

================================================================================
                                  6890 GC METHOD
================================================================================


OVEN
   Initial temp:  45 'C (On)                 Maximum temp:  320 'C
   Initial time:  5.00 min                   Equilibration time:  0.50 min
   Ramps:
      #  Rate  Final temp  Final time   CRYO (N2)
      1  5.00       80        3.00        Cryo:  Off
      2 15.00      150        3.00        Cryo fault:  Off
      3 15.00      250        8.00        Cryo timeout:  120.00 min (Off)
      4   0.0(Off)                       Quick cryo cool:  Off
   Post temp:  260 'C                     Ambient temp:  50 'C
   Post time:  0.00 min
   Run time:  37.33 min


FRONT INLET (SPLIT/SPLITLESS)           BACK INLET (UNKNOWN)
   Mode:  Split
   Initial temp:  50 'C (Off)
   Pressure:  0.00 psi (Off)
   Total flow:  45.0 mL/min
   Gas saver:  Off
   Gas type:  Helium


COLUMN 1                                COLUMN 2
   Capillary Column                        Capillary Column
   Model Number:  J&W 113-4362             Model Number:  Agilent 19091S-433
   GS-GasPro                               HP-5MS  5% Phenyl Methyl Siloxane
   Max temperature:  260 'C                Max temperature:  325 'C
   Nominal length:  60.0 m                 Nominal length:  30.0 m
   Nominal diameter:  320.00 um            Nominal diameter:  250.00 um
   Nominal film thickness:  0.00 um        Nominal film thickness:  0.25 um
   Mode:  constant flow                    Mode:  constant flow
   Initial flow:  2.0 mL/min               Initial flow:  1.5 mL/min
```

APPENDIX A (continued)

```
   Nominal init pressure:  15.85 psi
   Average velocity:  28 cm/sec
   Inlet:  Aux 4 Pressure Controller
   Outlet:  Front Detector
   Outlet pressure:  ambient

FRONT DETECTOR (FID)
   Temperature:  320 'C (On)
   Hydrogen flow:  40.0 mL/min (On)
   Air flow:  450.0 mL/min (On)
   Mode:  Constant makeup flow
   Makeup flow:  30.0 mL/min (On)
   Makeup Gas Type: Helium
   Flame:  On
   Electrometer:  On
   Lit offset:  2.0

SIGNAL 1
   Data rate:  20 Hz
   Type:  front detector
   Save Data:  On
   Zero:  0.0 (Off)
   Range:  0
   Fast Peaks:  Off
   Attenuation:  0

COLUMN COMP 1
   Derive from front detector

THERMAL AUX 2
   Use:  Valve Box Heater
   Description:
   Initial temp:  150 'C (On)
   Initial time:  0.00 min
      #  Rate  Final temp  Final time
      1   0.0(Off)

AUX PRESSURE 4
   Description:
   Gas Type:  Helium
   Driving Column 1
   Initial pressure:  15.84 psi (On)

   Nominal init pressure:  16.03 psi
   Average velocity:  34 cm/sec
   Inlet:  Aux 3 Pressure Controller
   Outlet:  Back Detector
   Outlet pressure:  ambient

BACK DETECTOR (FID)
   Temperature:  320 'C (On)
   Hydrogen flow:  40.0 mL/min (On)
   Air flow:  450.0 mL/min (On)
   Mode:  Constant makeup flow
   Makeup flow:  30.0 mL/min (On)
   Makeup Gas Type: Helium
   Flame:  On
   Electrometer:  On
   Lit offset:  2.0

SIGNAL 2
   Data rate:  20 Hz
   Type:  back detector
   Save Data:  On
   Zero:  0.0 (Off)
   Range:  0
   Fast Peaks:  Off
   Attenuation:  0

COLUMN COMP 2
   Derive from back detector

AUX PRESSURE 3
   Description:
   Gas Type:  Helium
   Driving Column 2
   Initial pressure:  16.02 psi (On)

AUX PRESSURE 5
   Description:
   Gas Type:  Helium
   Initial pressure:  0.00 psi (Off)

POST RUN
   Post Time: 0.00 min

TIME TABLE
```

APPENDIX A (continued)

Time	Specifier	Parameter & Setpoint

GC Injector

Front Injector:		
Sample Washes	0	
Sample Pumps	6	
Injection Volume	1.00	microliters
Syringe Size	10.0	microliters
Nanoliter Adapter	Off	
PostInj Solvent A Washes	0	
PostInj Solvent B Washes	0	
Viscosity Delay	0	seconds
Plunger Speed	Fast	
Back Injector:		
Sample Washes	0	
Sample Pumps	6	
Injection Volume	1.00	microliters
Syringe Size	10.0	microliters
Nanoliter Adapter	Off	
PostInj Solvent A Washes	0	
PostInj Solvent B Washes	0	
Viscosity Delay	0	seconds
Plunger Speed	Fast	

Column 1 Inventory Number : AB004
Column 2 Inventory Number : AB010

END OF INSTRUMENT CONTROL PARAMETERS

APPENDIX A (continued)

GC Method for the GC containing the Supelco Petrocol column.

```
                          INSTRUMENT CONTROL PARAMETERS:    Instrument #1
                          ---------------------------------------------

   C:\MSDCHEM\1\METHODS\LPSTMETHOD4.M

Control Information
------- -----------

Sample Inlet      :  GC
Injection Source  :  Manual
Injection Location:  Front
Mass Spectrometer :  Disabled

================================================================================
                                6890 GC METHOD
================================================================================


OVEN
   Initial temp:  35 'C (On)                 Maximum temp:  290 'C
   Initial time:  15.00 min                  Equilibration time:  0.50 min
   Ramps:
      #  Rate  Final temp  Final time   CRYO (N2)
      1  1.00       50        0.00        Cryo:  Off
      2 15.00      250        5.00        Cryo fault:  Off
      3   0.0(Off)                       Cryo timeout:  120.00 min (Off)
   Post temp:  270 'C                    Quick cryo cool:  Off
   Post time:  0.00 min                  Ambient temp:  30 'C
   Run time:  48.33 min


FRONT INLET (SPLIT/SPLITLESS)            BACK INLET (VOLATILES)
   Mode:  Split                              Mode:  Split
   Initial temp:  50 'C (Off)                Initial temp:  50 'C (Off)
   Pressure:  0.00 psi (Off)                 Pressure:  0.00 psi (Off)
   Total flow:  45.0 mL/min                  Total flow:  45.0 mL/min
   Gas saver:  Off                           Gas saver:  Off
   Gas type:  Helium                         Gas type:  Hydrogen


COLUMN 1                                 COLUMN 2
   Capillary Column                          Capillary Column
   Model Number:  J&W 19095P-MS0E            Model Number:  Supelco 24160-U
   HP-MOLSIV Megabore                        Petrocol DH
   Max temperature:  300 'C                  Max temperature:  320 'C
   Nominal length:  30.0 m                   Nominal length:  100.0 m
   Nominal diameter:  530.00 um              Nominal diameter:  250.00 um
   Nominal film thickness:  50.00 um         Nominal film thickness:  0.50 um
   Mode:  constant flow                      Mode:  constant pressure
```

APPENDIX A (continued)

```
   Initial flow:  2.0 mL/min
   Nominal init pressure:  3.64 psi
   Average velocity:  21 cm/sec
   Inlet:  Aux 5 Pressure Controller
   Outlet:  Front Detector
   Outlet pressure:  ambient

FRONT DETECTOR (TCD)
   Temperature:  250 'C (On)
   Reference flow:  20.0 mL/min (On)
   Mode:  Constant column+makeup flow
   Combined flow:  7.0 mL/min
   Makeup flow:  On
   Makeup Gas Type: Helium
   Filament:  On
   Negative polarity:  Off

SIGNAL 1
   Data rate:  20 Hz
   Type:  front detector
   Save Data:  On
   Zero:  0.0 (Off)
   Range:  0
   Fast Peaks:  Off
   Attenuation:  0

COLUMN COMP 1
   Derive from front detector

THERMAL AUX 1
   Use:  MSD Transfer Line Heater
   Description:
   Initial temp:  250 'C (On)
   Initial time:  0.00 min
      #  Rate  Final temp  Final time
      1   0.0(Off)

AUX PRESSURE 3
   Description:
   Gas Type:  Helium
   Initial pressure:  0.00 psi (Off)

AUX PRESSURE 5
   Description:
   Gas Type:  Argon methane 5%
   Driving Column 1
   Pressure:  44.00 psi
   Nominal initial flow:  2.1 mL/min
   Average velocity:  26 cm/sec
   Inlet:  Aux 4 Pressure Controller
   Outlet:  Back Detector
   Outlet pressure:  ambient

BACK DETECTOR (FID)
   Temperature:  300 'C (On)
   Hydrogen flow:  30.0 mL/min (On)
   Air flow:  300.0 mL/min (On)
   Mode:  Constant makeup flow
   Makeup flow:  30.0 mL/min (On)
   Makeup Gas Type: Helium
   Flame:  On
   Electrometer:  On
   Lit offset:  0.5

SIGNAL 2
   Data rate:  10 Hz
   Type:  back detector
   Save Data:  On
   Zero:  0.0 (Off)
   Range:  0
   Fast Peaks:  Off
   Attenuation:  0

COLUMN COMP 2
   Derive from back detector

THERMAL AUX 2
   Use:  Valve Box Heater
   Description:
   Initial temp:  150 'C (On)
   Initial time:  0.00 min
      #  Rate  Final temp  Final time
      1   0.0(Off)

AUX PRESSURE 4
   Description:
   Gas Type:  Helium
   Driving Column 2
   Initial pressure:  44.00 psi (On)
```

APPENDIX A (continued)

```
   Initial pressure:  3.64 psi (On)

                                          POST RUN
                                             Post Time: 0.00 min


TIME TABLE
   Time       Specifier                     Parameter & Setpoint



                                GC Injector


     Front Injector:
        Sample Washes                 0
        Sample Pumps                  6
        Injection Volume           1.00 microliters
        Syringe Size               10.0 microliters
        Nanoliter Adapter           Off
        PostInj Solvent A Washes      0
        PostInj Solvent B Washes      0
        Viscosity Delay               0 seconds
        Plunger Speed              Fast

     Back Injector:
        Sample Washes                 0
        Sample Pumps                  6
        Injection Volume           1.00 microliters
        Syringe Size               10.0 microliters
        Nanoliter Adapter           Off
        PostInj Solvent A Washes      0
        PostInj Solvent B Washes      0
        Viscosity Delay               0 seconds
        Plunger Speed              Fast

 Column 1 Inventory Number : AB007
 Column 2 Inventory Number : AB011



                           TUNE PARAMETERS for SN:
                         ----------------------------

 EMISSION    :      34.610
 ENERGY      :      69.922
 REPELLER    :      17.893
 IONFOCUS    :      74.973
 ENTRANCE_LE :      14.500
 EMVOLTS     :    1905.882
 AMUGAIN     :    2079.000
 AMUOFFSET   :     117.000
```

APPENDIX A (continued)

```
FILAMENT    :       1.000
DCPOLARITY  :       0.000
ENTLENSOFFS :      18.071
MASSGAIN    :      23.000
MASSOFFSET  :     -10.000

                    END OF TUNE PARAMETERS
                  ----------------------------------


                          END OF INSTRUMENT CONTROL PARAMETERS
                          ----------------------------------
```

APPENDIX B

Short Python script used to remove oxygen containing reactions and species from RMG kinetic libraries and species dictionary.

```
#Written by Miroslaw Liszka
#Short script used to remove oxygen containing reactions and species from RMG
kinetic libraries
#and species dictionary. It can be easily modified to remove species
containing other elements.

speciesdict = {}
oxyspeciesdict = {}

with open('dictionary.txt', 'r') as olddict, open('stripped_dictionary.txt',
'w') as newdict:
    for line in olddict:
        cleanline = line.strip().split()
        if len(cleanline) == 1:
            currentspecies = cleanline[0]
            speciesdict[currentspecies] = []
        elif not cleanline:
            continue
        else:
            speciesdict[currentspecies].append(cleanline)

    for key in speciesdict:
        adjlist = speciesdict[key]
        for row in adjlist:
            if str(row[1]).lower() == 'o':
                oxyspeciesdict[key] = []
            else:
                continue

    for key in speciesdict:
        if key not in oxyspeciesdict:
            newdict.write('\n' + key + '\n')
            adjlist = speciesdict[key]
            for row in adjlist:
                outputline = ''
                for col in row:
                    outputline += str(col) + ' '
                newdict.write(outputline + '\n')
    olddict.close()
    newdict.close()

with open('reactions.py', 'r') as oldreact, open('stripped_reactions.py',
'w') as newreact:
    i = 1
    nowrite = False
    oxyreact = False
    for line in oldreact:
        if 'entry(' in line:
            nowrite = True
        if 'label' in line:
            oxyreact = False
```

APPENDIX B (continued)

```
        newline = line.replace('"', ' ').strip().split()
        for val in newline:
            if val in oxyspeciesdict:
                nowrite = True
                oxyreact = True
                break
        if not oxyreact:
            newreact.write('entry(' +'\n')
            newreact.write('    index = ' + str(i) +',\n')
            newreact.write(line)
            nowrite = False
            i += 1
            continue
    if not nowrite:
        newreact.write(line)
oldreact.close()
newreact.close()
```

APPENDIX B (continued)

Short Python script for preparing the mechanism for MC analysis by assigning an uncertainty factor to all the reactions in the mechanism.

```
#Originally Written by Alexksandr Fridlyand
#Modified by Miroslaw Liszka

import os.path
import sys

'''Function to take a clean chemistry file (filein) and for each reaction add
a coded string
specifying the reaction index nominal A, uncertainty, and uncertainty mode
for each reaction.
See writechemkin.py for details of string format'''

def
writeuncertall(filein='chem.inp',fileout='uncertchem.inp',uncert=0.3,mode='a'
):

      #Keywords in CHEMKIN files that tell this script to ignore line
    chemkinkeys = ['/','DUP','CHEB','END', 'DUPLICATE', 'PLOG', 'duplicate']
    ##keyword to replace in chemkin file to ensure proper formatting of
mechanism
    rdash = [' / ', '/ ', ' /']
    requal = [' = ', ' =', '= ']
    rplus = [' + ', ' +', '+ ']
    rforward = [' => ', ' =>', '=> ']
    rreverse = [' <= ', ' <=', '<= ']
    rboth = [' <=> ', ' <=>', '<=> ']

    #Code to check if filein exists
    if os.path.exists(filein)==False:
        sys.exit(filein+" not found in working directory, check file name")

    with open(filein,'r') as chemin, open(fileout,'w') as chemout:
        rxn_section = False
        rxn_index = 1
        for line in chemin:
            #check whether we're at the reaction section
            if 'REACTIONS' in line:
                rxn_section = True
                chemout.write(line)
                continue #skip to next line

            #if  at the reaction section write uncertainty string
            ## skip blank lines since code originally couldn't even do that
without failing
            if rxn_section and not line.isspace() and line:
                ##properly formatting the mechanism for main script
                for symbol in rdash:
                    line = line.replace(symbol, '/')
                for symbol in requal:
                    line = line.replace(symbol, '=')
                for symbol in rplus:
```

APPENDIX B (continued)

```
                    line = line.replace(symbol, '+')
                for symbol in rforward:
                    line = line.replace(symbol, '=>')
                for symbol in rreverse:
                    line = line.replace(symbol, '<=')
                for symbol in rboth:
                    line = line.replace(symbol, '<=>')
                line = line.replace(' (+', '(+')
                line = line.replace('!#', '! ')
                ## added check for and removal of existing comments
                ## comment out plog coefficients
                if 'PLOG' in line:
                    chemout.write('!' + line)
                    continue
                if '!' in line:
                    rcline = line.split('!')
                    if rcline[0] and not rcline[0].isspace() and not
checkline(rcline[0],chemkinkeys):
                        line = rcline[0]
                    else:
                        chemout.write(line)
                        continue
                if not checkline(line, chemkinkeys):
                    cleanline = line.strip().split()
                    A = cleanline[len(cleanline)-3]
                    chemout.write(line.strip()+' !#'+str(rxn_index)+' =
'+str(A)+'u'+str(uncert)+'m'+mode+'\n')
                    rxn_index += 1
                else:
                    chemout.write(line)
            else:
                chemout.write(line)

def checkline(line='something',keylist=['/','DUP','CHEB','END']):
    #returns true if item on keylist exists in the line string
    for i in keylist:
        if i in line:
            return(True)
        else:
            continue
    return(False)
```

APPENDIX B (continued)

Python script for comparing to chemical kinetic mechanisms in Chemkin format. The script utilizes a more general way of reading the reaction string which could be extended to the mechanism preparation script.

```
#Written by Miroslaw Liszka
speciesdict = {}
reactiondict = {}
speciesdict2 = {}
reactiondict2 = {}
speciesstart = False
reactionsstart = False
speciesstart2 = False
reactionsstart2 = False

def isfloat(string):
    try:
        float(string)
        return True
    except ValueError:
        return False

with open('mech.txt', 'r') as mech1:
    for line in mech1:
        if 'end' == line.lower().strip() and speciesstart:
            speciesstart = False
        if 'end' == line.lower().strip() and reactionsstart:
            reactionsstart = False
        if 'species' == line.lower().strip():
            speciesstart = True
            continue
        if 'reactions' == line.lower().strip():
            reactionsstart = True
            continue
        if speciesstart:
            splitline = line.strip().split()
            for item in splitline:
                speciesdict[item] = []
        if reactionsstart:
            react = ''
            if line[0] == '!':
                continue
                #line = line[1:]
            line = line.split('!')
            line = line[0].strip().split()
            for val in line:
                reacconsts = []
                if not isfloat(val):
                    react += val
                if isfloat(val) and len(react) > 0:
                    try:
                        reacconsts.append(val)
                        reacconsts.append(line[line.index(val) + 1])
                        reacconsts.append(line[line.index(val) + 2])
                        reactiondict[react] = reacconsts
```

APPENDIX B (continued)

```
                        break
                    except IndexError:
                        break
            #reactiondict[react] = []
    mech1.close()
with open('jetsurf.txt', 'r') as mech2:
    for line in mech2:
        if 'end' == line.lower().strip() and speciesstart2:
            speciesstart2 = False
        if 'end' == line.lower().strip() and reactionsstart2:
            reactionsstart2 = False
        if 'species' == line.lower().strip():
            speciesstart2 = True
            continue
        if 'reactions' == line.lower().strip():
            reactionsstart2 = True
            continue
        if speciesstart2:
            splitline = line.strip().split()
            for item in splitline:
                speciesdict2[item] = []
        if reactionsstart2:
            react = ''
            if line[0] == '!':
                continue
                #line = line[1:]
            line = line.split('!')
            line = line[0].strip().split()
            for val in line:
                reacconsts = []
                if not isfloat(val):
                    react += val
                if isfloat(val) and len(react) > 0:
                    try:
                        reacconsts.append(val)
                        reacconsts.append(line[line.index(val) + 1])
                        reacconsts.append(line[line.index(val) + 2])
                        reactiondict2[react] = reacconsts
                        break
                    except IndexError:
                        break
            #reactiondict2[react] = []
    mech2.close()
for key in reactiondict:
    if key not in reactiondict2 or reactiondict.get(key) !=
reactiondict2.get(key):
        print(key, reactiondict[key])
with open('compareresults.txt', 'w') as results:
    for key in reactiondict:
        if key not in reactiondict2 or reactiondict.get(key) !=
reactiondict2.get(key):
            results.write(key + '\t' + str(reactiondict[key]) + '\n')
```

APPENDIX B (continued)

Python script for reading the PLOG data and updating it in the reaction line.

```
#Written by Miroslaw Liszka
import os.path
import sys
import math
from decimal import Decimal

def isfloat(string):
    try:
        float(string)
        return True
    except ValueError:
        return False

def interpplog(filein='cleanchem.inp', fileout='spmcchem.inp', pressure=200,
saveplog = True):
    ## dictionary for the plog data with keys later used as the reaction
number tag
    plogdict = {}
    plogvals = []
    appendA = 'A'
    appendn = 'n'
    appendE = 'E'
    linecounter = 1
    insertline = 0
    if not os.path.exists(filein):
        sys.exit(filein+" not found in working directory, check file name")
    with open(filein,'r') as chemin, open(fileout,'w') as chemout:
        rxn_section = False
        rxn_index = 1
        ## we loop through the mechanism line by line to collect the plog
data
        for line in chemin:
            #check whether we're at the reaction section
            if 'REACTIONS' in line:
                rxn_section = True
                continue #skip to next line
            ## skip blank lines since code originally couldn't even do that
without failing
            if rxn_section and not line.isspace() and line:
                ##check if we are at line with plog data and save it in a
list
                if 'PLOG' in line:
                    line = line.replace('/',' ')
                    plogline = line.strip().split()
                    plogvals.append(plogline)
                ##check for uncertainty tag
                if '!#' in line:
                    ## check if plog values exist if yes save them with
previous reaction tag
                    if plogvals:
                        plogdict[cleanline[4]] = plogvals
                        ## clear plog value list
```

APPENDIX B (continued)

```
                        plogvals = []
                    cleanline = line.strip().split()
                    ## check if at end of reaction section
                if 'END' in line:
                    ## check if plog values exist if yes save them with
previous reaction tag
                    if plogvals:
                        plogdict[cleanline[4]] = plogvals
                        ## clear plog value list
                        plogvals = []
        # return plogdict
        ## now we loop once again through the mechanism line by line
        ## this time we check whether each tag matches any of those in the
        ## plog value dictionary, and if it does we replace the coefficients
        ## with the appropriate ones at the desired pressure
        chemin.seek(0)
        rxn_section = False
        for line in chemin:
            #check whether we're at the reaction section
            if 'REACTIONS' in line:
                rxn_section = True
                chemout.write(line)
                continue #skip to next line
            ## skip blank lines since code originally couldn't even do that
without failing
            if rxn_section and not line.isspace() and line and '!#' in line:
                cleanline = line.strip().split()
                ## check if reaction tag has plog values
                if cleanline[4] in plogdict:
                    plogcoeffs = plogdict[cleanline[4]]
                    ## check which plog coefficients to use
                    if pressure < float(plogcoeffs[0][2]):
                        print(cleanline[4], ' ', plogcoeffs[0][:])
                        line = line.replace(cleanline[1], plogcoeffs[0][3])
                        #n and E have to be replaced only once each,
otherwise problems arise if they were both set to 0 originally
                        line = line.replace(cleanline[2], plogcoeffs[0][4],
1)
                        line = line.replace(cleanline[3], plogcoeffs[0][5],
1)
                        appendA = plogcoeffs[0][3]
                        appendn = plogcoeffs[0][4]
                        appendE = plogcoeffs[0][4]
                        chemout.write(line)
                        insertline = linecounter
                    elif pressure >= 0.99*float(plogcoeffs[-1][2]):
                        print(cleanline[4], ' ', plogcoeffs[-1][:])
                        line = line.replace(cleanline[1], plogcoeffs[-1][3])
                        #n and E have to be replaced only once each,
otherwise problems arise if they were both set to 0 originally
                        line = line.replace(cleanline[2], plogcoeffs[-1][4],
1)
                        line = line.replace(cleanline[3], plogcoeffs[-1][5],
1)
```

APPENDIX B (continued)

```
                        appendA = plogcoeffs[-1][3]
                        appendn = plogcoeffs[-1][4]
                        appendE = plogcoeffs[-1][5]
                        chemout.write(line)
                        insertline = linecounter + len(plogcoeffs)
                    else:
                        for i in range(0,len(plogcoeffs)-1):
                            ## chemkin uses the plog coefficients directly if
they are given at pressure within 1% of the specified pressure
                            if 0.99*float(plogcoeffs[i][2]) <= pressure <=
1.01*float(plogcoeffs[i][2]):
                                print(cleanline[4], ' ', plogcoeffs[i][:])
                                line = line.replace(cleanline[1],
plogcoeffs[i][3])
                                #n and E have to be replaced only once each,
otherwise problems arise if they were both set to 0 originally
                                line = line.replace(cleanline[2],
plogcoeffs[i][4], 1)
                                line = line.replace(cleanline[3],
plogcoeffs[i][5], 1)
                                chemout.write(line)
                                break
                            if  1.01*float(plogcoeffs[i][2]) < pressure <
0.99*float(plogcoeffs[i+1][2]):
                                ## interpolate plog coefficients if they fall
between two pressure values

#print(math.log(float(plogcoeffs[i+1][3]))*(math.log(pressure/float(plogcoeff
s[i][2]))/(math.log(float(plogcoeffs[i+1][2])/float(plogcoeffs[i][2]))))
                                A =
math.exp(math.log(float(plogcoeffs[i][3]))+math.log(float(plogcoeffs[i+1][3])
/float(plogcoeffs[i][3]))*(math.log(pressure/float(plogcoeffs[i][2]))/math.lo
g(float(plogcoeffs[i+1][2])/float(plogcoeffs[i][2]))))
                                n = float(plogcoeffs[i][4]) +
(float(plogcoeffs[i+1][4]) -
float(plogcoeffs[i][4]))*(math.log(pressure/float(plogcoeffs[i][2]))/math.log
(float(plogcoeffs[i+1][2])/float(plogcoeffs[i][2])))
                                E = float(plogcoeffs[i][5]) +
(float(plogcoeffs[i+1][5]) -
float(plogcoeffs[i][5]))*(math.log(pressure/float(plogcoeffs[i][2]))/math.log
(float(plogcoeffs[i+1][2])/float(plogcoeffs[i][2])))
                                print(cleanline[4], ' ', pressure, ' ',
'{:.4E}'.format(Decimal(A)), ' ', '{:.3f}'.format(n), ' ',
'{:.3f}'.format(E))
                                appendA = str('{:.3E}'.format(Decimal(A)))
                                appendn = str('{:.3f}'.format(n))
                                appendE = str('{:.3f}'.format(E))
                                line = line.replace(cleanline[1], appendA)
                                #n and E have to be replaced only once each,
otherwise problems arise if they were both set to 0 originally
                                line = line.replace(cleanline[2], appendn, 1)
                                line = line.replace(cleanline[3], appendE, 1)
                                chemout.write(line)
                                insertline = linecounter + i + 1
```

APPENDIX B (continued)

```
                            break
                    ## write line unmodified if no plog data is included
                    else:
                        chemout.write(line)
                else:
                    chemout.write(line)
                ## save plog data if desired
                if linecounter == insertline and saveplog:
                    chemout.write('! PLOG/' + str(pressure) + ' '*35 + appendA +
' '*5 + appendn + ' '*5 + appendE + '/' + '\n')
                linecounter += 1
```

APPENDIX C

Input file used to generate the methylcyclohexane mechanism with RMG.

```
database(
    thermoLibraries = ['Chernov', 'JetSurF2.0', 'primaryThermoLibrary'],
    reactionLibraries = [],
    seedMechanisms = ['ChernovPyrolysis', 'JetSurF2.0PyrolysisPDep'],
    kineticsDepositories = 'default',
    kineticsFamilies = 'default',
    kineticsEstimator = 'rate rules',
)

species(
    label = "CH3cC6H11",
    reactive = True,
    structure = adjacencyList(
"""
1  C u0 p0 c0 {2,S} {3,S} {7,S} {8,S}
2  C u0 p0 c0 {1,S} {4,S} {9,S} {10,S}
3  C u0 p0 c0 {1,S} {6,S} {17,S} {18,S}
4  C u0 p0 c0 {2,S} {5,S} {11,S} {12,S}
5  C u0 p0 c0 {4,S} {6,S} {13,S} {14,S}
6  C u0 p0 c0 {3,S} {5,S} {15,S} {16,S}
7  C u0 p0 c0 {1,S} {19,S} {20,S} {21,S}
8  H u0 p0 c0 {1,S}
9  H u0 p0 c0 {2,S}
10 H u0 p0 c0 {2,S}
11 H u0 p0 c0 {4,S}
12 H u0 p0 c0 {4,S}
13 H u0 p0 c0 {5,S}
14 H u0 p0 c0 {5,S}
15 H u0 p0 c0 {6,S}
16 H u0 p0 c0 {6,S}
17 H u0 p0 c0 {3,S}
18 H u0 p0 c0 {3,S}
19 H u0 p0 c0 {7,S}
20 H u0 p0 c0 {7,S}
21 H u0 p0 c0 {7,S}
"""),
)

species(
    label = "AR",
    reactive = False,
    structure = adjacencyList(
"""
1 Ar u0 p4 c0
"""),
)

species(
    label = "methylenecyclopentane",
    reactive = True,
    structure = adjacencyList(
"""
```

APPENDIX C (continued)

```
1  C u0 p0 c0 {2,D} {7,S} {8,S}
2  C u0 p0 c0 {1,D} {3,S} {6,S}
3  C u0 p0 c0 {2,S} {4,S} {9,S} {10,S}
4  C u0 p0 c0 {3,S} {5,S} {11,S} {12,S}
5  C u0 p0 c0 {4,S} {6,S} {13,S} {14,S}
6  C u0 p0 c0 {2,S} {5,S} {15,S} {16,S}
7  H u0 p0 c0 {1,S}
8  H u0 p0 c0 {1,S}
9  H u0 p0 c0 {3,S}
10 H u0 p0 c0 {3,S}
11 H u0 p0 c0 {4,S}
12 H u0 p0 c0 {4,S}
13 H u0 p0 c0 {5,S}
14 H u0 p0 c0 {5,S}
15 H u0 p0 c0 {6,S}
16 H u0 p0 c0 {6,S}
"""),
)

species(
    label = "dimethylcyclopentane",
    reactive = True,
    structure = adjacencyList(
"""
1  C u0 p0 c0 {2,S} {8,S} {9,S} {10,S}
2  C u0 p0 c0 {1,S} {3,S} {4,S} {7,S}
3  C u0 p0 c0 {2,S} {11,S} {12,S} {13,S}
4  C u0 p0 c0 {2,S} {5,S} {14,S} {15,S}
5  C u0 p0 c0 {4,S} {6,S} {16,S} {17,S}
6  C u0 p0 c0 {5,S} {7,S} {18,S} {19,S}
7  C u0 p0 c0 {2,S} {6,S} {20,S} {21,S}
8  H u0 p0 c0 {1,S}
9  H u0 p0 c0 {1,S}
10 H u0 p0 c0 {1,S}
11 H u0 p0 c0 {3,S}
12 H u0 p0 c0 {3,S}
13 H u0 p0 c0 {3,S}
14 H u0 p0 c0 {4,S}
15 H u0 p0 c0 {4,S}
16 H u0 p0 c0 {5,S}
17 H u0 p0 c0 {5,S}
18 H u0 p0 c0 {6,S}
19 H u0 p0 c0 {6,S}
20 H u0 p0 c0 {7,S}
21 H u0 p0 c0 {7,S}
"""),
)

species(
    label = "benzene",
    reactive = True,
    structure = adjacencyList(
"""
1  C u0 p0 c0 {2,D} {6,S} {7,S}
```

APPENDIX C (continued)

```
2  C u0 p0 c0 {1,D} {3,S} {8,S}
3  C u0 p0 c0 {2,S} {4,D} {9,S}
4  C u0 p0 c0 {3,D} {5,S} {10,S}
5  C u0 p0 c0 {4,S} {6,D} {11,S}
6  C u0 p0 c0 {1,S} {5,D} {12,S}
7  H u0 p0 c0 {1,S}
8  H u0 p0 c0 {2,S}
9  H u0 p0 c0 {3,S}
10 H u0 p0 c0 {4,S}
11 H u0 p0 c0 {5,S}
12 H u0 p0 c0 {6,S}
"""),
)

species(
    label = "cyclohexadiene",
    reactive = True,
    structure = adjacencyList(
"""
1  C u0 p0 c0 {2,S} {6,S} {7,S} {8,S}
2  C u0 p0 c0 {1,S} {3,S} {9,S} {10,S}
3  C u0 p0 c0 {2,S} {4,D} {11,S}
4  C u0 p0 c0 {3,D} {5,S} {12,S}
5  C u0 p0 c0 {4,S} {6,D} {13,S}
6  C u0 p0 c0 {1,S} {5,D} {14,S}
7  H u0 p0 c0 {1,S}
8  H u0 p0 c0 {1,S}
9  H u0 p0 c0 {2,S}
10 H u0 p0 c0 {2,S}
11 H u0 p0 c0 {3,S}
12 H u0 p0 c0 {4,S}
13 H u0 p0 c0 {5,S}
14 H u0 p0 c0 {6,S}
"""),
)

species(
    label = "butene1",
    reactive = True,
    structure = adjacencyList(
"""
1  C u0 p0 c0 {2,S} {5,S} {6,S} {7,S}
2  C u0 p0 c0 {1,S} {3,S} {8,S} {9,S}
3  C u0 p0 c0 {2,S} {4,D} {10,S}
4  C u0 p0 c0 {3,D} {11,S} {12,S}
5  H u0 p0 c0 {1,S}
6  H u0 p0 c0 {1,S}
7  H u0 p0 c0 {1,S}
8  H u0 p0 c0 {2,S}
9  H u0 p0 c0 {2,S}
10 H u0 p0 c0 {3,S}
11 H u0 p0 c0 {4,S}
12 H u0 p0 c0 {4,S}
"""),
```

```
)

species(
    label = "isobutylene",
    reactive = True,
    structure = adjacencyList(
"""
1  C u0 p0 c0 {2,S} {5,S} {6,S} {7,S}
2  C u0 p0 c0 {1,S} {3,S} {4,D}
3  C u0 p0 c0 {2,S} {8,S} {9,S} {10,S}
4  C u0 p0 c0 {2,D} {11,S} {12,S}
5  H u0 p0 c0 {1,S}
6  H u0 p0 c0 {1,S}
7  H u0 p0 c0 {1,S}
8  H u0 p0 c0 {3,S}
9  H u0 p0 c0 {3,S}
10 H u0 p0 c0 {3,S}
11 H u0 p0 c0 {4,S}
12 H u0 p0 c0 {4,S}
"""),
)

species(
    label = "cyclopentadiene",
    reactive = True,
    structure = adjacencyList(
"""
1  C u0 p0 c0 {2,S} {5,S} {6,S} {7,S}
2  C u0 p0 c0 {1,S} {3,D} {8,S}
3  C u0 p0 c0 {2,D} {4,S} {9,S}
4  C u0 p0 c0 {3,S} {5,D} {10,S}
5  C u0 p0 c0 {1,S} {4,D} {11,S}
6  H u0 p0 c0 {1,S}
7  H u0 p0 c0 {1,S}
8  H u0 p0 c0 {2,S}
9  H u0 p0 c0 {3,S}
10 H u0 p0 c0 {4,S}
11 H u0 p0 c0 {5,S}
"""),
)

simpleReactor(
    temperature = (1200,"K"),
    pressure = (199,"bar"),
    initialMoleFractions={
        "AR": 0.999819,
        "CH3cC6H11": 0.000181,
        "methylenecyclopentane": 0,
        "dimethylcyclopentane": 0,
        "benzene": 0,
        "cyclohexadiene": 0,
        "butene1": 0,
        "isobutylene": 0,
        "cyclopentadiene": 0,
```

```
    },
    terminationTime = (2.2,"ms"),
)

simpleReactor(
    temperature = (1400,"K"),
    pressure = (199,"bar"),
    initialMoleFractions={
        "AR": 0.999819,
        "CH3cC6H11": 0.000181,
        "methylenecyclopentane": 0,
        "dimethylcyclopentane": 0,
        "benzene": 0,
        "cyclohexadiene": 0,
        "butene1": 0,
        "isobutylene": 0,
        "cyclopentadiene": 0,
    },
    terminationTime = (2.2,"ms"),
)

simpleReactor(
    temperature = (1600,"K"),
    pressure = (199,"bar"),
    initialMoleFractions={
        "AR": 0.999819,
        "CH3cC6H11": 0.000181,
        "methylenecyclopentane": 0,
        "dimethylcyclopentane": 0,
        "benzene": 0,
        "cyclohexadiene": 0,
        "butene1": 0,
        "isobutylene": 0,
        "cyclopentadiene": 0,
    },
    terminationTime = (2.2,"ms"),
)

simulator(
    atol = 1e-16,
    rtol = 1e-08,
    sens_atol = 1e-06,
    sens_rtol = 0.0001,
)

model(
    toleranceMoveToCore = 0.1,
    toleranceKeepInEdge = 0,
    toleranceInterruptSimulation = 1,
    maximumEdgeSpecies = 100000,
    minCoreSizeForPrune = 50,
    minSpeciesExistIterationsForPrune = 2,
    filterReactions = 0,
)
```

APPENDIX C (continued)

```
pressureDependence(
    method = 'modified strong collision',
    maximumGrainSize = (0.5,"kcal/mol"),
    minimumNumberOfGrains = 250,
    temperatures = (300,2000,"K",8),
    pressures = (40,200,"bar",8),
    interpolation = ('pdeparrhenius',),
    maximumAtoms = 22,
)

generatedSpeciesConstraints(
      #allows exceptions to the following restrictions
    allowed=['input species','seed mechanisms','reaction libraries'],
      #maximum number of each atom in a molecule
    maximumCarbonAtoms=8,
    maximumOxygenAtoms=0,
    maximumNitrogenAtoms=0,
    maximumSiliconAtoms=0,
    maximumSulfurAtoms=0,
      #max number of non-hydrogen atoms
    #maximumHeavyAtoms=20,
      #maximum radicals on a molecule
    maximumRadicalElectrons=1,
)

options(
    units = "si",
    saveRestartPeriod = None,
    generateOutputHTML = False,
    generatePlots = False,
    saveSimulationProfiles = False,
    saveEdgeSpecies = False,
    keepIrreversible = None,
    verboseComments = False,
)
```

APPENDIX C (continued)

Input file used to generate the cyclohexane mechanism with RMG.

```
database(
    thermoLibraries = ['Chernov', 'JetSurF2.0', 'primaryThermoLibrary'],
    reactionLibraries = [],
    seedMechanisms = ['ChernovPyrolysis', 'JetSurF2.0PyrolysisPDep'],
    kineticsDepositories = 'default',
    kineticsFamilies = 'default',
    kineticsEstimator = 'rate rules',
)

species(
    label = "cC6H12",
    reactive = True,
    structure = adjacencyList(
"""
1  C u0 p0 c0 {2,S} {6,S} {7,S} {8,S}
2  C u0 p0 c0 {1,S} {3,S} {9,S} {10,S}
3  C u0 p0 c0 {2,S} {4,S} {11,S} {12,S}
4  C u0 p0 c0 {3,S} {5,S} {13,S} {14,S}
5  C u0 p0 c0 {4,S} {6,S} {15,S} {16,S}
6  C u0 p0 c0 {1,S} {5,S} {17,S} {18,S}
7  H u0 p0 c0 {1,S}
8  H u0 p0 c0 {1,S}
9  H u0 p0 c0 {2,S}
10 H u0 p0 c0 {2,S}
11 H u0 p0 c0 {3,S}
12 H u0 p0 c0 {3,S}
13 H u0 p0 c0 {4,S}
14 H u0 p0 c0 {4,S}
15 H u0 p0 c0 {5,S}
16 H u0 p0 c0 {5,S}
17 H u0 p0 c0 {6,S}
18 H u0 p0 c0 {6,S}
"""),
)

species(
    label = "AR",
    reactive = False,
    structure = adjacencyList(
"""
1 Ar u0 p4 c0
"""),
)

species(
    label = "methylenecyclopentane",
    reactive = True,
    structure = adjacencyList(
"""
1  C u0 p0 c0 {2,D} {7,S} {8,S}
2  C u0 p0 c0 {1,D} {3,S} {6,S}
```

```
3  C u0 p0 c0 {2,S} {4,S} {9,S} {10,S}
4  C u0 p0 c0 {3,S} {5,S} {11,S} {12,S}
5  C u0 p0 c0 {4,S} {6,S} {13,S} {14,S}
6  C u0 p0 c0 {2,S} {5,S} {15,S} {16,S}
7  H u0 p0 c0 {1,S}
8  H u0 p0 c0 {1,S}
9  H u0 p0 c0 {3,S}
10 H u0 p0 c0 {3,S}
11 H u0 p0 c0 {4,S}
12 H u0 p0 c0 {4,S}
13 H u0 p0 c0 {5,S}
14 H u0 p0 c0 {5,S}
15 H u0 p0 c0 {6,S}
16 H u0 p0 c0 {6,S}
"""),
)

species(
    label = "dimethylcyclopentane",
    reactive = True,
    structure = adjacencyList(
"""
1  C u0 p0 c0 {2,S} {8,S} {9,S} {10,S}
2  C u0 p0 c0 {1,S} {3,S} {4,S} {7,S}
3  C u0 p0 c0 {2,S} {11,S} {12,S} {13,S}
4  C u0 p0 c0 {2,S} {5,S} {14,S} {15,S}
5  C u0 p0 c0 {4,S} {6,S} {16,S} {17,S}
6  C u0 p0 c0 {5,S} {7,S} {18,S} {19,S}
7  C u0 p0 c0 {2,S} {6,S} {20,S} {21,S}
8  H u0 p0 c0 {1,S}
9  H u0 p0 c0 {1,S}
10 H u0 p0 c0 {1,S}
11 H u0 p0 c0 {3,S}
12 H u0 p0 c0 {3,S}
13 H u0 p0 c0 {3,S}
14 H u0 p0 c0 {4,S}
15 H u0 p0 c0 {4,S}
16 H u0 p0 c0 {5,S}
17 H u0 p0 c0 {5,S}
18 H u0 p0 c0 {6,S}
19 H u0 p0 c0 {6,S}
20 H u0 p0 c0 {7,S}
21 H u0 p0 c0 {7,S}
"""),
)

species(
    label = "benzene",
    reactive = True,
    structure = adjacencyList(
"""
1  C u0 p0 c0 {2,D} {6,S} {7,S}
2  C u0 p0 c0 {1,D} {3,S} {8,S}
3  C u0 p0 c0 {2,S} {4,D} {9,S}
```

```
4  C u0 p0 c0 {3,D} {5,S} {10,S}
5  C u0 p0 c0 {4,S} {6,D} {11,S}
6  C u0 p0 c0 {1,S} {5,D} {12,S}
7  H u0 p0 c0 {1,S}
8  H u0 p0 c0 {2,S}
9  H u0 p0 c0 {3,S}
10 H u0 p0 c0 {4,S}
11 H u0 p0 c0 {5,S}
12 H u0 p0 c0 {6,S}
"""),
)

species(
    label = "cyclohexadiene",
    reactive = True,
    structure = adjacencyList(
"""
1  C u0 p0 c0 {2,S} {6,S} {7,S} {8,S}
2  C u0 p0 c0 {1,S} {3,S} {9,S} {10,S}
3  C u0 p0 c0 {2,S} {4,D} {11,S}
4  C u0 p0 c0 {3,D} {5,S} {12,S}
5  C u0 p0 c0 {4,S} {6,D} {13,S}
6  C u0 p0 c0 {1,S} {5,D} {14,S}
7  H u0 p0 c0 {1,S}
8  H u0 p0 c0 {1,S}
9  H u0 p0 c0 {2,S}
10 H u0 p0 c0 {2,S}
11 H u0 p0 c0 {3,S}
12 H u0 p0 c0 {4,S}
13 H u0 p0 c0 {5,S}
14 H u0 p0 c0 {6,S}
"""),
)

species(
    label = "butene1",
    reactive = True,
    structure = adjacencyList(
"""
1  C u0 p0 c0 {2,S} {5,S} {6,S} {7,S}
2  C u0 p0 c0 {1,S} {3,S} {8,S} {9,S}
3  C u0 p0 c0 {2,S} {4,D} {10,S}
4  C u0 p0 c0 {3,D} {11,S} {12,S}
5  H u0 p0 c0 {1,S}
6  H u0 p0 c0 {1,S}
7  H u0 p0 c0 {1,S}
8  H u0 p0 c0 {2,S}
9  H u0 p0 c0 {2,S}
10 H u0 p0 c0 {3,S}
11 H u0 p0 c0 {4,S}
12 H u0 p0 c0 {4,S}
"""),
)
```

APPENDIX C (continued)

```
species(
    label = "isobutylene",
    reactive = True,
    structure = adjacencyList(
"""
1  C u0 p0 c0 {2,S} {5,S} {6,S} {7,S}
2  C u0 p0 c0 {1,S} {3,S} {4,D}
3  C u0 p0 c0 {2,S} {8,S} {9,S} {10,S}
4  C u0 p0 c0 {2,D} {11,S} {12,S}
5  H u0 p0 c0 {1,S}
6  H u0 p0 c0 {1,S}
7  H u0 p0 c0 {1,S}
8  H u0 p0 c0 {3,S}
9  H u0 p0 c0 {3,S}
10 H u0 p0 c0 {3,S}
11 H u0 p0 c0 {4,S}
12 H u0 p0 c0 {4,S}
"""),
)

species(
    label = "cyclopentadiene",
    reactive = True,
    structure = adjacencyList(
"""
1  C u0 p0 c0 {2,S} {5,S} {6,S} {7,S}
2  C u0 p0 c0 {1,S} {3,D} {8,S}
3  C u0 p0 c0 {2,D} {4,S} {9,S}
4  C u0 p0 c0 {3,S} {5,D} {10,S}
5  C u0 p0 c0 {1,S} {4,D} {11,S}
6  H u0 p0 c0 {1,S}
7  H u0 p0 c0 {1,S}
8  H u0 p0 c0 {2,S}
9  H u0 p0 c0 {3,S}
10 H u0 p0 c0 {4,S}
11 H u0 p0 c0 {5,S}
"""),
)

simpleReactor(
    temperature = (1200,"K"),
    pressure = (199,"bar"),
    initialMoleFractions={
        "AR": 0.999810,
        "cC6H12": 0.000190,
        "methylenecyclopentane": 0,
        "dimethylcyclopentane": 0,
        "benzene": 0,
        "cyclohexadiene": 0,
        "butene1": 0,
        "isobutylene": 0,
        "cyclopentadiene": 0,
    },
    terminationTime = (2.2,"ms"),
```

```
)

simpleReactor(
    temperature = (1400,"K"),
    pressure = (199,"bar"),
    initialMoleFractions={
        "AR": 0.999810,
        "cC6H12": 0.000190,
        "methylenecyclopentane": 0,
        "dimethylcyclopentane": 0,
        "benzene": 0,
        "cyclohexadiene": 0,
        "butene1": 0,
        "isobutylene": 0,
        "cyclopentadiene": 0,
    },
    terminationTime = (2.2,"ms"),
)

simpleReactor(
    temperature = (1600,"K"),
    pressure = (199,"bar"),
    initialMoleFractions={
        "AR": 0.999810,
        "cC6H12": 0.000190,
        "methylenecyclopentane": 0,
        "dimethylcyclopentane": 0,
        "benzene": 0,
        "cyclohexadiene": 0,
        "butene1": 0,
        "isobutylene": 0,
        "cyclopentadiene": 0,
    },
    terminationTime = (2.2,"ms"),
)

simulator(
    atol = 1e-16,
    rtol = 1e-08,
    sens_atol = 1e-06,
    sens_rtol = 0.0001,
)

model(
    toleranceMoveToCore = 0.1,
    toleranceKeepInEdge = 0,
    toleranceInterruptSimulation = 1,
    maximumEdgeSpecies = 100000,
    minCoreSizeForPrune = 50,
    minSpeciesExistIterationsForPrune = 2,
    filterReactions = 0,
)

pressureDependence(
```

APPENDIX C (continued)

```
    method = 'modified strong collision',
    maximumGrainSize = (0.5,"kcal/mol"),
    minimumNumberOfGrains = 250,
    temperatures = (300,2000,"K",8),
    pressures = (40,200,"bar",8),
    interpolation = ('pdeparrhenius',),
    maximumAtoms = 22,
)

generatedSpeciesConstraints(
      #allows exceptions to the following restrictions
    allowed=['input species','seed mechanisms','reaction libraries'],
      #maximum number of each atom in a molecule
    maximumCarbonAtoms=8,
    maximumOxygenAtoms=0,
    maximumNitrogenAtoms=0,
    maximumSiliconAtoms=0,
    maximumSulfurAtoms=0,
      #max number of non-hydrogen atoms
    #maximumHeavyAtoms=20,
      #maximum radicals on a molecule
    maximumRadicalElectrons=1,
)

options(
    units = "si",
    saveRestartPeriod = None,
    generateOutputHTML = False,
    generatePlots = False,
    saveSimulationProfiles = False,
    saveEdgeSpecies = False,
    keepIrreversible = None,
    verboseComments = False,
)
```

APPENDIX C (continued)

Input file used to generate the hex-5-en-1-yl/1,5-hexadiene mechanism with RMG.

```
database(
    thermoLibraries = ['Chernov', 'JetSurF2.0', 'primaryThermoLibrary'],
    reactionLibraries = [],
    seedMechanisms = ['ChernovPyrolysis', 'JetSurF2.0PyrolysisPDep'],
    kineticsDepositories = 'default',
    kineticsFamilies = 'default',
    kineticsEstimator = 'rate rules',
)

species(
    label = "hex5en1yl",
    reactive = True,
    structure = adjacencyList(
"""
multiplicity 2
1  C u1 p0 c0 {2,S} {3,S} {4,S}
2  H u0 p0 c0 {1,S}
3  H u0 p0 c0 {1,S}
4  C u0 p0 c0 {1,S} {5,S} {9,S} {10,S}
5  C u0 p0 c0 {4,S} {6,S} {11,S} {12,S}
6  C u0 p0 c0 {5,S} {7,S} {13,S} {14,S}
7  C u0 p0 c0 {6,S} {8,D} {15,S}
8  C u0 p0 c0 {7,D} {16,S} {17,S}
9  H u0 p0 c0 {4,S}
10 H u0 p0 c0 {4,S}
11 H u0 p0 c0 {5,S}
12 H u0 p0 c0 {5,S}
13 H u0 p0 c0 {6,S}
14 H u0 p0 c0 {6,S}
15 H u0 p0 c0 {7,S}
16 H u0 p0 c0 {8,S}
17 H u0 p0 c0 {8,S}
"""),
)

species(
    label = "C6H815",
    reactive = True,
    structure = adjacencyList(
"""
1  C u0 p0 c0 {2,D} {7,S} {8,S}
2  C u0 p0 c0 {1,D} {3,S} {9,S}
3  C u0 p0 c0 {2,S} {4,S} {10,S} {11,S}
4  C u0 p0 c0 {3,S} {5,S} {12,S} {13,S}
5  C u0 p0 c0 {4,S} {6,D} {14,S}
6  C u0 p0 c0 {5,D} {15,S} {16,S}
7  H u0 p0 c0 {1,S}
8  H u0 p0 c0 {1,S}
9  H u0 p0 c0 {2,S}
10 H u0 p0 c0 {3,S}
11 H u0 p0 c0 {3,S}
12 H u0 p0 c0 {4,S}
```

```
13 H u0 p0 c0 {4,S}
14 H u0 p0 c0 {5,S}
15 H u0 p0 c0 {6,S}
16 H u0 p0 c0 {6,S}

"""),
)

species(
    label = "AR",
    reactive = False,
    structure = adjacencyList(
"""
1 Ar u0 p4 c0
"""),
)

species(
    label = "methylenecyclopentane",
    reactive = True,
    structure = adjacencyList(
"""
1  C u0 p0 c0 {2,D} {7,S} {8,S}
2  C u0 p0 c0 {1,D} {3,S} {6,S}
3  C u0 p0 c0 {2,S} {4,S} {9,S} {10,S}
4  C u0 p0 c0 {3,S} {5,S} {11,S} {12,S}
5  C u0 p0 c0 {4,S} {6,S} {13,S} {14,S}
6  C u0 p0 c0 {2,S} {5,S} {15,S} {16,S}
7  H u0 p0 c0 {1,S}
8  H u0 p0 c0 {1,S}
9  H u0 p0 c0 {3,S}
10 H u0 p0 c0 {3,S}
11 H u0 p0 c0 {4,S}
12 H u0 p0 c0 {4,S}
13 H u0 p0 c0 {5,S}
14 H u0 p0 c0 {5,S}
15 H u0 p0 c0 {6,S}
16 H u0 p0 c0 {6,S}
"""),
)

species(
    label = "dimethylcyclopentane",
    reactive = True,
    structure = adjacencyList(
"""
1  C u0 p0 c0 {2,S} {8,S} {9,S} {10,S}
2  C u0 p0 c0 {1,S} {3,S} {4,S} {7,S}
3  C u0 p0 c0 {2,S} {11,S} {12,S} {13,S}
4  C u0 p0 c0 {2,S} {5,S} {14,S} {15,S}
5  C u0 p0 c0 {4,S} {6,S} {16,S} {17,S}
6  C u0 p0 c0 {5,S} {7,S} {18,S} {19,S}
7  C u0 p0 c0 {2,S} {6,S} {20,S} {21,S}
8  H u0 p0 c0 {1,S}
```

```
9  H u0 p0 c0 {1,S}
10 H u0 p0 c0 {1,S}
11 H u0 p0 c0 {3,S}
12 H u0 p0 c0 {3,S}
13 H u0 p0 c0 {3,S}
14 H u0 p0 c0 {4,S}
15 H u0 p0 c0 {4,S}
16 H u0 p0 c0 {5,S}
17 H u0 p0 c0 {5,S}
18 H u0 p0 c0 {6,S}
19 H u0 p0 c0 {6,S}
20 H u0 p0 c0 {7,S}
21 H u0 p0 c0 {7,S}
"""),
)

species(
    label = "benzene",
    reactive = True,
    structure = adjacencyList(
"""
1  C u0 p0 c0 {2,D} {6,S} {7,S}
2  C u0 p0 c0 {1,D} {3,S} {8,S}
3  C u0 p0 c0 {2,S} {4,D} {9,S}
4  C u0 p0 c0 {3,D} {5,S} {10,S}
5  C u0 p0 c0 {4,S} {6,D} {11,S}
6  C u0 p0 c0 {1,S} {5,D} {12,S}
7  H u0 p0 c0 {1,S}
8  H u0 p0 c0 {2,S}
9  H u0 p0 c0 {3,S}
10 H u0 p0 c0 {4,S}
11 H u0 p0 c0 {5,S}
12 H u0 p0 c0 {6,S}
"""),
)

species(
    label = "cyclohexadiene",
    reactive = True,
    structure = adjacencyList(
"""
1  C u0 p0 c0 {2,S} {6,S} {7,S} {8,S}
2  C u0 p0 c0 {1,S} {3,S} {9,S} {10,S}
3  C u0 p0 c0 {2,S} {4,D} {11,S}
4  C u0 p0 c0 {3,D} {5,S} {12,S}
5  C u0 p0 c0 {4,S} {6,D} {13,S}
6  C u0 p0 c0 {1,S} {5,D} {14,S}
7  H u0 p0 c0 {1,S}
8  H u0 p0 c0 {1,S}
9  H u0 p0 c0 {2,S}
10 H u0 p0 c0 {2,S}
11 H u0 p0 c0 {3,S}
12 H u0 p0 c0 {4,S}
13 H u0 p0 c0 {5,S}
```

```
14 H u0 p0 c0 {6,S}
"""),
)

species(
    label = "butene1",
    reactive = True,
    structure = adjacencyList(
"""
1  C u0 p0 c0 {2,S} {5,S} {6,S} {7,S}
2  C u0 p0 c0 {1,S} {3,S} {8,S} {9,S}
3  C u0 p0 c0 {2,S} {4,D} {10,S}
4  C u0 p0 c0 {3,D} {11,S} {12,S}
5  H u0 p0 c0 {1,S}
6  H u0 p0 c0 {1,S}
7  H u0 p0 c0 {1,S}
8  H u0 p0 c0 {2,S}
9  H u0 p0 c0 {2,S}
10 H u0 p0 c0 {3,S}
11 H u0 p0 c0 {4,S}
12 H u0 p0 c0 {4,S}
"""),
)

species(
    label = "isobutylene",
    reactive = True,
    structure = adjacencyList(
"""
1  C u0 p0 c0 {2,S} {5,S} {6,S} {7,S}
2  C u0 p0 c0 {1,S} {3,S} {4,D}
3  C u0 p0 c0 {2,S} {8,S} {9,S} {10,S}
4  C u0 p0 c0 {2,D} {11,S} {12,S}
5  H u0 p0 c0 {1,S}
6  H u0 p0 c0 {1,S}
7  H u0 p0 c0 {1,S}
8  H u0 p0 c0 {3,S}
9  H u0 p0 c0 {3,S}
10 H u0 p0 c0 {3,S}
11 H u0 p0 c0 {4,S}
12 H u0 p0 c0 {4,S}
"""),
)

species(
    label = "cyclopentadiene",
    reactive = True,
    structure = adjacencyList(
"""
1  C u0 p0 c0 {2,S} {5,S} {6,S} {7,S}
2  C u0 p0 c0 {1,S} {3,D} {8,S}
3  C u0 p0 c0 {2,D} {4,S} {9,S}
4  C u0 p0 c0 {3,S} {5,D} {10,S}
5  C u0 p0 c0 {1,S} {4,D} {11,S}
```

```
6  H u0 p0 c0 {1,S}
7  H u0 p0 c0 {1,S}
8  H u0 p0 c0 {2,S}
9  H u0 p0 c0 {3,S}
10 H u0 p0 c0 {4,S}
11 H u0 p0 c0 {5,S}
"""),
)

simpleReactor(
    temperature = (1000,"K"),
    pressure = (199,"bar"),
    initialMoleFractions={
        "AR": 0.999839,
        "hex5en1yl": 0.0000805,
        "C6H815": 0.0000805,
        "methylenecyclopentane": 0,
        "dimethylcyclopentane": 0,
        "benzene": 0,
        "cyclohexadiene": 0,
        "butene1": 0,
        "isobutylene": 0,
        "cyclopentadiene": 0,
    },
    terminationTime = (2.2,"ms"),
)

simpleReactor(
    temperature = (1200,"K"),
    pressure = (199,"bar"),
    initialMoleFractions={
        "AR": 0.999810,
        "hex5en1yl": 0.0000805,
        "C6H815": 0.0000805,
        "methylenecyclopentane": 0,
        "dimethylcyclopentane": 0,
        "benzene": 0,
        "cyclohexadiene": 0,
        "butene1": 0,
        "isobutylene": 0,
        "cyclopentadiene": 0,
    },
    terminationTime = (2.2,"ms"),
)

simpleReactor(
    temperature = (1400,"K"),
    pressure = (199,"bar"),
    initialMoleFractions={
        "AR": 0.999810,
        "hex5en1yl": 0.0000805,
        "C6H815": 0.0000805,
        "methylenecyclopentane": 0,
        "dimethylcyclopentane": 0,
```

APPENDIX C (continued)

```
        "benzene": 0,
        "cyclohexadiene": 0,
        "butene1": 0,
        "isobutylene": 0,
        "cyclopentadiene": 0,
    },
    terminationTime = (2.2,"ms"),
)

simulator(
    atol = 1e-16,
    rtol = 1e-08,
    sens_atol = 1e-06,
    sens_rtol = 0.0001,
)

model(
    toleranceMoveToCore = 0.1,
    toleranceKeepInEdge = 0,
    toleranceInterruptSimulation = 1,
    maximumEdgeSpecies = 100000,
    minCoreSizeForPrune = 50,
    minSpeciesExistIterationsForPrune = 2,
    filterReactions = 0,
)

pressureDependence(
    method = 'modified strong collision',
    maximumGrainSize = (0.5,"kcal/mol"),
    minimumNumberOfGrains = 250,
    temperatures = (300,2000,"K",8),
    pressures = (40,200,"bar",8),
    interpolation = ('pdeparrhenius',),
    maximumAtoms = 22,
)

generatedSpeciesConstraints(
      #allows exceptions to the following restrictions
    allowed=['input species','seed mechanisms','reaction libraries'],
      #maximum number of each atom in a molecule
    maximumCarbonAtoms=8,
    maximumOxygenAtoms=0,
    maximumNitrogenAtoms=0,
    maximumSiliconAtoms=0,
    maximumSulfurAtoms=0,
      #max number of non-hydrogen atoms
    #maximumHeavyAtoms=20,
      #maximum radicals on a molecule
    maximumRadicalElectrons=1,
)

options(
    units = "si",
    saveRestartPeriod = None,
```

```
    generateOutputHTML = False,
    generatePlots = False,
    saveSimulationProfiles = False,
    saveEdgeSpecies = False,
    keepIrreversible = None,
    verboseComments = False,
)
```

APPENDIX D

The species names for the experimental data present in the following pages is given in the table below. All the species data is provided in ppm.

Species Symbol	Species Name
CH4	Methane
C2H6	Ethane
C2H4	Ethylene
C2H2	Acetylene
C3H8	Propane
cC3H6	Cyclopropene
C3H6	Propene
aC3H4	Propadiene
1-C4H8	1-Butene
2-C4H8	2-Butene
pC3H4	Propyne
C4H6	1,3-Butadiene
C4H2	Diacetylene
C4H8	Isobutylene
C4H6-12	1,2-Butadiene
C4H4	Vinylacetylene
C5H6	Cyclopentadiene
C6H10-15	1,5-Hexadiene
C6H12-1	1-Hexene
CH2cC5H8	Methylenecyclopentane
C6H6	Benzene
cC6H12	Cyclohexane
cC6H8	1,3-Cyclohexadiene
cC6H10	Cyclohexene
CH3cC6H11	Methylcyclohexane
C7H8	Toluene
6B1H	6-Bromo-1-hexene

APPENDIX D (continued)

Species data for experiments conducted at 40 bar with 186 ppm of cyclohexane as the fuel.

P (bar)	T (K)	t (s)	CH4	C2H6	C2H4	C2H2	C3H8	C3H6	aC3H4	1-C4H8	pC3H4
40.40	1389	0.002107	49.73	7.64	227.17	151.38	0.00	7.82	9.22	0.16	20.09
42.62	1254	0.002218	8.65	2.55	108.52	26.82	0.08	8.78	4.54	1.30	3.67
37.72	1199	0.002277	3.08	0.59	44.05	8.27	0.00	3.75	1.77	0.90	0.77
39.21	1248	0.002224	8.54	2.55	105.46	25.50	0.05	8.63	4.47	1.25	3.46
38.50	1307	0.002182	22.25	8.39	196.41	73.17	0.00	13.13	8.85	0.62	13.97
39.16	1111	0.002507	0.00	0.00	1.64	0.25	0.00	0.19	0.00	0.00	0.00
39.42	1068	0.002697	1.03	0.00	0.19	0.00	0.00	0.00	0.00	0.00	0.00
39.34	1020	0.003068	0.00	0.00	0.00	0.00	0.00	0.00	0.00	0.00	0.00
35.95	1103	0.002432	0.00	0.00	2.23	0.33	0.00	0.21	0.00	0.00	0.00
36.23	1134	0.002299	0.64	0.07	7.47	1.10	0.00	0.63	0.22	0.19	0.08
38.93	1248	0.002241	7.02	2.02	91.90	20.96	0.00	7.63	3.81	1.30	2.65
38.58	1209	0.002255	3.20	0.65	47.50	9.04	0.00	4.06	1.82	0.90	0.86
39.63	1238	0.002167	6.67	1.72	86.73	19.08	0.06	7.16	3.51	1.28	2.32
36.40	1263	0.002221	11.66	4.12	134.09	36.21	0.06	10.68	5.87	1.17	5.78
36.68	1292	0.002181	19.98	7.86	184.36	64.46	0.08	12.96	8.40	0.73	12.43
37.06	1272	0.002165	19.63	7.51	183.29	62.70	0.09	12.92	8.19	0.78	11.80
37.95	1339	0.002169	26.35	9.28	208.07	85.12	0.08	12.91	9.28	0.44	16.22
36.56	1297	0.002193	20.21	7.91	186.79	65.06	0.05	13.09	8.37	0.78	12.43
34.33	1094	0.002455	0.00	0.00	0.79	0.10	0.00	0.11	0.00	0.00	0.00
36.70	1167	0.002282	1.13	0.16	13.68	2.24	0.00	1.13	0.44	0.28	0.12
33.97	1372	0.002158	37.23	10.12	224.20	115.22	0.00	10.77	9.86	0.29	20.29
36.10	1450	0.002072	70.55	2.94	189.95	238.80	0.00	3.01	6.06	0.08	13.89
32.91	1676	0.002137	68.33	0.79	78.83	377.57	0.00	0.61	2.32	0.00	5.44
37.39	1542	0.001989	73.60	1.07	110.08	342.38	0.00	1.01	3.04	0.00	7.13
35.61	1585	0.002051	71.12	0.98	100.89	356.20	0.00	0.87	2.84	0.00	6.83
37.03	1577	0.002049	69.70	0.89	92.72	363.11	0.00	0.81	2.64	0.00	6.45
34.48	1627	0.002096	68.17	0.88	85.25	372.42	0.00	0.70	0.72	0.00	6.03
33.28	1324	0.002171	25.87	9.67	205.66	83.72	0.00	12.82	9.40	0.59	16.58
36.87	1446	0.002057	77.68	5.67	236.95	221.78	0.00	6.60	8.10	0.42	18.59
38.38	1478	0.002042	74.55	2.54	191.33	242.23	0.00	2.87	5.76	0.14	13.40
37.90	1494	0.002042	72.91	3.08	197.67	235.32	0.00	3.20	6.30	0.07	14.46
37.98	1441	0.002085	63.02	5.00	216.46	192.98	0.00	5.02	7.86	0.09	17.94
37.62	1445	0.002076	68.31	4.47	216.05	210.55	0.00	4.73	7.41	0.14	17.11
35.31	1387	0.002142	51.39	7.55	226.05	155.93	0.00	7.34	9.17	0.19	20.42

APPENDIX D (continued)

Species data for experiments conducted at 40 bar with 186 ppm of cyclohexane as the fuel (continued).

C4H6	C4H2	C4H8	C4H6-12	C4H4	C5H6	C6H10-15	C6H12-1	CH2cC5H8	C6H6	cC6H12	cC6H10	C7H8
22.26	2.98	0.05	0.54	10.28	0.98	0.00	0.05	0.00	5.24	7.65	0.09	0.30
50.80	0.00	0.14	0.47	1.75	0.92	0.07	0.43	0.14	0.49	95.64	0.88	0.00
25.34	0.00	0.00	0.14	0.30	0.32	0.10	0.54	0.11	0.11	146.24	1.30	0.00
50.11	0.00	0.11	0.47	1.69	0.86	0.06	0.45	0.14	0.42	97.54	0.88	0.00
54.78	0.82	0.13	0.93	6.67	1.59	0.03	0.17	0.08	1.55	34.12	0.27	0.00
1.08	0.00	0.00	0.00	0.00	0.00	0.00	0.06	0.00	0.00	184.25	0.28	0.00
0.00	0.00	0.00	0.00	0.00	0.00	0.00	0.00	0.00	0.00	185.66	0.06	0.00
0.00	0.00	0.00	0.00	0.00	0.00	0.00	0.00	0.00	0.00	186.07	0.00	0.00
1.43	0.00	0.00	0.00	0.00	0.00	0.00	0.11	0.00	0.00	182.41	0.37	0.00
4.74	0.00	0.00	0.00	0.00	0.05	0.05	0.30	0.03	0.01	177.33	0.80	0.00
45.96	0.00	0.14	0.39	1.25	0.71	0.07	0.53	0.12	0.37	107.53	1.01	0.00
27.38	0.00	0.07	0.13	0.33	0.34	0.07	0.54	0.10	0.15	143.69	1.41	0.00
44.14	0.00	0.12	0.35	1.09	0.71	0.09	0.54	0.13	0.34	111.65	1.03	0.00
55.93	0.51	0.12	0.63	2.82	1.11	0.06	0.37	0.13	0.67	76.29	0.65	0.00
56.34	0.74	0.15	0.87	5.87	1.57	0.02	0.19	0.09	1.32	40.82	0.29	0.00
57.74	0.79	0.17	0.82	5.58	1.53	0.03	0.20	0.09	1.22	41.28	0.32	0.00
50.30	1.03	0.13	0.88	7.79	1.69	0.00	0.13	0.07	1.94	24.47	0.18	0.00
56.87	0.80	0.16	0.86	5.85	1.55	0.02	0.20	0.06	1.25	39.58	0.30	0.00
0.51	0.00	0.00	0.00	0.00	0.00	0.00	0.02	0.00	0.00	183.80	0.13	0.00
8.73	0.00	0.00	0.00	0.00	0.11	0.09	0.40	0.05	0.00	171.75	1.11	0.00
35.52	1.80	0.09	0.77	9.87	1.47	0.00	0.06	0.03	3.46	13.10	0.10	0.00
6.78	8.01	0.00	0.22	6.40	0.36	0.00	0.00	0.00	8.14	3.07	0.04	0.34
1.22	23.51	0.00	0.00	1.94	0.14	0.00	0.00	0.00	5.66	0.94	0.00	0.00
2.00	17.57	0.00	0.09	2.66	0.17	0.00	0.00	0.00	7.03	1.20	0.00	0.00
1.81	19.72	0.00	0.00	2.50	0.15	0.00	0.00	0.00	6.55	1.07	0.00	0.00
1.78	21.18	0.00	0.08	2.28	0.17	0.00	0.00	0.00	6.38	1.16	0.00	0.00
1.49	22.91	0.00	0.00	2.13	0.14	0.00	0.00	0.00	5.78	1.02	0.00	0.00
50.12	1.07	0.13	0.87	7.74	1.64	0.00	0.12	0.07	1.87	26.04	0.19	0.00
11.86	6.23	0.07	0.34	9.21	0.92	0.00	0.04	0.02	9.73	3.04	0.06	0.75
6.86	8.36	0.00	0.18	6.50	0.36	0.00	0.00	0.00	8.89	2.19	0.04	0.34
7.43	7.64	0.05	0.23	7.03	0.40	0.00	0.00	0.02	8.55	2.59	0.03	0.34
12.67	5.16	0.00	0.35	9.05	0.59	0.00	0.03	0.00	7.23	3.74	0.06	0.38
11.03	6.06	0.05	0.31	8.50	0.62	0.00	0.03	0.00	8.17	3.21	0.06	0.54
21.06	3.34	0.08	0.59	10.48	0.95	0.04	0.05	0.00	5.59	7.61	0.10	0.40

APPENDIX D (continued)

Species data for experiments conducted at 100 bar with 189 ppm of cyclohexane as the fuel.

P (bar)	T (K)	t (s)(	CH4	C2H6	C2H4	C2H2	C3H8	C3H6	aC3H4	1-C4H8	pC3H4
99.35	1288	0.002153	27.59	5.80	210.58	87.25	0.05	12.55	7.43	0.49	12.94
90.72	1038	0.002651	0.00	0.00	0.31	0.00	0.00	0.00	0.00	0.00	0.00
92.84	980	0.002429	0.00	0.00	0.00	0.00	0.00	0.00	0.00	0.00	0.00
94.37	1085	0.002417	0.00	0.00	1.17	0.17	0.00	0.10	0.00	0.00	0.00
101.97	1122	0.002265	0.00	0.00	2.74	0.45	0.00	0.29	0.05	0.00	0.00
113.28	1188	0.002234	3.48	0.31	50.66	9.90	0.00	3.97	1.45	0.81	0.59
95.81	1107	0.002345	0.00	0.00	2.48	0.40	0.00	0.23	0.05	0.00	0.00
100.91	1155	0.002313	2.18	0.18	30.31	5.55	0.00	2.44	0.89	0.53	0.30
98.44	1210	0.002329	5.90	0.80	78.13	17.36	0.00	6.12	2.59	1.14	1.46
96.68	1125	0.002409	0.00	0.00	5.17	0.78	0.00	0.40	0.13	0.05	0.00
99.19	1165	0.002344	1.62	0.14	19.99	3.52	0.00	1.58	0.57	0.38	0.17
94.11	1229	0.002303	8.04	1.35	102.93	24.88	0.00	7.92	3.38	1.27	2.44
92.07	1240	0.002347	9.53	1.77	115.38	29.62	0.07	8.85	4.01	1.29	3.30
103.57	1336	0.002184	32.46	5.98	220.47	102.10	0.05	11.89	7.76	0.40	14.71
97.42	1297	0.002265	23.15	5.17	196.32	74.18	0.07	12.62	7.04	0.67	11.08
88.23	1221	0.002355	7.83	1.34	97.48	23.38	0.00	7.67	3.43	1.31	2.40
97.37	1301	0.002259	22.67	5.04	193.99	72.30	0.00	12.60	7.07	0.64	10.62
92.46	1220	0.002207	9.22	1.67	115.34	28.76	0.05	8.87	3.91	1.28	3.16
98.19	1254	0.002182	15.82	3.47	161.27	49.88	0.00	11.69	5.76	0.98	6.77
90.48	1249	0.002305	8.82	1.62	107.34	26.66	0.00	8.25	3.72	1.28	2.88
90.55	1372	0.002208	48.15	5.11	226.07	146.64	0.00	8.00	7.76	0.25	16.92
86.81	1404	0.002186	57.09	3.65	220.26	175.94	0.00	5.96	7.11	0.17	15.80
82.83	1382	0.002236	61.95	2.73	209.87	194.40	0.00	4.59	6.42	0.14	14.33
88.65	1488	0.002162	71.95	1.31	166.18	266.79	0.00	2.32	4.03	0.06	9.14
86.82	1412	0.002216	68.65	3.94	243.71	195.35	0.00	6.60	7.14	0.18	15.92
85.60	1482	0.002123	73.11	1.69	188.31	248.40	0.00	2.82	4.58	0.13	10.76
87.24	1463	0.002149	69.46	1.99	198.13	227.76	0.00	3.41	5.17	0.10	11.85
84.00	1504	0.002104	74.02	1.03	134.48	304.11	0.00	1.63	3.00	0.09	7.20
90.44	1556	0.002097	50.01	0.48	34.61	399.61	0.00	0.53	1.49	0.00	3.55

APPENDIX D (continued)

Species data for experiments conducted at 100 bar with 189 ppm of cyclohexane as the fuel (continued).

C4H6	C4H2	C4H8	C4H6-12	C4H4	C5H6	C6H10-15	C6H12-1	CH2cC5H8	C6H6	cC6H12	cC6H10	C7H8
50.15	0.00	0.15	0.72	7.72	2.04	0.02	0.13	0.06	2.44	23.62	0.27	0.24
0.24	0.00	0.00	0.00	0.00	0.00	0.00	0.00	0.00	0.00	188.40	0.14	0.00
0.00	0.00	0.00	0.00	0.00	0.00	0.00	0.00	0.00	0.00	188.55	0.07	0.00
0.71	0.00	0.00	0.00	0.00	0.00	0.01	0.04	0.00	0.00	187.14	0.23	0.00
1.78	0.00	0.00	0.00	0.00	0.02	0.02	0.13	0.03	0.00	186.18	0.47	0.00
28.61	0.00	0.05	0.15	0.34	0.38	0.10	0.54	0.16	0.17	143.75	1.69	0.00
1.61	0.00	0.00	0.00	0.00	0.02	0.02	0.13	0.03	0.00	186.18	0.46	0.00
18.04	0.00	0.05	0.08	0.14	0.20	0.10	0.54	0.11	0.07	160.57	1.62	0.00
40.11	0.00	0.11	0.28	0.85	0.65	0.12	0.56	0.18	0.34	120.49	1.34	0.00
3.25	0.00	0.00	0.00	0.00	0.03	0.04	0.24	0.04	0.01	183.62	0.70	0.00
12.37	0.00	0.00	0.05	0.07	0.13	0.10	0.50	0.08	0.04	169.76	1.41	0.00
48.94	0.00	0.13	0.39	1.49	0.91	0.08	0.49	0.19	0.50	101.92	1.16	0.00
52.39	0.00	0.17	0.46	1.96	1.05	0.07	0.46	0.18	0.56	91.78	0.96	0.00
44.43	1.25	0.12	0.69	8.84	2.07	0.02	0.10	0.04	2.99	17.51	0.22	0.38
55.37	0.79	0.16	0.75	6.55	1.91	0.03	0.18	0.08	1.88	33.43	0.35	0.19
47.09	0.00	0.12	0.36	1.38	0.87	0.08	0.50	0.19	0.47	105.38	1.10	0.00
56.12	0.34	0.13	0.75	6.36	1.87	0.03	0.19	0.09	1.81	34.82	0.35	0.00
53.02	0.00	0.20	0.49	1.89	1.06	0.07	0.44	0.19	0.65	91.57	1.04	0.00
59.17	0.11	0.19	0.70	4.09	1.58	0.05	0.29	0.15	1.17	57.03	0.57	0.00
49.75	0.00	0.16	0.41	1.68	1.00	0.09	0.48	0.18	0.54	96.67	1.02	0.00
24.22	2.59	0.11	0.44	10.09	1.49	0.00	0.04	0.03	5.46	7.76	0.10	0.62
16.06	3.64	0.00	0.29	9.16	1.08	0.00	0.03	0.02	6.88	5.22	0.06	0.63
12.29	4.72	0.05	0.22	8.15	0.80	0.00	0.03	0.02	7.72	5.42	0.08	0.55
5.72	8.71	0.00	0.10	4.48	0.42	0.01	0.02	0.01	9.18	1.95	0.04	0.31
15.42	4.23	0.09	0.27	9.55	1.31	0.00	0.03	0.01	8.47	3.73	0.07	0.89
6.58	7.20	0.00	0.15	5.54	0.56	0.00	0.01	0.01	9.54	1.97	0.03	0.51
8.47	6.17	0.05	0.17	6.45	0.64	0.00	0.02	0.01	9.08	2.36	0.03	0.51
3.85	11.09	0.00	0.11	3.36	0.36	0.00	0.00	0.00	9.21	1.04	0.00	0.26
1.29	31.16	0.00	0.00	2.05	0.17	0.00	0.00	0.00	3.72	0.30	0.00	0.07

APPENDIX D (continued)

Species data for experiments conducted at 200 bar with 192 ppm of cyclohexane as the fuel.

P (bar)	T (K)	t (s)	CH4	C2H6	C2H4	C2H2	C3H8	C3H6	aC3H4	1-C4H8	pC3H4
172.68	956	0.002283	0.00	0.00	0.18	0.00	0.00	0.00	0.00	0.00	0.00
185.34	1009	0.002236	0.00	0.00	0.42	0.09	0.00	0.00	0.00	0.00	0.00
190.11	1087	0.002314	0.00	0.00	1.50	0.21	0.00	0.14	0.00	0.00	0.00
196.09	1152	0.002288	0.91	0.00	6.53	1.07	0.00	0.61	0.15	0.09	0.00
242.60	1276	0.002092	13.35	1.50	147.16	39.57	0.10	11.02	3.96	1.34	3.86
182.27	1140	0.002277	0.76	0.00	3.43	0.51	0.00	0.34	0.05	0.00	0.00
192.28	1195	0.002294	1.33	0.10	13.78	2.33	0.00	1.20	0.27	0.22	0.10
190.07	1197	0.002208	1.56	0.12	20.21	3.43	0.00	1.67	0.45	0.29	0.18
179.55	1204	0.002254	1.78	0.14	24.23	4.12	0.00	2.06	0.53	0.42	0.18
194.16	1362	0.002072	25.71	3.87	209.59	78.56	0.14	13.40	6.29	0.84	10.12
196.47	1263	0.002107	8.76	0.94	109.82	26.25	0.04	8.44	3.11	1.53	2.39
200.69	1279	0.002119	8.63	0.83	107.22	24.26	0.05	8.28	3.01	1.51	2.15
187.66	1203	0.002228	1.78	0.18	24.13	4.24	0.00	1.99	0.63	0.42	0.19
180.85	1196	0.002279	1.73	0.09	19.52	3.30	0.00	1.58	0.45	0.32	0.14
194.25	1254	0.002132	6.74	0.66	91.71	20.77	0.00	7.12	2.54	1.40	1.72
210.16	1353	0.002062	23.58	3.25	211.37	72.35	0.10	14.25	6.20	0.92	8.74
193.99	1236	0.002132	4.59	0.41	64.51	13.14	0.05	5.07	1.75	1.08	0.87
211.92	1351	0.002058	29.12	4.14	228.02	91.39	0.09	14.07	6.95	0.70	11.80
188.67	1305	0.002154	13.11	1.61	148.24	39.09	0.06	11.12	4.30	1.63	4.02
190.48	1374	0.002084	24.67	3.72	215.83	77.01	0.19	14.32	6.68	0.99	9.94
201.05	1386	0.002048	33.00	4.63	241.69	102.70	0.11	14.19	7.41	0.49	13.48
190.43	1390	0.002107	36.35	5.02	246.29	111.38	0.11	13.63	7.54	0.44	14.63
176.61	1370	0.002177	29.69	4.71	230.95	91.73	0.09	14.24	7.17	0.80	12.41
189.79	1557	0.001971	78.32	1.13	205.85	262.35	0.00	2.87	4.80	0.10	11.68
206.54	1320	0.002082	21.47	3.10	195.37	66.92	0.09	13.31	5.84	1.18	8.08
207.05	1349	0.002068	27.89	4.01	217.46	86.49	0.08	13.43	6.55	0.92	11.03
222.92	1539	0.001964	74.19	1.06	193.43	249.50	0.00	2.75	4.25	0.44	10.04
195.36	1386	0.002051	36.69	4.67	236.52	112.57	0.12	12.46	7.21	1.27	14.23
205.79	1514	0.001987	66.62	2.54	230.76	192.94	0.00	5.69	6.19	1.46	14.71
191.88	1416	0.002041	41.15	4.71	241.67	124.53	0.00	11.63	7.20	0.85	14.88
203.25	1515	0.001994	65.57	2.32	230.66	194.57	0.00	5.49	6.09	0.75	14.26
198.27	1461	0.00202	52.80	3.53	241.52	158.08	0.00	8.36	6.87	0.22	15.20
217.34	1485	0.001986	67.53	1.70	223.07	211.16	0.00	4.66	5.78	0.32	13.27

APPENDIX D (continued)

Species data for experiments conducted at 200 bar with 192 ppm of cyclohexane as the fuel (continued).

C4H6	C4H2	C4H8	C4H6-12	C4H4	C5H6	C6H10-15	C6H12-1	CH2cC5H8	C6H6	cC6H12	cC6H10	C7H8
0.10	0.00	0.00	0.00	0.00	0.00	0.00	0.00	0.00	0.00	192.62	0.04	0.00
0.29	0.00	0.00	0.00	0.00	0.00	0.00	0.00	0.00	0.00	176.78	0.10	0.00
1.03	0.00	0.00	0.00	0.00	0.01	0.02	0.03	0.02	0.00	186.71	0.30	0.00
4.34	0.00	0.00	0.00	0.00	0.04	0.03	0.18	0.03	0.01	169.47	0.81	0.00
62.83	0.69	0.27	0.62	3.08	1.48	0.06	0.35	0.15	1.19	68.08	0.96	0.00
2.24	0.00	0.00	0.00	0.00	0.00	0.02	0.08	0.04	0.00	180.08	0.59	0.00
8.80	0.00	0.00	0.00	0.00	0.09	0.06	0.33	0.06	0.03	164.43	1.34	0.00
12.83	0.00	0.05	0.04	0.06	0.12	0.08	0.41	0.08	0.04	160.57	1.59	0.00
15.25	0.00	0.05	0.07	0.09	0.17	0.09	0.44	0.10	0.05	159.70	1.82	0.00
59.23	0.93	0.24	0.77	7.28	2.16	0.03	0.14	0.08	2.29	24.56	0.29	0.25
54.01	0.00	0.20	0.42	1.66	0.94	0.08	0.48	0.17	0.60	91.69	1.25	0.00
52.81	0.44	0.27	0.38	1.55	0.81	0.08	0.49	0.04	0.75	97.27	1.31	0.00
15.16	0.00	0.05	0.06	0.08	0.15	0.09	0.44	0.08	0.05	158.99	1.64	0.00
12.46	0.00	0.00	0.00	0.05	0.11	0.07	0.42	0.06	0.04	160.89	1.50	0.00
48.54	0.00	0.17	0.39	1.22	0.70	0.09	0.49	0.15	0.42	102.69	1.37	0.00
69.40	0.94	0.29	0.82	6.69	1.79	0.03	0.17	0.06	1.69	32.96	0.41	0.00
36.71	0.00	0.10	0.21	0.58	0.44	0.10	0.56	0.12	0.26	130.92	1.81	0.00
61.29	1.05	0.18	0.79	8.67	2.04	0.03	0.13	0.00	2.38	21.33	0.24	0.31
66.30	0.62	0.22	0.61	2.91	1.24	0.06	0.39	0.13	0.86	71.19	0.91	0.00
67.79	0.83	0.22	0.84	7.12	2.02	0.02	0.19	0.07	2.03	32.02	0.36	0.17
57.96	1.20	0.20	0.80	9.78	2.12	0.01	0.09	0.01	2.81	15.86	0.17	0.29
52.31	1.44	0.18	0.73	10.26	2.36	0.02	0.07	0.00	3.39	12.88	0.14	0.54
61.39	1.13	0.25	0.85	8.68	2.21	0.02	0.12	0.03	2.63	21.64	0.24	0.34
5.43	7.44	0.00	0.11	7.22	0.62	0.00	0.01	0.00	8.92	0.68	0.01	0.57
64.26	0.77	0.22	0.76	5.94	2.10	0.04	0.21	0.12	2.00	38.36	0.44	0.14
57.06	0.95	0.19	0.75	7.89	2.32	0.03	0.14	0.08	2.58	23.38	0.28	0.34
5.43	6.41	0.03	0.10	6.23	0.68	0.00	0.01	0.00	8.85	0.96	0.02	0.58
45.60	1.39	0.14	0.66	9.83	2.32	0.02	0.07	0.04	3.51	11.81	0.15	0.45
12.17	3.84	0.05	0.20	9.64	1.37	0.01	0.01	0.01	7.53	1.55	0.02	0.87
39.49	1.63	0.03	0.59	10.32	2.28	0.02	0.06	0.03	4.14	9.10	0.12	0.61
11.82	3.85	0.05	0.19	9.56	1.34	0.01	0.01	0.01	7.19	1.75	0.03	0.87
23.67	2.58	0.10	0.39	10.99	1.71	0.01	0.03	0.01	5.30	3.53	0.06	0.65
10.18	4.82	0.06	0.20	8.95	1.00	0.01	0.02	0.00	6.80	1.56	0.02	0.66

APPENDIX D (continued)

Species data for experiments conducted at 40 bar with 484 ppm of cyclohexane as the fuel.

P (bar)	T (K)	t (s)	CH4	C2H6	C2H4	C2H2	C3H8	C3H6	aC3H4	1-C4H8	pC3H4
40.59	1154	0.002405	1.49	0.00	15.74	2.15	0.00	1.52	0.33	0.21	0.09
41.03	1277	0.002153	38.70	7.67	395.71	113.40	0.18	30.02	13.83	3.05	14.94
40.23	1228	0.002213	13.28	1.57	180.87	36.42	0.08	14.82	5.75	2.98	3.16
42.61	1413	0.002041	129.11	13.24	601.22	396.35	0.11	22.07	19.82	0.48	42.23
40.85	1489	0.00204	184.91	4.09	471.53	668.00	0.00	7.03	11.90	0.16	27.29
41.57	1320	0.002087	58.00	12.40	497.90	175.82	0.21	33.89	17.71	2.09	25.72
40.85	1299	0.002139	47.87	10.10	449.79	142.74	0.18	32.56	15.88	2.64	20.26
41.05	1368	0.00203	86.29	16.30	577.58	264.94	0.14	31.97	20.49	1.02	37.80
38.42	1235	0.002241	16.51	2.31	215.41	45.82	0.09	17.57	7.12	3.30	4.44
39.71	1298	0.002115	52.16	11.53	471.30	158.47	0.19	33.15	17.04	2.36	23.20
38.49	1367	0.002109	86.60	16.72	576.45	266.27	0.13	31.71	20.73	1.02	38.34
40.88	1433	0.002007	161.03	8.24	561.13	515.90	0.00	13.48	16.74	0.27	37.26
39.95	1396	0.002108	119.22	14.49	598.14	365.42	0.06	24.13	20.49	0.60	42.72
38.79	1198	0.002256	7.14	0.71	106.58	19.17	0.10	8.81	3.32	1.98	1.46
41.80	1286	0.00214	34.62	6.61	370.24	101.91	0.18	28.35	12.80	3.23	12.97
40.65	1256	0.00219	20.98	3.45	260.04	59.61	0.14	20.85	8.77	3.45	6.45
41.08	1378	0.002078	110.48	15.77	600.85	338.56	0.11	26.61	20.76	0.59	42.39
42.82	1354	0.002033	78.68	15.62	561.37	241.30	0.16	32.80	19.94	1.21	35.31
39.07	1351	0.002142	77.33	15.98	557.67	237.27	0.13	32.99	20.16	1.24	35.13
37.85	1147	0.002415	0.96	0.00	8.60	1.14	0.00	0.80	0.19	0.10	0.00
35.93	1075	0.002799	0.00	0.00	0.77	0.09	0.00	0.10	0.00	0.00	0.00
36.05	1120	0.002636	0.00	0.00	1.45	0.15	0.00	0.17	0.00	0.00	0.00
43.48	1265	0.002183	27.52	4.80	317.19	79.48	0.17	24.88	10.68	3.49	9.32

APPENDIX D (continued)

Species data for experiments conducted at 40 bar with 484 ppm of cyclohexane as the fuel (continued).

C4H6	C4H2	C4H8	C4H6-12	C4H4	C5H6	C6H10-15	C6H12-1	CH2cC5H8	C6H6	cC6H12	cC6H10	C7H8
10.48	0.00	0.00	0.00	0.00	0.10	0.11	0.62	0.08	0.03	466.38	2.07	0.00
155.55	1.40	0.51	1.69	9.96	4.10	0.16	0.87	0.34	2.89	167.85	1.66	0.00
98.55	0.00	0.24	0.61	1.93	1.62	0.27	1.44	0.43	0.77	326.85	3.55	0.00
63.57	7.34	0.18	1.13	27.61	4.24	0.03	0.10	0.05	14.83	18.55	0.21	1.73
15.24	20.73	0.00	0.33	15.17	1.37	0.01	0.00	0.01	23.13	6.19	0.07	1.21
152.14	2.21	0.46	2.04	16.93	5.16	0.11	0.51	0.23	4.87	98.90	0.89	0.28
157.44	1.82	0.59	1.91	13.25	4.74	0.13	0.69	0.33	3.90	130.98	1.21	0.26
117.76	3.63	0.33	1.85	24.49	5.62	0.06	0.26	0.13	8.31	46.10	0.42	0.98
112.59	0.00	0.30	0.80	2.80	2.02	0.25	1.38	0.46	1.04	299.67	3.12	0.00
153.97	1.98	0.48	2.01	15.03	4.93	0.11	0.61	0.26	4.28	115.32	0.98	0.31
116.11	3.80	0.44	1.90	24.68	5.63	0.07	0.26	0.13	8.32	45.89	0.40	1.01
32.89	12.75	0.13	0.66	23.03	2.55	0.00	0.05	0.03	19.80	9.81	0.10	1.72
73.54	6.48	0.18	1.27	27.87	4.52	0.04	0.13	0.06	13.15	24.73	0.25	1.38
62.91	0.00	0.23	0.36	0.71	0.92	0.27	1.47	0.35	0.35	386.02	3.88	0.00
152.45	1.40	0.47	1.58	8.67	3.84	0.19	0.95	0.42	2.52	186.17	1.78	0.00
126.25	1.01	0.42	1.03	4.20	2.44	0.24	1.27	0.31	1.51	261.57	2.70	0.00
84.34	5.39	0.25	1.51	27.82	5.12	0.05	0.14	0.07	11.89	26.03	0.27	1.52
126.73	3.12	0.40	2.06	23.08	5.64	0.06	0.29	0.13	7.36	55.31	0.52	0.66
128.09	3.08	0.35	1.98	22.67	5.63	0.08	0.32	0.14	7.16	57.56	0.51	0.70
5.69	0.00	0.00	0.00	0.00	0.06	0.07	0.46	0.05	0.04	473.69	1.22	0.00
0.50	0.00	0.00	0.00	0.00	0.01	0.00	0.03	0.00	0.00	482.06	0.28	0.00
0.97	0.00	0.00	0.00	0.00	0.01	0.00	0.08	0.01	0.00	481.20	0.32	0.00
142.63	1.22	0.56	1.37	6.22	3.27	0.20	1.10	0.47	1.91	223.79	2.22	0.00

APPENDIX D (continued)

Species data for experiments conducted at 200 bar with 3195 ppm of cyclohexane as the fuel.

P (bar)	T (K)	t (s)	CH4	C2H6	C2H4	C2H2	C3H8	C3H6	aC3H4	1-C4H8	pC3H4
187.88	1237	0.002191	46.45	15.51	770.11	64.12	0.35	68.89	6.69	9.39	2.61
194.91	1197	0.002196	21.92	9.50	407.39	30.04	0.17	37.90	3.27	5.09	1.03
186.21	1121	0.002245	1.72	0.98	23.23	1.35	0.00	2.57	0.18	0.38	0.00
200.29	1138	0.002234	2.16	1.27	29.42	1.68	0.00	3.22	0.20	0.50	0.00
196.00	1359	0.002091	462.76	64.82	3347.09	531.94	3.99	259.18	33.48	20.25	49.93
199.23	1474	0.00203	1000.37	70.72	4017.95	1244.27	3.07	200.08	43.39	5.56	94.29
203.75	1427	0.002035	767.66	76.52	3939.81	901.63	4.18	252.08	42.50	10.52	82.79
212.10	1369	0.002039	486.82	68.66	3394.18	547.57	4.34	263.05	34.67	19.47	54.06
203.19	1315	0.002051	286.48	50.24	2638.96	340.27	2.78	217.83	25.59	23.57	28.74
205.66	1311	0.002122	226.39	44.65	2292.61	265.04	2.17	193.02	21.05	22.97	20.24
200.24	1275	0.00211	199.53	40.52	2132.36	240.39	1.89	179.84	19.40	22.26	17.78
200.28	1419	0.002046	816.92	75.75	3968.70	972.27	3.69	241.25	43.21	8.93	86.80
184.61	1506	0.002052	1204.55	53.57	3806.10	1658.81	1.66	135.45	39.34	2.74	90.86
178.11	1638	0.001922	1549.47	23.25	2212.34	2533.19	0.36	37.96	20.88	0.70	55.54

Species data for experiments conducted at 200 bar with 3195 ppm of cyclohexane as the fuel (continued).

C4H6	C4H2	C4H8	C4H6-12	C4H4	C5H6	C6H10-15	C6H12-1	CH2cC5H8	C6H6	cC6H12	cC6H10	C7H8
430.95	3.50	4.39	1.64	3.76	8.33	0.88	8.23	2.90	5.60	2430.27	42.43	0.25
237.67	1.68	2.08	0.68	1.29	3.75	0.67	6.18	1.46	1.77	2660.72	33.02	0.05
14.64	0.20	0.19	0.06	0.04	0.29	0.07	0.95	0.11	0.07	3068.64	3.76	0.00
18.66	0.00	0.23	0.10	0.00	0.32	0.09	1.13	0.15	0.00	3092.91	4.75	0.00
1081.40	5.14	11.35	9.60	74.38	73.35	0.39	3.85	2.24	101.25	600.69	11.93	15.15
498.98	12.16	4.60	5.81	135.13	72.16	0.08	0.58	0.35	240.06	83.79	1.84	38.72
774.81	11.98	7.60	8.14	117.34	84.26	0.18	1.37	0.91	183.25	207.05	4.14	30.13
1067.30	8.98	11.68	9.58	80.02	73.48	0.33	3.31	0.87	103.94	528.61	10.36	14.80
1079.71	3.23	12.15	8.71	44.49	51.40	0.56	5.92	3.07	52.73	1039.26	20.77	6.41
999.02	4.37	10.64	6.52	31.74	41.59	0.67	6.86	4.25	37.17	1268.53	25.93	4.70
971.66	3.80	10.75	6.50	27.91	37.34	0.77	7.37	3.86	33.88	1405.44	29.08	3.93
704.81	12.03	7.00	7.95	122.47	82.25	0.17	1.17	0.77	195.38	166.84	3.38	32.48
294.66	14.33	2.29	3.60	140.10	53.93	0.00	0.32	0.18	276.53	36.98	0.82	39.28
87.16	19.76	0.63	1.24	137.55	20.82	0.00	0.05	0.02	321.60	5.57	0.12	21.08

APPENDIX D (continued)

Species data for experiments conducted at 40 bar with 187 ppm of methylcyclohexane as the fuel.

P (bar)	T (K)	t (s)	CH4	C2H6	C2H4	C2H2	C3H8	C3H6	aC3H4	1-C4H8	pC3H4	C4H6
35.68	998	0.003106	0.00	0.00	0.00	0.00	0.00	0.00	0.00	0.00	0.00	0.00
41.65	1483	0.001994	112.49	4.67	191.03	303.42	0.00	3.84	6.25	0.09	14.60	6.04
26.11	902	0.003645	0.00	0.00	0.00	0.00	0.00	0.00	0.00	0.00	0.00	0.00
25.36	960	0.003501	0.00	0.00	0.00	0.00	0.00	0.00	0.00	0.00	0.00	0.00
37.97	1222	0.002239	12.94	7.57	48.31	7.76	0.00	15.28	2.83	3.17	2.50	28.11
33.52	1101	0.002582	1.37	0.26	1.99	0.23	0.00	0.81	0.15	0.19	0.00	1.25
36.21	1119	0.002598	1.39	0.19	1.98	0.21	0.00	0.77	0.10	0.16	0.09	1.22
25.89	888	0.003711	0.00	0.00	0.00	0.00	0.00	0.00	0.00	0.00	0.00	0.00
35.57	1133	0.002466	2.67	0.71	5.45	0.63	0.00	2.07	0.31	0.50	0.28	3.44
36.69	1178	0.002277	7.09	3.05	21.61	2.88	0.00	7.51	1.25	1.74	1.01	13.46
37.76	1182	0.00226	9.10	4.45	30.23	4.34	0.00	10.14	1.76	2.29	1.45	18.47
35.90	1146	0.002287	3.87	1.18	8.96	1.08	0.00	3.28	0.51	0.83	0.44	5.72
35.19	1168	0.002411	4.56	1.46	11.38	1.42	0.00	4.18	0.65	1.00	0.51	7.30
37.82	1247	0.002219	24.20	17.87	104.57	22.65	0.10	27.63	6.52	3.80	6.74	51.35
40.13	1253	0.00221	24.80	17.60	105.76	22.83	0.13	28.18	6.56	3.90	6.74	52.14
38.58	1223	0.00222	18.87	12.51	76.73	14.34	0.07	22.30	4.69	3.87	4.39	41.10
35.29	1197	0.00226	10.79	5.89	38.18	5.84	0.00	12.43	2.29	2.66	1.86	22.74
34.74	1206	0.002252	14.17	8.92	54.84	9.18	0.07	16.97	3.29	3.35	2.89	31.51
27.02	1125	0.002524	2.80	0.82	5.97	0.71	0.00	2.34	0.36	0.48	0.29	3.87
37.06	1323	0.002113	46.44	32.40	201.35	73.63	0.13	32.96	11.53	1.29	18.94	61.49
38.82	1333	0.002137	51.09	32.11	211.62	84.36	0.10	31.16	11.72	1.04	20.79	57.56
37.54	1245	0.002223	21.50	15.40	91.74	18.77	0.09	25.34	5.68	3.81	5.52	47.06
37.23	1273	0.002209	32.50	25.17	145.56	38.82	0.14	32.93	9.07	3.07	11.07	61.43
35.81	1250	0.002225	26.07	20.36	116.36	26.84	0.11	29.42	7.38	3.60	7.88	54.87
38.29	1339	0.002143	53.32	31.88	216.17	90.55	0.10	29.99	11.86	0.94	21.66	55.24
39.93	1354	0.002105	57.71	30.94	223.65	100.21	0.00	28.34	11.96	0.70	22.45	51.12
37.59	1308	0.002165	43.77	31.38	191.11	66.51	0.14	33.23	11.01	1.46	17.39	61.78
37.18	1285	0.002173	37.45	28.69	167.39	49.84	0.00	34.01	10.20	2.32	13.91	63.54
34.66	1295	0.002193	47.42	32.52	203.71	76.28	0.00	32.03	11.45	1.13	19.36	59.57
36.34	1344	0.002139	57.03	31.35	223.74	101.33	0.08	27.67	11.94	0.71	22.85	50.66
35.67	1420	0.002092	87.17	18.08	239.91	184.23	0.00	13.43	10.77	0.26	23.89	22.88
35.80	1386	0.002128	69.64	26.24	235.91	135.19	0.00	20.87	11.64	0.40	24.19	37.03
36.94	1352	0.002142	64.93	28.31	232.49	121.50	0.04	23.39	11.78	0.52	23.96	42.00
35.82	1340	0.002134	60.25	30.25	228.11	110.85	0.06	25.68	11.88	0.63	23.53	46.73
36.69	1411	0.002098	78.75	22.10	240.13	159.26	0.00	16.90	11.36	0.33	24.73	29.27
35.65	1379	0.002134	64.59	28.73	233.77	122.71	0.09	23.58	11.88	0.49	24.26	42.53
36.44	1436	0.00208	95.11	13.99	235.89	209.78	0.00	10.40	10.02	0.19	22.48	17.24
38.05	1493	0.002028	110.91	4.75	189.37	301.09	0.00	3.88	6.22	0.10	14.36	6.05
38.44	1478	0.002357	109.07	7.37	215.01	267.73	0.00	5.85	7.73	0.13	17.99	9.17
37.37	1438	0.002052	97.00	12.66	232.15	217.40	0.00	9.57	9.66	0.19	21.81	15.67
38.44	1550	0.002004	110.11	2.60	144.90	370.51	0.00	2.15	4.39	0.05	10.49	3.39
39.39	1549	0.001997	109.71	2.55	141.39	371.75	0.00	2.02	4.21	0.00	10.15	3.20
37.43	1487	0.002032	110.44	5.67	196.97	296.49	0.00	4.49	6.64	0.10	15.48	7.10
39.88	1554	0.001994	110.26	2.62	145.94	363.76	0.00	2.14	4.40	0.00	10.60	3.41
37.72	1574	0.00198	100.11	1.64	97.97	425.05	0.00	1.24	3.21	0.00	7.77	2.07
36.62	1577	0.001976	101.47	1.76	104.53	416.47	0.00	1.34	3.29	0.04	8.10	2.17

APPENDIX D (continued)

Species data for experiments conducted at 40 bar with 187 ppm of methylcyclohexane as the fuel (continued).

C4H2	C4H8	C4H6-12	C4H4	C5H6	C6H10-15	C6H12-1	CH2cC5H8	C6H6	cC6H12	cC6H8	cC6H10	CH3cC6H11	C7H8
0.00	0.00	0.00	0.00	0.00	0.00	0.00	0.00	0.00	0.01	0.00	0.01	187.96	0.00
12.25	0.07	0.23	7.50	0.55	0.00	0.00	0.01	11.85	0.02	0.00	0.00	1.64	0.56
0.00	0.00	0.00	0.00	0.00	0.00	0.00	0.00	0.00	0.00	0.00	0.00	187.09	0.00
0.00	0.00	0.00	0.00	0.00	0.00	0.00	0.00	0.00	0.02	0.00	0.00	187.10	0.00
0.70	0.14	0.32	0.54	1.33	0.04	0.00	0.20	0.46	0.02	0.29	1.43	133.20	0.00
0.00	0.00	0.00	0.00	0.00	0.00	0.00	0.00	0.01	0.02	0.00	0.40	185.34	0.00
0.00	0.00	0.00	0.00	0.03	0.00	0.00	0.00	0.01	0.02	0.01	0.44	185.04	0.00
0.00	0.00	0.00	0.00	0.00	0.00	0.00	0.00	0.00	0.00	0.00	0.00	187.54	0.00
0.06	0.00	0.00	0.00	0.15	0.00	0.00	0.04	0.02	0.02	0.03	0.79	180.30	0.00
0.42	0.09	0.10	0.12	0.56	0.02	0.00	0.12	0.12	0.02	0.16	1.43	160.65	0.00
0.47	0.11	0.18	0.22	0.83	0.03	0.00	0.15	0.21	0.02	0.21	1.50	151.77	0.00
0.12	0.00	0.00	0.00	0.24	0.02	0.00	0.06	0.04	0.02	0.06	1.06	176.29	0.00
0.20	0.05	0.07	0.00	0.31	0.02	0.00	0.07	0.06	0.02	0.08	1.17	172.51	0.00
1.25	0.31	0.90	2.32	2.69	0.05	0.00	0.21	1.29	0.01	0.30	0.88	84.47	0.00
1.21	0.33	0.85	2.36	2.61	0.05	0.00	0.22	1.34	0.01	0.32	0.90	83.97	0.00
0.99	0.22	0.58	1.25	2.04	0.06	0.00	0.23	0.87	0.02	0.34	1.19	108.12	0.00
0.55	0.11	0.25	0.33	1.03	0.04	0.00	0.18	0.34	0.02	0.26	1.48	144.45	0.00
0.73	0.19	0.39	0.64	1.48	0.04	0.00	0.21	0.52	0.02	0.30	1.38	127.82	0.00
0.10	0.00	0.00	0.00	0.15	0.00	0.00	0.05	0.02	0.02	0.03	0.82	179.43	0.00
1.80	0.31	1.35	9.34	4.38	0.03	0.00	0.11	3.56	0.00	0.11	0.20	21.81	0.00
1.98	0.26	1.30	10.64	4.31	0.03	0.00	0.08	4.01	0.00	0.09	0.16	17.41	0.14
1.06	0.25	0.80	1.85	2.38	0.05	0.00	0.23	1.08	0.02	0.33	1.03	95.12	0.00
1.50	0.35	1.17	4.60	3.57	0.05	0.00	0.24	2.03	0.00	0.24	0.55	55.36	0.00
1.34	0.33	0.95	2.92	2.92	0.05	0.00	0.21	1.45	0.01	0.28	0.80	76.27	0.00
2.15	0.23	1.29	11.40	4.17	0.03	0.00	0.07	4.30	0.00	0.09	0.15	16.04	0.16
2.23	0.22	1.21	12.21	4.13	0.07	0.00	0.05	4.86	0.00	0.09	0.11	12.00	0.15
1.55	0.27	1.32	8.37	4.29	0.03	0.00	0.11	3.30	0.00	0.14	0.25	27.02	0.08
1.67	0.36	1.35	6.15	3.92	0.04	0.00	0.18	2.50	0.00	0.17	0.39	40.29	0.00
1.84	0.24	1.30	9.70	4.30	0.03	0.00	0.08	3.61	0.00	0.10	0.18	21.00	0.00
2.36	0.22	1.21	12.35	4.03	0.02	0.01	0.05	4.82	0.00	0.09	0.11	12.63	0.19
5.13	0.10	0.70	14.07	2.05	0.00	0.00	0.02	8.66	0.00	0.11	0.04	4.24	0.70
3.20	0.14	0.97	14.05	3.26	0.00	0.01	0.02	6.49	0.00	0.12	0.07	7.30	0.28
2.70	0.17	1.09	13.66	3.56	0.00	0.00	0.03	5.82	0.00	0.08	0.09	9.27	0.33
2.50	0.18	1.15	13.05	3.79	0.00	0.00	0.05	5.29	0.00	0.11	0.11	10.87	0.25
4.00	0.11	0.87	14.47	2.61	0.00	0.00	0.02	7.61	0.00	0.09	0.06	5.59	0.46
2.71	0.15	1.08	13.75	3.60	0.00	0.00	0.04	5.80	0.00	0.08	0.08	8.63	0.34
6.35	0.10	0.57	13.13	1.55	0.00	0.00	0.01	9.72	0.00	0.00	0.04	3.36	0.74
12.02	0.07	0.25	7.29	0.56	0.00	0.00	0.00	11.42	0.00	0.00	0.03	1.74	0.41
9.64	0.07	0.34	9.78	0.83	0.00	0.00	0.00	11.52	0.00	0.00	0.02	1.94	0.67
6.80	0.08	0.52	12.60	1.40	0.02	0.00	0.01	10.07	0.00	0.00	0.03	2.93	1.09
18.35	0.05	0.15	4.68	0.36	0.00	0.00	0.01	10.68	0.00	0.00	0.04	1.12	0.37
18.52	0.00	0.11	4.47	0.35	0.00	0.00	0.00	10.59	0.00	0.00	0.02	1.07	0.30
11.71	0.09	0.28	8.06	0.64	0.00	0.00	0.01	11.34	0.00	0.00	0.01	1.78	0.45
17.73	0.00	0.13	4.70	0.35	0.00	0.00	0.00	10.79	0.00	0.00	0.02	1.11	0.48
26.28	0.00	0.12	3.17	0.25	0.00	0.00	0.00	8.33	0.00	0.00	0.00	0.79	0.17
24.54	0.00	0.09	3.23	0.26	0.00	0.00	0.01	8.63	0.00	0.00	0.02	0.87	0.00

APPENDIX D (continued)

Species data for experiments conducted at 100 bar with 188 ppm of methylcyclohexane as the fuel.

P (bar)	T (K)	t (s)	CH4	C2H6	C2H4	C2H2	C3H8	C3H6	aC3H4	1-C4H8	pC3H4	C4H6
99.45	1012	0.002351	0.55	0.00	0.30	0.00	0.00	0.15	0.00	0.00	0.00	0.15
99.03	1059	0.002413	0.96	0.00	0.90	0.12	0.00	0.42	0.06	0.00	0.00	0.51
83.89	1067	0.002516	0.91	0.00	0.93	0.15	0.00	0.44	0.07	0.00	0.00	0.52
98.93	1200	0.002231	21.31	8.26	70.53	12.86	0.08	21.81	3.82	4.22	3.83	37.77
108.86	1248	0.0022	38.55	17.28	136.90	34.77	0.18	33.85	7.76	3.73	9.39	57.97
114.38	1260	0.00216	43.03	19.53	152.64	43.66	0.17	34.59	8.82	2.94	11.68	59.35
99.84	1130	0.002391	4.67	0.88	10.26	1.37	0.00	3.95	0.52	0.90	0.49	6.37
81.23	1080	0.002491	1.46	0.17	1.97	0.23	0.00	0.80	0.10	0.15	0.10	1.23
103.94	1234	0.002205	29.17	12.62	102.52	21.71	0.13	28.78	5.76	4.56	6.16	50.02
101.69	1266	0.002189	49.00	22.49	175.07	57.00	0.18	34.54	9.68	2.02	14.72	59.67
99.62	1323	0.002195	65.41	22.60	210.84	94.86	0.10	28.26	10.59	0.91	20.65	47.51
108.57	1221	0.002203	27.18	11.11	92.69	19.00	0.12	27.00	5.13	4.64	5.48	46.88
115.75	1213	0.002201	24.01	9.43	80.82	15.67	0.09	24.15	4.44	4.45	4.56	41.90
98.55	1101	0.002385	4.52	0.66	8.44	1.00	0.00	3.43	0.45	0.73	0.44	5.16
117.76	1240	0.002172	30.55	10.98	97.55	18.38	0.13	28.66	5.21	10.68	7.22	47.45
106.28	1390	0.002106	95.58	12.64	229.97	166.55	0.00	15.17	9.68	0.52	21.35	22.87
90.66	1204	0.002281	28.79	14.10	105.89	23.65	0.14	28.67	6.13	4.21	6.70	49.96
106.26	1367	0.002105	79.60	18.73	225.71	125.98	0.00	22.45	10.45	0.69	21.85	36.05
112.75	1383	0.002099	94.43	13.15	231.63	167.08	0.00	15.77	9.74	0.42	21.45	23.95
99.94	1305	0.002219	55.04	23.68	190.79	70.78	0.17	32.92	10.32	1.53	17.46	56.41
94.74	1263	0.002289	42.48	20.67	155.18	44.84	0.14	34.57	9.03	3.04	12.12	60.34
99.93	1203	0.002357	20.63	8.21	69.00	12.61	0.11	21.36	3.92	4.15	3.78	36.87
98.19	1160	0.002371	7.92	1.81	19.58	2.63	0.00	7.18	1.01	1.72	0.99	11.96
96.09	1312	0.002145	65.25	22.74	209.98	95.90	0.09	27.57	10.69	0.88	20.62	46.43
93.30	1402	0.002139	99.14	10.29	224.73	188.85	0.00	11.83	9.04	0.32	20.26	17.86
94.99	1504	0.002105	115.24	2.48	154.93	324.50	0.00	2.98	4.20	0.08	9.97	4.31
85.04	1409	0.002225	96.64	11.64	227.65	182.68	0.00	12.64	9.19	0.32	20.60	19.14
88.03	1490	0.002021	111.52	5.39	208.91	247.86	0.00	6.17	6.95	0.17	16.47	8.85
102.27	1510	0.002019	114.52	2.48	149.94	327.30	0.00	2.98	4.09	0.08	9.70	4.29
89.02	1492	0.002161	114.06	3.41	175.32	292.14	0.00	3.97	4.95	0.11	11.64	5.85
95.12	1531	0.002113	99.36	1.81	82.09	401.81	0.00	1.87	2.81	0.00	6.75	2.94
87.38	1602	0.002033	82.50	1.02	47.13	439.11	0.00	1.04	2.06	0.00	4.94	1.64
83.67	1590	0.002077	89.60	1.09	57.76	428.37	0.00	1.12	2.23	0.10	5.40	1.73
85.03	1493	0.002202	105.22	2.12	106.70	379.37	0.00	2.24	3.23	0.08	7.65	3.53

APPENDIX D (continued)

Species data for experiments conducted at 100 bar with 188 ppm of methylcyclohexane as the fuel (continued).

C4H2	C4H8	C4H6-12	C4H4	C5H6	C6H10-15	C6H12-1	CH2cC5H8	C6H6	cC6H12	cC6H8	cC6H10	CH3cC6H11	C7H8
0.00	0.00	0.00	0.00	0.00	0.00	0.00	0.00	0.00	0.07	0.00	0.08	188.14	0.00
0.00	0.00	0.00	0.00	0.00	0.00	0.00	0.00	0.00	0.07	0.00	0.22	186.55	0.00
0.00	0.00	0.00	0.00	0.00	0.00	0.00	0.00	0.00	0.07	0.00	0.21	185.55	0.00
0.00	0.22	0.52	1.08	1.96	0.06	0.00	0.18	0.97	0.05	0.38	1.33	109.00	0.03
1.42	0.35	1.04	4.01	3.47	0.07	0.00	0.05	2.46	0.03	0.29	0.64	55.38	0.16
1.45	0.38	1.14	5.39	3.93	0.07	0.00	0.12	2.99	0.03	0.21	0.49	44.77	0.19
0.15	0.00	0.00	0.00	0.29	0.04	0.00	0.06	0.06	0.07	0.07	1.24	172.30	0.00
0.04	0.00	0.00	0.00	0.04	0.00	0.00	0.00	0.00	0.07	0.00	0.42	183.61	0.00
1.10	0.28	0.79	2.18	2.80	0.07	0.00	0.18	1.58	0.04	0.35	0.96	80.67	0.06
1.63	0.33	1.19	7.21	4.29	0.05	0.00	0.13	3.62	0.02	0.16	0.34	30.93	0.30
2.12	0.22	1.01	11.51	4.27	0.00	0.00	0.05	5.89	0.00	0.11	0.17	13.69	0.61
1.17	0.30	0.74	1.81	2.48	0.09	0.00	0.18	1.52	0.06	0.38	1.13	90.30	0.00
1.04	0.26	0.59	1.44	2.29	0.08	0.00	0.18	1.25	0.05	0.37	1.21	101.38	0.00
0.19	0.00	0.00	0.00	0.25	0.02	0.00	0.07	0.08	0.07	0.08	1.24	173.97	0.00
1.20	0.30	0.90	1.63	2.51	0.06	0.00	0.18	1.61	0.04	0.38	1.14	84.89	0.07
3.99	0.11	0.58	12.83	2.64	0.00	0.00	0.02	9.86	0.00	0.08	0.08	4.28	1.07
1.23	0.30	0.84	2.44	2.79	0.09	0.00	0.26	1.60	0.04	0.36	0.91	78.98	0.07
2.76	0.19	0.81	13.02	3.68	0.00	0.00	0.04	7.84	0.00	0.10	0.12	7.92	0.86
4.11	0.11	0.56	13.17	2.85	0.00	0.00	0.02	10.02	0.00	0.10	0.08	4.05	1.12
1.73	0.29	1.15	8.97	4.49	0.06	0.00	0.09	4.30	0.00	0.16	0.29	23.24	0.41
1.52	0.35	1.16	5.54	4.09	0.06	0.00	0.18	2.90	0.03	0.28	0.48	44.01	0.19
0.89	0.20	0.50	1.04	1.89	0.06	0.00	0.23	0.86	0.05	0.40	1.37	111.17	0.00
0.34	0.09	0.09	0.08	0.48	0.00	0.00	0.09	0.15	0.08	0.15	1.59	161.43	0.00
2.03	0.23	0.95	11.49	4.14	0.00	0.00	0.06	5.75	0.00	0.09	0.17	14.33	0.58
5.03	0.10	0.42	12.15	2.04	0.00	0.00	0.03	10.92	0.00	0.13	0.05	3.78	1.05
12.25	0.00	0.11	4.96	0.55	0.00	0.00	0.00	13.50	0.00	0.00	0.00	0.77	0.53
4.66	0.08	0.45	12.33	2.23	0.00	0.00	0.00	10.38	0.00	0.07	0.05	3.80	1.02
7.70	0.06	0.24	9.29	1.09	0.00	0.00	0.00	12.84	0.00	0.00	0.04	1.32	0.98
12.52	0.08	0.13	4.64	0.52	0.00	0.00	0.00	13.17	0.00	0.00	0.00	0.74	0.53
10.14	0.08	0.14	6.06	0.69	0.00	0.00	0.00	13.22	0.00	0.00	0.00	1.14	0.62
21.47	0.00	0.09	3.20	0.41	0.00	0.00	0.00	10.03	0.00	0.00	0.00	0.57	0.20
30.31	0.00	0.00	2.81	0.28	0.00	0.00	0.00	6.71	0.00	0.00	0.00	0.31	0.11
18.94	0.00	0.07	2.88	0.32	0.00	0.00	0.00	8.04	0.00	0.00	0.00	0.37	0.17
18.14	0.00	0.11	3.52	0.45	0.00	0.00	0.00	11.28	0.00	0.00	0.00	0.80	0.27

APPENDIX D (continued)

Species data for experiments conducted at 200 bar with 181 ppm of methylcyclohexane as the fuel.

P (bar)	T (K)	t (s)	CH4	C2H6	C2H4	C2H2	C3H8	C3H6	aC3H4	1-C4H8	pC3H4	C4H6
153.40	879	0.002336	0.00	0.00	0.00	0.00	0.00	0.00	0.00	0.00	0.00	0.00
172.27	984	0.002276	0.00	0.00	0.00	0.00	0.00	0.00	0.00	0.00	0.00	0.00
161.64	1013	0.002335	0.00	0.00	0.21	0.00	0.00	0.08	0.00	0.00	0.00	0.10
158.99	1024	0.00237	0.00	0.00	0.37	0.00	0.00	0.18	0.00	0.00	0.00	0.24
175.54	1162	0.002337	4.03	0.45	7.71	0.99	0.00	3.12	0.37	0.66	0.44	4.90
174.17	1135	0.002305	3.42	0.32	6.04	0.71	0.00	2.49	0.32	0.54	0.35	3.88
168.42	1192	0.002254	8.29	1.37	19.48	2.58	0.00	7.50	0.99	1.68	1.03	12.31
173.83	1246	0.002138	30.04	9.23	94.30	17.67	0.11	28.22	5.04	5.08	5.58	48.85
181.02	1288	0.002161	37.90	11.78	117.36	26.33	0.13	33.04	6.30	5.31	7.40	55.87
168.84	1203	0.0023	10.65	1.88	25.72	3.61	0.00	9.71	1.29	2.25	1.35	15.77
175.53	1206	0.002248	10.96	1.89	26.77	3.74	0.00	10.02	1.39	2.28	1.38	16.47
185.13	1309	0.002082	46.64	15.42	147.48	38.06	0.21	37.48	8.00	4.66	10.31	63.11
187.17	1266	0.002117	40.19	12.97	126.41	30.03	0.18	34.60	6.99	5.14	8.35	58.48
181.33	1246	0.002188	28.06	7.89	84.16	16.18	0.14	26.22	4.40	5.07	4.79	44.41
168.21	1179	0.002241	9.23	1.63	22.32	3.12	0.00	8.34	1.13	1.90	1.12	13.66
180.65	1274	0.002119	39.51	13.21	125.68	29.76	0.17	34.32	6.93	5.01	8.26	58.06
190.09	1371	0.002055	71.52	20.62	214.38	86.99	0.14	34.65	10.72	1.35	19.34	55.75
166.39	1256	0.002226	27.02	7.72	81.21	15.25	0.10	25.54	4.26	5.02	4.61	43.62
166.94	1245	0.002193	28.28	8.51	86.56	16.95	0.11	26.60	4.61	5.09	5.03	45.48
183.10	1372	0.002068	68.47	20.86	208.90	80.86	0.15	35.51	10.60	1.51	18.49	57.58
182.42	1413	0.002048	85.93	17.80	233.66	124.83	0.09	25.76	10.58	0.57	22.02	39.50
175.49	1401	0.002063	78.06	19.94	226.34	107.22	0.10	29.57	10.80	0.82	21.37	46.99
164.22	1459	0.002086	102.18	11.25	236.30	177.10	0.00	15.27	9.58	0.28	21.73	22.05
197.77	1587	0.001949	125.19	1.41	163.80	309.67	0.00	2.62	4.27	0.00	10.14	3.20
182.50	1505	0.002003	112.58	7.02	226.57	204.16	0.00	10.44	8.23	0.19	18.90	13.99
183.09	1450	0.002039	98.44	12.66	234.45	157.40	0.00	17.98	9.82	0.36	21.38	25.97
219.36	1759	0.00183	77.04	0.24	22.73	415.39	0.00	0.26	1.29	0.00	3.30	0.36
200.71	1633	0.001911	123.37	0.73	128.51	345.98	0.00	1.50	3.29	0.00	7.93	1.84
225.01	1664	0.001879	110.18	0.47	71.99	390.84	0.00	0.78	2.33	0.00	5.88	1.04
204.54	1579	0.00194	125.29	1.83	180.34	287.11	0.00	3.41	4.87	0.06	11.62	4.13
190.41	1462	0.002021	98.61	12.74	236.27	156.70	0.00	18.31	9.74	0.34	21.51	26.18
200.54	1549	0.001965	121.21	3.59	210.50	244.09	0.00	6.11	6.55	0.13	15.73	7.52
223.78	1500	0.001976	116.88	5.34	220.74	214.60	0.00	9.11	7.66	0.11	17.48	11.64
181.53	1304	0.002106	49.91	17.05	159.07	45.27	0.19	37.50	8.87	3.75	12.07	63.14
185.72	1348	0.002073	61.93	19.83	192.09	67.42	0.17	36.40	10.14	2.09	16.37	59.98
179.15	1254	0.002133	30.23	8.97	92.68	18.50	0.11	27.96	4.92	5.18	5.52	48.00
176.83	1239	0.002243	18.52	4.32	51.35	8.39	0.06	17.53	2.72	3.88	2.72	29.86
187.48	1310	0.002095	51.18	17.08	161.66	46.24	0.19	38.15	9.02	3.74	12.22	64.30

APPENDIX D (continued)

Species data for experiments conducted at 200 bar with 181 ppm of methylcyclohexane as the fuel (continued).

C4H2	C4H8	C4H6-12	C4H4	C5H6	C6H10-15	C6H12-1	CH2cC5H8	C6H6	cC6H12	cC6H8	cC6H10	CH3cC6H11	C7H8
0.00	0.00	0.00	0.00	0.00	0.00	0.00	0.00	0.00	0.04	0.00	0.00	181.10	0.00
0.00	0.00	0.00	0.00	0.00	0.00	0.00	0.00	0.00	0.05	0.00	0.02	180.88	0.00
0.00	0.00	0.00	0.00	0.00	0.00	0.00	0.00	0.00	0.05	0.00	0.05	176.81	0.00
0.00	0.00	0.00	0.00	0.00	0.00	0.00	0.00	0.00	0.03	0.00	0.09	174.66	0.00
0.19	0.03	0.05	0.00	0.21	0.04	0.00	0.00	0.00	0.03	0.06	1.11	169.63	0.00
0.16	0.00	0.00	0.00	0.17	0.02	0.00	0.10	0.00	0.04	0.04	0.93	169.68	0.00
0.40	0.10	0.11	0.10	0.53	0.04	0.00	0.07	0.14	0.04	0.15	1.61	151.65	0.00
1.10	0.33	0.76	1.92	2.27	0.08	0.00	0.11	1.43	0.03	0.37	1.13	82.31	0.11
1.31	0.35	0.93	2.97	3.17	0.08	0.00	0.25	2.08	0.01	0.42	0.95	69.20	0.13
0.45	0.10	0.14	0.17	0.65	0.05	0.00	0.12	0.19	0.03	0.21	1.75	147.08	0.01
0.45	0.09	0.15	0.19	0.70	0.05	0.00	0.11	0.20	0.03	0.21	1.68	141.41	0.00
1.59	0.42	1.14	4.70	3.82	0.09	0.00	0.22	2.91	0.02	0.35	0.65	47.68	0.15
1.42	0.41	1.02	3.50	3.29	0.08	0.00	0.26	2.10	0.02	0.37	0.85	61.22	0.08
1.09	0.27	0.65	1.53	2.21	0.07	0.00	0.18	1.11	0.02	0.40	1.31	91.60	0.01
0.38	0.07	0.11	0.15	0.60	0.04	0.00	0.10	0.18	0.02	0.18	1.70	154.42	0.01
1.54	0.40	0.99	3.46	3.29	0.08	0.00	0.20	2.12	0.02	0.37	0.82	62.40	0.08
2.01	0.34	1.08	11.07	4.56	0.03	0.00	0.06	5.54	0.00	0.13	0.14	11.18	0.66
1.02	0.24	0.61	1.43	2.02	0.07	0.00	0.19	1.05	0.02	0.44	1.36	95.67	0.00
1.06	0.26	0.65	1.65	2.37	0.09	0.00	0.29	1.21	0.02	0.44	1.27	93.37	0.00
2.00	0.35	1.15	10.36	4.58	0.04	0.00	0.06	5.15	0.00	0.13	0.16	12.96	0.47
2.67	0.22	0.82	13.55	4.30	0.00	0.00	0.03	7.95	0.00	0.11	0.06	4.35	1.07
2.32	0.24	0.96	12.74	4.60	0.03	0.00	0.03	6.95	0.00	0.14	0.08	6.36	0.88
4.31	0.10	0.47	13.77	3.00	0.00	0.00	0.00	10.76	0.00	0.06	0.03	1.84	1.36
10.29	0.00	0.08	5.91	0.63	0.00	0.00	0.00	13.98	0.00	0.00	0.00	0.46	0.77
5.20	0.08	0.33	11.85	2.05	0.00	0.00	0.00	12.16	0.00	0.11	0.03	6.19	1.33
3.54	0.11	0.57	13.63	3.35	0.00	0.00	0.02	10.17	0.00	0.10	0.04	2.97	1.46
26.18	0.00	0.00	4.19	0.00	0.00	0.00	0.00	0.00	0.00	0.00	0.00	0.00	0.00
12.52	0.00	0.06	4.70	0.47	0.00	0.00	0.00	13.94	0.00	0.00	0.00	0.24	0.46
17.09	0.00	0.00	3.95	0.35	0.00	0.00	0.00	11.68	0.00	0.00	0.00	0.19	0.26
9.00	0.00	0.11	6.94	0.82	0.00	0.00	0.00	13.83	0.00	0.00	0.00	0.66	0.78
3.48	0.13	0.59	13.77	3.32	0.00	0.00	0.02	9.45	0.00	0.08	0.04	2.71	1.19
6.91	0.06	0.17	9.77	1.28	0.00	0.00	0.00	12.09	0.00	0.04	0.00	0.57	1.08
5.68	0.08	0.27	11.31	1.95	0.00	0.00	0.01	13.23	0.00	0.09	0.02	1.09	1.38
1.67	0.42	1.21	5.85	4.15	0.07	0.00	0.19	3.25	0.02	0.29	0.49	39.48	0.31
1.88	0.36	1.16	8.96	4.76	0.05	0.00	0.10	4.97	0.05	0.18	0.24	19.15	0.58
1.11	0.29	0.72	1.94	2.53	0.09	0.00	0.28	1.45	0.01	0.47	1.25	90.02	0.06
0.74	0.15	0.33	0.61	1.50	0.07	0.00	0.20	0.58	0.02	0.41	1.77	127.59	0.02
1.67	0.44	1.24	6.03	4.23	0.07	0.00	0.17	3.42	0.02	0.30	0.49	38.90	0.27

APPENDIX D (continued)

Species data for experiments conducted at 40 bar with 507 ppm of methylcyclohexane as the fuel.

P (bar)	T (K)	t (s)	CH4	C2H6	C2H4	C2H2	C3H8	C3H6	aC3H4	1-C4H8	pC3H4	C4H6
36.31	1381	0.002119	229.60	46.99	628.27	407.45	0.17	51.02	27.47	1.15	56.75	81.67
40.33	1313	0.002133	144.61	61.38	497.53	166.96	0.53	94.04	26.85	6.15	40.40	164.71
41.11	1624	0.001911	209.36	1.77	122.05	1223.77	0.00	1.84	5.08	0.08	12.24	2.76
38.78	1481	0.002018	301.85	12.03	523.00	765.86	0.00	14.00	16.17	0.31	37.05	19.44
39.36	1370	0.002078	229.62	47.88	632.09	396.13	0.00	53.64	27.42	1.23	57.17	85.16
39.75	1375	0.002074	206.80	56.76	620.45	331.65	0.21	65.75	28.73	1.71	56.98	108.43
41.16	1478	0.002012	298.51	14.51	557.99	699.45	0.15	17.32	18.13	0.34	41.03	24.08
43.55	1508	0.001959	307.20	7.55	453.67	862.08	0.00	9.41	12.98	0.23	29.76	12.77
40.74	1413	0.00207	280.70	23.77	605.46	586.84	0.11	27.28	22.04	0.55	48.89	39.52
41.89	1374	0.002032	226.73	48.86	630.11	383.46	0.20	56.06	27.99	1.38	57.42	89.55
41.99	1339	0.002035	200.45	58.15	610.63	307.65	0.24	71.22	28.75	2.08	55.86	117.75
40.48	1307	0.002081	156.55	63.29	529.88	195.51	0.41	90.80	27.86	4.81	45.13	157.72
38.97	1315	0.002139	154.30	63.64	526.97	191.98	0.41	91.22	27.93	4.90	44.37	159.05
39.38	1329	0.002107	175.09	63.54	571.89	243.55	0.36	82.71	28.74	3.30	50.96	141.93
37.99	1242	0.00217	93.24	40.91	321.59	74.83	0.44	83.33	17.90	11.63	20.53	148.71
41.97	1280	0.002145	118.06	50.98	406.42	111.05	0.47	93.33	22.41	9.75	29.01	164.81
36.39	1173	0.002282	23.26	5.72	60.07	7.94	0.12	21.48	3.05	4.82	2.80	37.02
38.83	1295	0.002163	147.03	62.74	507.65	175.18	0.49	93.45	27.19	5.76	41.79	163.72
37.94	1157	0.002446	14.55	2.61	32.77	3.92	0.04	12.41	1.65	2.73	1.54	20.82
39.24	1182	0.002259	37.90	11.11	108.56	16.20	0.17	36.44	5.58	7.86	5.29	63.98
41.19	1225	0.002225	70.86	27.14	230.60	45.12	0.32	67.17	12.49	11.82	13.28	119.35
38.88	1184	0.00227	33.56	9.41	94.26	13.69	0.14	32.15	4.82	7.00	4.53	56.27
41.44	1558	0.001953	281.39	3.84	275.45	1085.33	0.00	4.31	8.19	0.13	19.73	6.11
38.22	1383	0.002119	232.26	46.20	631.42	410.57	0.22	51.03	27.14	1.16	56.96	81.39
38.34	1385	0.002089	238.38	42.99	629.83	430.21	0.16	47.04	26.91	1.04	56.46	74.11
41.41	1223	0.002267	65.36	24.07	209.49	38.99	0.29	62.64	11.31	11.62	11.57	111.40
38.28	1157	0.002283	22.46	5.43	57.70	7.61	0.07	20.85	2.97	4.64	2.71	35.90
39.61	1109	0.002518	4.63	0.41	7.37	0.75	0.00	3.12	0.40	0.57	0.37	4.83
38.49	1123	0.002499	7.54	0.97	14.24	1.55	0.00	5.79	0.74	1.22	0.68	9.28
40.10	1097	0.002526	3.97	0.29	5.96	0.59	0.00	2.51	0.32	0.43	0.28	3.93
38.05	1435	0.002086	273.52	27.06	615.59	565.28	0.17	29.70	23.04	0.57	50.83	43.92
35.92	1373	0.002128	226.61	48.98	631.01	399.80	0.20	53.32	27.75	1.23	57.44	85.88
37.74	1044	0.002772	0.90	0.00	0.71	0.00	0.00	0.35	0.00	0.00	0.00	0.44

APPENDIX D (continued)

Species data for experiments conducted at 40 bar with 507 ppm of methylcyclohexane as the fuel (continued).

C4H2	C4H8	C4H6-12	C4H4	C5H6	C6H10-15	C6H12-1	CH2cC5H8	C6H6	cC6H12	cC6H8	cC6H10	CH3cC6H11	C7H8
9.95	0.35	1.87	37.31	9.51	0.05	0.00	0.08	24.48	0.00	0.19	0.18	15.43	3.13
4.58	1.11	3.40	22.48	12.78	0.16	0.02	0.41	11.34	0.06	0.58	0.84	76.06	1.04
85.83	0.00	0.16	8.11	0.70	0.00	0.00	0.00	17.52	0.00	0.00	0.00	0.91	0.33
26.34	0.14	0.51	21.86	2.80	0.00	0.00	0.02	35.18	0.00	0.04	0.05	4.29	2.21
9.39	0.33	1.92	37.59	9.98	0.08	0.01	0.08	24.27	0.00	0.25	0.21	15.80	3.02
7.44	0.55	2.39	36.50	11.72	0.09	0.00	0.12	20.65	0.11	0.27	0.25	20.74	2.76
22.56	0.14	0.62	25.17	3.45	0.00	0.00	0.02	34.72	0.00	0.14	0.06	4.78	2.71
31.77	0.19	0.36	16.64	1.95	0.00	0.00	0.02	35.37	0.00	0.12	0.05	3.31	1.88
16.99	0.23	0.97	31.47	5.42	0.04	0.00	0.04	32.05	0.00	0.12	0.00	7.66	3.06
9.14	0.52	2.04	37.64	10.45	0.07	0.00	0.09	23.95	0.00	0.32	0.21	17.96	3.10
7.08	0.55	2.53	35.45	12.32	0.08	0.01	0.14	19.65	0.09	0.38	0.30	26.01	2.57
4.90	0.89	3.20	26.06	13.25	0.13	0.02	0.36	13.06	0.08	0.53	0.67	61.42	1.59
4.85	0.98	3.23	25.52	13.24	0.12	0.01	0.34	12.79	0.06	0.49	0.67	61.33	1.59
5.69	0.92	3.08	30.91	13.04	0.11	0.02	0.24	15.79	0.08	0.45	0.46	41.62	2.10
3.69	1.03	2.58	9.21	9.16	0.21	0.00	0.85	5.68	0.12	1.15	2.34	193.01	0.46
3.95	1.19	3.11	14.60	11.27	0.20	0.02	0.67	8.20	0.09	0.90	1.50	132.40	0.71
1.08	0.18	0.30	0.41	1.79	0.11	0.00	0.51	0.50	0.23	0.56	4.27	434.32	0.04
4.82	1.05	3.32	23.49	12.85	0.15	0.01	0.39	11.76	0.08	0.59	0.03	71.43	1.33
0.62	0.10	0.14	0.14	1.00	0.10	0.00	0.34	0.14	0.24	0.30	3.49	463.54	0.03
1.65	0.37	0.66	1.19	3.34	0.15	0.02	0.73	1.22	0.20	0.96	4.51	379.23	0.11
2.87	0.78	1.78	4.94	6.96	0.22	0.00	0.92	3.51	0.14	1.24	3.35	266.17	0.23
1.33	0.29	0.57	0.92	2.84	0.14	0.00	0.71	0.95	0.21	0.86	4.54	395.94	0.07
52.84	0.00	0.21	10.42	1.10	0.00	0.00	0.01	29.45	0.02	0.00	0.00	1.92	0.91
9.87	0.38	1.84	37.42	9.63	0.06	0.00	0.08	24.70	0.00	0.23	0.19	16.14	3.06
10.80	0.41	1.81	37.31	8.92	0.03	0.00	0.07	25.59	0.00	0.18	0.18	15.25	3.09
2.61	0.72	1.58	4.03	6.21	0.21	0.00	0.88	3.08	0.15	1.26	3.59	283.11	0.26
0.93	0.18	0.29	0.38	1.79	0.13	0.00	0.52	0.49	0.23	0.59	4.23	432.45	0.05
0.18	0.03	0.03	0.00	0.22	0.04	0.00	0.11	0.03	0.25	0.04	1.48	496.23	0.00
0.34	0.06	0.03	0.00	0.49	0.06	0.00	0.06	0.26	0.00	0.11	2.29	488.34	0.00
0.15	0.00	0.00	0.00	0.18	0.05	0.00	0.10	0.02	0.25	0.03	1.27	499.06	0.00
16.13	0.24	1.07	32.90	5.81	0.00	0.00	0.04	30.75	0.00	0.14	0.09	8.03	3.22
9.65	0.33	1.90	37.69	9.91	0.06	0.00	0.08	23.85	0.00	0.22	0.18	16.25	2.97
0.00	0.00	0.00	0.00	0.02	0.01	0.00	0.00	0.00	0.27	0.00	0.20	507.03	0.00

APPENDIX D (continued)

Species data for experiments conducted at 40 bar with 164 ppm of 6-bromo-1-hexene as the fuel.

P (bar)	T (K)	t (s)	CH4	C2H6	C2H4	C2H2	C3H8	cC3H6	C3H6	aC3H4	1-C4H8	pC3H4	2-C4H8
30.58	1152	0.002402	16.25	0.77	44.44	9.04	0.19	2.29	113.65	9.20	3.18	3.79	0.55
30.02	1082	0.002592	8.32	1.06	31.21	1.66	0.21	4.02	52.17	1.33	3.11	0.27	0.52
30.32	1004	0.003153	1.19	0.27	8.32	0.12	0.04	1.11	5.04	0.03	0.36	0.00	0.20
29.93	1020	0.003069	2.02	0.38	12.33	0.22	0.00	1.67	9.75	0.11	0.72	0.00	0.27
29.90	1022	0.002908	1.97	0.39	12.72	0.29	0.04	1.80	10.66	0.13	0.78	0.00	0.32
30.10	1035	0.002802	2.43	0.45	13.25	0.28	0.04	2.04	13.03	0.17	1.01	0.00	0.30
31.05	1012	0.003124	2.26	0.43	12.50	0.22	0.05	1.89	11.73	0.12	0.69	0.00	0.35
34.03	1089	0.002691	12.51	1.26	37.14	3.31	0.30	4.36	78.92	2.64	3.93	0.69	0.58
32.68	1045	0.002906	5.30	0.86	23.02	0.79	0.16	3.36	32.26	0.57	2.01	0.00	0.47
29.54	1026	0.002948	2.26	0.41	12.33	0.25	0.00	1.89	11.68	0.12	0.74	0.00	0.34
29.95	1057	0.002824	6.33	0.90	24.17	0.98	0.16	3.70	39.04	0.79	2.53	0.00	0.49
32.11	1101	0.002487	13.53	1.18	37.97	4.16	0.31	4.27	87.32	3.36	4.37	0.94	0.64
30.04	1098	0.00254	10.29	1.10	32.39	2.49	0.26	4.42	67.54	2.08	4.08	0.57	0.56
31.42	1094	0.002663	13.60	1.14	37.46	4.26	0.30	4.20	88.24	3.59	4.10	1.03	0.67
41.62	1374	0.002069	42.47	0.24	57.89	49.99	0.00	0.11	37.33	30.65	0.00	61.57	0.00
40.84	1299	0.00217	28.58	0.32	52.25	28.24	0.06	0.29	75.81	26.70	0.41	40.19	0.00
40.04	1259	0.002221	22.91	0.42	48.94	19.70	0.07	0.45	97.52	21.42	0.76	23.10	0.09

Species data for experiments conducted at 40 bar with 164 ppm of 6-bromo-1-hexene as the fuel (continued).

C4H6	C4H2	C4H8	C4H6-12	C4H4	C5H6	C6H10-15	C6H12-1	C6H6	cC6H12	cC6H8	cC6H10	C7H8	6B1H
18.04	0.00	0.43	0.22	2.26	6.15	3.92	0.12	40.29	0.00	0.48	0.00	0.61	8.54
17.52	0.00	0.36	0.00	0.37	4.75	27.45	0.81	19.14	0.02	2.62	3.01	0.27	41.66
7.47	0.00	0.00	0.00	0.00	0.53	20.43	0.50	2.11	0.03	1.19	6.91	0.03	120.99
10.75	0.00	0.20	0.00	0.00	1.01	26.07	0.68	3.61	0.04	1.71	6.01	0.04	109.83
11.28	0.00	0.22	0.00	0.00	1.15	26.98	0.69	3.70	0.03	1.82	5.87	0.10	105.25
11.07	0.00	0.00	0.00	0.00	1.03	28.17	0.79	5.45	0.02	1.37	7.99	0.07	89.22
10.70	0.00	0.12	0.00	0.00	1.16	26.95	0.76	4.54	0.03	1.92	7.70	0.11	97.40
23.69	0.00	0.49	0.21	0.74	5.95	16.02	0.57	30.95	0.01	1.71	2.21	0.45	22.89
19.07	0.00	0.33	0.00	0.14	3.08	30.43	0.94	11.73	0.03	2.83	5.33	0.15	58.94
10.41	0.00	0.18	0.00	0.00	1.27	27.38	0.76	4.18	0.03	2.14	7.79	0.08	95.89
19.24	0.00	0.41	0.00	0.25	3.22	29.73	1.00	14.99	0.03	2.27	6.02	0.20	46.97
23.42	0.00	0.65	0.00	0.95	5.90	13.27	0.48	34.45	0.00	1.41	2.01	0.52	15.67
25.62	0.00	0.57	0.00	0.54	5.65	21.73	0.72	24.85	0.02	2.44	3.39	0.33	24.18
16.53	0.00	0.61	0.16	0.96	6.25	12.68	0.47	35.01	0.00	1.48	2.11	0.49	15.80
1.24	2.74	0.00	0.20	9.62	0.00	0.23	0.00	41.40	0.00	0.00	0.16	1.17	1.72
12.64	0.97	0.14	0.14	6.93	4.47	0.56	0.01	39.02	0.00	0.10	0.13	0.79	2.24
10.90	0.29	0.00	0.23	5.09	5.52	0.85	0.03	40.93	0.00	0.16	0.21	0.69	2.41

APPENDIX D (continued)

Species data for experiments conducted at 100 bar with 162 ppm of 6-bromo-1-hexene as the fuel.

P (bar)	T (K)	t (s)	CH4	C2H6	C2H4	C2H2	C3H8	cC3H6	C3H6	aC3H4	1-C4H8	pC3H4	2-C4H8
82.16	976	0.003035	1.07	0.27	9.27	0.00	0.00	0.77	3.83	0.00	0.23	0.00	0.00
101.62	1140	0.002345	20.18	2.29	55.72	5.24	0.52	3.07	103.15	3.07	2.34	1.48	0.00
69.74	966	0.002538	0.69	0.13	3.70	0.00	0.00	0.29	0.96	0.00	0.13	0.00	0.10
89.80	1076	0.002564	16.07	2.81	50.16	2.48	0.64	4.66	80.84	1.47	3.10	0.45	0.00
103.76	1118	0.002333	20.11	2.32	55.18	5.95	0.51	3.04	104.56	3.19	2.04	1.69	0.78
92.70	1062	0.002464	15.56	2.73	48.98	2.45	0.60	4.57	78.69	1.38	3.03	0.60	1.04
105.65	1090	0.002441	20.34	2.83	56.26	4.53	0.64	4.05	102.36	2.54	2.32	1.03	0.96
95.16	1065	0.002377	15.07	2.73	46.42	2.28	0.66	4.70	77.44	1.28	2.97	0.28	0.00
91.98	1019	0.00245	7.43	1.75	31.94	0.89	0.31	3.69	39.90	0.46	1.66	0.00	0.68
101.84	1076	0.002406	17.55	2.97	49.61	3.14	0.70	4.54	88.60	1.72	2.27	0.67	0.94
87.17	1032	0.002591	4.87	1.28	23.74	0.46	0.19	2.97	25.44	0.22	1.24	0.00	0.58
96.34	1066	0.002538	13.90	2.69	42.82	1.93	0.61	4.41	69.83	1.13	2.19	0.28	0.76
88.24	992	0.00252	2.19	0.55	15.84	0.17	0.00	1.48	9.17	0.09	0.48	0.00	0.39
92.00	1018	0.002541	5.52	1.42	29.52	0.60	0.22	2.86	27.94	0.30	1.34	0.00	0.67
101.63	1069	0.002455	15.47	3.07	51.34	2.21	0.64	4.53	76.03	1.26	2.40	0.42	0.98
84.17	985	0.00261	1.23	0.23	7.34	0.09	0.00	0.63	2.86	0.00	0.15	0.00	0.16
108.03	1211	0.002211	22.75	1.33	57.39	12.56	0.28	0.65	113.26	7.34	0.89	6.19	0.51
106.32	1236	0.002197	25.94	0.97	57.70	16.71	0.16	0.44	106.23	11.07	0.57	11.39	0.22
86.07	1179	0.00235	22.14	1.31	54.48	11.21	0.28	0.80	113.96	7.14	0.97	5.18	0.61
94.57	1329	0.002204	39.48	0.33	63.93	42.77	0.05	0.10	55.67	23.57	0.18	45.01	0.00
81.24	969	0.003031	1.02	0.23	3.16	0.00	0.00	0.54	2.00	0.00	0.19	0.00	0.00
91.43	1399	0.002174	55.81	0.18	71.74	73.64	0.00	0.08	28.88	26.68	0.00	57.99	0.00
99.17	1298	0.002154	36.15	0.47	62.57	34.96	0.07	0.16	68.29	20.87	0.00	36.11	0.07
109.21	1371	0.002163	47.30	0.26	65.33	59.33	0.00	0.08	33.81	23.34	0.00	49.17	0.15
102.45	1334	0.002224	40.78	0.42	70.17	44.15	0.06	0.15	67.18	25.03	0.00	45.86	0.00
70.42	942	0.002613	0.00	0.00	0.82	0.00	0.00	0.10	0.25	0.00	0.00	0.00	0.00
68.03	908	0.002678	0.00	0.00	0.26	0.00	0.00	0.00	0.07	0.00	0.00	0.00	0.00
81.78	986	0.002654	0.87	0.21	5.26	0.04	0.00	0.64	2.57	0.00	0.31	0.00	0.21
105.70	1291	0.002163	26.71	0.63	58.57	22.46	0.10	0.28	95.83	14.58	0.20	18.57	0.00
99.62	1165	0.002309	22.34	1.56	54.15	9.53	0.31	1.06	109.09	5.68	1.26	3.91	0.62
106.99	1323	0.002194	38.02	0.33	62.95	39.59	0.06	0.12	58.39	21.67	0.00	39.73	0.00

APPENDIX D (continued)

Species data for experiments conducted at 100 bar with 162 ppm of 6-bromo-1-hexene as the fuel (continued).

C4H6	C4H2	C4H8	C4H6-12	C4H4	C5H6	C6H10-15	C6H12-1	C6H6	cC6H12	cC6H8	cC6H10	C7H8	6B1H
9.14	0.00	0.12	0.00	0.00	0.34	15.96	0.37	3.24	0.04	0.60	12.80	0.02	76.63
44.11	0.00	0.74	0.21	1.66	4.31	2.90	0.16	39.15	0.00	0.15	1.30	0.81	1.92
3.53	0.05	0.00	0.00	0.00	0.09	8.74	0.16	3.50	0.03	0.34	18.81	0.00	86.22
43.06	0.00	1.04	0.21	0.74	5.04	13.00	0.62	32.89	0.02	0.98	2.50	0.68	16.84
6.93	0.00	0.74	0.14	1.58	5.82	3.54	0.21	42.31	0.00	0.47	0.77	0.94	5.13
9.43	0.00	1.00	0.00	0.70	5.75	13.25	0.64	31.18	0.04	1.62	2.42	0.63	19.84
4.44	0.00	0.93	0.16	1.24	6.05	5.55	0.32	39.90	0.01	0.80	1.19	0.96	9.02
29.10	0.00	0.99	0.11	0.67	5.21	14.39	0.71	30.77	0.02	1.52	3.29	0.62	21.23
6.62	0.00	0.65	0.00	0.23	3.50	24.47	1.04	15.02	0.05	2.55	5.95	0.26	50.46
4.60	0.00	1.12	0.00	0.79	6.24	9.44	0.53	36.49	0.04	1.37	2.20	0.79	14.62
8.46	0.00	0.49	0.00	0.11	2.52	25.97	1.08	10.15	0.08	2.71	7.17	0.19	68.09
4.93	0.00	0.92	0.16	0.52	5.81	14.85	0.81	30.67	0.03	1.97	3.25	0.65	23.77
14.76	0.00	0.24	0.00	0.00	0.98	21.84	0.65	3.61	0.07	1.36	4.76	0.05	101.31
16.31	0.00	0.47	0.00	0.00	2.82	25.54	0.94	11.00	0.06	2.24	4.42	0.21	64.22
5.26	0.00	1.04	0.00	0.53	5.90	13.91	0.67	29.82	0.03	1.77	2.23	0.73	22.83
6.88	0.00	0.00	0.00	0.00	0.32	14.10	0.32	1.40	0.04	0.75	5.21	0.02	118.38
6.49	0.00	0.44	0.15	3.75	5.57	0.66	0.04	45.09	0.00	0.13	0.17	1.03	1.23
12.60	0.31	0.30	0.23	5.17	5.86	0.44	0.03	45.23	0.00	0.08	0.11	1.03	0.74
2.44	0.27	0.52	0.00	2.99	6.04	1.29	0.07	45.66	0.00	0.19	0.29	0.92	2.11
26.38	1.92	0.00	0.20	11.65	2.59	0.11	0.00	42.02	0.00	0.04	0.09	1.27	0.24
2.91	0.00	0.00	0.00	0.00	0.22	11.21	0.32	2.62	0.03	0.88	19.74	0.00	129.10
0.47	5.22	0.00	0.13	13.60	1.93	0.08	0.00	48.44	0.00	0.00	0.18	1.69	0.53
0.34	1.32	0.00	0.00	8.31	4.24	0.16	0.00	47.08	0.00	0.08	0.11	1.39	1.01
0.45	3.93	0.00	0.00	11.82	2.53	0.08	0.00	49.82	0.00	0.00	0.00	1.83	0.97
0.63	1.96	0.00	0.00	10.83	3.85	0.11	0.00	46.51	0.00	0.00	0.10	0.00	1.33
0.62	0.00	0.00	0.00	0.00	0.00	3.95	0.07	2.07	0.00	0.21	12.74	0.00	161.05
0.26	0.00	0.00	0.00	0.00	0.00	1.42	0.05	1.90	0.00	0.11	12.03	0.00	171.22
4.81	0.00	0.00	0.00	0.00	0.25	13.74	0.38	2.21	0.03	0.79	11.03	0.04	144.23
0.58	0.59	0.00	0.00	6.17	5.29	0.25	0.01	44.39	0.00	0.07	0.10	1.21	1.26
9.63	0.00	0.35	0.00	2.92	5.71	1.60	0.08	46.20	0.00	0.19	0.35	1.06	4.14
2.14	1.77	0.00	0.00	10.00	3.09	0.00	0.00	44.90	0.00	0.07	0.10	1.49	0.64

APPENDIX D (continued)

Species data for experiments conducted at 200 bar with 161 ppm of 6-bromo-1-hexene as the fuel.

P (bar)	T (K)	t (s)	CH4	C2H6	C2H4	C2H2	C3H8	cC3H6	C3H6	aC3H4	1-C4H8	pC3H4	2-C4H8
182.62	1198	0.002218	27.32	2.35	66.61	11.35	0.48	0.77	124.60	5.16	0.92	4.68	0.75
167.76	1212	0.002349	24.80	2.20	61.69	10.54	0.45	0.88	118.16	4.76	0.59	4.01	0.86
171.86	1105	0.002356	19.48	4.01	57.13	2.75	1.02	4.05	87.75	1.37	2.68	0.60	1.01
176.34	1060	0.002385	10.19	2.91	43.88	0.87	0.56	3.50	45.92	0.42	1.51	0.00	0.99
173.14	1104	0.002361	17.59	4.15	55.00	2.06	1.01	4.28	78.46	1.05	2.44	0.46	1.15
154.77	1079	0.002823	19.55	4.18	54.55	2.39	1.04	4.20	86.29	1.25	2.46	0.51	1.07
166.27	928	0.002293	0.34	0.00	2.25	0.00	0.00	0.13	0.55	0.00	0.00	0.00	0.00
173.49	990	0.002268	1.75	0.51	13.13	0.11	0.05	0.86	4.96	0.00	0.46	0.00	0.31
179.35	985	0.00227	1.74	0.51	14.31	0.09	0.00	1.01	5.88	0.00	0.54	0.00	0.44
233.47	1133	0.002235	23.46	4.04	62.06	4.90	0.94	2.82	103.92	2.20	2.23	1.32	0.97
172.20	983	0.002372	1.72	0.58	13.46	0.17	0.05	1.06	6.48	0.00	0.41	0.00	0.38
152.59	953	0.002303	0.78	0.23	4.30	0.00	0.00	0.35	1.33	0.00	0.00	0.00	0.17
174.38	1085	0.002369	15.30	3.98	50.67	1.57	0.95	4.24	68.57	0.77	1.82	0.25	1.21
173.56	1160	0.002328	22.26	3.41	59.17	5.26	0.78	3.00	103.26	2.43	1.14	1.52	1.23
198.21	1417	0.002039	48.82	0.29	66.30	64.61	0.00	0.00	27.35	19.27	0.00	44.00	0.00
219.87	1439	0.00202	51.47	0.20	65.49	72.61	0.00	0.00	20.34	18.31	0.00	42.84	0.00
189.29	1310	0.002192	26.65	0.94	63.37	22.17	0.12	0.14	94.43	10.38	0.00	14.80	0.23
227.96	1140	0.002175	22.65	3.73	61.65	5.04	0.82	2.65	97.18	2.17	0.58	1.40	1.23
208.21	1404	0.002072	43.70	0.41	68.60	51.76	0.00	0.00	44.16	19.37	0.00	41.65	0.00
208.89	1359	0.002064	33.21	0.57	66.12	34.70	0.07	0.07	65.45	15.85	0.00	29.04	0.00
205.29	1323	0.002076	29.58	0.95	66.81	24.67	0.19	0.17	92.35	11.29	0.34	17.28	0.00
209.58	1272	0.002104	27.54	1.30	64.69	18.55	0.24	0.19	99.58	8.23	0.00	10.46	0.36
184.51	1198	0.002251	23.39	2.62	60.39	8.17	0.55	1.44	106.05	3.55	0.40	2.67	1.04
188.06	1246	0.002232	23.85	1.64	60.21	12.55	0.34	0.43	108.79	5.60	0.35	5.49	0.81
213.94	1332	0.002133	32.68	0.77	66.48	29.30	0.15	0.09	76.00	13.45	0.00	22.37	0.00
254.24	1495	0.001959	65.46	0.21	49.78	120.92	0.00	0.00	5.49	8.57	0.00	21.35	0.00

APPENDIX D (continued)

Species data for experiments conducted at 200 bar with 161 ppm of 6-bromo-1-hexene as the fuel (continued).

C4H6	C4H2	C4H8	C4H6-12	C4H4	C5H6	C6H10-15	C6H12-1	C6H6	cC6H12	cC6H8	cC6H10	C7H8	6B1H
1.82	0.00	0.39	0.15	3.48	5.30	0.40	0.05	43.23	0.00	0.09	0.15	1.21	0.81
0.88	0.00	0.45	0.13	2.96	5.79	0.46	0.04	46.14	0.00	0.10	0.17	1.20	0.97
18.09	0.00	1.27	0.23	0.84	4.77	5.94	0.37	35.84	0.01	0.60	1.54	0.96	10.08
3.50	0.00	1.01	0.24	0.31	3.50	18.25	0.87	19.20	0.06	1.62	4.66	0.45	46.69
5.16	0.00	1.53	0.00	0.68	5.19	8.78	0.53	31.82	0.04	1.07	2.31	0.93	17.16
9.12	0.00	1.32	0.22	0.85	5.08	7.04	0.44	39.75	0.00	0.74	2.01	1.11	13.20
2.29	0.00	0.00	0.00	0.00	0.06	4.80	0.09	1.26	0.00	0.16	5.08	0.00	160.31
13.23	0.00	0.12	0.00	0.00	0.44	15.52	0.46	2.70	0.08	0.69	4.88	0.03	125.05
13.69	0.00	0.28	0.00	0.00	0.44	0.03	0.47	3.61	0.07	0.64	7.21	0.05	99.06
48.80	0.00	1.22	0.21	1.61	3.45	1.35	0.12	38.61	0.03	0.06	0.45	1.05	1.28
11.97	0.00	0.19	0.00	0.00	0.55	17.23	0.58	3.54	0.08	0.87	6.76	0.05	125.61
4.24	0.00	0.00	0.00	0.00	0.14	8.28	0.22	1.99	0.05	0.39	8.28	0.02	157.11
3.17	0.00	1.61	0.00	0.43	5.06	12.38	0.71	32.35	0.07	1.41	3.34	2.31	22.65
1.73	0.00	0.79	0.00	1.42	4.40	0.00	0.15	42.81	0.00	0.23	0.56	1.16	3.21
4.66	5.09	0.00	0.11	16.20	0.58	0.03	0.00	43.41	0.00	0.00	0.07	2.22	0.13
5.72	6.25	0.00	0.00	12.98	1.13	0.03	0.00	44.31	0.10	0.00	0.00	2.46	0.34
0.42	0.46	0.22	0.00	5.91	2.41	0.10	0.00	38.12	0.00	0.00	0.06	1.16	0.50
0.00	0.00	0.93	0.00	1.31	3.76	1.40	0.11	37.20	0.00	0.19	0.49	1.02	1.42
3.27	3.58	0.00	0.00	11.78	1.04	0.04	0.00	44.08	0.00	0.00	0.07	0.00	0.10
1.39	1.52	0.00	0.00	9.02	2.30	0.07	0.00	35.71	0.00	0.00	0.05	1.40	0.45
0.68	0.74	0.38	0.00	5.97	1.77	0.09	0.00	34.79	0.00	0.00	0.12	1.10	0.35
0.33	0.36	0.00	0.00	4.80	2.94	0.15	0.00	39.26	0.00	0.11	0.11	1.17	0.58
0.00	0.00	0.58	0.00	1.84	3.57	0.64	0.07	43.23	0.00	0.00	0.28	1.18	1.37
0.18	0.20	0.44	0.00	3.27	3.20	0.25	0.03	40.60	0.00	0.06	0.11	1.05	0.37
1.10	1.21	0.00	0.00	6.78	1.80	0.08	0.00	41.90	0.00	0.00	0.08	1.46	0.35
12.87	14.08	0.00	0.00	7.47	0.48	0.03	0.00	47.17	0.00	0.00	0.03	1.88	0.38

APPENDIX D (continued)

Species data for experiments conducted at 40 bar with 358 ppm of 6-bromo-1-hexene as the fuel.

P (bar)	T (K)	t (s)	CH4	C2H6	C2H4	C2H2	C3H8	cC3H6	C3H6	aC3H4	1-C4H8	pC3H4	2-C4H8
38.67	1150	0.002398	44.32	4.15	128.98	15.14	0.87	6.05	249.77	11.39	4.61	5.80	2.19
40.57	1201	0.002254	46.16	2.98	131.95	23.05	0.54	2.51	258.72	16.98	1.98	12.08	1.66
39.20	1064	0.002308	26.01	5.25	98.45	2.96	1.12	9.21	134.58	2.33	4.26	0.57	2.28
38.63	964	0.002334	1.20	0.42	14.13	0.00	0.00	1.11	4.72	0.00	0.35	0.00	0.40
39.25	1006	0.002385	7.37	2.14	50.61	0.56	0.27	4.64	39.46	0.47	1.87	0.00	1.23
40.61	1059	0.002424	26.48	5.37	95.92	2.98	1.19	9.44	137.07	2.37	4.69	0.59	2.14
39.20	1096	0.002559	41.61	5.63	120.05	8.42	1.31	9.45	213.84	6.23	1.67	2.23	2.83
36.64	1114	0.002575	43.18	5.07	122.21	10.62	1.13	8.42	227.72	8.12	1.66	3.34	2.46
39.61	1028	0.002346	9.26	2.64	53.86	0.72	0.33	5.52	50.24	0.51	1.65	0.00	1.51
38.78	926	0.002373	0.00	0.14	2.91	0.00	0.00	0.22	0.64	0.00	0.00	0.00	0.00
37.84	1011	0.002359	7.61	2.22	47.21	0.62	0.25	5.00	42.20	0.42	1.85	0.00	1.25
36.13	1019	0.002353	6.69	1.98	42.87	0.54	0.24	4.54	36.23	0.36	1.52	0.00	1.17
38.90	1046	0.002437	17.18	4.12	71.87	1.54	0.74	8.02	90.66	1.24	3.46	0.17	1.82
39.43	994	0.002372	3.81	1.30	27.88	0.27	0.09	3.18	20.52	0.18	0.95	0.00	0.86
37.77	1073	0.002488	30.50	5.58	97.12	3.79	1.31	9.97	153.46	2.83	1.70	0.71	2.50
35.72	1051	0.002424	22.10	4.67	80.81	2.31	0.93	8.98	114.60	1.87	1.50	0.31	2.14
40.01	1293	0.002124	71.79	0.96	142.32	70.78	0.14	0.52	165.84	49.13	0.14	80.06	0.31
38.45	1367	0.002078	113.72	0.47	145.54	150.64	0.05	0.20	57.74	53.71	0.00	115.69	0.00
38.30	1191	0.002249	48.88	2.75	127.50	24.87	0.47	2.04	247.90	19.29	0.42	14.21	1.60
41.13	1270	0.002113	64.44	1.23	138.52	56.29	0.18	0.60	201.43	41.95	0.17	58.73	0.42
41.70	1274	0.002106	60.88	1.31	136.61	51.89	0.21	0.65	201.92	38.31	0.00	51.51	0.58
38.33	1203	0.002262	49.95	2.65	126.24	25.58	0.47	1.84	245.96	19.59	0.51	14.86	1.47
36.62	1180	0.002258	49.72	2.58	124.50	24.85	0.45	2.01	250.06	19.57	0.73	14.26	1.53
40.85	1357	0.002057	110.92	0.48	148.41	135.52	0.08	0.18	65.46	50.25	0.18	105.47	0.10
40.95	1326	0.002108	89.30	0.73	145.73	93.08	0.07	0.29	110.60	50.79	0.09	95.22	0.15
39.35	1224	0.002208	55.92	2.11	124.53	31.79	0.36	1.06	229.64	24.80	0.44	22.67	0.92
37.21	1212	0.002228	54.90	2.25	123.24	29.76	0.36	1.22	232.08	23.41	0.44	20.07	1.07
37.67	1253	0.002116	64.09	1.46	130.82	46.57	0.19	0.68	198.02	36.16	0.31	45.65	0.47
36.64	1482	0.002036	150.67	0.20	77.67	354.38	0.00	0.00	6.81	13.00	0.00	30.60	0.00
36.92	1451	0.00201	148.59	0.24	113.30	277.90	0.00	0.10	12.52	22.84	0.00	52.76	0.00
38.03	1403	0.002047	130.97	0.35	137.81	191.78	0.00	0.12	27.99	38.81	0.00	87.14	0.00

APPENDIX D (continued)

Species data for experiments conducted at 40 bar with 358 ppm of 6-bromo-1-hexene as the fuel (continued).

C4H6	C4H2	C4H8	C4H6-12	C4H4	C5H6	C6H10-15	C6H12-1	C6H6	cC6H12	cC6H8	cC6H10	C7H8	6B1H
97.23	0.00	1.27	0.38	5.19	12.52	5.58	0.21	86.55	0.00	1.08	0.88	2.01	8.43
2.34	0.17	0.74	0.18	6.90	12.21	2.83	0.09	87.14	0.00	0.47	0.45	1.80	3.66
5.46	0.00	1.67	0.15	0.80	9.51	41.17	1.46	50.41	0.15	3.58	5.79	1.00	73.86
12.18	0.00	0.18	0.00	0.00	0.44	26.68	0.48	1.39	0.09	1.20	7.77	0.07	301.93
18.47	0.00	0.71	0.00	0.15	3.42	54.09	1.51	13.58	0.16	3.49	8.08	0.29	193.71
4.54	0.00	1.67	0.12	0.81	9.28	40.93	1.59	51.94	0.15	3.48	6.43	1.02	71.79
2.43	0.00	1.22	0.11	1.97	11.82	14.28	0.64	81.05	0.00	1.72	2.32	1.78	21.40
2.16	0.00	1.05	0.00	2.50	11.49	10.25	0.45	84.79	0.00	1.26	1.74	1.69	15.83
1.72	0.00	0.84	0.00	0.23	4.14	55.53	1.68	18.09	0.17	4.07	10.49	0.33	171.21
2.83	0.00	0.00	0.00	0.00	0.04	8.45	0.15	2.05	0.04	0.37	14.14	0.07	319.51
7.29	0.00	0.69	0.00	0.20	3.43	54.86	1.59	15.19	0.16	3.84	11.34	0.28	183.81
3.12	0.00	0.57	0.00	0.13	3.17	53.87	1.55	12.72	0.17	4.03	11.28	0.26	199.81
2.69	0.00	1.12	0.00	0.45	6.34	53.39	1.94	34.68	0.23	4.09	10.60	0.65	115.37
3.90	0.00	0.37	0.00	0.00	1.59	45.63	1.24	8.46	0.15	2.96	17.28	0.17	224.15
2.64	0.00	1.47	0.00	0.87	10.57	35.71	1.52	59.75	0.16	3.65	6.41	1.18	57.33
2.13	0.00	1.07	0.00	0.53	8.64	48.43	1.83	43.93	0.17	4.56	8.88	0.89	89.65
0.23	2.73	0.11	0.09	15.40	8.43	0.62	0.02	84.31	0.00	0.25	0.12	2.45	0.96
0.00	12.53	0.00	0.00	22.02	3.58	0.18	0.00	96.98	0.00	0.00	0.06	3.22	0.28
0.68	0.25	0.37	0.00	5.93	11.61	2.87	0.10	89.16	0.00	0.46	0.60	1.78	4.34
0.24	1.60	0.15	0.11	12.74	8.59	0.72	0.01	84.93	0.00	0.33	0.16	2.07	1.00
0.31	1.40	0.14	0.00	11.74	9.21	0.81	0.02	84.70	0.00	0.28	0.20	2.06	0.83
0.66	0.22	0.34	0.11	6.21	11.10	2.66	0.09	88.51	0.00	0.38	0.63	1.72	3.47
0.70	0.20	0.37	0.09	5.90	11.07	2.84	0.11	88.16	0.00	0.40	0.73	1.72	4.12
0.27	10.33	0.09	0.13	25.47	3.62	0.18	0.00	96.65	0.00	0.00	0.10	3.41	0.95
0.14	4.99	0.18	0.14	19.76	6.52	0.35	0.00	90.94	0.00	0.15	0.18	3.02	1.60
0.56	0.41	0.24	0.12	7.76	11.79	1.56	0.06	92.54	0.00	0.66	0.64	1.99	3.31
0.53	0.34	0.32	0.09	7.28	12.57	1.74	0.07	93.27	0.00	0.69	0.68	2.00	3.51
0.35	1.09	0.18	0.12	11.28	11.26	0.93	0.04	90.74	0.00	0.44	0.39	2.12	1.99
0.00	46.33	0.00	0.00	9.92	0.58	0.04	0.00	105.31	0.00	0.00	0.04	1.40	0.62
0.00	34.60	0.00	0.00	17.87	1.01	0.05	0.00	112.30	0.00	0.00	0.06	2.28	0.30
0.00	19.99	0.00	0.00	23.62	2.21	0.11	0.00	108.01	0.22	0.00	0.07	3.25	2.17

APPENDIX D (continued)

Species data for experiments conducted at 100 bar with 170 ppm of 1,5-hexadiene as the fuel.

P (bar)	T (K)	t (s)	CH4	C2H6	C2H4	C2H2	cC3H6	C3H6	aC3H4	1-C4H8	pC3H4
84.40	980	0.002599	0.00	0.00	0.00	0.00	0.00	0.60	0.00	0.00	0.00
96.77	989	0.002482	0.00	0.00	0.19	0.00	0.00	0.69	0.00	0.12	0.00
105.04	990	0.002357	0.00	0.00	0.20	0.00	0.00	0.81	0.04	0.12	0.00
110.30	1133	0.002254	0.76	0.00	7.81	2.77	0.00	36.98	16.41	6.14	2.95
114.81	1141	0.002311	0.74	0.00	7.81	2.65	0.00	36.50	15.35	6.14	2.72
80.96	955	0.002961	0.00	0.00	0.12	0.00	0.00	0.38	0.00	0.07	0.00
94.34	1033	0.002532	0.00	0.00	0.48	0.06	0.00	2.23	0.29	0.47	0.00
93.01	1061	0.002506	0.00	0.00	0.95	0.21	0.00	4.38	0.99	0.87	0.13
99.40	1155	0.002393	0.62	0.00	7.48	2.49	0.00	34.72	16.00	5.73	2.74
86.95	1040	0.002636	0.00	0.00	0.66	0.12	0.00	2.72	0.53	0.56	0.00
98.59	1094	0.002402	0.18	0.00	2.63	0.75	0.00	12.38	4.41	2.25	0.59
92.88	1142	0.002366	0.78	0.00	11.56	4.62	0.09	53.56	29.75	8.51	6.59
114.08	1287	0.002163	19.04	6.60	43.17	28.47	0.09	103.27	48.79	5.77	61.72
114.63	1282	0.002172	20.21	7.16	43.44	29.73	0.10	97.63	45.57	4.70	61.58
92.30	1128	0.002398	0.00	0.00	6.54	2.27	0.00	31.50	15.59	5.05	2.60
99.65	1172	0.002241	1.30	0.14	18.90	7.92	0.08	80.16	43.90	13.84	13.80
110.51	1223	0.002211	10.64	3.70	35.48	19.85	0.10	103.39	54.27	10.71	45.69
86.44	1124	0.002432	0.17	0.00	6.62	2.35	0.08	31.68	15.79	5.07	2.65
97.44	1274	0.002274	15.28	5.87	39.73	24.93	0.11	102.84	51.42	6.77	57.61
99.53	1243	0.002255	10.58	3.97	35.46	20.04	0.09	104.80	56.09	10.81	47.12
100.31	1204	0.002278	6.23	2.03	30.85	15.85	0.09	102.61	57.41	14.66	35.56
87.82	1132	0.002407	0.69	0.00	9.31	3.50	0.00	43.74	23.39	6.82	4.56
98.23	1190	0.002287	3.98	0.96	27.84	13.58	0.10	100.82	57.75	16.69	29.25
91.54	1297	0.002268	23.59	8.07	44.05	34.61	0.10	94.73	45.76	3.34	70.99
93.34	1333	0.002203	42.38	9.50	55.49	64.02	0.06	67.49	38.12	1.72	71.78
100.66	1449	0.002117	88.18	3.76	61.36	160.60	0.00	17.74	17.22	0.47	36.21
94.93	1494	0.002121	95.38	2.30	53.83	191.79	0.00	10.49	11.16	0.25	24.03

APPENDIX D (continued)

Species data for experiments conducted at 100 bar with 170 ppm of 1,5-hexadiene as the fuel (continued).

C4H6	C4H2	C4H8	C4H6-12	C4H4	C5H6	C6H10-15	C6H12-1	C6H6	cC6H8	cC6H10	C7H8
0.00	0.00	0.00	0.00	0.00	0.03	168.61	0.55	0.05	0.08	0.02	0.00
0.07	0.00	0.00	0.00	0.00	0.05	171.88	0.57	0.05	0.12	0.00	0.00
0.13	0.00	0.00	0.00	0.00	0.06	172.28	0.56	0.05	0.14	0.02	0.00
6.40	0.00	0.00	0.00	0.29	2.66	122.27	0.27	2.06	3.19	0.23	0.04
6.38	0.00	0.00	0.00	0.27	2.74	122.48	0.28	2.07	3.28	0.23	0.05
0.06	0.00	0.00	0.00	0.00	0.04	172.28	0.57	0.04	0.06	0.00	0.00
0.42	0.00	0.00	0.00	0.00	0.22	170.12	0.57	0.15	0.40	0.05	0.00
0.83	0.00	0.00	0.00	0.00	0.44	167.18	0.53	0.27	0.77	0.07	0.00
6.18	0.00	0.00	0.00	0.25	2.49	125.07	0.27	1.92	2.98	0.22	0.00
0.50	0.00	0.00	0.00	0.00	0.28	169.12	0.55	0.17	0.53	0.05	0.00
2.40	0.00	0.00	0.00	0.00	1.09	156.18	0.43	0.64	1.69	0.13	0.00
8.59	0.00	0.00	0.00	0.46	3.16	99.33	0.19	2.66	3.11	0.22	0.06
15.78	0.70	0.48	1.11	3.22	6.25	5.26	0.03	13.50	0.60	0.00	0.65
15.29	0.71	0.44	1.03	3.29	6.28	6.86	0.03	13.99	0.60	0.00	0.71
5.53	0.00	0.00	0.00	0.21	2.22	130.40	0.29	1.50	2.81	0.20	0.04
11.94	0.21	0.16	0.11	0.84	4.61	60.62	0.11	4.78	3.18	0.20	0.13
15.24	0.52	0.46	0.99	2.30	6.34	13.94	0.07	10.36	1.11	0.05	0.40
5.62	0.00	0.00	0.00	0.21	2.19	129.29	0.28	1.52	2.79	0.20	0.00
15.02	0.63	0.50	1.13	2.80	6.17	7.99	0.04	12.04	0.73	0.03	0.53
15.17	0.53	0.50	1.01	2.25	6.23	12.77	0.06	10.12	1.10	0.05	0.36
14.46	0.39	0.41	0.63	1.81	5.91	20.02	0.06	8.33	1.58	0.07	0.30
7.23	0.00	0.00	0.00	0.33	2.72	112.18	0.23	2.09	3.00	0.21	0.05
14.12	0.30	0.30	0.40	1.52	5.68	26.65	0.07	7.47	2.05	0.10	0.21
14.07	0.81	0.38	0.98	3.41	5.25	4.22	0.02	13.98	0.37	0.02	0.70
12.61	1.55	0.21	0.77	5.37	3.32	1.79	0.00	20.23	0.21	0.00	1.19
5.27	6.19	0.10	0.38	6.48	0.76	0.29	0.00	33.18	0.03	0.00	1.62
2.98	8.03	0.00	0.15	4.65	0.47	0.14	0.00	33.42	0.02	0.00	1.25

APPENDIX E

Due to their size, the RMG mechanisms, the optimized Wang mechanisms, and the thermodynamic data are included as digital files in the supplemental information. “CH RMG Unmodified Mech and Thermo.inp” is the RMG mechanism for methylcyclohexane with all the necessary species thermochemistry. “CH RMG Optimized Mech and Thermo.inp” is the optimized version of the RMG mechanism for methylcyclohexane with all the necessary species thermochemistry. “CH Wang Optimized Mech and Thermo.inp” is the optimized Wang mechanism with respect to the cyclohexane experimental data with all the necessary species thermochemistry. “MCH RMG Unmodified Mech and Thermo.inp” is the RMG mechanism for methylcyclohexane with all the necessary species thermochemistry. “MCH RMG Optimized Mech and Thermo.inp” is the optimized version of the RMG mechanism for methylcyclohexane with all the necessary species thermochemistry. “MCH Wang Optimized Mech and Thermo.inp” is the optimized Wang mechanism with respect to the methylcyclohexane experimental data with all the necessary species thermochemistry. “hex5en1yl 15HD RMG Mech and Thermo.inp” is the RMG mechanism for hex-5-en-1-yl radical and 1,5-hexadiene with all the necessary species thermochemistry.

VITA

Education

- Ph.D. in Mechanical Engineering, University of Illinois at Chicago, *August 2018*
- B.S. in Mechanical Engineering, University of Illinois at Chicago**,** *May 2013*

Experience

- Engineer (Part Time) at Gas Technology Institute, *January 2018 - Present*
- Research Assistant at University of Illinois at Chicago, *August 2013 - Present*
- Teaching Assistant at University of Illinois at Chicago, *August 2013 - August 2015*

Awards

- 2014, 2016 Illinois Space Grant Consortium Fellowship
- Ogden Livermore Award for excelling in Modern Physics, Fall 2012

Publications

- M. Liszka, K. Brezinsky, "Variable High Pressure and Concentration Study of Cyclohexane Pyrolysis at High Temperatures," *International Journal of Chemical Kinetics* (submitted)
- M. Liszka, K. Brezinsky, "Experimental and Comparative Modeling Study of High Temperature and Very High Pressure Methylcyclohexane Pyrolysis," *Fuel* (submitted)
- M. Liszka, K. Brezinsky, "Experimental and Modeling Study of Hex-5-en-1-yl Radical Pyrolysis at Very High Pressure and Temperature," *Combustion and Flame* (submitted)
- X. Han, M. Liszka, R. Xu, K. Brezinsky, H. Wang, "A high pressure shock tube study of the pyrolysis of real jet fuel Jet A," *Proc. Combust. Inst.*, vol. 37 (accepted)

Presentations

- K. Brezinsky (presenter), M. Liszka, "Experimental and Comparative Modeling Study of High Temperature and Very High Pressure Cyclohexane, Methylcyclohexane, and 6-Bromo-1-hexene Pyrolysis," *The 4th International Workshop on Flame Chemistry*, Dublin, Ireland, July 2018.

Poster Presentations

- M. Liszka, (presenter), K. Brezinsky, "High Pressure and Temperature Pyrolysis of Cyclohexane, Methylcyclohexane, and 6-Bromo-1-hexene,"*37th International Symposium on Combustion*, Dublin, Ireland, July-August 2018.
- M. Liszka (presenter), K. Brezinsky, X. Han, "Reactions of hex-5-en-1-yl radicals, 1,5-hexadiene, and cyclohexane," *10th International Conference on Chemical Kinetics*, Chicago, May 2017.
- M. Liszka, (presenter), K. Brezinsky, X. Han, "Reactions of hex-5-en-1-yl radicals, 1,5-hexadiene, and cyclohexane," *10th US National Combustion Meeting*, Hyattsville, Maryland, April 2017.